CORA Cork Open Research Archive
Cartlann Taighde Oscailte Chorcaí

| | |
|---|---|
| Title | Properties and applications of injection locking in 1.55 μm quantum-dash mode-locked semiconductor lasers |
| Authors | Sooudi, Ehsan |
| Publication date | 2013 |
| Original Citation | Sooudi, E. 2013. Properties and applications of injection locking in 1.55 μm quantum-dash mode-locked semiconductor lasers. PhD Thesis, University College Cork. |
| Type of publication | Doctoral thesis |
| Rights | © 2013, Ehsan Sooudi. - http://creativecommons.org/licenses/by-nc-nd/3.0/ |
| Download date | 2026-11-04 21:52:48 |
| Item downloaded from | https://hdl.handle.net/10468/1292 |

UCC
University College Cork, Ireland
Coláiste na hOllscoile Corcaigh

# Properties and Applications of Injection Locking in 1.55 $\mu$m Quantum-Dash Mode-Locked Semiconductor Lasers

Ehsan Sooudi
MSC ELECTRICAL ENGINEERING



NATIONAL UNIVERSITY OF IRELAND, CORK

School of Science

Department of Physics

**Thesis submitted for the degree of Doctor of Philosophy**

September 2013

Supervisor: Professor John G. McInerney

Head of Department/School: Professor John G. McInerney

# Contents

Abstract . . . iv
List of Publications . . . v
Acknowledgements . . . viii
List of Figures . . . ix
List of Tables . . . xix

**1 Introduction** **1**
1.1 Brief History of Semiconductor Lasers . . . 1
1.2 Density of States . . . 2
1.3 Mode-Locked Laser Diodes . . . 3
1.3.1 Quantum Well and Bulk Mode-Locked Lasers . . . 6
1.3.2 GaAs Based Quantum Dot Mode-Locked Lasers at 1300 nm . . . 8
1.3.3 InP based Quantum Dash/Dot Mode-Locked Lasers (QDMLLs) at 1550 nm . . . 9
1.4 Optical Injection of Semiconductor Lasers . . . 11
1.4.1 Mode-Locked Lasers . . . 12
1.4.2 Other Lasers . . . 16
1.5 Application of Mode-Locked Lasers in Optical Communication Systems 18
1.5.1 Microwave/Millimeter-Wave Generation and Transmission . . . 18
1.5.2 Optical Time/Wavelength Division Multiplexing . . . 19
1.6 Motivation For This Work . . . 21
1.7 Thesis Organisation . . . 22

**2 Basic Characterisations of Quantum-Dash Mode-Locked Lasers** **24**
2.1 Introduction . . . 24
2.2 Device Structures and Fabrication . . . 24
2.2.1 Device Structures . . . 24
2.2.2 Device Fabrication . . . 26
2.3 Measurement Techniques . . . 27
2.3.1 Light-Current (L-I) and Power Measurements . . . 27
2.3.2 Optical and RF Spectrum Measurement . . . 29
2.3.3 Optical Linewidth Measurement . . . 30
2.3.4 Time-Domain Measurement . . . 31
2.3.5 Intensity Autocorrelation Measurement . . . 32
2.4 Characterisation of Self Mode-Locked Lasers (SML) . . . 34
2.4.1 Pulse Compression in SML Devices . . . 37
2.5 Characterisation of Saturable-Absorber Mode-Locked Lasers (SAML) 43
2.5.1 21 GHz Devices . . . 43
2.5.2 52 GHz Devices . . . 47
2.6 Summary and Discussions . . . 49

**3 Optical Injection of Self-Mode-Locked Lasers (SML)** **51**
3.1 Introduction . . . 51
3.2 Experimental Arrangement . . . 51
3.3 Injection Locking: General Properties . . . 53
3.4 Dynamics of DWELL Device . . . 55
3.4.1 Analysis of Dynamics Versus Injection Parameters . . . 59
3.5 Microwave Generation in DWELL Device . . . 60

3.6 Microwave Generation in DBARR Device . . . 66
3.7 Tuning and Scaling Properties . . . 69
3.8 Comparison of DWELL and DBARR Devices . . . 74
3.9 Summary and Discussions . . . 76

**4 Optical Injection of Saturable-Absorber Dominated Mode-Locked Lasers (SAMLs) 77**
4.1 Introduction . . . 77
4.2 CW Injection . . . 77
4.2.1 Pulse Measurement and Time-Bandwidth Product Control . . 80
4.3 Dual-Mode Injection . . . 82
4.3.1 Timing Jitter Reduction . . . 84
4.3.2 Optical Linewidth . . . 87
4.4 Analysis of Repetition Rate Tuning . . . 88
4.4.1 Free Running . . . 89
4.4.2 CW Optical Injection . . . 90
4.5 Versatile Optical Frequency Comb Generation Using Dual-Mode Optical Injection . . . 92
4.5.1 Wide RF Locking-Range . . . 93
4.5.2 Optical Spectral Properties . . . 96
4.5.3 On the Scaling Properties . . . 97
4.6 Summary and Discussions . . . 98

**5 All Optical Stabilisation of Quantum Dash Mode-Locked Lasers 100**
5.1 Introduction . . . 100
5.2 Experimental Arrangement and Results . . . 103
5.2.1 Mechanism in Filtered Feedback . . . 109
5.3 Summary and Discussions . . . 110

**6 Application of Injection-Locked Mode-Locked Lasers for Phase Sensitive Amplifiers 112**
6.1 Introduction . . . 112
6.2 Basics of Phase Sensitive Amplifiers . . . 113
6.3 PSA Schemes . . . 114
6.3.1 Practical Implementation of Carrier-Extraction and Frequency Replication . . . 115
6.4 PSA Based on Injection-Locked Quantum Dash Mode-Locked Lasers . 117
6.4.1 Experimental Arrangement . . . 118
6.4.2 Analysis of Four-Wave Mixing Terms . . . 119
6.4.3 Injection-Locking Performance . . . 122
6.4.4 Phase-Sensitive Performance . . . 129
6.5 Summary and Discussions . . . 131

**7 Conclusions 133**
7.1 Introduction . . . 133
7.2 Technical Contributions . . . 133
7.3 Future Works . . . 135

I, Ehsan Sooudi, certify that this thesis is my own work and I have not obtained a degree in this university or elsewhere on the basis of the work submitted in this thesis.

*Ehsan Sooudi*

# Abstract

Mode-locked semiconductor lasers are compact pulsed sources with ultra-narrow pulse widths and high repetition-rates. In order to use these sources in real applications, their performance needs to be optimised in several aspects, usually by external control. We experimentally investigate the behaviour of recently-developed quantum-dash mode-locked lasers (QDMLLs) emitting at 1.55 $\mu$m under external optical injection. Single-section and two-section lasers with different repetition frequencies and active-region structures are studied. Particularly, we are interested in a regime which the laser remains mode-locked and the individual modes are simultaneously phase-locked to the external laser.

Injection-locked self-mode-locked lasers demonstrate tunable microwave generation at first or second harmonic of the free-running repetition frequency with sub-MHz RF linewidth. For two-section mode-locked lasers, using dual-mode optical injection (injection of two coherent CW lines), narrowing the RF linewidth close to that of the electrical source, narrowing the optical linewidths and reduction in the time-bandwidth product is achieved. Under optimised bias conditions of the slave laser, a repetition frequency tuning ratio >2% is achieved, a record for a monolithic semiconductor mode-locked laser.

In addition, we demonstrate a novel all-optical stabilisation technique for mode-locked semiconductor lasers by combination of CW optical injection and optical feedback to simultaneously improve the time-bandwidth product and timing-jitter of the laser. This scheme does not need an RF source and no optical to electrical conversion is required and thus is ideal for photonic integration.

Finally, an application of injection-locked mode-locked lasers is introduced in a multi-channel phase-sensitive amplifier (PSA). We show that with dual-mode injection-locking, simultaneous phase-synchronisation of two channels to local pump sources is realised through one injection-locking stage. An experimental proof of concept is demonstrated for two 10 Gbps phase-encoded (DPSK) channels showing more than 7 dB phase-sensitive gain and less than 1 dB penalty of the receiver sensitivity.

# List of Publications

## Journal Papers:

- **E. Sooudi**, C. de Deios, G. Huyet, J. G. McInerney, F. Lelarge, R. Rosales, K. Merghem, A. Martinez, A. Ramdane, and S. P. Hegarty, "A novel scheme for two-level stabilization of semiconductor mode-locked lasers using simultaneous optical injection and optical feedback," *IEEE Journal of Selected Topics in Quantum Electronics*, vol.19, no.4, pp.1101208,1101208, July-Aug. 2013.
- **E. Sooudi**, S. Sygletos, A. D. Ellis, G. Huyet, J. McInerney, F. Lelarge, K. Merghem, R. Rosales, A. Martinez, A. Ramdane, and S. Hegarty, "Optical frequency comb generation using dual-mode injection-locking of quantum-dash mode locked lasers: properties and applications," *IEEE Journal of Quantum Electronics*, vol. 48, no. 10, pp. 1327 –1338, Oct. 2012.
- **E. Sooudi**, G. Huyet, J. McInerney, F. Lelarge, K. Merghem, R. Rosales, A. Martinez, A. Ramdane, and S. Hegarty, "Injection-locking properties of InAs/InP-based mode-locked quantum-dash lasers at 21 GHz," *IEEE Photonics Technology Letters*, vol. 23, no. 20, pp. 1544 –1546, Oct. 2011.
- **E. Sooudi**, G. Huyet, J. McInerney, F. Lelarge, K. Merghem, A. Martinez, A. Ramdane, and S. Hegarty, "Observation of harmonic-mode-locking in a mode-locked InAs/InP-based quantum-dash laser with CW optical injection," *IEEE Photonics Technology Letters*, vol. 23, no. 9, pp. 549 –551, May 2011.

## International Conference Papers:

- **E. Sooudi**, C. de Dios, G. Huyet, J. G. McInerney, F. Lelarge, R. Rosales, K. Merghem, A. Martinez, A. Ramdane, and S. P. Hegarty, "All optical passive stabilization of a two-section InAs/InP based quantum-dash mode-locked laser with simultaneous CW injection-locking and selective optical feedback," in *Proc. Conference on Lasers and Electro-Optics (CLEO)*. Optical Society of America, 2012, p. JW2A.84.
- **E. Sooudi**, S. Sygletos, P. Frascella, A. D. Ellis, G. Huyet, J. G. McInerney, F. Lelarge, K. Merghem, R. Rosales, A. Martinez, A. Ramdane, and S. P. Hegarty, "Phase synchronization of a two-channel phase-sensitive amplifier based on optical injection-locking of InP quantum-dash mode-locked lasers," in *Proc. Optical Fiber Communication Conference (OFC)*. Optical Society of America, 2012, p. OTh1C.2.
- **E. Sooudi**, J. McInerney, G. Huyet, S. Hegarty, F. Lelarge, K. Merghem, A. Martinez, and A. Ramdane, "Dynamics of mode-locked InP based quantum dash lasers for optical communications," in *Proc. 13th International Conference on Transparent Optical Networks (ICTON 2011)*, Jun. 2011, pp. 1 –4.
- **E. Sooudi**, J. McInerney, S. Hegarty, G. Huyet, K. Merghem, A. Martinez, and A. Ramdane, "Scaling and tuning properties of microwave generation in CW injection locked InP-based mode-locked quantum dash lasers," in *Proc. IEEE Photonics Conference (PHO), (formerly known as LEOS)*, Oct. 2011, pp. 113 –114.
- **E. Sooudi**, H. N. Fernando, S. P. Hegarty, G. Huyet, J. G. McInerney, F. Lelarge,

K. Merghem, A. Martinez, and A. Ramdane, "Generation of microwave signal in a mode-locked InAs/InP based quantum dash laser with CW optical injection," in *Proc. Conference on Lasers and Electro-Optics (CLEO)*. Optical Society of America, 2010, p. CMII4.

- **E. Sooudi**, H. N. Fernando, and J. G. McInerney, "Observation of injection locking in a long-cavity InAs/InP 1.56 µm quantum dash laser," in *Proc. Frontiers in Optics (FIO)*. Optical Society of America, 2009, p. FThK6.

## National Conference Papers:

- **E. Sooudi**, S. P. Hegarty and J. G. McInerney, "Tunable microwave generation using injection-locked 1.5 $\mu$m mode-locked quantum dash lasers," in *Proc. Photonics Ireland 2011*, 2011, p. B42.
- H. N. J. Fernando, **E. Sooudi** and J. G. McInerney, "Injection-locking of long-cavity InAs/InP 1.56 $\mu$m quantum-dash laser at threshold," in *Proc. Photonics Ireland 2009*, 2009, p. B7.

*To Samane, Kian, & My Parents*

# Acknowledgements

Successful accomplishment of a PhD relies on one's capabilities but is not possible without help and support of many people. I would like to thank Prof. Erich Ippen and Prof. Nabeel Riza, my Viva examiners, for taking time to read my thesis and for valuable discussions. I thank my PhD supervisor, Prof. John G. McInerney for giving me a unique opportunity to do my PhD on semiconductor lasers at UCC and Tyndall National Institute, particularly for his support and giving freedom during the course of this work. I also thank Dr. Guillaume Huyet and Dr. Steve Hegarty for their kind support in all aspects of my PhD; particularly kindly letting me be one of their group members. Guillaume has made me feel that I have a second supervisor. I am also grateful for assistance of Prof. Jim Greer and Prof. Paul Townsend from Tyndall National Institute. Thanks to Science Foundation Ireland (SFI) and European Communities Seventh Framework Programme FP/2007-2013 under PHASORS project for financial support of this work.

Special thanks to Prof. Andrew Ellis for the generous support of my PhD for one year. Close collaboration with Andrew's team and using their facilities was a great chance to investigate this project in an application level, ending up in interesting and fruitful results.

During my PhD, I had a chance to have valuable discussions with Prof. Evgeny Viktorov on laser physics aspects of this project. I thank him for his patience to elaborate the discussions down to the level of my understanding. Many thanks to Dr. François Lelarge from III-V lab, a joint Laboratory of "Alcatel Lucent Bell Labs," "Thales Research & Technology" and "CEA-LETI" France, and Prof. Abderrahim Ramdane from LPN, CNRS, France for providing quantum-dash semiconductor laser samples. Thank you Dr. Bob Manning for the reading of one of the papers from my PhD work and interesting discussions. I also thank Dr. Stylianos Sygletos for help and technical support for the PSA experiment, Dr. Cristina De dios for a three months visit to Cork, which made it possible to work on the combined injection and feedback experiment and also Dr. Harendra Fernando for working with me in the first year of my PhD.

Many thanks to Dr. Peter O'Brien, Marc Rensing and Noreen Nudds from Advanced Packaging Group in Tyndall for their support with packaging of the lasers. Thanks to Dr. David Bitauld, Dr. Simon Osborne, and Dr. Patrycja Heinricht from Tyndall PTG for the loan of equipments. In UCC Department of Physics, thanks to all in general and in particular to Christy Roche and Robin (Bob) Gillen. A big thank you to current and former Optoelectronic Group members of Tyndall: David Goulding, Bryan Kelleher, David Williams, Shane, Jiri, Nicola, Boguslaw, Tomasz Piwonski, Tomasz Ochalski, Beatriz, Natalia, and Tanya and also to my Iranian friends and colleagues at Tyndall.

Finally, a very special thank you to my wife, my love, and my best friend, Samane, for her endless love, precious support, tolerance and encouraging for the last five years, particularly during the difficult days of my PhD.

# List of Figures


1.1 Quantum confinement and density of states. (a), (b). Bulk structure (no quantum confinement). (c), (d). Quantum confinement in one dimension (quantum-well). (e), (f). Quantum confinement in two dimensions (quantum-wire). (g), (h). Quantum confinement in three dimensions (quantum-dot). . . . . 4

1.2 The three main techniques for mode-locking in semiconductor lasers. (a). Passive mode-locking. (b). Temporal evolution of gain and absorption in the steady state. (c). Active mode-locking. (d). Temporal evolution of gain and absorption. (e). Hybrid mode-locking. . . . . 5

1.3 Colliding-pulse mode-locking (CPM) techniques. (a). CPM at second harmonic: $2f_{ML}$, [26–28]. (b). Multiple CPM at 6th harmonic: $6f_{ML}$, [29, 30]. (c). Asymmetric CPM: $mf_{ML}$, [31]. (d). Asymmetric CPM with relatively prime ratios for $m$ and $n$ ($m > n$): $mf_{ML}$, [32]. The fundamental repetition-rate of the cavity is $f_{ML}$ and $L$ is the total cavity length. . . . . 7

1.4 The diagram of InP QDMLLs for mode-locking operation based on cavity structure. . . . . 10

1.5 Basic diagram for optical injection-locking; if the light is injected unidirectionally from the Laser 1 to the Laser 2, the Laser 1 is known as master laser and the laser 2 is known as slave laser. . . . . 12

1.6 Schematic diagram of different scenarios for optical injection of mode-locked lasers. . . . . 13

1.7 Schematic diagram for coherent combining of beams from injection-locked lasers. Reproduced with permission from [118], ©(1999) Optical Society of America. . . . . 17

1.8 Schematic diagram for utilisation of mode-locked lasers for generation and transmission of microwave/millimeter wave signals. (a). Radio over fibre (RoF) microwave/millimeter-wave transmission. (b). Wireless transmission of microwave/millimeter-wave signals. (c). Millimeter-wave/THz generation. . . . . 19

1.9 Schematic diagram for OTDM system from semiconductor mode-locked lasers. . . . . 20

1.10 Schematic diagram for WDM system using semiconductor mode-locked lasers. . . . . 21

2.1 Active region structure of the devices. (a). DWELL type. (b). DBARR type. Acronyms: QD: Quantum-Dash layer, QW: Quantum-Well layer, BARR: Barrier layer. . . . . 25

2.2 Cavity structure of the devices. (a). Single-section device (SML) laser (b). Two-section device (SAML) laser. . . . . 26

2.3 Layer structures of the devices. (a). DWELL laser (b). DBARR laser. The thickness of layers are not scaled to the actual size. . . . . 28

2.4 Photo of a mounted device on a AlN submount. The electrical contacts were made using ball-type wire bonding. . . . . 29

2.5 Schematic of measurement setup for (L-I) and optical power measurement, DUT: Device Under test. . . . . 29

2.6 Schematic of measurement setup for optical and RF spectra measurement. DUT: Device Under test, ISO: Free space isolator, OSA: Optical Spectrum Analyser, ESA: Electrical (RF) Spectrum Analyser, PD: High speed Photodetector, RF Amp.: RF Amplifier. . . . . 30
2.7 Schematic of measurement setup heterodyne measurement. DUT: Device Under test, ISO: Free space isolator, OSA: Optical Spectrum Analyser, ESA: Electrical (RF) Spectrum Analyser, PD: High speed Photodetector, RF Amp.: RF Amplifier., PC: Polarization Controller, ECL: External Cavity Laser. . . . . 31
2.8 Schematic diagram of an intensity autocorrelator. BS: Beam splitter, M: Mirror. . . . . 32
2.9 Schematic of measurement setup for pulse-width using intensity autocorrelator. DUT: Device Under test, ISO: Free space isolator, PC: Polarization Controller, AC: Autocorrelator. . . . . 33
2.10 Light-Current (L-I) measurement of SML devices with different cavity length and active region structures. . . . . 34
2.11 RF linewidth of repetition-rate for SML devices of different cavity lengths and active layer structures for excess currents above threshold $(I - I_{th})$. . . . . 35
2.12 Zoom of measured RF linewidth of the repetition-rate frequency for SML devices (red-line) and Lorentzian fit (blue-line). (a). 4 mm single-section DWELL (10.5 GHz), $I = 220$ mA. Resolution bandwidth: 10 kHz, Video bandwidth: 0.1 kHz. (b). 2 mm, two-section DBARR (21 GHz), $I = 155$ mA, absorber: open. Resolution bandwidth: 10 kHz, Video bandwidth: 1 kHz. $\Delta\nu$: Full-width at half maximum (FWHM) of RF linewidth. . . . . 36
2.13 Examples of optical spectra for SML devices with DWELL and DBARR strcutures. (a). 4 mm single-section DWELL (10.5 GHz), $I = 300$ mA. (b). 2 mm single-section DWELL (21 GHz), $I = 252.4$ mA. (c). 2 mm two-section DBARR with 2% absorber (21 GHz), $I = 190.4$ mA, absorber: float. . . . . 37
2.14 Measured autocorrelation trace for SML devices with different cavity length and active region. Devices: DWELL, 4 mm, $I = 300$ mA. DWELL, 2 mm, $I = 300$ mA. DBARR, 2 mm, $I = 120$ mA, absorber (2.0%): float. DBARR, 0.8 mm, $I = 120$ mA, absorber (14.8%): float. 38
2.15 Schematic of measurement arrangement for pulse compression of SML device using filter. Acronyms: BPF: Band-pass filter. . . . . 38
2.16 (a). Optical spectra of the 21 GHz laser without filtering (black) and filtered (colored) at different center wavelengths shown by $\lambda_1$ to $\lambda_7$. (b). Autocorrelation traces of pulses using the whole spectrum (black) and filtered at $\lambda_5$ (1559.75 nm). (c). Dependence of the pulse duration with filtered spectrum on the center wavelength of the filter. Inset shows three consecutive pulses from the autocorrelator. . . . . 39
2.17 (a). Optical spectra of the 10.5 GHz laser without filtering (black) and filtered (colored) at different center wavelengths shown by $\lambda_1 - \lambda_3$. (b). Autocorrelation traces of pulses using the whole spectrum (black) and filtered at $\lambda_2$ (1564.54 nm). (c). Dependence of the pulse duration of filtered spectrum on the center wavelength of the filter. Inset shows single captured pulse from the autocorrelator. . . . . 40

2.18 Schematic of experimental arrangement for pulse compression of SML device using single-mode fibre with variable length. . . . . 41
2.19 Autocorrelation traces for the 2 mm long DBARR, (absorber, 2%: floating), $I$ =125 mA, fibre length varied from 20 to 200 m. . . . . 41
2.20 Autocorrelation traces for the 2 mm long DBARR, (absorber, 2%: floating), with fibre length of 200 m. Bias current varied from 100-200 mA. 42
2.21 Gaussian fit (blue curve) to the measured autocorrelation trace (red curve) for the 2 mm long DBARR, (absorber, 2%: floating), with fibre length of 200 m. Bias current: 150 mA. The pulse duration after deconvolution was 0.65 ps. . . . . 43
2.22 Light-Current (L-I) measurement of I3-4 for different values of absorber bias voltage. Regimes of SML and SAML operation are shown in the curves. . . . . 44
2.23 Dependence of the pulse-width (Gaussian fit, left Y axis) and RF linewidth (Lorentzian fit, right Y axis) on the gain current for two absorber voltages. Device: I3-4. . . . . 44
2.24 Dependence of the pulse-width (Gaussian fit, left Y axis) and TBP (right Y axis) on the bias parameters the same as Fig. 2.23. Device: I3-4. 45
2.25 RF spectra of the mode-locked beat frequency (repetition-rate) of for different gain currents and $V_{Abs}$ = 0.2 V (Device: I3-4). . . . . 46
2.26 RF linewidth of the repetition-rate frequency (red curve) with its Lorentzian fit (blue curve). Device: I3-4, $I_{Gain}$ = 180 mA, $V_{Abs}$ = 0.2 V. . . . . 46
2.27 Dependence of the pulse-width (Gaussian fit, left Y axis) and TBP (right Y axis) on the bias parameters the same as Fig. 2.23 ($V_{Abs}$ = 0.2 V). Device: I3-4. . . . . 47
2.28 Dependence of the pulse-width (Gaussian fit, left Y axis) and TBP (right Y axis) on the bias parameters the same as Fig. 2.23 ($V_{Abs}$ = 0.2 V). Device: I3-4. . . . . 47
2.29 Measurement of pulsewidth for 52 GHz SAML device. (a). Measured pulsewidth versus gain current for different absorber voltages. (b). Single pulse captured with its $Sech^2$ fit, the inset shows the autocorrelation trace of seven consecutive pulses. . . . . 48
2.30 Dependence of the pulse-width (Gaussian fit, left Y axis) and TBP (right Y axis) on the absorber bias voltage for a fixed gain current (140 mA). Device: G4-3. . . . . 49

3.1 Schematic diagram of CW injection experiment for SML device. List of acronyms: Att.: Variable Optical Attenuator, PC: Polarization Controller, PWM: Optical Power Meter, QDML: Quantum-Dash Mode-Locked, ISO: Isolator, OSA: Optical Spectrum Analyzer, PD: Photodetector, RF Amp.: RF Amplifier, ESA: Electrical Spectrum Analyzer, OSC: Digital Sampling Oscilloscope. . . . . 52
3.2 Optical spectrum of slave laser at the unlocked (blue-dashed) and locked (red-solid) states. The injected power is ≈257 $\mu$W (Injection ratio ≈36.7%). . . . . 54
3.3 RF spectrum of the slave laser under stable locking with the same injection parameters as Fig. 3.2. The feature around 2.5 GHz corresponds to the noise of the ESA. . . . . 54

3.4 Optical linewidth measurement. (a). Slave laser linewidth free running (dashed line/blue) and stable-locked (solid-line/red) (b). Slave laser linewidth at stable-locked region (solid-line/red) with Master laser linewidth (dashed-line/blue). . . . . 55
3.5 Measured RF spectra of the slave laser in the unlocked region. The beating (mixing) tone between master and slave and subsequent generated mixing tones between the master and adjacent modes can be distinguished. The repetition rate and its second harmonic are also denoted by arrows. . . . . 56
3.6 (a). Measured time-trace of the slave laser in the period-one region. (b). Calculated RF spectrum. . . . . 56
3.7 (a). Measured time-trace of the slave laser in the period-two region. (b). Calculated RF spectrum. . . . . 57
3.8 (a). The measured time-trace of the slave laser at period-four region. (b). Calculated RF spectrum. . . . . 57
3.9 (a) Measured time-trace of the slave laser in the chaotic oscillation. (b) Calculated RF spectrum. . . . . 58
3.10 Optical spectrum of the slave laser in the microwave oscillation region. (a)Zoom of the spectrum. The injected mode is denoted in the figure; the excited mode is spaced at twice of mode-locked frequency. (b) Wider span of the spectrum. The injected mode is denoted by an arrow. . . 58
3.11 Heterodyne measurements of the optical linewidth of the injected mode at the microwave oscillation (solid-line/blue) and stable-locked (solid-line/red) regions. The optical line-shape of the master (solid-line/black) is also shown for comparison. . . . . 59
3.12 The intensity graph for dynamics at injection level of ≈28%. The dynamics are as follows: 1: Unlocked, 2: Period-One, 3: Period-Two, 4: Period-Four, 5: Period-Two, 6: Period-Four, 7: Period-Two, 8: Period-One, 9: Chaos. . . . . 60
3.13 Optical spectrum of the slave laser in microwave oscillation region. (a). Optical spectrum versus changing the current. The injected mode is denoted by an arrow. (b). Zoom of the optical spectrum of the slave laser when free running (blue-dashed) and MWO regime (red-solid). The Gaussian fit of the envelope is shown in green-dotted curve. Bias current was $1.6I_{th}$ and injection ratio 3%. The injected mode is 0. . . . . 61
3.14 RF spectrum of free running (dashed-line/blue) and injection (solid-line/red) corresponding to the optical spectrum of Fig. 3.13(b). . . . . 62
3.15 Measured optical linewidths of individual modes when free running (blue-diamonds) and injected, MWO (red-circles) for three wavelengths of injection shown by arrows. The free running optical spectrum in linear scale is shown on the right axis. . . . . 63
3.16 (a). 50 MHz span of the microwave tone (injected, red curve) and second harmonic of mode-locked tone (free running, black curve). Resolution band-width (RBW) was 300 kHz and video band-width (VBW) wass 30 kHz. The blue curve shows the Lorentzian fit of the microwave tone. (b). Autocorrelation trace of the laser under MWO region (solid-curve/red) and free running (solid-curve/blue). . . . . 64

3.17 Spectral tunability in the MWO regime. The dashed curve is the optical spectrum of the slave laser when free running ($1.6I_{th}$). The arrows show the location of the optical injection. . . . . 65
3.18 2D operational map of dynamics at $1.6I_{th}$. The symbol definitions are as follows: MWO: Microwave oscillation, MWO+RO: Narrow tone MWO with undamped RO. P2: Period doubling oscillation. URO: Undamped RO only. Inc MWO: Incomplete MWO (refer to the text). P1: Period one oscillation. SL: Stable locking or phase locked with single-mode operation. . . . . 65
3.19 (a). RF spectrum of MWO + RO region (solid-line/red curve). The RF spectrum of MWO is also shown for comparison (dashed-line/blue curve). (b). Optical spectrum of MWO + RO region (solid-line/red curve). The optical spectrum of MWO is also shown in dashed-line/blue. The arrow denotes the location of injection; the OSA resolution bandwidth for both cases was at the minimum (0.01 nm). . . . . 66
3.20 (a). Optical spectrum of the DBARR SML (I3-1, $I = 85$ mA, Absorber: 2.0%, floating), injection ratio≈7%) at free running (dashed-line/blue) and locked (solid-line/red). (b). Corresponding RF spectrum; free running (dashed-line/blue) and locked (solid-line/red). . . . . 67
3.21 Autocorrelation trace of SML DBARR device, CW injection-locked (solid-line, red) and free running (solid-line, blue), injection ratio ≈16.6%. 68
3.22 Optical locking range of CW injection for SML 21 GHz DBARR device (I3-1, 85 mA) versus injection power ratio. . . . . 69
3.23 RF tuning of generated microwave signal for DBARR SML device at 21 GHz (filled triangles) and DWELL SML at 10.5 GHz ($A_1$, filled squares). The bias current for DBARR and DWELL devices were 85 mA and 250 mA, respectively ($1.6I_{th}$). . . . . 70
3.24 RF tuning of generated microwave frequency within the locking range (red) and second harmonic of repetition rate when free running (blue). 70
3.25 RF tuning range as wide as 700 MHz for injection-locked DBARR SMLL with injection ratio ≈13.6%. The frequency of the injection-locked laser decreased while the frequency detuning between the master and slave was increased. The free running RF frequency is shown in blue curve. 71
3.26 The optical spectrum of the injection-locked slave laser (injection ratio 13.6%) at selected points in the locking range. The generated frequency is shown for each spectrum and injection wavelength denoted by arrow. The spcetra were offset for clear view. . . . . 71
3.27 Optical spectra of CW injection-locked 52 GHz DBARR SML (solid-line/red, bias current of 120 mA, $2.3I_{th}$) and injection-locked (solid-line/blue) 21 GHz device with the same active region. The arrows denote the wavelength of injection. . . . . 72
3.28 Intensity graph of heterodyne beat notes measured automatically while the master laser was sweeping for a few of modes around injection wavelength for 52 GHz DBARR device. (a). The mode adjacent to the injected mode on the blue side ($M_{-1}$). (b). Second mode after injection on the red side ($M_2$). (c). Third mode after injection on red side ($M_3$). 73

3.29 Comparison of dynamics of DWELL and DBARR devices under CW optical injection. (a). Intensity graph of RF spectra for DWELL SML (B3, $I$ =120 mA, $1.4I_{th}$), injection ratio≈ 9%. (b). Intensity graph of RF spectra for DBARR SML (I3-1, $I$ =85 mA, $2I_{th}$ Absorber: 2.0%, floating) , injection ratio≈ 9%. . . . . 75

4.1 Schematic diagram of CW injection experiment for SAML device. List of acronyms: AC: Autocorrelator, Att.: Variable Optical Attenuator, PC: Polarization Controller, QDML: Quantum-Dash Mode-Locked, ISO: Isolator, OSA: Optical Spectrum Analyser, PD: Photodetector, RF Amp.: RF Amplifier, ESA: Electrical Spectrum Analyser, OSC: Digital Oscilloscope, ECL: External Cavity Laser. . . . . 78

4.2 (a) Optical spectrum of the SAML laser (I3-3, Absorber: 6.9%, $I$ =110 mA, $V_{Abs}$ =0.0 V), injection ratio ≈2%) free running (dashed-line/blue) and locked (solid-line/red). The injected mode is denoted by an arrow. (b). RF spectrum corresponding to Fig. 4.2(a), free running (dashed-line/blue) and locked (solid-line/red). . . . . 79

4.3 Autocorrelation traces of a single pulse for SAML laser (I3-3, Absorber: 6.9%, $I$ =110 mA, $V_{Abs}$ =0.0 V) free running (dotted-line/blue), CW injection-locked (solid-line/red), and their Gaussian (solid-line/blue) and $\text{Sech}^2$ fit (solid-line/black) with the same injection power as Fig. 4.2. The inset shows the time trace of three consecutive injection-locked pulses. 80

4.4 Flowchart for calculation of transform limited pulse and autocorrelation trace from the captured optical spectrum for exact time-bandwidth product calculation. . . . . 81

4.5 Measured pulsewidth (left axis) and calculated time-bandwidth product (right axis) for CW injection-locked SAML (I3-4, Absorber: 9.4%, $I$ =160 mA, $V_{Abs}$ =0.1 V) versus master laser wavelength change within the locking range for different injection powers. . . . . 82

4.6 (a). Optical spectra of slave SAML laser (I3-4, $I$ =160 mA, Absorber: 9.4%, $V_{abs}$ =0.1 V) for two master-slave detunings around the boundaries inside the locking range, injection ratio ≈0.8%. The spectra were offset for better viewing. (b). Corresponding autocorrelation traces with their $\text{Sech}^2$ fit; the traces were offset for better viewing. . . . . 83

4.7 Schematic diagram of dual-mode injection experiment for SAML device. List of acronyms: AC: Autocorrelator, Att.: Variable Optical Attenuator, PC: Polarization Controller, QDML: Quantum-Dash Mode-Locked, ISO: Isolator, OSA: Optical Spectrum Analyser, PD: Photodetector, RF Amp.: RF Amplifier, ESA: Electrical Spectrum Analyser, OSC: Digital Oscilloscope, ECL: External Cavity Laser. . . . . 84

4.8 (a). RF spectrum of free running SAML laser (I3-4, $I$ =160 mA, Absorber: 9.4%, $V_{abs}$ =0.1 V), solid-line/blue and dual-mode injection, solid-line/red. (b). Zoom of the RF spectra for free-running and dual-mode injection with the peak frequency shifted to zero. Resolution bandwidths for free running and dual-mode injection were 100 kHz and 1 kHz (instrument limit), respectively. . . . . 85

4.9 The measured SSB noise spectra for free-running (solid-line/blue), CW injection (solid-line/green) and dual-mode injection (solid-line/red) for SAML laser (I3-4, $I$ =160 mA, Absorber: 9.4%, $V_{abs}$ =0.1 V). . . . . 86

4.10 (a). Heterodyne beat note of several modes at different locations of the OFC (solid-lines) along with free running (dashed-line/blue) 20th mode away from second injected mode. The modes are denoted based on their relative modal distance from injected modes; mode with negative indice located at the blue side of injection. (b). Zoom (30 MHz span) of the normalised RF beat note for the mode (solid-line/red) and one of the master's modulated side bands (dashed-line/black), injected power ratio ≈3%. . . . . 87
4.11 Optical spectra of two-section QDMLLs in free running operation. (a) I3-4, Gain current: 160 mA, Absorber voltage: 0.1 V and Gain current: 200 mA, Absorber voltage: -0.5 V. (b) I3-3, Gain current: 110 mA, Absorber voltage: 0.0 V and Gain current: 135 mA, Absorber voltage: -1.0 V. . . . . 88
4.12 Autocorrelation measurement of two-section QDMLLs in free running operation. (a) I3-4 corresponding to Fig. 4.11(a). (b) I3-3 corresponding to Fig. 4.11(b). . . . . 88
4.13 Free-running repetition rate of I3-4 for different bias parameters. (a) Absorber voltages: 0.2 V and -0.5 V, mount temperature: 20.0 $^{o}$C, gain current ranging from 130 to 210 mA. (b) Absorber voltages: 0.1 V and -0.5 V, gain current: 160 mA and mount temperature 15-23.5 $^{o}$C. . . . 90
4.14 Optical locking-range (left axis) at positive absorber voltage (full circles) and negative absorber voltage (full triangles) and repetition rate tuning (right axis) at positive absorber voltage (empty circles), and negative absorber voltage (empty triangles) versus injected power ratio. The bias parameters are the same as in Fig 4.11(a). . . . . 91
4.15 Repetition rate within the locking-range as a function of master laser frequency change for positive absorber voltage (circles, injected power ratio ≈1.1%) and negative absorber voltage (triangles, injected power ratio ≈1.2%). Bias parameters were the same as Fig. 4.14. . . . . 92
4.16 Intensity graphs for the RF spectrum under dual-mode injection with negative absorber voltage, injected power ratio ≈2.1%, the locking regions denoted by arrows (resolution bandwidth: 100 kHz). (a) Master laser wavelength: $\lambda_m$. (b) Master laser wavelength: $\lambda_m$ + 0.015 nm (1.85 GHz). (c) Master laser wavelength: $\lambda_m$ + 0.024 nm (2.90 GHz). (d) Master laser wavelength: $\lambda_m$ + 0.028 nm (3.45 GHz). . . . . 94
4.17 RF locking-range for dual-mode injection versus injected power for positive absorber voltage (blue marks) for I3-3 (6.9% absorber, square), I3-4 (9.4%, diamond), and I3-5 (11.9%, circle). The negative absorber voltage (red triangle) was demonstrated for I3-4 with the same bias parameters as Fig. 4.12(a). . . . . 94
4.18 (a) Repetition rate coverage of dual-mode injection versus injected power for positive absorber voltage (region surrounded by filled triangles) and negative absorber voltage (region surrounded by filled circles) and same bias parameters as Fig. 4.12 for I3-4. (b). Demonstration of wide (≈ 440 MHz) repetition rate tuning by combining the locking-ranges for negative and positive absorber voltages. The RF spectrum of the free-running mode-locked laser is shown for comparison. . . . . 95

4.19 Comb pulse-width (filled marks, left axis) and number of comb lines within 10 dB spectral width (empty marks, right axis) versus repetition rate of injection-locked laser ($f_{rep}$) for injection ratios of ≈2.9% and ≈4.6%). . . . . 96
4.20 Optical spectra of OFC for injection ratio of ≈4.6% at selected frequencies with the step of 60 MHz corresponding to Fig. 4.19. (a) $f_{rep}$ = 21.09 GHz. (b) $f_{rep}$ = 21.15 GHz. (c) $f_{rep}$ = 21.21 GHz. (d) $f_{rep}$ = 21.27 GHz. (e) $f_{rep}$ = 21.33 GHz. (f) $f_{rep}$ = 21.39 GHz. The arrows denote the spectral location of injected dual-modes. . . . . 97
4.21 Autocorrelation traces (blue/solid-lines) along with $Sech^2$ fit (red/dashed-line) and transform limited autocorrelation traces (black/dashed-dot line) corresponding to the optical spectra in Fig. 4.20. $\Delta\tau$: Actual pulsewidth after deconvolution, $\Delta\nu$: Spectral width (Hz). . . . . 98

5.1 The basic diagram of the proposed scheme for stabilisation of semiconductor mode-locked lasers. . . . . 102
5.2 Schematic of the experimental arrangement for simultaneous optical injection and feedback. A: Optical injection monitor point. B: Optical feedback monitor point. Acronyms: AC: Autocorrelator, Att.: Attenuator, ECL: External cavity laser, ESA: Electrical spectrum analyser, ISO: Isolator, OSA: Optical spectrum analyser, PC: Polarisation controller. 103
5.3 (a) Optical spectra of QDMLL when free-running ($I_{Gain}$ = 320 mA, $V_{Abs.}$ = -0.06 V). (b) Autocorrelation trace (solid-line, blue) with Gaussian fit (dashed-line, red) of QDMLL when free-running. (c) Optical spectrum of QDMLL under CW optical injection (injection strength ≈ -13.7 dB). (d) Autocorrelation trace (solid-line, blue) with Gaussian fit (dashed-line, red) of QDMLL under CW optical injection. (e) Optical spectrum of QDMLL under optical feedback (feedback strength ≈ -22.8 dB). (f) Autocorrelation trace (solid-line, blue) with Gaussian fit (dashed-line, red) of QDMLL with optical feedback (g) Optical spectrum of QDMLL under optical injection and optical feedback (-22.8 dB). The filtered spectrum used to re-inject to the laser was denoted by arrow. (h) Autocorrelation trace (solid-line, blue) with Gaussian fit (dashed-line, red) of QDMLL with optical injection and optical feedback. . . . 105
5.4 RF spectra of the mode-locked laser when free-running (dashed curve) and optical feedback only (solid curve), CW optical injection only (dashed curve) and both with CW optical injection and optical feedback (solid curve). Each case was denoted by an arrow. . . . . 106
5.5 Minimum RF linewidth of the injection-locked QDMLL with additional optical feedback loop using SMF with different lengths. . . . . 107
5.6 SSB phase noise spectra for the laser when free-running (with its Lorentzian fit) and CW optical injection only and optical injection + feedback for minimum and maximum length of the external cavity. . . 108
5.7 The modal (optical) linewidth of the injection-locked laser (left axis) and their associated coherence length (right axis) versus modal index (relative distance from the injected mode). . . . . 109

6.1 Comparison of a phase-sensitive amplifier (PSA) and phase-insensitive amplifier (PIA) in terms of phase diagram. (a) Phase-insensitive amplifier. (b) A PSA. . . . . 113

6.2 Block diagram of a different PSA schemes experimentally realised [191]. 114
6.3 Schematic diagram of PSA with different schemes. (a) Degenerate PSA with pump at the same frequency of the signal in a nonlinear loop mirror. (b) Non degenerate PSA with single pump. (c) Degenerate PSA with two pumps (dual-pump) [191]. . . . . 115
6.4 (a) Carrier extraction using FWM in a nonlinear medium. The signal is depicted in green with frequency $\omega_S$ and the pump in blue with frequency $\omega_P$ (b) Phase diagram of a binary phase encoded signal (DPSK). . . . 116
6.5 Schematic diagram of a multi pump black-box PSA based on conventional injection-locking scheme. . . . . 117
6.6 Schematic diagram of a multi pump black-box PSA based on injection-locking of quantum-dash mode-locked laser. . . . . 118
6.7 Experimental arrangement for two-channel DPSK PSA based on QDML phase synchronisation. List of acronyms used: MZM: Mach-Zehnder Modulator, PC: Polarisation Controller, SMF: Single-Mode Fibre, Att. Variable Optical Attenuator, HNLF: Highly Nonlinear Fibre, PZT: Piezo-Electric Transducer, PD: Photodetector, QDML: Quantum-Dash Mode-Locked Laser, WSS: Wavelength Selective Switch, RX: Receiver. 119
6.8 Optical spectrum of the HNLF output for carrier extraction process. The arrows denote the two DPSK channels (Ch.1, Ch.2), the local pump (P1), and the pumps generated through FWM process. . . . . 120
6.9 Comparison of the optical spectra for the extracted carriers (after filtering) through FWM of local pump and two de-correlated DPSK channels (red curve) and original CW lines(blue curve). Broadening clearly seen in the spectrum of extracted carriers are denoted by arrows. . . . . 120
6.10 Comparison of the optical spectra for the extracted carriers through FWM of local pump and two de-correlated DPSK channels at 20 GHz spacing (blue curve) and 40 GHz spacing (red curve). Note that the spacing of carriers generated through FWM is twice of that of channels. Extra broadening of FWM carriers with larger channel spacing is denoted by an arrow. . . . . 121
6.11 Optical spectra for the extracted carriers with channels at 40 GHz spacing with correlated (blue curve) and de-correlated cases (red curve). . 122
6.12 RF spectrum of the slave laser when free-running (blue curve) and under optical injection to the FWM generated carriers (red curve), offset to the peak frequency. The modulated channels where de-correlated channels at 40 GHz spacing with two independent RF sources for comb generation and phase modulation. The resolution bandwidth for free-running and injection-locked was 10 kHz, and 3 kHz, respectively. . . . . 123
6.13 Optical spectrum of the slave laser under optical injection to the FWM generated carriers (blue curve), and spectral position of programmable filter (WSS) for each case. Case 1: Dotted black rectangle, Case 2: Dotted red rectangle, Case 3: Green dashed rectangle. The injected modes are denoted by arrows. . . . . 124
6.14 RF linewidth of mode beating around each injected mode (red curve) along with its Lorentzian fit (blue curve) corresponding to spectral filtering cases in Fig. 6.13. (a). Case 1. (b). Case 2. (c) Case 3. Resolution bandwidth for all the cases was 3 kHz, $\Delta\nu$: RF linewidth. . . . . 124

6.15 RF spectra of the slave laser (SAML) under optical injection for three scenarios. Case A (blue curve): Independent clocks (RF sources) with de-correlated channels. Case B (green curve): Same (synchronised) clocks with de-correlated channels. Case C (red curve): Same (synchronised) clocks with correlated channels. The RF frequency of injection-locked laser was the same for all the cases and the traces were offset for better viewing. The resolution bandwidth was 3 kHz for case A and 1 kHz for case B and case C. . . . . 125
6.16 RF spectra of the the injected signal (blue curve, FWM carriers) and injection-locked laser (red curve). The modulated channels were de-correlated and same clock was utilised for comb generation and modulation (case B). . . . . 126
6.17 RF spectrum of free running (dashed-line/blue) and injection-locked SML (solid-line/red), the inset shows a zoom of the RF tone with 80 Hz span and RBW of 1 Hz. the 20 dB linewidth is $\approx$ 3 Hz. The FWM carriers were generated through case B scenario. . . . . 127
6.18 Comparison of optical spectra for SML and SAML lasers under optical injection to the extracted carriers. The FWM carriers were generated through case B scenario: same (synchronised) clocks with de-correlated channels. The arrows denote the location of injection. . . . . 128
6.19 (a) Optical spectrum of PSA input, after removing un-wanted components using WSS, the spectrum of OFC from QDMLL is depicted in dashed curve. (b) The zoom of the optical spectrum at the PSA output around channels for maximum (dashed line-red) and minimum (solid-line/blue) gain. . . . . 129
6.20 (a). BER measurements of both channels versus total received power. (b). Error free eye diagrams for both channels at the input and output of the PSA. . . . . 130

# List of Tables

2.1 Details of devices used in this work. For the two-section devices, the absorber length ratio (in percentage) is shown. Acronyms: Rep. Rate: Repetition Rate ($f_{ML} = \frac{c}{2nL}$, where $n$ is the refractive index of the cavity and $L$ is the cavity length). . . . . 26

5.1 Comparison of different techniques for stabilisation of mode-locked lasers based on external control. . . . . 101

6.1 Injection-locking performance versus different configurations for clock (RF) source and channel correlation/de-correlation. Channel spacing was 40 GHz for all the cases. . . . . 125

# Chapter 1

# Introduction

Invention and development of semiconductor lasers can be regarded as one of the major breakthroughs in the science and technology of the 20th century. Semiconductor lasers can be found in many everyday applications such as bar code readers, CD and DVD players, laser pointers, laser printers and so on. Without semiconductor lasers, optical fibre communication systems could not exist in their current form. Semiconductor lasers also have wide applications in many other fields such as defence, security, metrology, medical systems, and many other emerging areas. While the available market has been mostly in the form of individual device modules or arrays of devices until few years ago, semiconductor lasers have been also realised in the form of Photonic Integrated Circuits (PICs). PICs can be regarded as the *optical* equivalent of ICs with an integration scale with 10s-100s of active or passive components fabricated on the same chip.

While the technology and physics of these devices is established and understood in many aspects, open problems exist in many areas, mainly drived by emerging or potential applications. In this chapter, a basic overview of semiconductor lasers, particularly pulsed mode-locked sources, is presented with essential discussions on the state of the art relevant to the work carried out in this thesis.

## 1.1 Brief History of Semiconductor Lasers

The first experimental demonstration of a semiconductor laser was reported almost simultaneously (September-November 1962) by four different groups, IBM, GE Schenectady, GE Syracuse, and MIT Lincoln Lab [1]. The structures were based on a p-n junction based on GaAs of GaAsP material with optical feedback to enable lasing operation through stimulated emission. It should be mentioned that the possibility of stimulated emission in semiconductor material, electrical injection of minority carriers through p-n junctions of possible materials and the need for an optical resonator were predicted and suggested in published or unpublished communications as well as patents

before these experimental reports [2]. The main drive towards making lasers from GaAs and GaAsP semiconductor compounds was attributed to the frequent reports on efficient electroluminescence observed from those material systems (For a full history see [2] and references therein).

The first report of laser diodes involved high amount of threshold current densities with very low efficiencies in pulsed current mode at very low temperatures. The two main obstacles were poor carrier confinement and also very high optical losses. An important contribution that resulted in significant improvement of the electrical and optical efficiency was the invention of double-heterostructure (DH) laser by Kroemer [3]. In this solution, he suggested using surrounding barrier layers with higher band-gap energy than that of the active region. This causes the injected carriers to be trapped inside the active region and leads to higher carrier injection efficiency. In addition, the surrounding semiconductor layer with wider band-gap results in lower absorption of light, reducing the optical losses significantly. This important discovery in semiconductor laser development history which resulted in a Nobel prize in Physics in 2000. Later, Alferov (Nobel prize winner jointly with Herbert Kroemer and Jack S. Kilby in 2000) et al. and another group at Bell Labs demonstrated the lasing of GaAs DH laser with CW operation at room temperature, showing a reduction of threshold current density by more than one order of magnitude from the initial demonstrations $\sim 10^4$ A/cm$^2$. The DH structure was further optimised to give confinement of the optical field by adding surrounding layers and by deliberate design of thickness and refractive index of the layers.

In the four decades since, remarkable breakthroughs have been demonstrated, towards optimisation and development of semiconductor lasers in all aspects including the optical and electrical confinement, the quantum-well active region, the extension of the emission wavelength towards long wavelengths suitable for telecommunications and visible ranges, vertical-cavity surface-emitting lasers (VCSELs), distributed feedback (DFB) or Bragg-grating lasers (DBR), quantum dot lasers, and quantum cascade lasers. For a review, see papers by Coleman [4] and other papers in this journal's special issue [5] and [6] and references therein.

## 1.2 Density of States

As mentioned in § 1.1, the introduction of electronic and optical confinement of carriers played a key role in the development of semiconductor lasers. In this section, we briefly introduce another breakthrough in this area by introducing the quantum confinement of carriers with reduced dimensionality in structures.

The energy states that carriers can occupy depends on many factors such as band gap, applied electric field, and quantum confinement effects. A useful term, indicating the

number of allowed states per material unit volume and unit energy is the Density of States (DoS) [7]. It can be shown that DoS (shown as $N(E)$ in this text) for a bulk structure is proportional to $E^{\frac{1}{2}}$:

$$N(E) \propto E^{\frac{1}{2}} \tag{1.1}$$

The diagram of a 3D semiconductor structure with its corresponding DoS is shown in Fig. 1.1(a),(b), respectively. Reducing the dimensionality from 3D (no quantum confinement) to 2D (quantum-well), by reducing the size of structure lower than the de Broglie wavelength (few 10s of nm for III-V compound semiconductors) [8] leads to reduced of DoS as shown in Fig. 1.1(c),(d), in the form of a Heavyside function [9]. The main advantages of quantum well structures as active regions for semiconductor lasers are higher differential gain, lower threshold current density, wavelength tunability (by engineering the parameters) and faster dynamic properties [6, 10]. The next level of quantum confinement is to reduce the size of the structure in two dimensions (quantum-wire) as shown in Fig. 1.1(e). The corresponding DoS will be more quantised compared to the quantum-well case. The maximum quantum confinement will occur when the structure has reduced size in all three dimensions, known as quantum-dots (Fig. 1.1(g)). The DoS for a quantum-dot structure is reduced to a delta function, indicating that the carriers can only occupy single state (or sub-band), as shown in Fig. 1.1(h).

In quantum-dots, the limited number of available states directly leads to rapid filling of the states, by carrier injection, resulting in lower carrier density required to achieve transparency. This in turn can result in lower threshold current density in devices and higher optical material gain [8].

## 1.3 Mode-Locked Laser Diodes

Semiconductor mode-locked lasers are pulsed compact sources with simple, efficient, robust and reliable performance. Electrical injection with a very short cavity ($\sim$ 0.1-1 mm) have given the capabilities for ultra-high speed ($\sim$ 1-100 GHz) operation with low power consumption. The first demonstrations of a semiconductor based mode-locked lasers were the external cavity schemes where an external reflector was used to form the second mirror in late 70's by MIT group [11] and early 80's by others (see [12, 13] and references therein for a review). Since then, significant improvement in terms of pulsation performance (pulse-width, time-bandwidth product) or timing (jitter, RF linewidth), repetition rate, spectral width have been demonstrated. These were achieved through advancement in the active region and/or optimisations in the cavity structure.

Mode-locking in semiconductor lasers can be implemented by three basic techniques: passive-mode-locking, active mode-locking and hybrid mode-locking [14]. In all these techniques, the phase of the longitudinal modes are forced to become locked together.

This is in contrast to a Fabry-Pérot cavity without mode-locking mechanism, where the relative phase of the modes fluctuate randomly. The basic schematics of these three methods are shown in Fig. 1.2(a-e). In the passive mode-locking (Fig. 1.2(a)) the laser cavity consists of a gain section, a saturable-absorber section and mirrors to enable lasing which can be implemented in a monolithic arrangement in a semiconductor laser, as shown in Fig. 1.2(a). After a few hundreds of round-trips, the pulses are generated in a steady state by temporal interaction of gain and absorber dynamics of the laser where the absorber is saturated faster than gain, and recovers before the gain recovery,

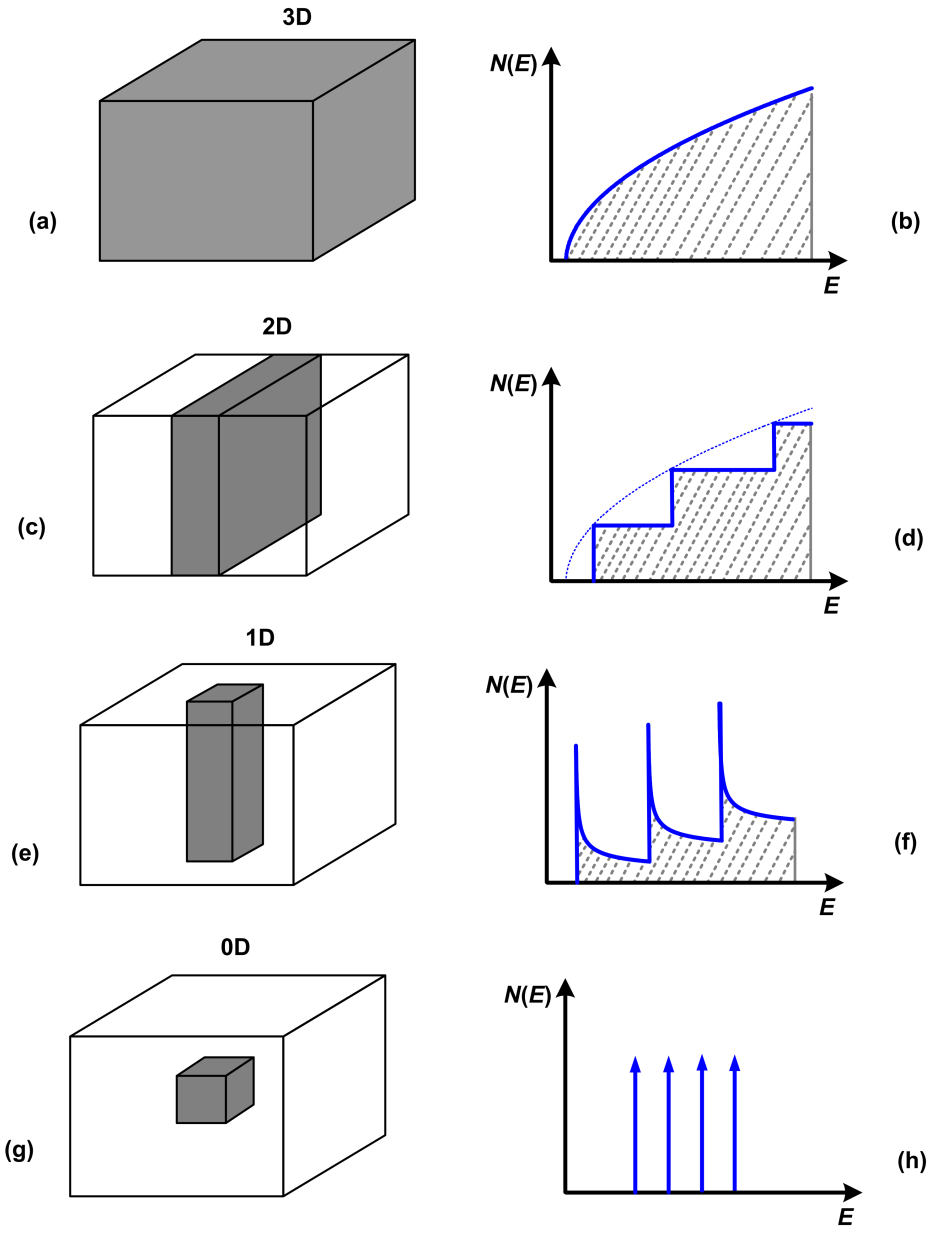



Figure 1.1: Quantum confinement and density of states. (a), (b). Bulk structure (no quantum confinement). (c), (d). Quantum confinement in one dimension (quantum-well). (e), (f). Quantum confinement in two dimensions (quantum-wire). (g), (h). Quantum confinement in three dimensions (quantum-dot).

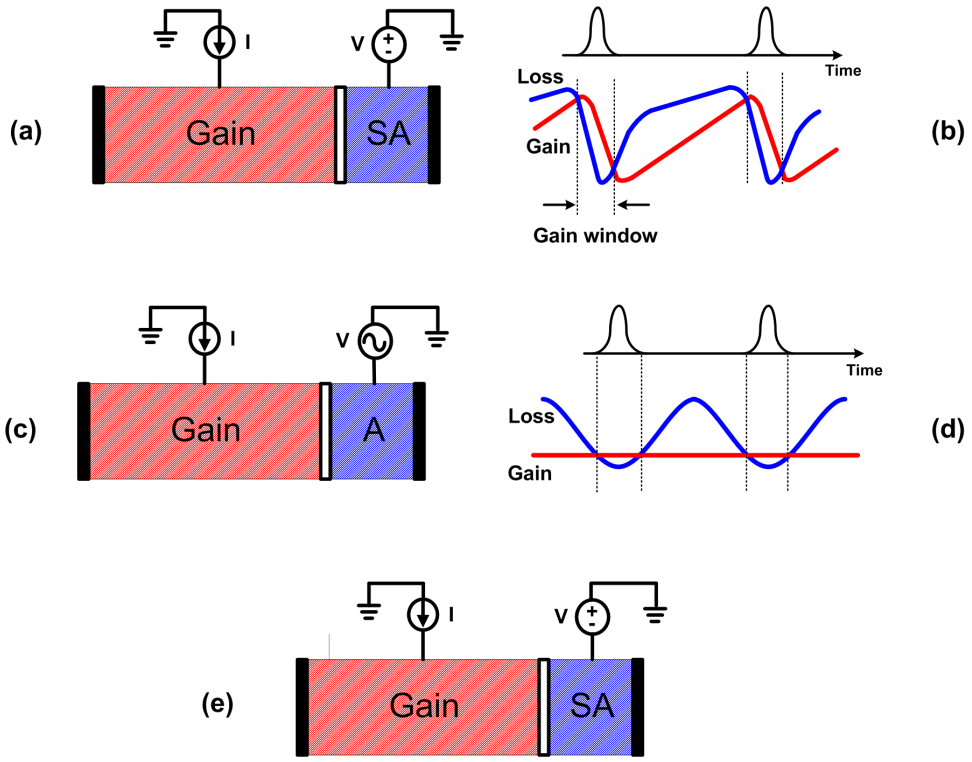



Figure 1.2: The three main techniques for mode-locking in semiconductor lasers. (a). Passive mode-locking. (b). Temporal evolution of gain and absorption in the steady state. (c). Active mode-locking. (d). Temporal evolution of gain and absorption. (e). Hybrid mode-locking.

enabling a positive net gain window which allows the pulses to generate and propagate in the cavity (shown in Fig. 1.2(b)). In this self-starting process, the repetition-rate of the pulses correspond to the round-trip time of the cavity. In passive mode-locking, the gain and absorber temporal dynamics (recovery times) play a critical role in pulse formation and pulse-width. Active mode-locking can be implemented by modulating the gain or absorption of the cavity. The schematic diagram of an actively mode-locked laser is shown in Fig. 1.2(c) where the absorption is modulated through a modulator (for example an electro-absorption modulator) monolithically embedded in the laser cavity. The modulation is applied through an external RF source at frequencies equal or sub-harmonic to the cavity round-trip time, modulating the loss of the modulator section. Therefore, a window of positive gain is generated (Fig. 1.2(d)) and the generated pulses are synchronized with the RF source, resulting in a very low phase noise (timing jitter). It should be noted that while a sinusoidal function is applied to the modulator, pulse shortening occurs due to the properties of the modulator transfer function and the propagation of pulses in the cavity for many round-trips [15].

The passive mode-locking and active mode-locking schemes can be combined in the scheme termed hybrid mode-locking, shown in Fig. 1.2(e). In this scheme, the DC biased saturable-absorber forms the pulsation and the RF modulation synchronises the

timing of the pulses with a stable external RF source through RF modulation.

### 1.3.1 Quantum Well and Bulk Mode-Locked Lasers

In this section, we will present a brief overview of developments and major advancements towards optimising semiconductor mode-locked lasers. We categorize them based on the type of active region: quantum-well and bulk, quantum dots at 1.3 $\mu$m and quantum dashes/dots at 1.55 $\mu$m. The first demonstrations of monolithic passive mode-locking (without an external cavity) in semiconductor lasers was reported by Sanders et at. in [16] and Vasil'ev in [17]. The first report was from a multi-quantum well GaAs based active region with emission around 860 nm and repetition-rate of 108 GHz with pulse-widths of 2.4 ps and time-bandwidth product of 1.1. The second report was demonstrated for a double-heterostructure bulk GaAs active region with 0.1 $\mu$m width emitting at the same wavelength range with repetition rate of 100 GHz and 2.3 ps $\text{Sech}^2$ pulses with 0.7 time-bandwidth product. Later, it was shown that embedding a passive section with higher band-gap in addition to the gain and absorber sections using quantum-well intermixing technology can reduce the threshold current, the pulse-width and associated time-bandwidth product for a longer cavity ($\approx$ 4 mm) [18]. The emission wavelength was extended to 1.3 $\mu$m with hybrid mode-locking scheme in [19] with 1.4 ps pulsewidth at 15 GHz. Active mode-locking with integration of electro-absorption modulator as the optical gating element rather than a saturable absorber has been reported for 1.55 $\mu$m mode-locked lasers with 2 ps pulse-width at 16.3 GHz [20] and 3.0 ps at 50 GHz [21].

Typical two-section mode-locked lasers show pulses with excess bandwidths making the time-bandwidth product much higher than the transform-limit range. This comes mainly from self-phase modulation which occurs due to the gain saturation which results in change of refractive index and instantaneous frequency within the duration of the pulse [22]. Therefore, a mechanism for spectral filtering, preferably within the cavity is desirable to overcome this problem. Using distributed-Bragg-reflectors (DBR) as filtering element within the cavity, lasers have demonstrated control over the centre wavelength, spectral width as well as transform-limited pulse generation [15, 23–25].

To increase the repetition-rate of semiconductor mode-locked lasers, one might consider of decreasing the cavity length to shorten the round-trip time of the laser. However, the threshold gain increases for shorter cavities and there are more effective techniques to make a mode-locked laser to emit pulses faster than its fundamental repetition rate, without making the whole cavity shorter. Colliding-pulse mode-locking (CPM) is a technique which enables pulses with repetition rates of higher harmonics from a cavity by placing the saturable absorber in the middle of the cavity rather than one end (Fig. 1.3(a)). Using this technique, transform-limited 1.4 ps pulses at 32.6 GHz from a 2.54 mm actively mode-locked quantum well emitting at 1.58 $\mu$m was

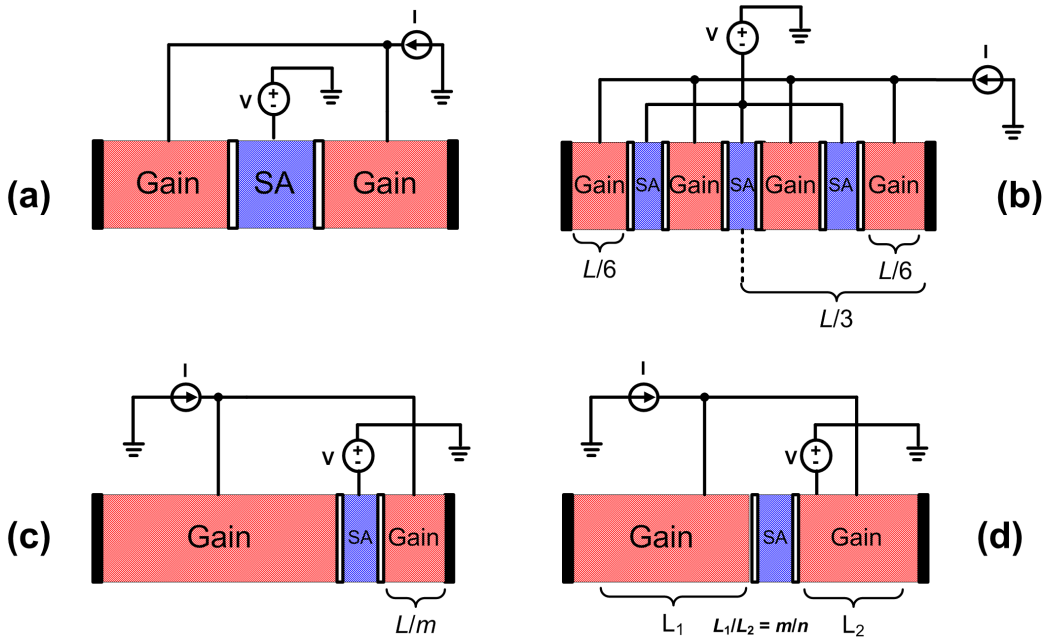



Figure 1.3: Colliding-pulse mode-locking (CPM) techniques. (a). CPM at second harmonic: $2f_{ML}$, [26–28]. (b). Multiple CPM at 6th harmonic: $6f_{ML}$, [29, 30]. (c). Asymmetric CPM: $mf_{ML}$, [31]. (d). Asymmetric CPM with relatively prime ratios for $m$ and $n$ ($m > n$): $mf_{ML}$, [32]. The fundamental repetition-rate of the cavity is $f_{ML}$ and $L$ is the total cavity length.

demonstrated by Wu et al. in [26]. The same group showed transform-limited sub-ps pulse generation at higher repetition rates, up to 350 GHz using the same technique with passive-mode-locking (without RF source) [27, 28]. Later, an actively CPM laser at 15.8 GHz was utilised for data transmission in an optical-time division multiplexing system and showed error free performance [33]. More works on dynamics and chirp of such lasers can be found in [34–36]. The CPM cavity can be extended to generate pulses with higher harmonics from a cavity with the same length; this scheme is known as multiple colliding-pulse mode-locking (Fig. 1.3(b)). Placing three absorbers (at 1/4, 1/2. and 3/4 of the cavity) has led to generate pulses with maximum repetition-rate of 4th times (240 GHz) the fundamental frequency [29, 30] and 192 GHz (6th harmonic, by placing the absorbers at 1/6, 1/2 and 5/6 of the cavity). It was shown that the multiple absorber sections can be removed and harmonic mode-locking is possible even with a single absorber section when the absorber is placed at location of $\frac{L}{m}$ where $L$ is the total cavity length and $m$ is the integer number (asymmetric CPM, shown in Fig. 1.3(c)). With this scheme, harmonic mode-locking at harmonics of 2, 3, 5 (175 GHz) and also 7th harmonic (350 GHz) from 800 $\mu$m cavity ($\approx$ 54 GHz) has been shown [31]. Note that when the harmonic number increases the absorber length might be large enough to cover the position $\frac{L}{m}$ and $\frac{L}{m+1}$. Higher repetition-rates is also possible if the absorber is placed inside the cavity to make the ratio of the two parts $\frac{m}{n}$ so that $m$ and $n$ are integers without common divisor (relatively prime) [32], shown in Fig. 1.3(d).

Shimizu et al. showed harmonic pulse generation at 580 GHz and 860 GHz with $\frac{3L}{8}$ and $\frac{5L}{12}$ from a laser with cavity length of 600 $\mu$m (fundamental frequency $\approx$ 72 GHz).

In addition to the significant improvements and contributions towards faster and better quality of pulsation in these lasers, efforts has been made on extending the tuning of the repetition-rate. For a practical application, it is important to synchronise the repetition-rate of the laser to that of the external source. For this purpose, the RF locking-range should cover any errors in the processing and cleaving procedures of the laser. The typical RF locking of a two-section hybrid-mode-locked laser is only a few 10s of MHz; this range is smaller than the cleaving/process error. Liu et al. demonstrated around 1 GHz total tuning of repetition-rate in a multi-section passive mode-locked laser at 38 GHz including a DBR and passive section. This wide range was achieved by changing the current of passive section, gain section, the voltage of the absorber section [37]. Kaiser et al. showed 500 MHz RF locking-range for a 40 GHz hybrid mode-locked, multi-section laser [38, 39] based on the same technique for repetition-rate tuning. The RF locking-range can also be improved by optimising the RF circuit for higher injection efficiency and less required power [40, 41]. A wide locking-range of 200 MHz for a 40 GHz multi-section laser was achieved with this circuit which is higher by an order of magnitude than the impedance matching (50 $\Omega$) circuit [40]. The record for the RF locking-range (1.9 GHz for a 40 GHz laser) was demonstrated for actively mode-locked lasers with optimised RF circuit [41].

### 1.3.2 GaAs Based Quantum Dot Mode-Locked Lasers at 1300 nm

Semiconductor mode-locked lasers based on GaAs based quantum dot material system have shown promising performance. This is mainly because of several advantages of quantum dots such as broad gain-bandwidth (due to inhomogeneous broadening), ultrafast carrier dynamics in the absorber section, lower threshold current and reduced amplified spontaneous emission [8, 42, 43]. Promising results have been demonstrated such as 390 fs pulse-width with 10s of mW power from a 21 GHz laser [44], simultaneous achievement of narrow pulses (2 ps) and with low RF linewidth (500 fs timing jitter) from a 8 GHz laser [45], stable operation up to temperatures of 80 $^{o}$C with narrow RF linewidth and decreasing trend of pulse-width [46, 47] and up to 110$^{o}$C with pulse-widths less than 19 ps [48].

The GaAs based quantum-dot mode-locked lasers showed mode-locking at ground-state (GS) or excited-state (ES) with change of bias conditions [49] with nearly similar pulse-widths. Also, dual operation at both GS and ES was demonstrated for a two-section mode-locked laser at high bias currents [50]. In addition to the control mechanism for this switching with bias conditions, Kim at el. showed that the two-section mode-locked laser can either operate at GS or ES mode-locking with controlled filtered feedback from a grating, without need to change the bias [51].

While few ps or sub-ps pulse generation has been demonstrated for such lasers, large TBP values were reported [44, 48–51]. Indeed, TBP is dependent on the bias conditions and is minimized at bias currents close to threshold and higher negative absorber voltages, with decreasing the gain/absorber length ratio [43]. In order to increase the average and peak power of the laser output, tapered gain sections were demonstrated with 10 mW average power (500 mW peak power) and 780 fs pulses (at 24 GHz) with TBP of 0.5 [52] and transform-limited 360 fs with 15 mW average power (2.2 W peak power) for a device with smaller gain/absorption length ratio [43].

Quantum-dot mode-locked lasers with hybrid mode-locking and higher repetition-rates (CPM techniques) were reported by several groups. Kuntz et al. demonstrated hybrid-mode-locking for a 35 GHz laser with wide RF locking-range of 90 MHz [53]; Schmeckebier et al. showed stabilisation of a 40 GHz laser with external RF source [54]. They reported total locking-range of 101 MHz for hybrid mode-locking to different bias conditions, while individual locking-range for fixed bias parameters was around 10 MHz. Another group showed the maximum 30 MHz RF locking-range of a 40 GHz laser with some investigations on the width of locking-range such as dependence on pulse-width and stability of mode-locking [55]. Using the demonstrated techniques for CPM in quantum-well lasers, Thompson et al. showed CPM operation at second harmonic from a 3.9 mm device with 7 ps pulses and little chirp (TBP $\approx$ 0.54) [56]. Asymmetric CPM technique, was also demonstrated for quantum-dot mode-locked lasers showing higher harmonics (7.2-50.7 GHz in [57] and 39, 79, 118, and 237 GHz in [43, 58]), with nearly transform-limited pulses with identical pulse-widths (1.4-1.8 ps).

### 1.3.3 InP based Quantum Dash/Dot Mode-Locked Lasers (QDMLLs) at 1550 nm

The first demonstration of mode-locking in InAs/InP quantum dot lasers were reported by Renaudier et al. in [59] showing a very coherent "self-pulsation" at 45 GHz with RF linewidth of less than 100 kHz. The second observation by Gosset et al. in [60, 61] showed complementary measurements of pulse-duration for a 134 GHz laser with nearly transform-limited, sub-ps pulse-width (800 fs) and also 50 kHz RF-linewidth for 42 GHz laser with few ps range pulse-width. Similar results have been published by another group from InAs/InP quantum-dash mode-locked lasers, showing the record of 312 fs, transform-limited pulses from a short, single-section cavity at 92 GHz [62]. The interesting part was the fact that these promising pulsation was observed for single-section Fabry-Pérot lasers without any passive (absorber section) or active mode-locking schemes. The presence of phase-locking between the longitudinal modes was attributed to the strong nonlinear effects inside the cavity such as four-wave-mixing (FWM) [62, 63].

While the presence of mode-locking inside the cavity are evident, from now on, we name

these lasers "self-mode-locked" (SML) lasers. The term "self-pulsating" usually corresponds to frequencies associated with the relaxation oscillation (RO) frequency and not the free-spectral-range of the cavity which is the case for single-section quantum-dash lasers. The presence of such self-mode-locking has been observed in GaAs bulk lasers [64], InP based bulk lasers [65] , and quantum well lasers emitting at 980 nm [66] and 1.55 $\mu$m [67–69]. While the mode-locking observed in these lasers were mostly attributed to "frequency-modulated (FM) mode-locking", conversion to amplitude modulation mode-locking (similar to passive mode-locking) is possible by using an optical fibre [67]. One important aspect of mode-locking observed in quantum-dash single-mode lasers is better phase coherence among the modes, which enables $\sim$ 1-10 kHz range for the linewidth of the beating tone [63] compared to $\sim$ 100 kHz-1 MHz range for quantum-well or bulk lasers. For a survey of development of such lasers one can see [70] and references therein.

Unlike the promising SML operation in single-section QDMLs, the conventional passive mode-locking from two-section quantum-dash lasers did not show outstanding performance in the first observations including high loss, low gain, and broad regions of Q-switching [71]. For these devices, the output of the laser showed significant amount of chirp so that the clear pulses were only observed by spectral filtering [71] or compression by single-mode standard fibre [72, 73]. This was attributed to the long relative delay in the pulses generated by each mode group in the lasing optical spectrum, leading to a broad intensity output when superimposing the mode groups as the whole spectrum.

Recently, the two-section mode-locking of QDMLLs by the same group in France show-

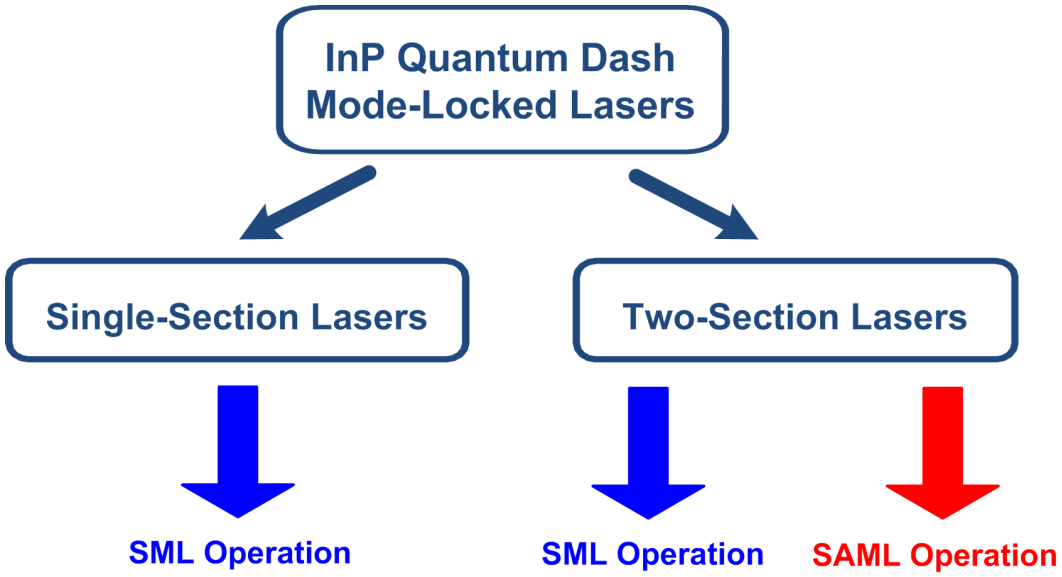



Figure 1.4: The diagram of InP QDMLLs for mode-locking operation based on cavity structure.

ing the SML operation in such lasers was reported [74]. These two-section lasers consisted the same active layers for the gain and absorber sections, similar to the single-section lasers. Broad optical spectrum, narrow RF linewidth (∼100 kHz) with ps pulses were reported, but the time-bandwidth product is still much higher than the Fourier-limit. Some differences in the performance of these lasers to the SML lasers were highlighted in [74]. From now on, to distinguish the mode-locking mechanism of two-section laser from SML lasers, we use the term "saturable-absorber dominated mode-locking" (SAML) for these lasers.

The focus of this thesis will be on these two type of lasers, as we will show in the following chapters. It is worth mentioning to schematically illustrate the types and diversity of devices we analyse in this work, shown in Fig. 1.4. As shown in Fig. 1.4, the Fabry-Pérot single-section laser only operate as SML lasers whereas for two-section (gain and saturable absorber) lasers, depending on bias conditions of the absorber, SML or SAML operation may be exhibited.

## 1.4 Optical Injection of Semiconductor Lasers

Locking (synchronisation) phenomenon can occur between oscillators of any type. This was described by Huygens for the first time in the locking between two swinging pendulums by in the 1600s. A theoretical prediction was awaited until the middle of the 20th century when Adler established a study on locking phenomena in electric oscillators [75]. He found that the oscillation frequency of a free running oscillator can be locked to the frequency of an injecting oscillator. This concept was adapted for using in a laser as an oscillator; the first injection locking was demonstrated by Stover and Steier using two HeNe lasers in 1966 [76]. In the area of semiconductor lasers, Kobayashi et al [77] showed in 1980 that injection locking (IL) a diode laser assured single-mode operation under high speed modulation. Afterwards, for more than three decades, injection locking of semiconductor lasers has been explored in order to develop and create widespread applications and performance improvement such as modulation bandwidth enhancement, noise reduction (in all aspects), pulsing enhancement, optical spectrum narrowing, comb generation, far-field (FF) beam enhancement and scanning, and generation of coherent high power beams. At the same time, from a pure physical point of view, many studies have been done on the analysis of stability and behavior of laser systems under optical injection as a system of nonlinear coupled oscillators. The basic schematic of an injection-locked system is shown in Fig. 1.5 where the light from laser1 was injected to the cavity of laser2. Both the lasers can be either CW or pulsed sources and the injected light can be uni-directionally coming from the laser1 (master-slave configuration) or bi-directionally travels between the cavities of laser1 and laser2 (mutual injection configuration). The locking-range (optical) is defined as the detuning (frequency/wavelength difference between master and slave) range in which the slave




Figure 1.5: Basic diagram for optical injection-locking; if the light is injected unidirectionally from the Laser 1 to the Laser 2, the Laser 1 is known as master laser and the laser 2 is known as slave laser.

remains injection-locked, based on a locking definition. For mode-locked lasers, we use an additional term as RF locking-range which refers to the repetition-rate range in which the slave laser remains synchronised (locked) to the external RF source.

The optical injection of a laser can be motivated by three main considerations: to improve and optimise performance of the laser, to force the laser operate in a region of interest which is not accessible without injection (such as chaos) or to look at dynamical regimes and transitions from a nonlinear dynamical point of view. A complete survey of injection-locking of semiconductor lasers is not within the scope of this thesis. Therefore, we present a survey on the works have been done on injection-locking of mode-locked lasers and also briefly on the lasers of other type (such as laser arrays, VCSELs) in this section.

### 1.4.1 Mode-Locked Lasers

Since the mode-locked lasers are pulsed sources; possible scenarios for optical injection include CW injection, side-band (dual-mode) injection, pulsed injection, or clock (data) injection. The master-slave schemes are shown in Fig. 1.6; the typical optical spectrum for different injection cases are shown on the left side. For the cases other than CW, the injection can be at the same harmonic (fundamental injection), higher harmonics (harmonic injection) or sub-harmonic (sub-harmonic injection) of the slave laser repetition-rate, as shown in right side of Fig. 1.6. The CW, dual, and pulsed injection schemes are based on optical injection-locking process where the optical lines of the injected signal interact with those of the slave laser. The data injection scheme is usually carried out for the purpose of optical clock-recovery from a data signal at the receiver end or in the middle of an optical communication system.

#### CW Optical Injection

Joneckis et al., in [78] demonstrated successful CW optical injection in selection of one super mode (group of phase-locked modes) and suppress the rest of super-modes in an external cavity mode-locked laser. Significant reduction of chirp and nearly transform limit pulses with optical injection was also achieved. Within a theoretical study, it was predicted that increasing the injection power, however, led to pulse broadening not

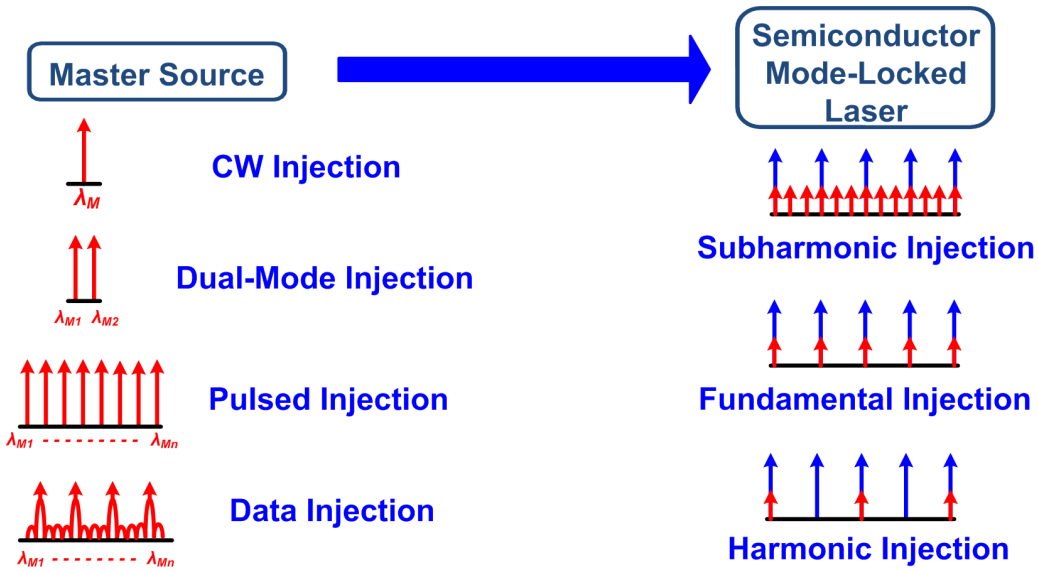



Figure 1.6: Schematic diagram of different scenarios for optical injection of mode-locked lasers.

only due to more suppression of modes but also due to prolonging the gain quenching for the formation of the pulses in gain-absorption competition. Margalit et al. [79] theoretically predicted that for mode-locked lasers with very long cavity (solid-state or fibre-lasers) CW injection would be inefficient as the power is distributed among many modes. However, for semiconductor mode-locked lasers CW injection is more efficient as fewer modes are lasing. The selection of a supermode with CW optical injection was also demonstrated for InP strained quantum-well harmonically CPM laser at 192 GHz [80]. The CW injection demonstrated the selection of harmonic mode at every mode injected, regardless of the free-running suppression of that mode. The reported locking-range was quite narrow (2.5 pm) and slight broadening of pulse-dwidth under optical injection was observed with the time-bandwidth product still transform-limited. Quinlan et al. in [81, 82] demonstrated super mode selection with CW optical injection in a semiconductor-based ring cavity mode-locked laser leading to amplitude and phase noise reduction due to super mode noise suppression. With CW optical injection, chirp reduction from 0.84 for a $\text{sech}^2$ pulse to nearly transform limited (0.34) for a Fabry-Pérot quantum-well actively mode-locked laser at 40 GHz and 1.55 $\mu$m was also demonstrated [83]. Narrowing of the optical linewidth of the individual modes close to the master laser was observed with CW injection of actively mode-locked ring laser at 10 GHz [84], an actively mode-locked laser (with integrated electro-absorption modulator) with repetition-rate of 25 GHz [85, 86], a supercontinuum generator based on hybrid mode-locked laser [87] and an external cavity hybrid mode-locked multi quantum well laser at 1 GHz [88]. In addition to the optical linewidth, the frequency stability of each individual mode can be controlled by injection of a CW light frequency stabilised with an accurate frequency source (molecular absorption line) [85]. Here, while no information on the locking-range was provided, a wider and flatter spectrum under

optical injection, than free-running with 3dB width of 14 nm was achieved. With a development of GaAs based quantum dot mode-locked lasers, CW injection-locking was also demonstrated for such lasers emitting at 1.3 $\mu$m [89, 90]. It was shown that CW injection can stabilise the pulsed again waveform instabilities with GHz optical locking-range [89]. Another theoretical study predicted that the optical locking range is wider at the corner of stable-unstable passive-mode locking where the slave laser is less stable [91].

**Dual-mode optical injection**

The extension of CW optical injection to dual-mode (side-band) optical injection, for the first time was proposed by Ahmed et al. in [92, 93] to injection-lock a double sideband suppressed carrier (DSBSC) modulation signal to a 37 GHz passively mode-locked laser. They showed significant reduction of phase-noise and control over the repetition rate with wide RF-locking range of 170 MHz. Later, Lee et al. in [94, 95] showed that not only the phase noise, but the phase of each mode can be locked to that of the master laser with injection of two-modes (from a hybrid mode-locked laser [95] or side-bands of a Mach-Zehnder intensity modulator [94]). Each mode in the spectrum of injection-locked laser can be used as a local oscillator in an optical heterodyne detection system. This method was later implemented successfully in a GaAs based quantum-dot passively mode-locked laser with significant reduction of timing jitter, significant reduction in time-bandwidth product and 20 MHz of RF-locking range for a 10 GHz laser [96]. The same group showed later that dual-mode injection at higher harmonics of the repetition rate is possible with generation of the comb with similar repetition rate [97].

**Pulsed optical injection**

Dual-mode injection can be extended for the case of multi-mode or pulsed optical injection to a mode-locked laser. The first observation of pulsed injection-locking to a semiconductor mode-locked laser was demonstrated by Margalit et al. in [98], with achievement spectral narrowing close to that of a master laser and also pulse-width narrowing. The same group reported harmonic injection-locking of a passively mode-locked fibre laser to a pulsed signal [99]. This harmonic mode-locking occurred as a result of slight detuning of modes between master and slave so that only a part of the two spectra overlap. As a result, the repetition-rate of the slave laser was an integer multiples of free-running laser and injection pulses. The method was extended to dual pulsed injection locking of two synchronized diode lasers (as the master) at 2.4 GHz to a passively mode-locked fibre laser as a slave. The resulting injection-locked slave laser had two pulsed spectra at wavelengths of 1.53 $\mu$m and 1.55 $\mu$m with repetition rate of 7.5 GHz [100]. The optical injection of several lines into the cavity of a mode-locked laser opens up the possibility of synchronisation of the slave laser to its subharmonic, this synchronisation is called *subharmonic injection-locking*. The main advantage of this

synchronisation scheme is to synchronise a high frequency laser to a slower master laser. Injection-locking to a 40 GHz (passively mode-locked) laser by optical injection of pulses from 1 GHz (external cavity hybrid mode-locked laser) pulses was demonstrated by Kurita et al. [101]. They showed no particular dependence of locking on the pulse shape, even when a pulse with 300 ps trailing tail was injected. Also, a directly modulated DFB at 10 GHz was used as the master laser; again, successful harmonic injection-locking occurred with the condition that at least two modes from slave laser should be injected. This reminds us the necessary condition for dual-mode optical injection of mode-locked lasers. Nirmalathas et al. carried out a study of sub-harmonic mode-locking and side-by side comparison with sub-harmonic hybrid mode-locking (electrical synchronisation) [102]. They showed that successful locking at 40th sub-harmonic was possible whereas with electrical only sub-harmonics of 2-6 were possible. Also, optical injection showed lower timing jitter and less amplitude modulation and wider RF locking-range (40 MHz) than electrical (4 MHz). In their study, strong dependence of locking performance (RF-locking range, RF power) observed versus pulsewidth (better with narrower pulses). In most cases mentioned above, the pulsewidth and time-bandwidth product of the slave laser remained almost unchanged under low injection levels and the main contribution of pulsed injection-locking was strong timing jitter reduction. Pulsed injection-locking of GaAs basedquantum-dot mode-locked laser (1.3 $\mu$m) was demonstrated by Kim et al. with the possibility for pulsed injection-locking at either excited state or ground states. In their scheme which consisted 4 GHz lasers as master and slave, it was shown that injection at the excited state could lock the slave laser lasing at ground state and vice versa. With excited state injection, a wide RF locking range was achieved (6.7 MHz) for up-shifted repetition-rates which was much larger than the case where injection spectrum was at ground state and slave laser emitted at excited state.

**Data optical injection**

For the data injection-locking, the synchronisation scheme could be coherent (injection-locking) or incoherent [103, 104]. The latter is based on the interaction of incoming signal with the carriers and the locking of the repetition-rate to that of the signal occurs through modulation of the carriers. A study on all optical clock recovery and comparison with electrical clock recovery and dependence on data signal was carried out by Arahira et al. in [104]. It was shown that the optical clock recovery is possible in the "resonant" case when the optical carrier coincides with one mode of the slave laser and "anti-resonant" case when the optical carrier is in the middle of the two adjacent modes. Modulation rate was the same as the repetition rate of the slave laser. The resonant optical clock recovery was the most robust technique against data format (in-phase or carrier suppressed), input data pattern and the intensity fluctuations of data signal compared to anti-resonant case and electrical injection. The optical clock recovery scheme based on resonant mode showed robustness against intensity and phase noise in the input data signals [105]. Particularly, the passively mode-locked laser

acted as an active filter with strong phase regeneration when the high frequency jitter component became greater than the RF-locking range of the system. An optimization in the saturable-absorber active layer to a tensile multi-quantum well structure led to have less wavelength and polarisation sensitivity with orthogonal optical clock recovery [106]. The same clock recovery scheme was used to study the effect of optical signal to noise ratio and data format modulation in [107]. It was shown that the system was almost independent of data modulation (on-off keying or phase-shift keying) and robust against degradation of optical signal to noise ratio. All optical clock recovery has been also demonstrated for InP based quantum-dot (dash) mode-locked lasers by Roncin et al. [108]. They showed successful 40 GHz clock recovery from a 40 GHz single-section laser with data injection at 40, 80, and 160 Gbps. Cascaded optical clock recovery with a polarisation insensitive bulk self-pulsation laser and a low phase noise quantum dot InP laser both at 40 GHz was demonstrated by Lavigne in [109]. The latter stage acts as a filter to absorb the additional jitter coming from the input clock from the previous stage.

### 1.4.2 Other Lasers

#### High-power semiconductor lasers

Since the early of 80's, injection-locking of edge-emitting laser arrays has been explored and implemented with the desire of having high coherent power and enhanced far-field beam quality. Goldberg et al. in [110] were successful to implement an injection locked coupled-stripe 10-element laser diode array by a laser diode master with 105 mW single-frequency with $0.5^{o}$ angular width at 3 mw injected single mode beam from the master laser. The locking range, defined as the input frequency range which the height of single lobe in the far-field pattern maintains at least half of its maximum value, was measured to be 16 GHz. Hohimer et al. achieved a continuous, wide locking-range of more than 60 GHz for injection power $\approx$ 12 mW with gain-guided laser array slave laser and a dye laser as the master [111] with optical injection to the single-end-element in the array. This was followed by works from other groups with 315 mW for a 20-element array [112], 450 mW from an array with phase-conjugate beam coupling arrangement [113], 510 mW for a 40-element array [114], and 1.0 W from an AlGaAs laser array, injection-locked to a CW external cavity master laser [115]. In addition, the change of the far-field emission angle with the injection frequency which is known as "beam steering" or "beam scanning" was observed in [111, 116] as well as broad area lasers [117].

Injection-locking of individual lasers on a broad-area laser bar has been demonstrated some years ago [119–121]. In this work, two individual broad-area lasers from a bar of 19 devices with emitting aperture width of 125 $\mu$m and separation of 500 $\mu$m for the lasers, and common current source. This is of particular interest as coherent coupling

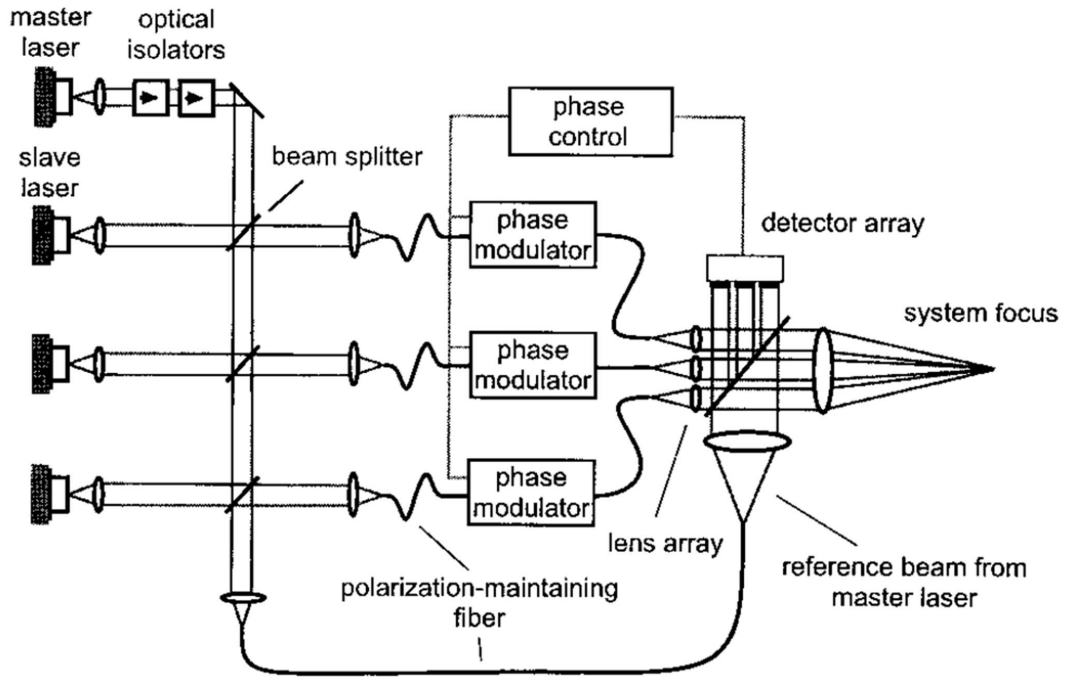



Figure 1.7: Schematic diagram for coherent combining of beams from injection-locked lasers. Reproduced with permission from [118], ©(1999) Optical Society of America.

of laser beams emitted from phase-locked lasers will result in a high intensity which is proportional to the square of the number of laser elements [122]. Simultaneous injection-locking of single-mode diode lasers has been also implemented with feedback based phase control of the lasers to generate a coupled coherent beam for two lasers [123], three lasers [124] and 19 individual lasers [118]. The schematic diagram of the experimental arrangement to simultaneously injection-lock 19 laser diodes in an array is shown in Fig. 1.7. As can be seen, each laser is individually injection-locked to the common master laser and the light was coupled to a separate single-mode fibre. The feedback loop stabilised the temporal phase of the slaves' light at the collimation point to ensure temporal and spatial coherence of the beams.

**VCSELs**

The major effort in research on optical injection of VCSELs was focused on improving the dynamic performance of the laser, particularly the modulation response and chirp reduction. These two improvements make direct modulation of semiconductor laser a practical way to implement a low cost and simple transmitter without need for external modulators. Improvement of dynamic range and modulation response for a 2.5 Gbps VCSEL transmitter [125], enhancement of resonance frequency by factor or ∼5-10 [126], modulation frequency more than 40 GHz [127], and a record of 66 GHz for modulation bandwidth from cascaded VCSEL injection-locking system [128]. It should be noted that all these achievements have been reported under so called strong optical injection. It is important to note that the injection ratio here is higher than the level used in the

mode-locked lasers by more than two orders of magnitude.

## 1.5 Application of Mode-Locked Lasers in Optical Communication Systems

In this section, we present a brief overview of important applications of semiconductor mode-locked lasers such as microwave/millimeter-wave generation and transmission, optical time-division multiplexing (OTDM), and wavelength division multiplexing (WDM). The applications are based on recruitment in frequency, time, or wavelength domains. In addition, to the above mentioned applications, optical clock recovery using optical injection of data signals into the cavity of the mode-locked laser, as discussed in § 1.4.1 is another area of application for such lasers.

### 1.5.1 Microwave/Millimeter-Wave Generation and Transmission

As we mentioned, semiconductor mode-locked lasers can generate pulse with repetition-rate of 40 GHz or higher. The generated signal can be used as a millimeter wave generation system, which can be modulated and transmitted over fibre or free space for short-haul communication systems. A schematic of possible scenarios to use mode-locked lasers for millimeter-wave generation and transmission is demonstrated in Fig. 1.8(a)-(c). Note that all of these schemes, the carrier signal is the generated electrical carrier (not the optical carrier or longitudinal modes) by converting the lasers's optical intensity oscillation to the electrical signal.

The data to be modulated can be applied to the laser directly; for example, Georges et al. in [129] showed transmission of error-free 50 Mb/s differential phase-shift keying (DPSK) data over few meters of fibre with a 45 GHz mode-locked laser (850 nm) by applying the superimposed signal (carrier and data) to the absorber section. The data can be modulated externally at the laser output [130, 131], shown in Fig. 1.8(a), (b). Ahmed et al. in [131] showed the extension of this work to lasers at long wavelength for both wireless and fibre transmission with a 37 GHz hybrid-mode-locked laser for wireless transmission up to 20 m of 500 Mb/s amplitude shift keying (ASK) and fibre based transmission (10 km single-mode fibre) of 200 Mb/s binary phase-shift keying (BPSK) modulated data. The lasing modes in the spectrum of a mode-locked laser could be recruited for generation of high quality millimeter-wave and THz signals at higher harmonics of a mode-locked lasers with low phase noise due to the fact that they are from the same cavity and are phase-locked together. This can be achieved by separate spectral filtering to select two modes located at higher harmonics of the repetition-rate to generate millimeter-wave up to 300 GHz (from a 38 GHz laser) [132]

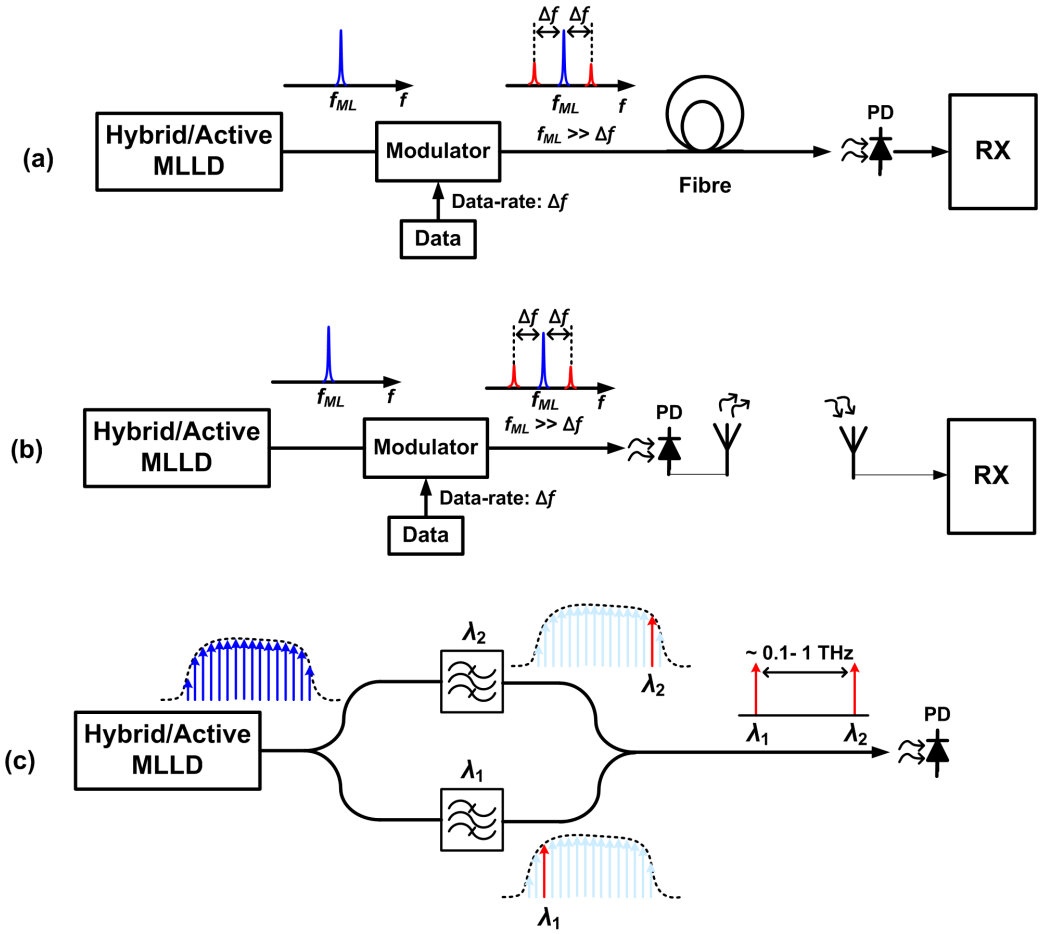



Figure 1.8: Schematic diagram for utilisation of mode-locked lasers for generation and transmission of microwave/millimeter wave signals. (a). Radio over fibre (RoF) microwave/millimeter-wave transmission. (b). Wireless transmission of microwave/millimeter-wave signals. (c). Millimeter-wave/THz generation.

and up to 1.34 THz from a 110 GHz CPM laser with sub-harmonic hybrid mode-locking [133], shown in basic diagram of Fig. 1.8(c).

### 1.5.2 Optical Time/Wavelength Division Multiplexing

The temporal pulsation of mode-locked lasers can be exploited to carry and distribute the data for long-haul transmission systems. In this scheme, the pulsation output of the laser is divided into time-slots, enabling separate information of data bits in each slot ("0" or "1"), which is known as Optical Time-Division Multiplexing (OTDM). The basic schematic diagram of an OTDM system using mode-locked lasers is shown in Fig. 1.9. In this system, the data is encoded in the serial form on the pulses. The data rate can be extended to harmonics of the repetition-rate using a multiplexer which separates the pulses and delays each pulse with respect to the other and recombines them to produce train of pulses with higher data rate. The suitable mode-locked laser for this

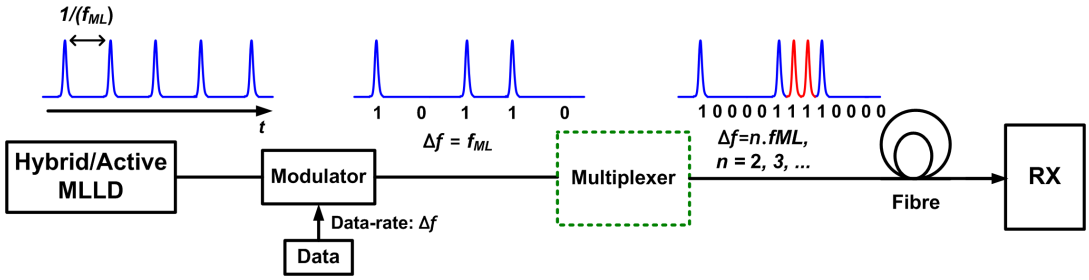



Figure 1.9: Schematic diagram for OTDM system from semiconductor mode-locked lasers.

application should have the necessary performance requirements such as transform-limited and short pulses, low timing jitter, and high extinction ratio of pulses [134]. The ability to lock to standard frequencies of the system is a key element like in many applications in optical communications.

The early OTDM demonstrations were reported for an extended-cavity active mode-locked laser at 4.9 GHz with error free transmission of 4.9 Gb/s data over 70 km of fibre (transform-limited 8 ps pulses) [135] and 8.2 GHz with the same data rate over 4200 km of optical fibre (transform-limited 8 ps pulses) [136]. The OTDM system was extended towards data rates at higher harmonics of the repetition-rate by the group in NTT Laboratories in 1996 [137], to demonstrate successful field experiments on transmission of 20 and 40 Gb/s data over 198 km of fibre in a sub-marine cable. The pulsed laser was a monolithic actively mode-locked laser (with integrated electro-absorption modulator [15]) at 20 GHz with transform limited 6 ps pulses. This was also the first 40 Gb/s transmission in a field environment for any optical communication system [138]. Another group reported increased data rate to 160 Gb/s from a 10 GHz mode-locked laser (transform limited 1.2 ps pulses) and transmitted over 116 km of field-installed fibre [139]. A group in Berlin also showed suitability of GaAs based quantum-dot mode-locked lasers for OTDM transmission up to 160 Gbps from a 40 GHz mode-locked laser [54].

Mode-locked lasers can be used for transmission of data using their spectral properties in the optical domain, to the well known wavelength division multiplexing (WDM) systems. The basic diagram of such a system is shown in Fig. 1.10 where the optical channels are separated using optical de-multiplexers and modulated and again multiplexed and sent through the fibre. At the destination, again the modulated channels are separated and processed individually. The main requirements for this application is matching of the absolute optical frequencies of the laser modes with those of the WDM grid and also precise matching of channel spacing (repetition-rate of laser) to that of the system. The wider the emission spectrum, more channels can be utilised for data encoding. As we discussed before, using a grating based structure in the cavity allows for precise control of emission wavelength; this allows for using an array of

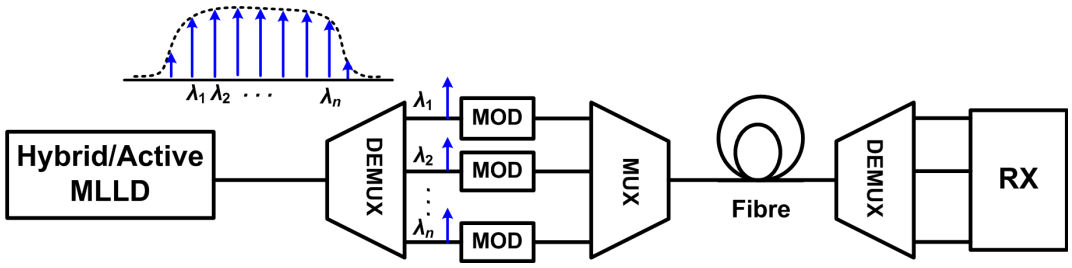



Figure 1.10: Schematic diagram for WDM system using semiconductor mode-locked lasers.

mode-locked lasers each spanning particular channels [140]. The WDM and OTDM schemes can be combined to increase the transmitted data rate from individual modes on a single mode-locked laser [141] or three separate mode-locked lasers each carrying 80 Gb/s OTDM modulation [142] over 600 km. WDM scheme can also be combined with millimeter-wave transmission to generate multiple millimeter waves, as different optical frequencies, each separately modulated and transmitted through 10 km of fibre [143].

## 1.6 Motivation For This Work

With the overview given so far, one can easily find the significant number of works that have been done in the area of mode-locked laser diodes in many aspects including optical injection. However, there are a number of important open problems that still exist in this area and should be investigated in depth.

**Stability:**

A semiconductor mode-locked laser can be regarded as a complex laser system; the addition of optical injection to this system can potentially induce many types of instabilities in the laser output. A recent study on CW injection of single-section quantum dash mode-locked lasers has shown typical classical dynamical regimes without any observation of injection-locking [144]. In fact, the stable-locked regime can be a narrow region in the dynamical map of optical injection versus detuning and injection ratio. In many cases no stable-locked region is observed for the laser under optical injection. In this regard, the first area of interest is to look at dynamical regimes under optical injection, particularly a region of injection-locked mode-locked operation. CW optical injection is an ideal candidate in terms of this study as the number of external parameters are limited, but essential to investigate this: power and (optical) frequency detuning. In a part of this work, we try to answer these relevant questions: Are quantum-dash mode-locked lasers stable under optical injection? If the answer is yes, what are the properties the stable regions? Also, regarding the two different mode-locking mechanisms (SML and SAMLs) what are the possible locking properties

associated with each mode-locking regime.

**Improvement of Locking and New Functionalities:** While many groups showed improvement in the performance of mode-locked lasers with optical injection, our interest in this sense is divided in two parts: first, to confirm this possibility for the newly developed quantum-dash mode-locked lasers. Second, to investigate further possible optimisations under optical injection, for example the tuning of repetition-rate. Again, any optimisation needs to be separately analysed for each mode-locking scheme.

**Stabilisation Techniques:** Apart from our interest in these lasers, we are looking for stabilisation schemes that can improve the pulsing performance of these lasers both in terms chirp and timing jitter. Note that, this capabilities might exist if the laser shows stable performance under optical injection. In this direction, we look for a technique that will not require optical to electrical conversion (all optical), an RF source or a reference, and can be potentially used for ultra highspeed lasers as well.

**Applications:** The mode-locked lasers have found several applications in optical communication systems as well as in optical metrology, and other fields. In this work, we also investigate the new applications for these devices, particularly with the advantages and capabilities (if exist) that optical injection creates. The particular area will be in the Phase-Sensitive Amplifiers (PSAs) where the concept of phase-locking and temporal coherence is of vital importance. The question here is whether there is a technique for the realisation of PSAs from semiconductor mode-locked lasers.

These general questions mentioned above will be tried to be investigated in this thesis.

## 1.7 Thesis Organisation

The thesis includes five technical chapters (2-6) and a final concluding chapter. In the next chapter (Chapter 2) we present the description and basics of experimental techniques carried out followed by an overview of basic characterisations of InP QDMLLs when free-running (without injection). We study the main performance characteristics of such lasers, in particular the major differences between SML and SAML lasers in their mode-locking performance. In Chapter 3, the behavior of SML lasers with different active layer structures are analysed under optical injection with the observations on stable performance under optical injection. In Chapter 4, the same study is carried out on SAML QDMLLs with optical injection and the general CW optical injection is also extended to dual-mode optical injection, enabling further improvements in laser performance. Following optical injection properties of QDMLL, a novel all optical stabilisation technique based on combination of CW optical injection and filtered optical feedback is introduced for SAML QDMLLs in Chapter 5.

In Chapter 6, a new application for injection-locked QDMLLs is demonstrated for

use in multi-wavelength phase-sensitive amplifiers for next generation of all optical regenerators. With an experiment as a proof of concept, we investigate the limitations of such system and possible improvements.

Finally, the thesis will be concluded in Chapter 7 with the highlights of our technical contributions in this work followed by suggested future works.

# Chapter 2

# Basic Characterisations of Quantum-Dash Mode-Locked Lasers

## 2.1 Introduction

In this chapter, we present the results on basic characterization of quantum dash mode-locked lasers (QDMLLs). Devices with two types of active region, dash-in-a-well (DWELL) and dash-in-a-barrier (DBARR) with different cavity types, single-section /self-mode-locked (SML) and two-section /saturable-absorber mode-locked (SAML) are investigated. After introducing the devices, the main measurement techniques will be briefly introduced. The results are categorised in two parts: SML and SAML devices.

## 2.2 Device Structures and Fabrication

The devices used in this work were categorized by their active region type and their cavity structure. The devices under test came from two types of active regions: DWELLs and DBARRs; the cavity structure was single-section with only gain section or two-section including a long gain section and a short absorber section.

### 2.2.1 Device Structures

The band diagram for DWELL type active region is shown in Fig. 2.1(a). As can be seen, the InAs quantum dash mono-layer was embedded within 8 nm thick InGaAsP lattice matched quantum-well layers ($\lambda_g = 1.45$ $\mu$m) and subsequent barrier layers (40 nm) and separate-confinement heterostructure (SCH) layers (280 nm) ($In_{0.8}Ga_{0.2}As_{0.4}P_{0.6}$,

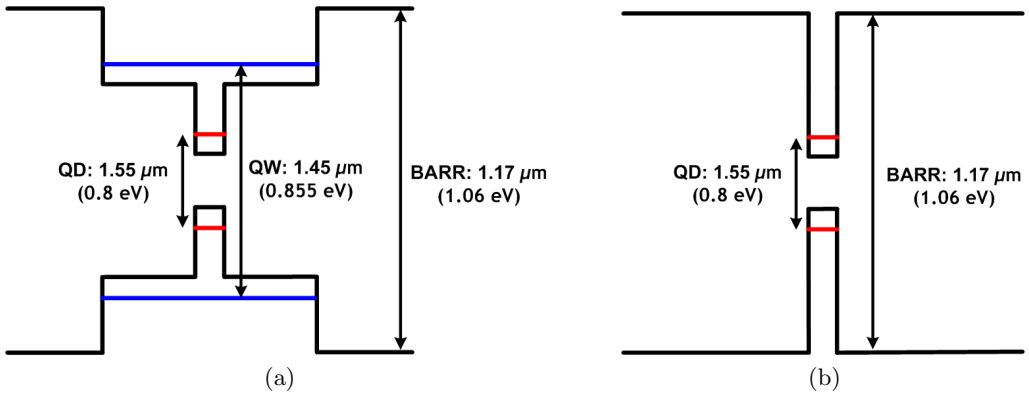
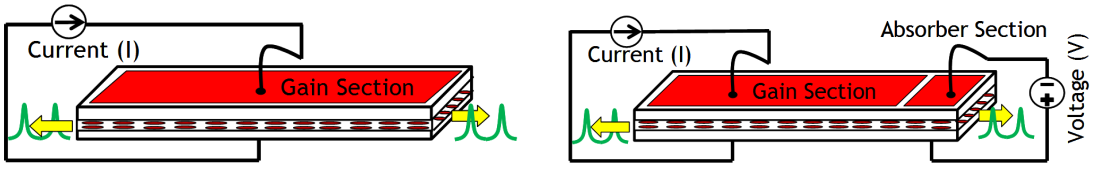



Figure 2.1: Active region structure of the devices. (a). DWELL type. (b). DBARR type. Acronyms: QD: Quantum-Dash layer, QW: Quantum-Well layer, BARR: Barrier layer.

$\lambda_g = 1.17$ $\mu$m, not shown). In the DBARR type, the quantum-dash mono-layer was embedded directly into the barrier and SCH layers as shown in Fig. 2.1(b). For both structures, the barrier and SCH layers were undoped. For the DWELL structures in this work, 6 quantum-dash monolayers in subsequent quantum-well and barriers were grown whereas the DBARR structure consisted 9 quantum-dash monolayers in barriers.

In addition to the active region type, the devices used had different cavity structures. The single-section devices had only gain sections (DC forward biased) operating as self-mode-locked (SML) lasers. The term self-mode-locked indicates the mode-locking without any deliberate passive/active scheme in the device. The origin of this phenomenon is still unclear but some hypotheses such as strong four-wave mixing (FWM) [63], or two-photon absorption[145] have been proposed. The other category of devices had two sections along the direction of light propagation; one was the gain section (similar to SML, forward biased), and the other one was the absorber section with the same active layer reverse biased with high electrical isolation from the gain section. Schematic of cavity structure for single-section and two-section devices are shown in Fig. 2.2. This structure forms the conventional passive mode-locking where the relative phases of the longitudinal modes are forced to be fixed by the mechanism of saturable-absorption. In this work, this mode-locking is termed saturable-absorber dominated mode-locking (SAML) to distinguish it from SML operation. One important difference between our two-section devices with other SAML devices (passively mode-locked lasers with InP quantum well or bulk active regions or GaAS based quantum dots) is that the two-section QDMLLs still operate as mode-locked lasers when the absorber is left open or is forward biased. In contrast with the other types of SAML devices, CW operation is usually observed when the absorber section does not operate as an absorber. The two-section QDMLL operates effectively as a single-section SML device when the absorber section was left open or forward biased above the transparency point. The list of devices used in this work, is shown in table 2.1.




(a) (b)

Figure 2.2: Cavity structure of the devices. (a). Single-section device (SML) laser (b). Two-section device (SAML) laser.

Table 2.1: Details of devices used in this work. For the two-section devices, the absorber length ratio (in percentage) is shown. Acronyms: Rep. Rate: Repetition Rate ($f_{ML} = \frac{c}{2nL}$, where $n$ is the refractive index of the cavity and $L$ is the cavity length).

| **Device** | **Active Region** | **Cavity Structure** | **Mode-Locking Mechanism** | **Length/Rep. Rate.** |
|---|---|---|---|---|
| A1 | DWELL | Single-section | SML | 4 mm/10.5 GHz |
| A2 | DWELL | Single-section | SML | 4 mm/10.5 GHz |
| B3 | DWELL | Single-Section | SML | 2 mm/21 GHz |
| I3-1 | DBARR | Two-section (2.0%) | SML | 2 mm/21 GHz |
| I3-3 | DBARR | Two-section (6.9%) | SML/SAML | 2 mm/21 GHz |
| I3-4 | DBARR | Two-section (9.4%) | SML/SAML | 2 mm/21 GHz |
| I3-5 | DBARR | Two-section (11.9%) | SML/SAML | 2 mm/21 GHz |
| G4-2 | DBARR | Two-section (11.7%) | SML | 0.8 mm/52 GHz |
| G4-3 | DBARR | Two-section (14.8%) | SML/SAML | 0.8 mm/52 GHz |

### 2.2.2 Device Fabrication

The growth of quantum-dash structures was carried out using gas-source molecular beam epitaxy (GSMBE) on a Silicon-doped InP substrate with (100) crystal direction using the Stransky-Krastanow growth method. The dash layer growth is based on deposition of a very thin layer (about 1 nm thick) of an InAs on InGaAsP layer; the mismatch between the lattice constant of the two layers causes the formation of quantum-dot islands [63]. However, due to the GSMBE growth conditions and surface anisotropy of InGaAsP layer, the formation of quantum-dots is usually modified to form nanostructures elongated in the direction perpendicular to the growth direction. These nanostructures are called quantum-dashes and have typical thickness $\sim$ 2 nm, width $\sim$ 15-20 nm and length $\sim$ 40-300 nm, depending on growth conditions [63].

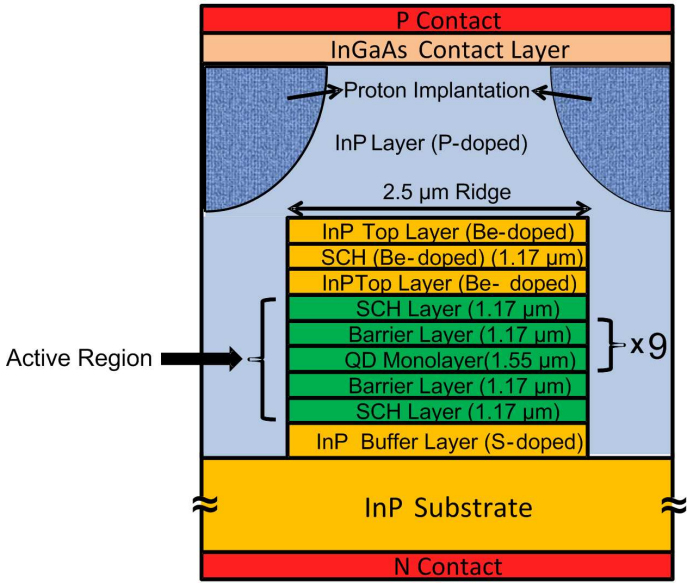
The DWELL or DBARR structures were processed into waveguides with either shallow ridge or buried ridge structures with well established InP processing technology for InP based quantum well or bulk devices [63]. For buried ridge stripe structures, waveguides were defined using contact lithography. Metal Organic Vapour Phase Epitaxy (MOVPE) was used to grow the p-doped InP cladding layer and GaInAs contact layers. For lateral confinement of carriers, proton implantation was utilized. P and n electrical contact pads were realized by ion beam sputtering of Ti/Pt/Au films [146]. For the two-section devices, interruption of the metal mask, etching of the ternary contact layer and implantation leads to forming two isolated section used as the gain and absorber sections with desired length ratios. Growth and processing of the devices were performed at III-V lab, a joint Laboratory of Alcatel Lucent Bell Labs, Thales Research & Technology and CEA-LETI, France [74]. The devices were cleaved to the required lengths at Laboratory for Photonics and Nanostructures (LPN), CNRS, France. The layer schematics of the DWELL and DBARR devices are shown in Figs. 2.3(a) and (b). The singulation of devices, mounting and wire-bonding were carried out at Tyndall. The devices were mounted on AlN submounts using silver epoxy as the bonder material. Then, the electrical connections to the devices using standard wire bonding. The submount was mounted on a copper block for active temperature control. A picture of a mounted device is shown in Fig. 2.4.

## 2.3 Measurement Techniques

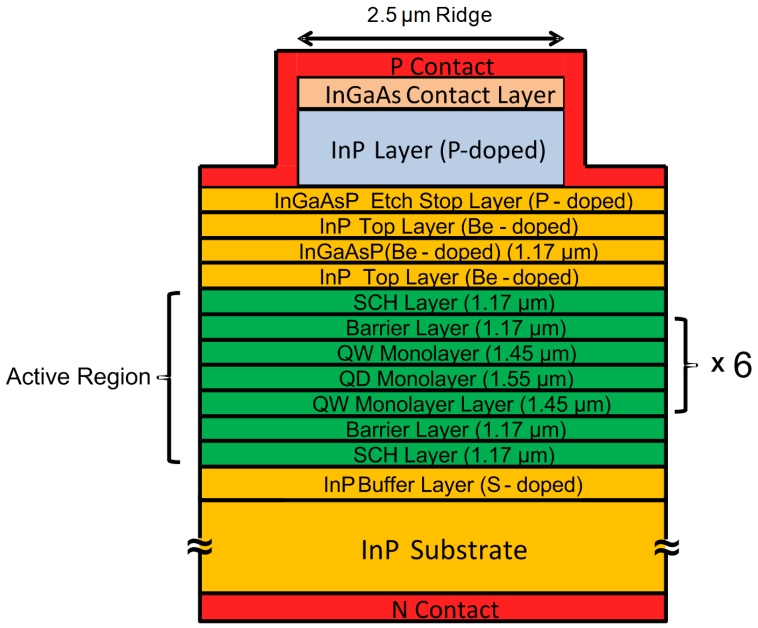
The measurement techniques we used in the course of this work gave information regarding the following parameters of the device under test (DUT): Optical power, optical spectrum, power spectrum (Fourier-transform of laser intensity), time-trace, optical linewidth, and measurement of the pulse duration of the laser intensity. The last is carried out using second-harmonic intensity autocorrelation and is based on certain hypotheses about the laser pulse shape which will be described in § 2.3.5.

### 2.3.1 Light-Current (L-I) and Power Measurements

The schematic of experimental arrangement for power measurement is shown in Fig.2.5. As can be seen the light from the laser is collected and collimated using free space lenses and a free space isolator and is shone onto a photodetector with large detection area connected to a power meter (Thorlabs Germanium PIN photodetector, model S122B with PM30 console system). The free space isolator was used to prevent any possible feedback from the photodetector to the laser. The photodetector is so slow that it could be assumed that it always measured the time-averaged power. This term will be used from now on for any correspondence about the emitted power, and the injection ratio used to evaluate the strength of external injection. For the L-I measurement,




(a)




(b)

Figure 2.3: Layer structures of the devices. (a). DWELL laser (b). DBARR laser. The thickness of layers are not scaled to the actual size.

LabView® is run on a computer connected to the power meter and current source to automatically change the current of the laser and read measurements from the power meter in a loop.

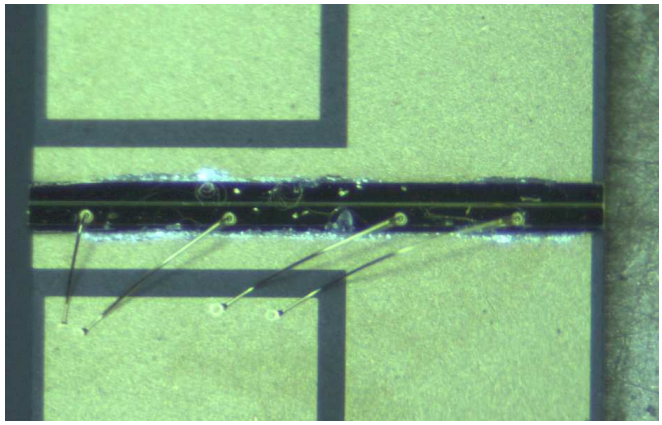


Figure 2.4: Photo of a mounted device on a AlN submount. The electrical contacts were made using ball-type wire bonding.

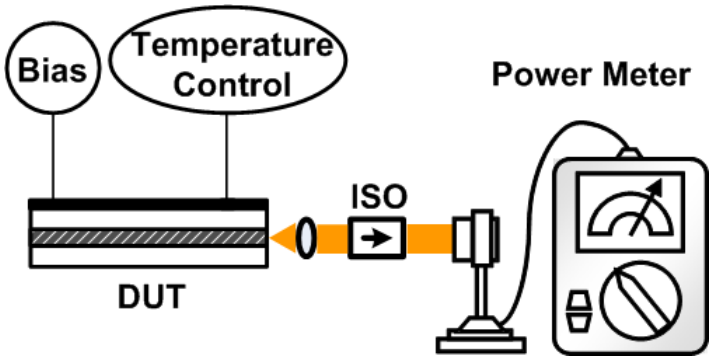



Figure 2.5: Schematic of measurement setup for (L-I) and optical power measurement, DUT: Device Under test.

### 2.3.2 Optical and RF Spectrum Measurement

The optical spectrum of the laser is measured using diffraction-grating based commercial optical spectrum analysers (Ando AQ6317B and Advantest Q8384) covering the infrared wavelength range up to 1700 nm with a minimum resolution bandwidth of 0.01 nm. While the optical spectrum analyser gives information about the optical spectral content of the laser (intensity VS wavelength), no information about the superposition of the spectral content could be retrieved from it. Analysis of power (RF) spectrum is a complementary measurement to the optical spectrum giving useful information about the device's performance. For example, in a mode-locked laser which is the core of this thesis, the RF spectrum gives information on the laser's repetition frequency, its frequency purity (phase-noise information), effective RF power, amplitude noise, and other nonlinear effects such as Q-switching. As we will see later in Chapter 3, in the analysis of the device under optical injection, the RF spectrum of the laser gives valuable information regarding the laser's behaviour. This information along with information coming from time-traces (§ 2.3.4) will give improved understanding of the dynamical regime; for example, whether the laser is injection-locked or unlocked; or if

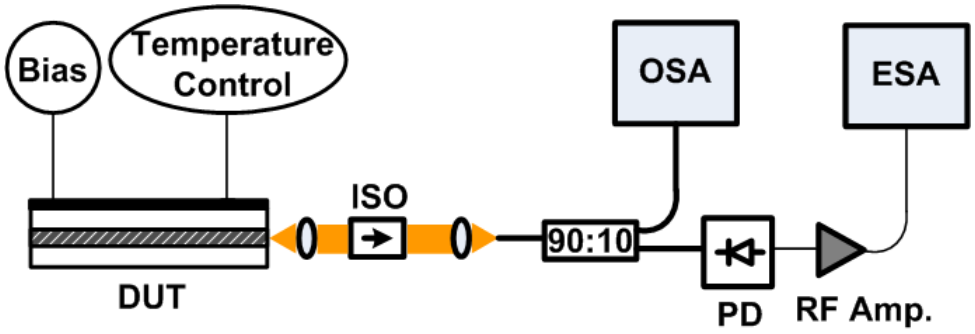



Figure 2.6: Schematic of measurement setup for optical and RF spectra measurement. DUT: Device Under test, ISO: Free space isolator, OSA: Optical Spectrum Analyser, ESA: Electrical (RF) Spectrum Analyser, PD: High speed Photodetector, RF Amp.: RF Amplifier.

it operated in unstable dynamical regimes, etc. In this experiment, we used the RF spectrum analyzer (Agilent, E-series, E4407B model) with minimum resolution bandwidth of 1 kHz and frequency range of 9 kHz-26.5 GHz. The schematic of experimental arrangement for the analysis of optical/RF spectra is shown in Fig. 2.6. As can be seen, an isolator was used to prevent any optical feedback. For automatic measurements, (for example the evolution of optical/RF spectra versus bias current), a computer was used to communicate through instruments under LabView® control.

### 2.3.3 Optical Linewidth Measurement

The optical spectrum analyser provides information on the spectral contents of the laser as described in § 2.3.2. However, high resolution measurements such as optical linewidth of individual modes of the laser could not be carried out using optical spectrum analyzer because of its resolution limitation. For example, a resolution bandwidth of 0.01 nm corresponds to the value of $\approx$ 1.25 GHz. Therefore, zoom around the mode of interest could not give any meaningful information of its linewidth if we expect modal linewidth of sub GHz range. As a result, we use a separate measurement technique for this purpose. In the course of this work, we utilized a heterodyne technique with a local source for optical linewidth measurement of DUT. The experimental arrangement for heterodyne measurement is depicted in Fig. 2.7.

This technique works as following: the light from DUT for linewidth measurements is mixed with the light from a local oscillator using a coupler. The coupler output is divided in two parts: one part goes to the optical spectrum analyzer and the other part is connected to a photodetector and RF spectrum analyzer after passing through a polarization controller. The mixing of light signals from DUT and local oscillator on the photodetector generates a beat signal. The frequency of this beat signal corresponds to the (optical) frequency difference of the mode from DUT and local oscillator. If they are close enough (in optical frequency) the beat frequency lies within the cut-off

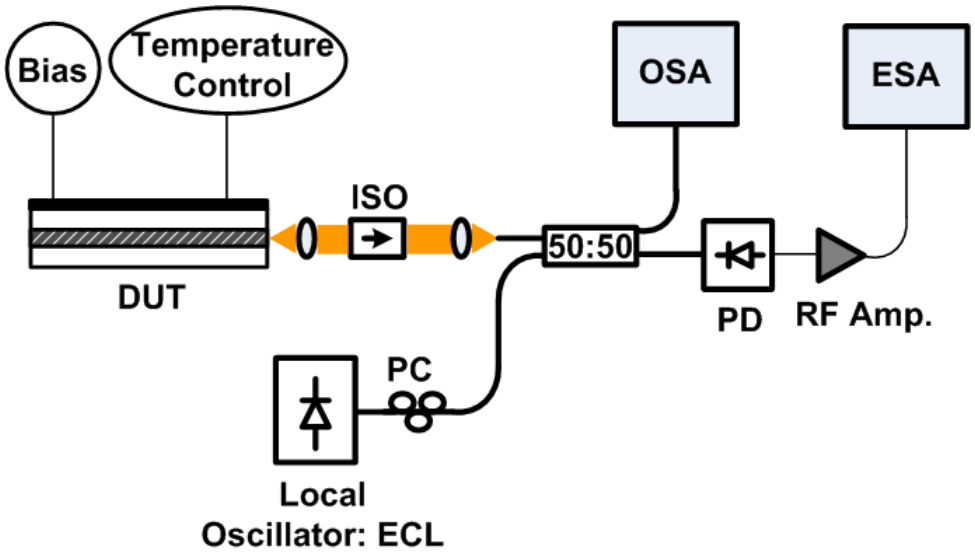



Figure 2.7: Schematic of measurement setup heterodyne measurement. DUT: Device Under test, ISO: Free space isolator, OSA: Optical Spectrum Analyser, ESA: Electrical (RF) Spectrum Analyser, PD: High speed Photodetector, RF Amp.: RF Amplifier., PC: Polarization Controller, ECL: External Cavity Laser.

frequency of the photodetector and it could be detected on the RF spectrum analyzer. Using the polarization controller the amplitude of this beat signal could be maximised provided the two light signals shining on the photodetector have the same polarization. If the phase noise of the local oscillator is much lower than that of DUT, the phase noise of the beat signal would be almost equal to that of the DUT. One advantage of this technique is that any asymmetry in the lineshape of DUT will transfer to that of the beat signal [147]. The local source is usually an external cavity laser with sub MHz optical linewidth.

### 2.3.4 Time-Domain Measurement

None of the techniques mentioned above provide information about the actual time-trace of laser's intensity output. As we will see later, in addition to the information from the RF spectrum, information about real time-trace of intensity will be useful to distinguish the dynamical regimes of laser in a particular scenario such as optical injection. For this purpose, we used a digital oscilloscope with maximum sampling rate of 40 GHz and input electrical bandwidth of 12 GHz. Considering Nyquist rate, any temporal feature with frequency band less than 20 GHz will be recovered using such a high sampling rate. However, the bandwidth limitation of the input port will suffice for a 10 GHz device to study the time-trace of dynamical regimes as the main components of the regimes will lie between 0 and 5 GHz.

### 2.3.5 Intensity Autocorrelation Measurement

Direct measurement of high-speed (GHz repetition range) ultrashort optical pulses with ps or less pulse duration is not possible using optical sampling or a fast photodetector. Therefore, an alternative technique is required for this purpose. Intensity autocorrelation is one of the popular techniques for measurement of such pulses. This method is based on measurement of pulsewidth using the pulse itself without any other references; a basic diagram of an intensity autocorrelator is shown in Fig. 2.8. For this purpose, the pulse is divided into two arms one with a fixed delay and the other one with variable delay. The two beams are recombined and focused on a nonlinear element for second harmonic generation (SHG)(usually an ultrathin nonlinear optical crystal) that generates a second harmonic signal which is proportional to $(E(t)+E(t-\tau))^2$. $E(t)$ is the electrical field of the original signal and $E(t-\tau)$ is the delayed signal. The term which is proportional to $E(t)E(t-\tau)$ is retained from the SHG generated signal and detected by a slow photodetector. The photocurrent generated by such a low photodetector will read:

$$i(\tau) \propto \int_{-\infty}^{+\infty} (E(t)E(t-\tau))^2\, dt = \int_{-\infty}^{+\infty} I(t)I(t-\tau)\, dt. \tag{2.1}$$

which integral equals $A(\tau)$, as the intensity autocorrelation.

Depending on the delay time ($\tau$), when the two pulses have better overlap, the SHG signal is stronger leading to higher autocorrelation intensity. An important fact about the intensity autocorrelation is that it does not give exact shape of the pulses. For example, symmetric and asymmetric pulse shapes can result in the same autocorrelation signal because of the nature of the autocorrelation coming from Eq. 2.1. Usually, the autocorrelation is measured with assumption of the pulse shape; for example, the autocorrelation of a Gaussian or $\text{Sech}^2$ pulse has the same temporal distribution with

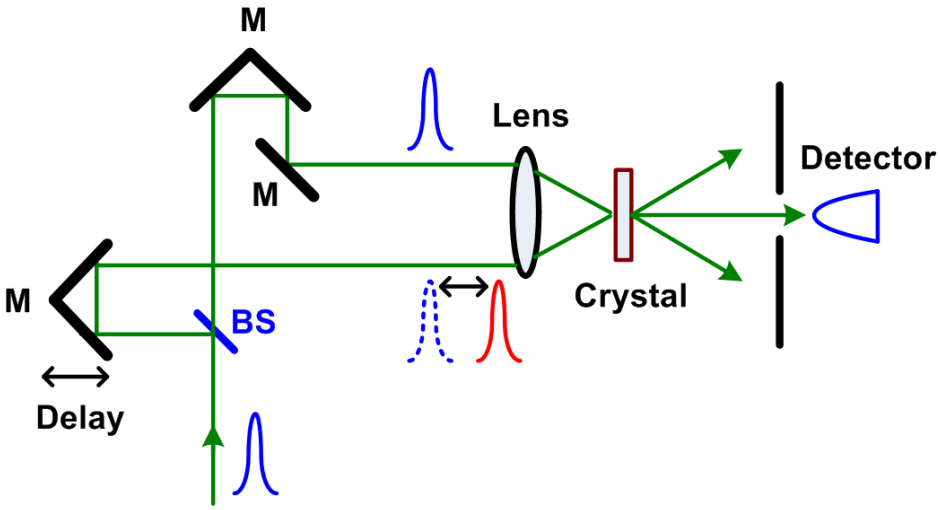



Figure 2.8: Schematic diagram of an intensity autocorrelator. BS: Beam splitter, M: Mirror.

broadening of the pulse duration. The actual pulse duration is calculated from the full-width at half maximum (FWHM) of the measured trace fitted to the function and divided by the de-convolution factor. This factor is 1.54 for $\text{Sech}^2$ pulse and $\sqrt{2}$ for Gaussian pulses. It has to be mentioned that the SHG autocorrelation in a non co-linear mode is a *background-free* autocorrelation which means that the intensity of the autocorrelation signal vanishes as the time delay becomes large; the autocorrelation traces shown in this thesis are of this type.

The schematic of the arrangement for SHG autocorrelation measurement is shown in Fig. 2.9. As can be seen, the signal passed through a polarization controller before the autocorrelator to remove the sensitivity of the instrument to the input polarization. The autocorrelator used in this work was an APE PulseCheck autocorrelator [148] with maximum scan range of 150 ps with sensitivity of $\sim 10^{-4}$ $\text{W}^2$. The sensitivity is defined as the product of averaged power ($P_{Av.}$) and peak power ($P_{Peak}$). The latter for a Gaussian pulse equals:

$$P_{Peak} = 0.94 \cdot \frac{E_P}{\Delta\tau} \tag{2.2}$$

where $\Delta\tau$ is the pulse duration and $E_P$ is the pulse energy:

$$E_P = P_{Av.} \cdot T \tag{2.3}$$

in which the $T$ is the period of the pulses. Substituting 2.3 into Eq. 2.2 yields:

$$P_{Av.} \cdot P_{Peak} = (P_{Av.})^2 \, \frac{0.94 \cdot T}{\Delta\tau}. \tag{2.4}$$

Care has to be taken for the average power requirement to have sensitivity above the instrument's limitation. As a rule of thumb, the minimum average power to have clean traces on the autocorrelator for a 5 ps Gaussian pulse with period 48 ps (21 GHz) will be a few mW. If amplification is required before the autocorrelator, it is very important to consider any dispersion compensation using an Erbium Doped Fibre Amplifier (EDFA) for a wide optical spectrum. This might lead to overestimation of

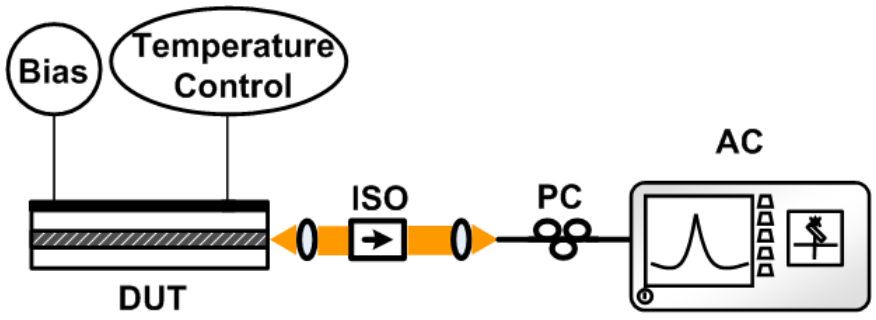



Figure 2.9: Schematic of measurement setup for pulse-width using intensity autocorrelator. DUT: Device Under test, ISO: Free space isolator, PC: Polarization Controller, AC: Autocorrelator.

the actual pulsewidth as the EDFA compensates the residual chirp coming from the mode-locked laser in addition to providing amplification.

## 2.4 Characterisation of Self Mode-Locked Lasers (SML)

In this section, we present measurement results on devices lasing in SML mode. The results are on the devices with single-section forward biased or two-section devices with the gain section forward biased and the absorber floating (open) or forward biased above the transparency point.

The L-I curves for a number of devices with SML operation are shown in Fig. 2.10. Devices with different cavity lengths and active region structures (DWELL, DBARR) are shown. As can be seen, for DWELL devices, the threshold current for the 4 mm long device was $\approx$ 145 mA which decreased to $\approx$ 82.5 mA for DWELL shorter device (2 mm long). For DBARR devices, the threshold current of the 2 mm long device was $\approx$ 42.5 mA decreasing to $\approx$ 34.5 mA for the device with the length of 0.8 mm. Comparing the values of threshold current and the length, an increase of threshold current density for shorter devices is confirmed regardless of the active region. This is due to increase in the cavity loss when shortening the cavity length. Also, by comparing DWELL and DBARR devices with the same length, one see lower threshold current for DBARR devices. This could be due to increased number of quantum-dash mono-layers in DBARR (9) compared to 6 layers for DWELL structure in this study. The slope

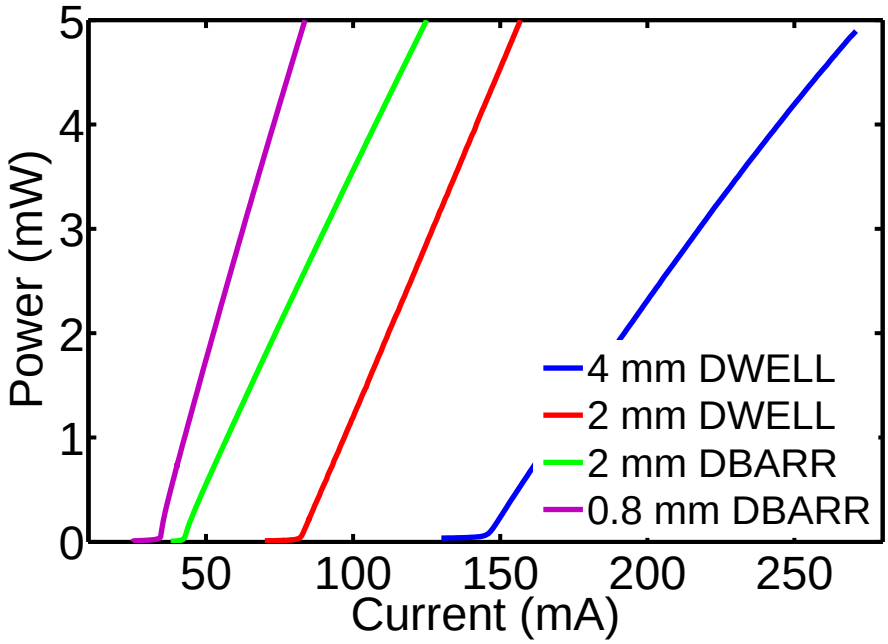



Figure 2.10: Light-Current (L-I) measurement of SML devices with different cavity length and active region structures.

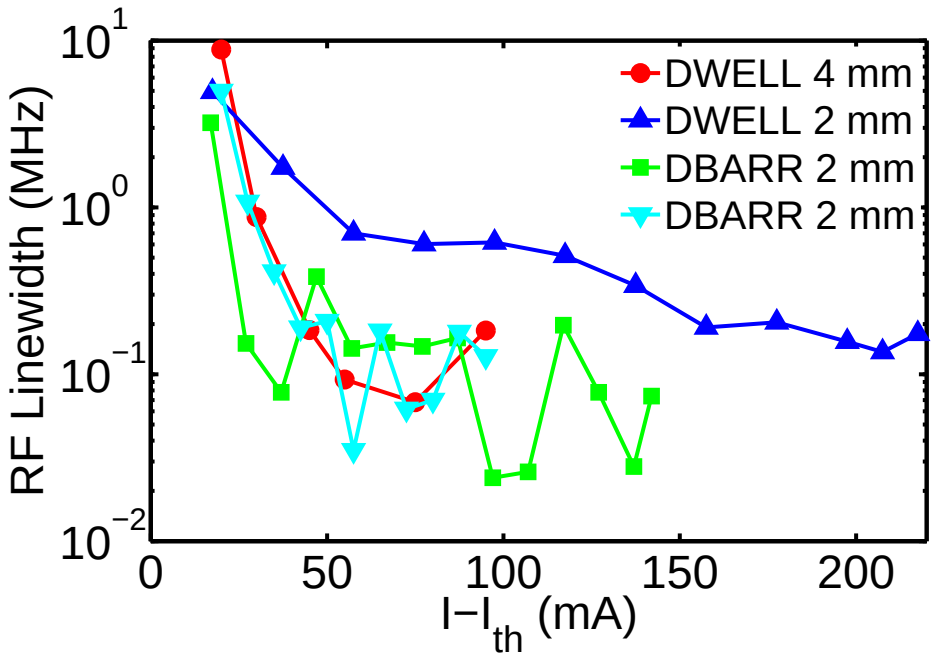



Figure 2.11: RF linewidth of repetition-rate for SML devices of different cavity lengths and active layer structures for excess currents above threshold ($I - I_{th}$).

efficiencies for the devices were 0.04 W/A for 4 mm DWELL, 0.07 W/A for 2 mm DWELL, 0.06 W/A for 2 mm DBARR, and 0.1 W/A for DBARR device with 0.8 mm length.

A number of SML devices were characterised in terms of RF linewidth of their repetition frequency for different bias currents; the results are shown in Fig. 2.11. The DWELL devices where 2 mm and 4 mm single-section devices and the DBARR devices were two-section devices with absorber lengths of 2% and 9.4% operating as SML with the absorber left floating (open). The values of RF linewidth measured has been plotted versus the excess current above threshold. As can be seen, the RF linewidth was quite broad (few to 10s of MHz) when the device is biased slightly above threshold. When the bias current was increased, the RF linewidth became narrower gradually. RF linewidth less than 100 kHz is achievable for both DBARR and DWELL devices; the lowest value was measured to be around 24 kHz (the DBARR device). The threshold currents for DBARR devices were 42.5 mA and 58 mA, respectively. It worth to mention that for all these devices there was no deliberate passive (such as saturable-absorber) mechanism to form mode-locking. For single-section devices, only the gain section was forward biased above the threshold point. For the two-section devices, when the absorber was left floating (open) the voltage was around 0.85 V. The absorption current decreases to zero at this voltage when the absorber was connected to a power-supply and biased at the same voltage. This indicates no effective absorption such that the absorber section operated at or above transparency point, performing as a passive section. The absorber could be biased above this point to operate as a gain-section if the voltage is increased

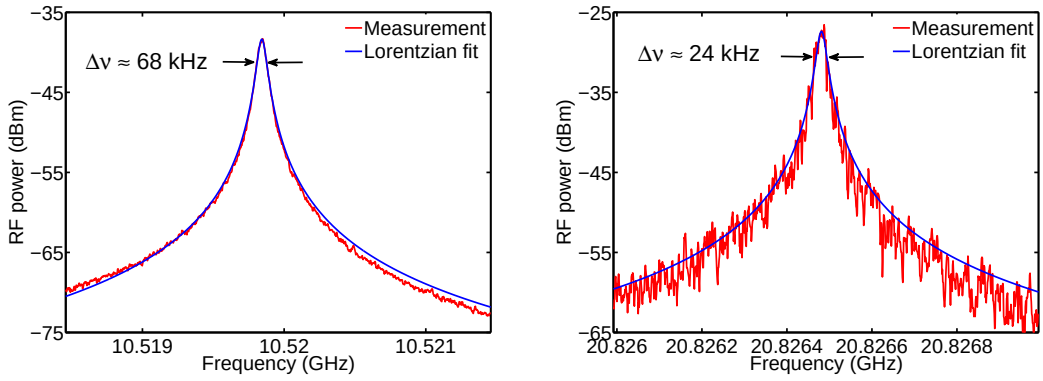



Figure 2.12: Zoom of measured RF linewidth of the repetition-rate frequency for SML devices (red-line) and Lorentzian fit (blue-line). (a). 4 mm single-section DWELL (10.5 GHz), $I = 220$ mA. Resolution bandwidth: 10 kHz, Video bandwidth: 0.1 kHz. (b). 2 mm, two-section DBARR (21 GHz), $I = 155$ mA, absorber: open. Resolution bandwidth: 10 kHz, Video bandwidth: 1 kHz. $\Delta\nu$: Full-width at half maximum (FWHM) of RF linewidth.

slightly above this point. In either these cases, the device operated as a *single-section* device.

The zoom of RF spectra for narrowest RF linewidth for DWELL device (10.5 GHz, 4 mm length) and DBARR device (21 GHz, 2 mm length) is shown in Fig. 2.12, along with their Lorentzian fit. The lowest value for the DWELL device was measured to be around 68 kHz and RF linewidth as narrow as 24 kHz was measured for DBARR device. Examples of optical spectra for DWELL and DBARR devices are shown in Fig. 2.13. Comparing the spectra for DWELL and DBARR devices, one can see wider optical spectra from DBARR devices (10 dB width about 12 nm). Such a wide optical spectrum, combined with narrow RF linewidth and reasonable amount of power is potentially an attractive solution in many applications. However, as we will see later, one limiting factor exists with the operation of such devices. Large amount of chirp in the cavity effectively prevents formation of any pulses directly from these lasers.

As shown in Fig. 2.14, the autocorrelator gives an indication of the pulsewidth based on some assumptions. The measured autocorrelation traces for SML devices with different cavity lengths and active region structure are shown in Fig. 2.14. As can be seen, for all of the devices no clear pulse traces exist in the measurements. The traces are almost flat for DWELL devices and for 2 mm long DBARR device a DC trace with small modulation content is observed; the time spacing of the peaks is measured to be around 49.8 ps, corresponding to 20.1 GHz which is close to the repetition rate of the laser. The trace for 0.8 mm DBARR device (absorber length fraction: 14.8%, floating), shows some spikes with high DC levels; the time spacing of the spikes was around 19.4 ps, corresponding to 51.5 GHz which is close to the actual repetition rate of the laser.

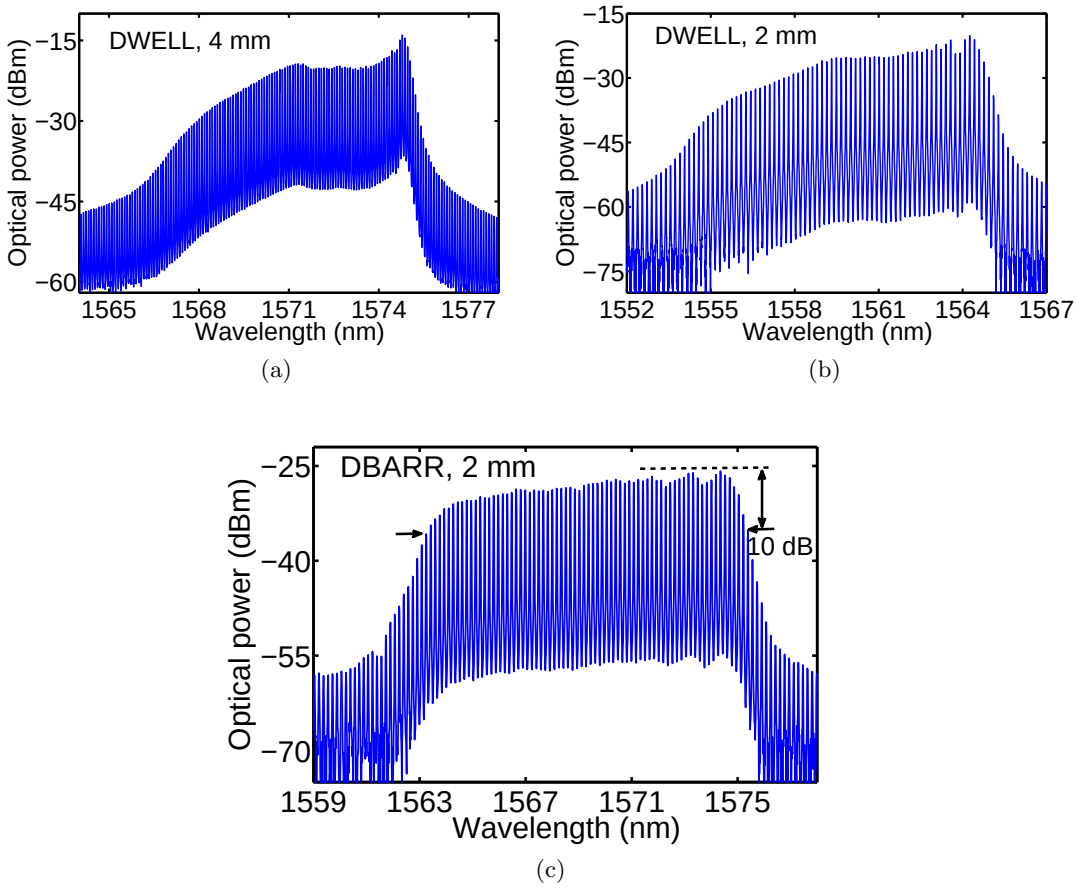



Figure 2.13: Examples of optical spectra for SML devices with DWELL and DBARR strcutures. (a). 4 mm single-section DWELL (10.5 GHz), $I = 300$ mA. (b). 2 mm single-section DWELL (21 GHz), $I = 252.4$ mA. (c). 2 mm two-section DBARR with 2% absorber (21 GHz), $I = 190.4$ mA, absorber: float.

This could be a clear indication of no *pulsed* operation in the time-domain. The physical mechanism behind this is not well understood, but it can be confirmed experimentally that high amount of dispersion comes from large deviation of static phase between the longitudinal modes [149]. This leads to less constructive superposition of the modes, and *suppressing* the pulsed intensity output of the laser. This phenomenon is less severe for shorter devices as fewer modes are present in the cavity. This could be seen for 0.8 mm device a trace of pulse/spikes with large DC background are present.

### 2.4.1 Pulse Compression in SML Devices

As shown in § 2.4, the direct autocorrelation trace from the SML devices did not show clear pulses. This could be a result of nonlinear phenomena in the cavity resulting in phase-locked modes with unequal static phases [149]. This leads to nondestructive superposition of the modes, effectively causing a high amount of chirp in the intensity of the laser. To overcome this problem, pulse compression is necessary to generate

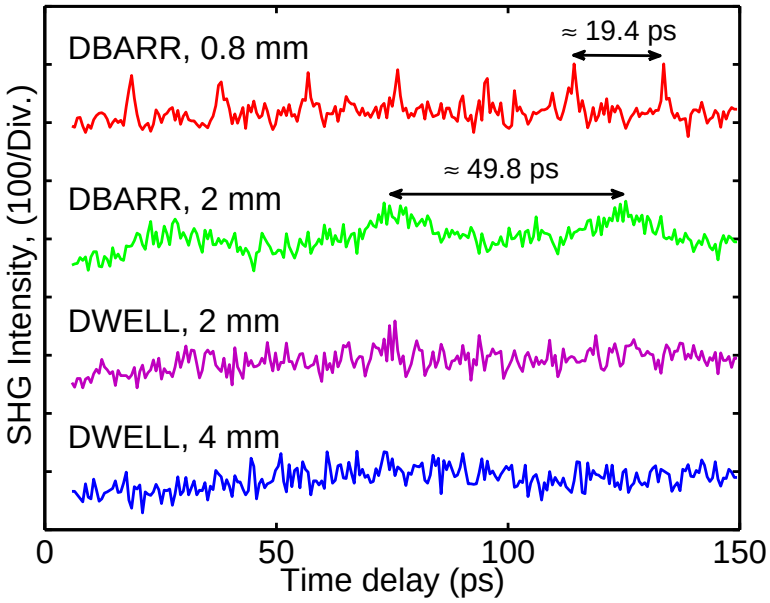



Figure 2.14: Measured autocorrelation trace for SML devices with different cavity length and active region. Devices: DWELL, 4 mm, $I = 300$ mA. DWELL, 2 mm, $I = 300$ mA. DBARR, 2 mm, $I = 120$ mA, absorber (2.0%): float. DBARR, 0.8 mm, $I = 120$ mA, absorber (14.8%): float.

pulses from some or all of the lasing modes. We present pulse generation from SML devices using two methods; filtering and compensation using a single-mode fibre with a certain length.

The experimental arrangement for the filtering method is shown in Fig. 2.15. As can be seen, light was coupled from one facet through a free space isolator (> 65 dB isolation) and a pair of lenses to a single-mode fibre, then amplified by an EDFA and passed through a tunable bandpass filter (C-Band) with fixed full-width at half maximum of 0.8 nm. The output of the filter was utilized for analysis of the optical and RF spectra and pulse-width measurements via the autocorrelator. DWELL devices with repetition frequencies of 21 and 10.5 GHz and DBARR devices with repetition rate of 21 GHz were studied in this experiment.

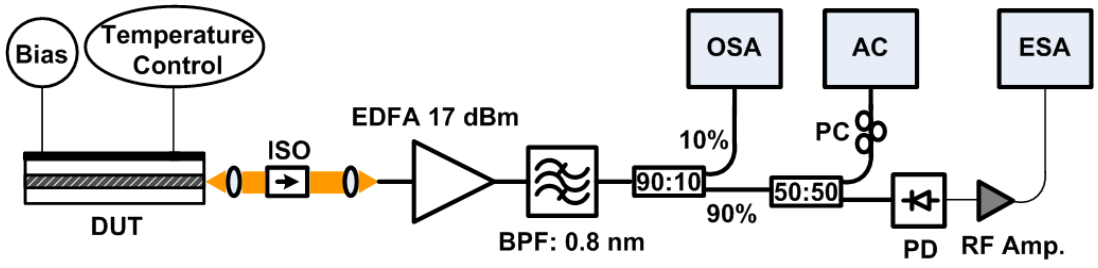



Figure 2.15: Schematic of measurement arrangement for pulse compression of SML device using filter. Acronyms: BPF: Band-pass filter.

Fig. 2.16(a) shows the optical spectrum of the 21 GHz laser without filtering at bias current of 300 mA ($3.6I_{th}$) at mount temperature 20°C, and filtered spectra at different regions of the whole optical spectrum. The autocorrelation trace of the laser before filtering (black) and after filtering (red) at the center wavelength of $\lambda_5$ (around 1560 nm) with Sech$^2$ pulses (blue) is shown in Fig. 2.16(b). As can be seen, the autocorrelation trace of the whole spectrum does not show pulses, but clean narrow pulse trains are produced after spectral filtering. This is because of the presence of a high level of dispersion in the cavity, causing large phase differences between the longitudinal modes and preventing generation of narrow pulses despite a broad optical spectrum. On the other hand, filtering a part of this spectrum actually reduces the chirp due to selection of a few pulses with closer static phase difference and thus clear pulses could be generated. The dependence of the pulse duration on the filter wavelength is shown

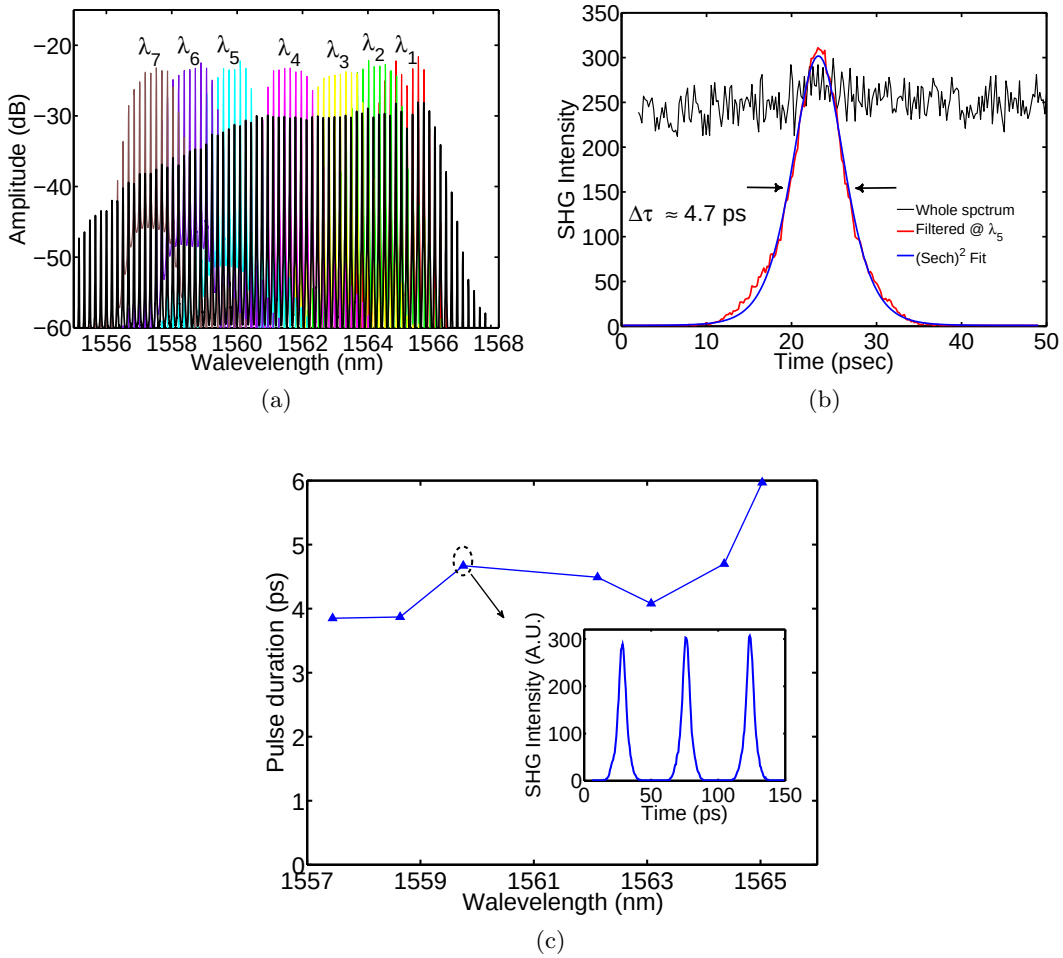



Figure 2.16: (a). Optical spectra of the 21 GHz laser without filtering (black) and filtered (colored) at different center wavelengths shown by $\lambda_1$ to $\lambda_7$. (b). Autocorrelation traces of pulses using the whole spectrum (black) and filtered at $\lambda_5$ (1559.75 nm). (c). Dependence of the pulse duration with filtered spectrum on the center wavelength of the filter. Inset shows three consecutive pulses from the autocorrelator.

in figure Fig. 2.16(c). The pulse-duration ranged from 3.9-4.7 ps except for pulses generated by filtering at the centre wavelength of ≈1565 nm which had ≈6 ps. The deviation could be due to modulation at the laser's optical spectrum around 1565 nm which was reproduced in the filtered spectrum. The time bandwidth product (TBP) of all the pulses, with 0.8 nm spectral width of the filter, was in the range 0.37 (transform limited) to 0.46 except at the centre wavelength which was 0.6.

We reproduced this pulse generation with longer single-section lasers with the same structure, repetition rate 10.5 GHz (4 mm cavity length). The emission wavelength of this laser was beyond 1565 nm (wavelength limit for the filter) so the temperature was reduced to 15°C to match the optical spectrum partially with the filter's limit. The optical spectra of the laser for both cases are shown in Fig. 2.17(a) with captured trace for single pulse in Fig. 2.17(b) . Similar results to the 21 GHz device have been reproduced by the longer device; with pulse durations ranging from 4.9-5.9 ps and

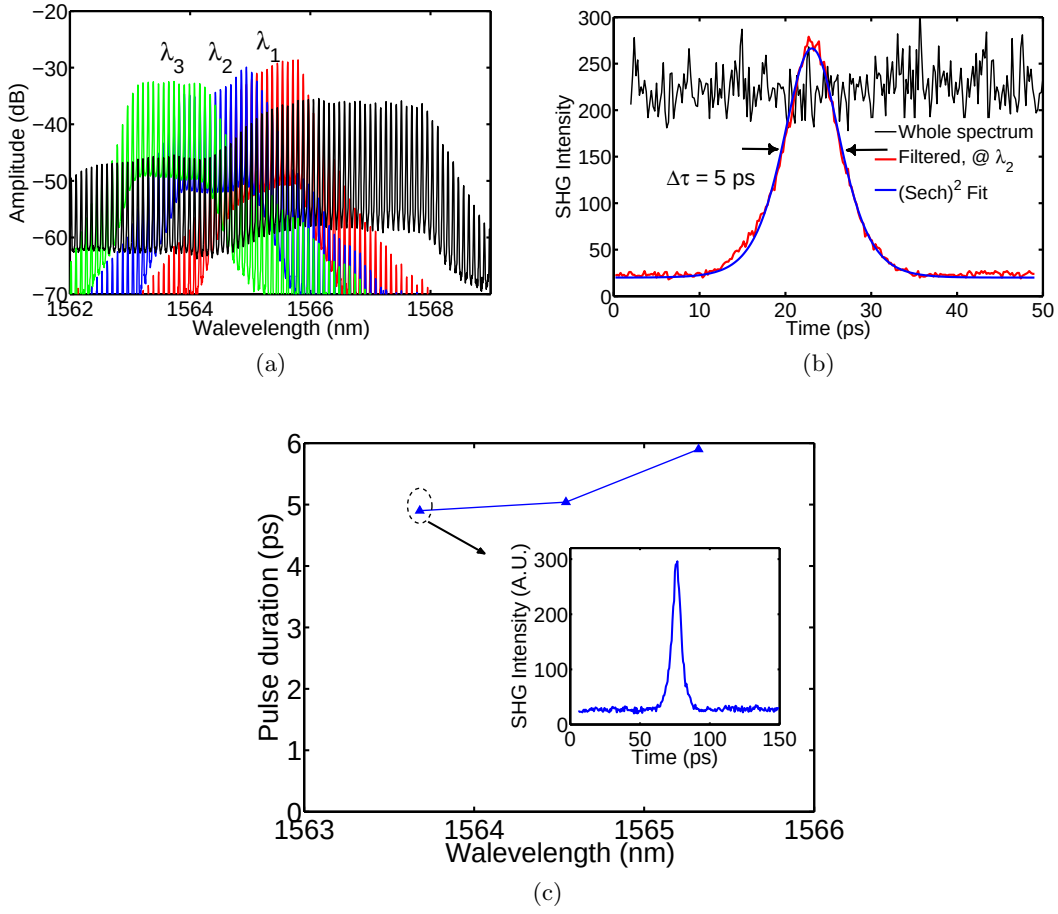



Figure 2.17: (a). Optical spectra of the 10.5 GHz laser without filtering (black) and filtered (colored) at different center wavelengths shown by $\lambda_1 - \lambda_3$. (b). Autocorrelation traces of pulses using the whole spectrum (black) and filtered at $\lambda_2$ (1564.54 nm). (c). Dependence of the pulse duration of filtered spectrum on the center wavelength of the filter. Inset shows single captured pulse from the autocorrelator.

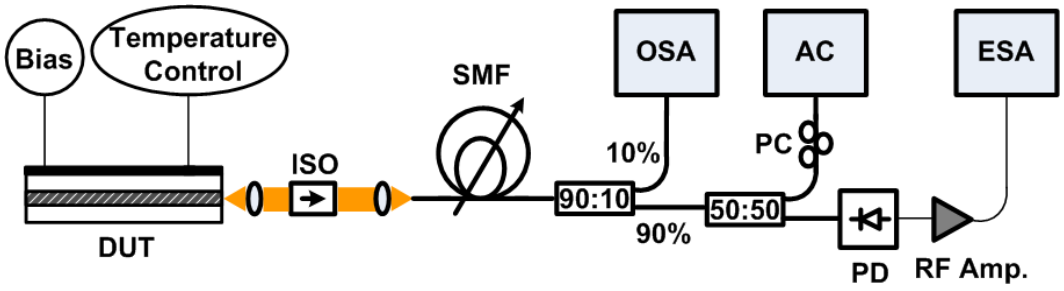



Figure 2.18: Schematic of experimental arrangement for pulse compression of SML device using single-mode fibre with variable length.

TBPs 0.34-0.6 (shown in Fig. 2.17(c)), confirming that the pulses were nearly transform limited. Similar results were observed using DBARR SML devices.

The high amount of chirp in the output of the SML device could be compensated using a single-mode fibre with proper selection of length of the device. In fact, the chromatic dispersion in the fibre can compensate the large static phase difference of the longitudinal modes of SML, provided the sign of the dispersion parameter matches with the trend of spectral phase. The schematic of the experimental arrangement for this measurement is shown in Fig. 2.18 where spools of single-mode fibre with different lengths (from 20 - 200 m) were used. The output of the fibre was analyzed using the autocorrelator. The device used in this experiment was the DBARR SML with 2 mm length and 2% absorber section left floating. The autocorrelation trace for the device biased at 125 mA with different lengths of fibre is shown in Fig. 2.19. As can be seen,

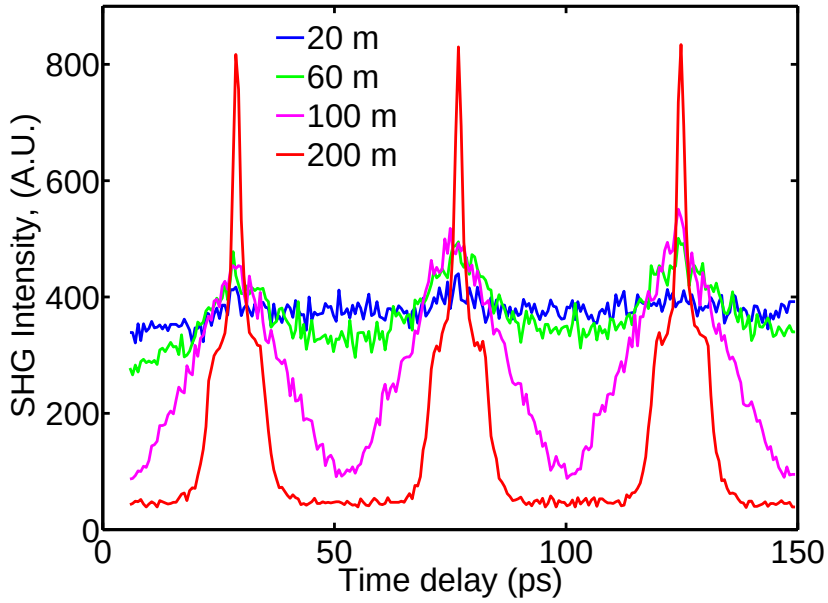



Figure 2.19: Autocorrelation traces for the 2 mm long DBARR, (absorber, 2%: floating), $I$ =125 mA, fibre length varied from 20 to 200 m.

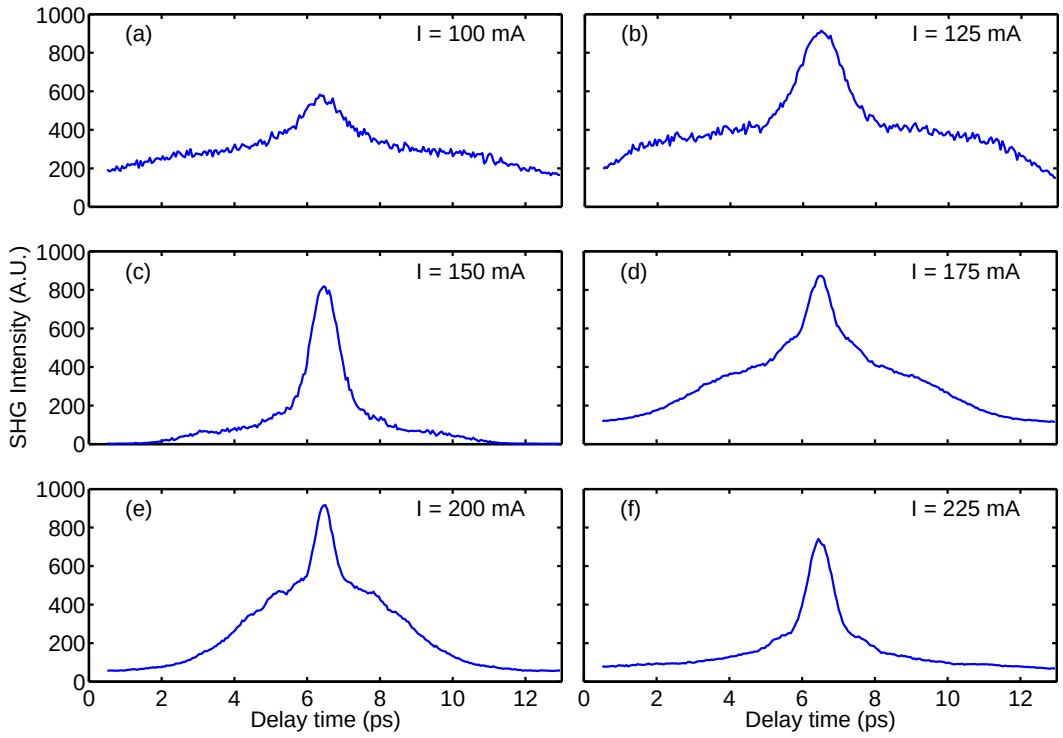



Figure 2.20: Autocorrelation traces for the 2 mm long DBARR, (absorber, 2%: floating), with fibre length of 200 m. Bias current varied from 100-200 mA.

by increasing the length of the fibre up to 100 m, the traces showed oscillation with more modulation depth. At length of 200 m a clear trend with high extinction ratio was observed confirming effectiveness of this method to compensate the dispersion.

This measurement was repeated keeping the fibre length fixed and varying the bias current, shown in Fig. 2.20(a-e). The fibre length was 200 m and the bias current varied from 100 mA to 225 mA with 25 mA current step. The shape of the traces consists of a peak which follows a Gaussian distribution on a pedestal; as the current increased, the ratio of the pedestal to the peak decreased up to 150 mA. At 150 mA a more regular autocorrelation trace was observed (Fig. 2.20(c)). Increasing the current beyond 150 mA changed the shape of trace back to that below 150 mA, with a large pedestal with a Gaussian distribution on top. This study reveals the fact that the spectral phase is dependent on bias current and for each current an optimized fibre length should be recruited to properly compensate the dispersion. The zoom of the autocorrelation trace with Gaussian fit at bias current of 150 mA is shown in Fig. 2.21. The pulsewidth after deconvolution was measured to be ≈0.65 ps. Considering the optical spectrum at this current, the spectral width was around 0.76 THz (6.2 nm) giving 0.49 for the TBP of the pulses. This value was slightly higher than the transform limit for the Gaussian pulse which is 0.44, a clear indication of almost complete dispersion compensation with this length of fibre.

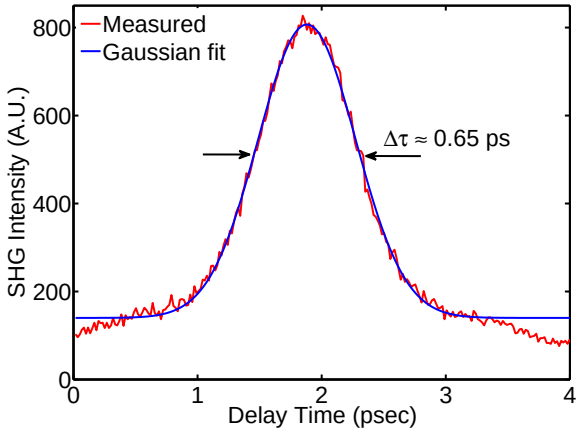



Figure 2.21: Gaussian fit (blue curve) to the measured autocorrelation trace (red curve) for the 2 mm long DBARR, (absorber, 2%: floating), with fibre length of 200 m. Bias current: 150 mA. The pulse duration after deconvolution was 0.65 ps.

## 2.5 Characterisation of Saturable-Absorber Mode-Locked Lasers (SAML)

In this section, we present measurement results on DBARR two-section devices with SAML operation. First, the results on 21 GHz devices are presented followed by results on 52 GHz devices.

### 2.5.1 21 GHz Devices

The Light-Current (L-I) curves for I3-4 (2 mm, absorber length ratio: 9.4%) for different absorber voltages are shown in Fig. 2.22. The regimes of SML and SAML operations are denoted in the L-I curves. For absorber biased above the transparency point, the absorbed current reduces to zero; thereby keeping the absorber as a passive section. Increasing the voltage slightly above this value (≈0.8 V) the absorber operates as a gain section. For both these cases the mode-locking mechanism was governed by the SML mechanism and the laser operates similar to a single-section device. The threshold current of the device was around 32 mA ($V_{Abs}$ = 0.95 V), increasing to ≈85 mA for $V_{Abs}$ = 0.3 V and ≈130 mA for $V_{Abs}$ = -0.5 V, when the laser operated as a SAML. As can be seen, this increase in the threshold current was followed by a decrease in the slope efficiency from ≈0.060 W/A ($V_{Abs}$ = 0.95 V) to ≈0.027 for $V_{Abs}$ = 0.3 V and ≈0.015 for $V_{Abs}$ = -0.5 V. No hysteresis was observed in the L-I curves for the laser operating as SML or SAML.

The bias parameters of the device for SAML operation were typically around 100-200 mA for gain current and approximate absorber voltage of -0.6 V to 0.3 V. More stable operation was usually observed when the absorber voltage slightly biased above 0 V,

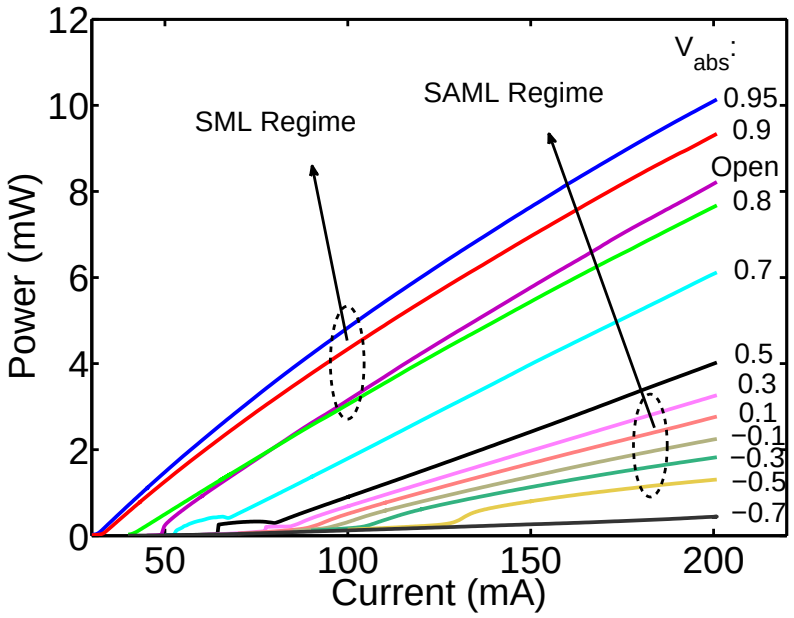



Figure 2.22: Light-Current (L-I) measurement of I3-4 for different values of absorber bias voltage. Regimes of SML and SAML operation are shown in the curves.

(0.1-0.2 V). Fig. 2.23 shows the dependence of the pulse-width (left Y axis) and RF linewidth (right Y axis) on bias current for two different absorber voltages. As can be seen, picosecond pulse generation without any pulse compression is possible. The trend of pulse-width against current is increasing for both voltages which is well understood

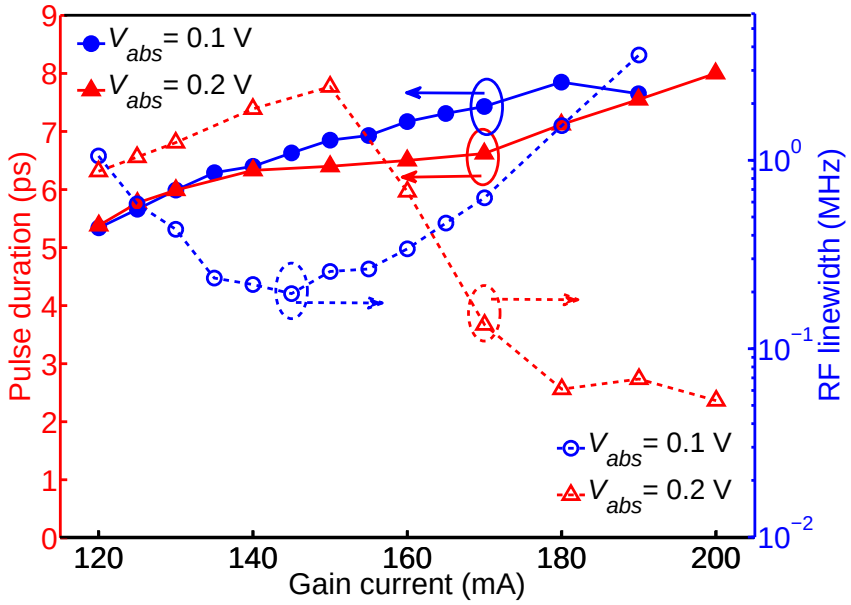



Figure 2.23: Dependence of the pulse-width (Gaussian fit, left Y axis) and RF linewidth (Lorentzian fit, right Y axis) on the gain current for two absorber voltages. Device: I3-4.

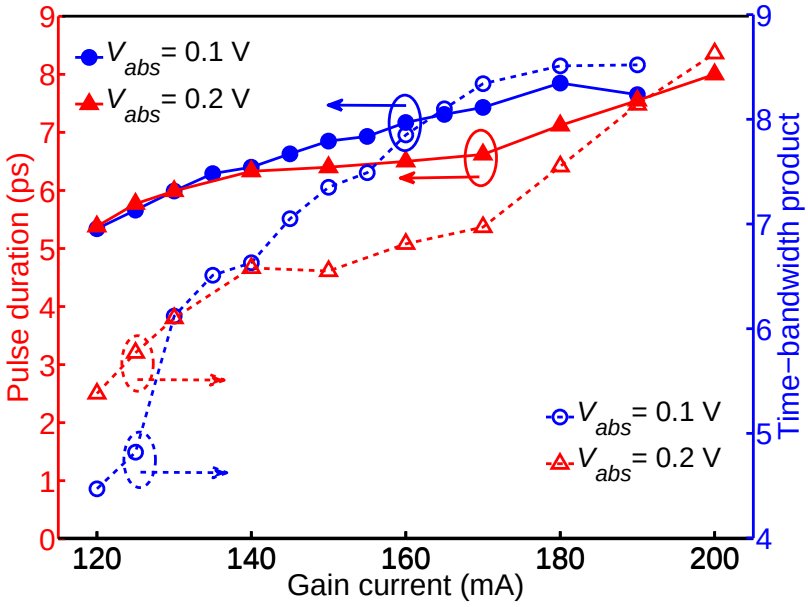



Figure 2.24: Dependence of the pulse-width (Gaussian fit, left Y axis) and TBP (right Y axis) on the bias parameters the same as Fig. 2.23. Device: I3-4.

in quantum-dot mode-locked lasers at 1.3 $\mu$m [150]. Slightly better pulse-widths were observed for $V_{Abs} = 0.2$ V. This is in contrast to what has been reported for quantum-dot mode-locked lasers at 1.3 $\mu$m where usually stable mode-locking operation occurs with the absorber negatively biased [43, 151]. Here, it looks like there is sufficient absorption at such positive voltages for the absorber. In addition, the RF linewidth is strongly dependent on the absorber voltage. For $V_{Abs} = 0.1$ V there is a decreasing and then increasing trend for the RF linewidth, whereas it follows a different trend for $V_{Abs} = 0.2$ V and sub 100 kHz RF linewidth is achievable at this absorber voltage.

An indication of the amount of chirp in these pulses is shown in Fig. 2.24 along with the pulse-width for the same bias conditions as Fig. 2.23. The TBP of the pulses has been calculated and depicted in the left Y axis. As can be seen, the TBP increases as the gain current increases. As shown in Fig. 2.23 regarding the increasing trend of the pulse-width, the optical spectrum also broadens with increase of bias current (not shown); therefore, the TBP should increase. The values of TBP range from 4.5-8.6 indicating significant chirp in the pulses related to the Fourier Limit for Gaussian pulses (0.44). As we will see later in Chapter 4, the TBP could be reduced significantly using optical injection-locking.

An example of the measured RF spectra for different gain currents is shown in Fig. 2.25 for $V_{Abs} = 0.2$ V and three different gain currents. As can be seen, by increasing the current the repetition frequency decreases while we see both broadening and narrowing of the RF linewidth. The traces for the RF linewidth followed the Lorentzian distribution very well as depicted in Fig. 2.26. Comparing the general trend of RF linewidth

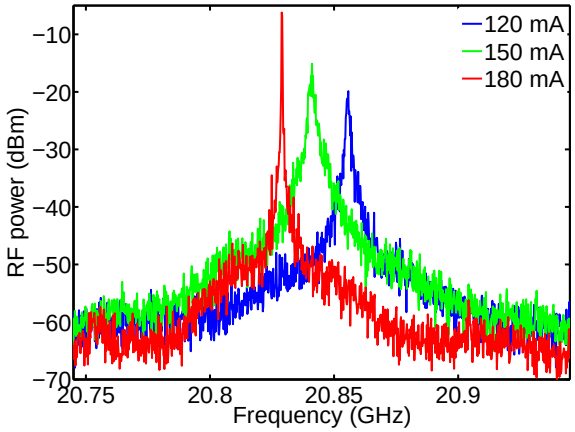



Figure 2.25: RF spectra of the mode-locked beat frequency (repetition-rate) of for different gain currents and $V_{Abs} = 0.2$ V (Device: I3-4).

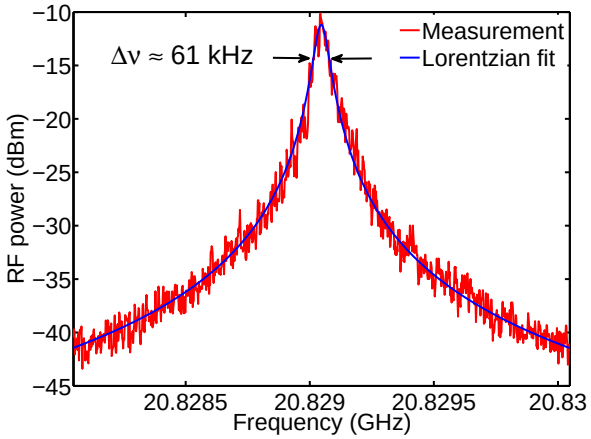



Figure 2.26: RF linewidth of the repetition-rate frequency (red curve) with its Lorentzian fit (blue curve). Device: I3-4, $I_{Gain} = 180$ mA, $V_{Abs} = 0.2$ V.

with SML, higher values were observed for SAML devices. On the other hand, the RF peak was usually higher by 10-15 dB than SML for similar average power even for lower RF linewidth operation of the latter. This could be an indication of more RF power available from SAML comparing to SML despite sub 100 kHz RF linewidth being easily achievable from SML devices.

Fig. 2.27 shows the optical spectrum of the device with the same absorber voltage and three different currents. With increase in current the optical spectrum shifts to longer wavelengths, as a result of ohmic heating. Also, the spectral width of the optical spectrum increases with current which contributed to the monotonic trend in the TBP with current in Fig. 2.24. The autocorrelation traces (solid-lines) with their Gaussian fit (dashed-lines) for the same bias parameters are shown in Fig. 2.28; the traces have been shifted for clear viewing. The traces fit by a Gaussian very well, and their calculated pulse-width after de-convolution increased with the current.

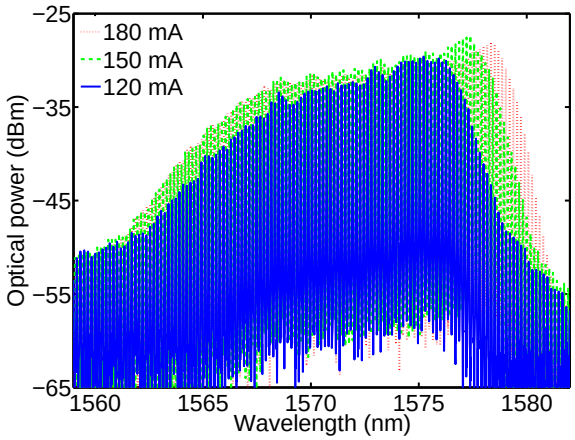



Figure 2.27: Dependence of the pulse-width (Gaussian fit, left Y axis) and TBP (right Y axis) on the bias parameters the same as Fig. 2.23 ($V_{Abs} = 0.2$ V). Device: I3-4.

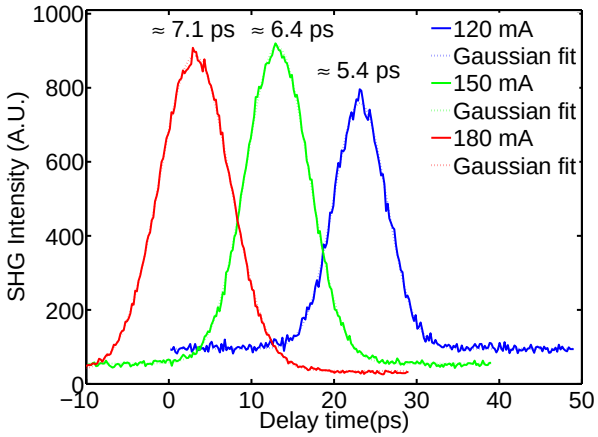
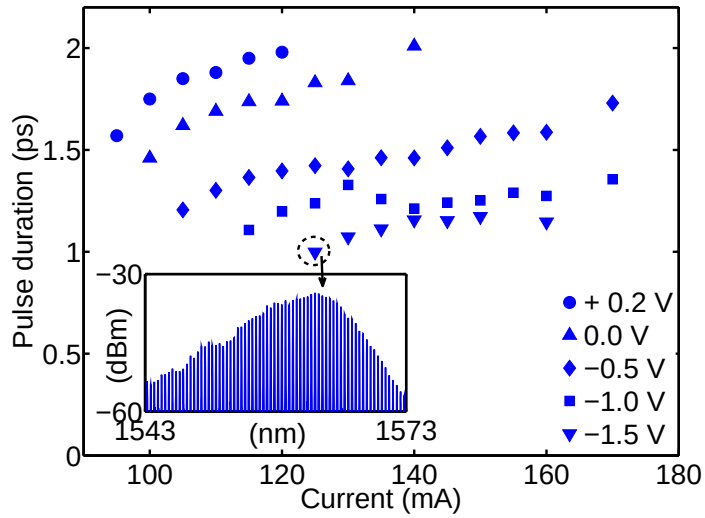



Figure 2.28: Dependence of the pulse-width (Gaussian fit, left Y axis) and TBP (right Y axis) on the bias parameters the same as Fig. 2.23 ($V_{Abs} = 0.2$ V). Device: I3-4.

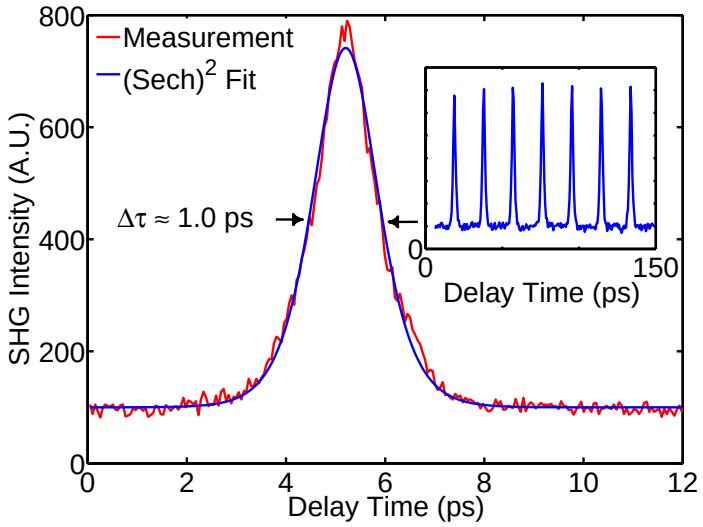
### 2.5.2 52 GHz Devices

The DUTs had a total cavity length of 810 $\mu$m with the absorber lengths of 70, 95, and 120 $\mu$m with isolation resistance of more than 15 k$\Omega$. The first two devices did not show SAML operation for absorber voltage down to -7 V. The third device with absorber length ratio of $\approx$ 14.8% showed SAML operation when the absorber voltage ranged from 0.2 V down to -1.8 V. The threshold current was about 35.5 mA with slope efficiency of 0.12 W/A when the absorber was forward biased above the gain point (SML operation). The threshold current and slope efficiency for 0.2 V biased absorber was around 72 mA and 0.09 W/A, respectively. For absorber biased at -2.0 V, the threshold current increased to 78.5 mA with a slope efficiency of 0.02 W/A.

The measured pulsewidth versus current for the absorber voltage range within the SAML regime is shown in Fig. 2.29(a). As can be seen, the pulsewidth decreased with




(a)




(b)

Figure 2.29: Measurement of pulsewidth for 52 GHz SAML device. (a). Measured pulsewidth versus gain current for different absorber voltages. (b). Single pulse captured with its Sech$^2$ fit, the inset shows the autocorrelation trace of seven consecutive pulses.

decreasing absorber voltage and increases for a fixed voltage when the current increased. The de-convolved pulsewidth with Sech$^2$ fit ranged from 1-2 ps. The inset shows the optical spectrum for the minimum observed pulsewidth. The autocorrelation trace with its Sech$^2$ fit is shown in Fig. 2.29(b) along with a trace of seven consecutive pulses in the inset. The estimated period of the device from the trace in the inset was measured to be $\approx$ 52.5 GHz with 0.8 GHz measurement error coming from the time resolution of the autocorrelator. This value was beyond the maximum frequency of the electronic spectrum analysers available in this experiment, making any direct measurement of

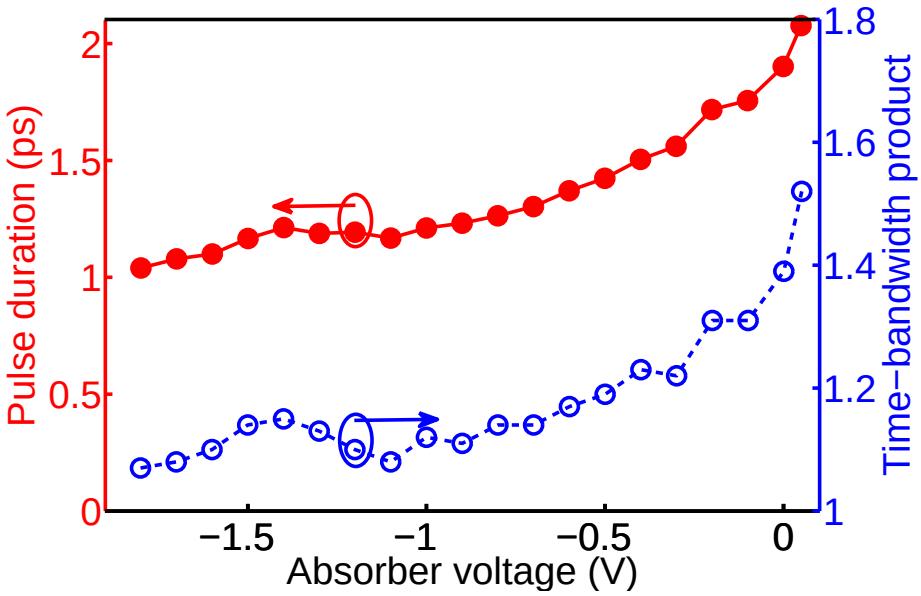



Figure 2.30: Dependence of the pulse-width (Gaussian fit, left Y axis) and TBP (right Y axis) on the absorber bias voltage for a fixed gain current (140 mA). Device: G4-3.

RF linewidth impossible. Within the SAML regime, the TBP of the pulses was also calculated, as shown in Fig. 2.30 in left and right axes, respectively. The gain current was fixed at 140 mA with absorber voltage ranging from -1.8 V to 0.05 V. Increasing the absorber voltage further leads to broadening in the pulses resulting in irregular autocorrelation traces which did not fit either $Sech^2$ or Gaussian. When the absorber voltage was increased from -1.8 V to 0.05 V, the pulsewidth increased from 1.0 ps to 2.1 ps. The TBP of the pulses also increased from 1.1 to 1.5 indicating chirp in the pulses compared to the Fourier Limit for $Sech^2$ pulses (0.351).

Comparing the pulse characteristics of 52 GHz SAML devices with 21 GHz SAML devices, two main differences can be found. First, narrower pulsewidth range was observed for shorter device, 1-2 ps compared to 5-7 ps for longer devices. This could be due to shorter gain recovery time in the 52 GHz devices because of higher carrier density. Note than the gain current was in the same range as those of 21 GHz devices leading to higher carrier density in the gain section. The second difference is the TBP which is significantly lower for 52 GHz devices. This could be due to fewer modes available in the gain spectrum and shorter cavity length, leading to less effective deviation of static phase between the longitudinal modes and less chirp. The latter can also contribute to shorter pulses observed experimentally.

## 2.6 Summary and Discussions

In this chapter, we discussed the structures of QDML lasers with basic measurement techniques used in this work. The QDML lasers were categorised by their mode-locking

mechanism: SML or SAML. For the SML lasers, RF linewidths 100 kHz observed regardless of active region type (DWELL or DBARR) with wider optical spectrum for DBARR devices. Such wide optical spectra, if followed by optimized timing jitter, could be useful for applications requiring such interesting spectral properties such as microwave and terahertz generation. One disadvantage of these devices was the need to utilize pulse compression techniques in order to generate pulses from them. We showed that the chirp can be compensated using a dispersive element with dispersion parameters of opposite sign such as a single-mode fibre of appropriate length. Selection of a few adjacent modes with low static phase deviation using a narrow band filter is another method of generating ps pulses from such devices. Despite the fact that the free-running (without optical injection) mode-locking behavior of DWELL and DBARR devices did not show clear difference, we will see in the next chapter that the dynamics of these devices are different under optical injection.

On the other hand, the two-section QDMLLs operating as SAML, show picosecond pulses without any compression. The TBP of the pulses are still significantly higher than the Fourier-limit indicating the presence of chirp. The TBP improves as the cavity length becomes shorter for SAML devices. As we will see in Chapter 4, the TBP of the SAML lasers can be reduced using optical injection. The RF linewidth of SAML devices were generally higher than SML devices indicating the potential of SML lasers for low jitter performance.

# Chapter 3

# Optical Injection of Self-Mode-Locked Lasers (SML)

## 3.1 Introduction

In this chapter, we analyse the behavior of SML devices under optical injection. All the results will be on CW injection of such devices giving a generic picture about the dynamics. The results can be divided into two categories: First, the general dynamical picture of self-mode-locked (SML) quantum dash lasers under optical injection: knowing the type of dynamics, stability and/or instabilities under optical injection. Second, as a mode-locked laser the possibility of performance improvement or new functionalities under optical injection. For the latter, we are looking for a region that the slave laser stably locks to the master and remains multi-mode. As we will see, this kind of dynamical regime exists for some of devices, and the locking characteristics look more attractive to microwave generation applications.

First, we introduce the experimental arrangement, then the different dynamical regimes will be introduced. Multi-mode injection-locked and mode-locked operation is presented for DWELL and DBARR devices. Finally, an analysis on frequency tuning and scaling of such regime is presented with some general comments on comparing DWELL and DBARR SML devices.

## 3.2 Experimental Arrangement

A schematic of the experimental arrangement for optical injection of SML devices is shown in Fig. 3.1. The master laser was a commercial external cavity tunable laser (New Focus 6328, 1520-1570 nm) with optical linewidth <1 MHz and fine tuning resolution of $\approx 0.5$ pm. The fiber pigtailed output of the master laser passed through a free-space

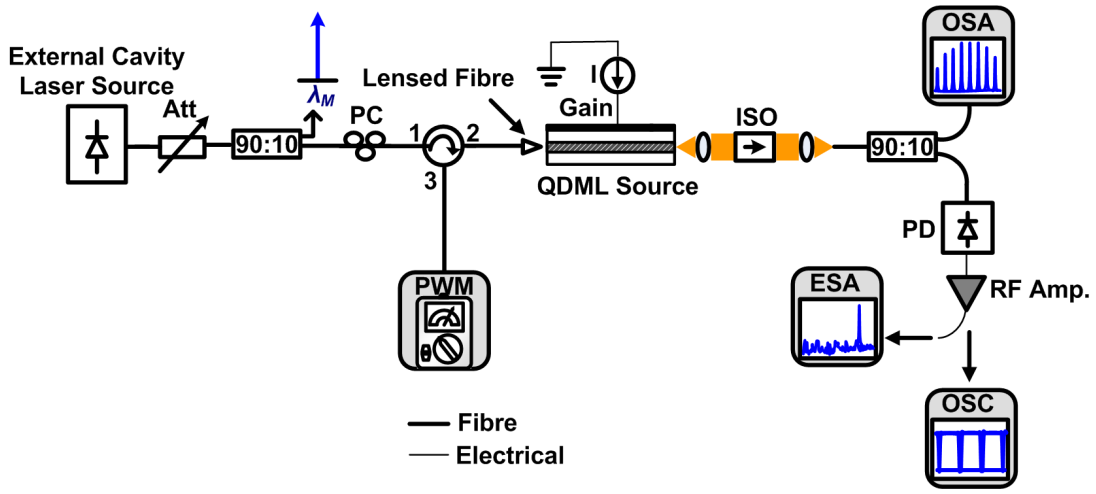



Figure 3.1: Schematic diagram of CW injection experiment for SML device. List of acronyms: Att.: Variable Optical Attenuator, PC: Polarization Controller, PWM: Optical Power Meter, QDML: Quantum-Dash Mode-Locked, ISO: Isolator, OSA: Optical Spectrum Analyzer, PD: Photodetector, RF Amp.: RF Amplifier, ESA: Electrical Spectrum Analyzer, OSC: Digital Sampling Oscilloscope.

isolator (> 60 dB total isolation), a variable optical attenuator, and 10/90 coupler to monitor the injection power. A polarization controller was used to align the polarization of the master laser with that of the slave. Then, the light was fed into port 1 of a circulator; the light from port 2 was coupled through one facet of the slave laser with a lensed fiber. The light from port 3 of the circulator enabled monitoring the power of the slave laser under injection.

The light passing a free space isolator (>60 dB isolation) was coupled to a single mode fiber using a pair of free space lenses. The light from the fibre was divided into to arms by a 10/90 coupler. The light from the other facet was utilized for optical spectrum analysis (using Ando AQ6317B OSA) and RF spectrum analysis or time-trace analysis using a 40 GSa/s digital oscilloscope with 12 GHz input bandwidth (Agilent Infiniium DSO91204A). For the RF spectrum analysis, the light was directed to a high speed photodetector (Newport D-25xr model with 17 GHz 3dB bandwidth and impulse response of 25 ps). The output of the photodetector was boosted by an RF amplifier (0.1-18 GHz, model number) connected to an electronic spectrum analyzer (Agilent E4407B, 26.5 GHz). A LabView® program was used to precisely control the master laser wavelength and subsequent measurement of the slave laser output. The slave laser (A1, DWELL, single-section, 10.5 GHz) was mounted on a ceramic submount sitting on a copper block. The temperature and drive current of the slave laser were controlled by a temperature controller with 0.1 $^o$C and laser diode controller with 0.01 mA accuracy, respectively.

The total loss from the master laser output to the slave's facet considering connector losses, components and 3 dB coupling loss for the lensed fiber was measured to be

≈8.6 dB. This means that around 14% of the master laser output power was injected to the slave laser cavity. We define the term injection ratio as the ratio of injected power to the free running power of the slave laser at the injected facet, $\frac{P_{Inj.}}{P_{Slave}}$. The measurement method for optical linewidth was the heterodyne technique as already described in § 2.3.3.

## 3.3 Injection Locking: General Properties

The behaviour of the slave laser when the external light is injected depends on three external parameters: injection strength, frequency detuning (frequency or wavelength difference between the master and the slave), and slave laser power. Under certain conditions, the slave laser goes to a particular region which is known as *locked*. In this region, the injected mode saturates the whole gain and the other longitudinal modes are suppressed because they can not avail of enough optical gain to lase. As a result, the slave laser becomes a single mode laser; now the frequency of this single mode laser follows the frequency of the master laser if it changes. The range of this frequency following is named as *locking range*.

At a part of this region, the phase of the slave laser is locked to that of the master; one indication of this behaviour is the narrowing of the optical linewidth of the slave laser close to that of the master laser. This region is known as stable-locking. As we see in experimental results, the slave laser at single mode or (locked) region does not necessarily have the stable-locked properties. The optical spectra of the laser in unlocked and locked states are shown in Fig. 3.2. The side-mode suppression ratio (SMSR) is about 45 dB which is a good indication of the single-mode (locked) operation, considering minimum resolution bandwidth of OSA (0.01 nm). To investigate the presence of stable-locking at this region, we need to look at the output of the slave in time/or frequency domain or at RF (power) spectra. The RF spectrum is shown in Fig. 3.3. The absence of any low-frequency (less than the resolution bandwidth of OSA) or high-frequency frequency components or continuum spectra is a confirmation of *stable* locking behavior. The mode-locked frequency is also absent because of single-mode operation of the slave laser. From this quiet spectrum, we can confirm that the slave laser does not have any particular unstable dynamics and the cavity of slave laser supports only one frequency/wavelength component which is that of the master (no beating tone).

Measurement of the optical linewidth of the slave laser in this region can be regarded as another indication of stable (or phase) locking. The optical linewidths of the slave laser under free running and stable-locking are shown in Fig. 3.4(a). The free running linewidth (3dB) was about 30 MHz which narrowed down to few hundred kHz when the laser was stable-locked. The optical linewidth of the slave laser at this region was

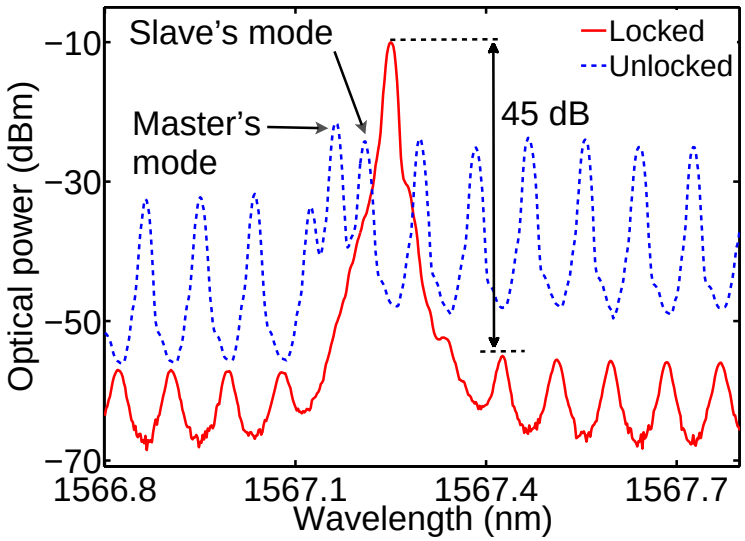



Figure 3.2: Optical spectrum of slave laser at the unlocked (blue-dashed) and locked (red-solid) states. The injected power is ≈257 $\mu$W (Injection ratio ≈36.7%).

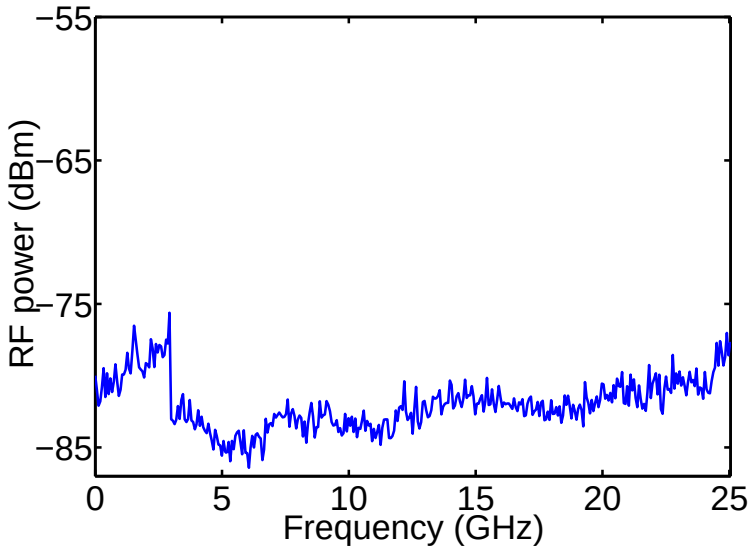
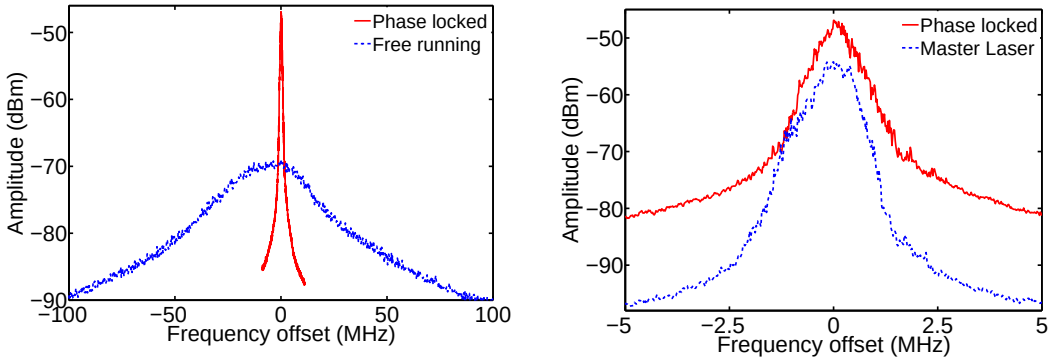



Figure 3.3: RF spectrum of the slave laser under stable locking with the same injection parameters as Fig. 3.2. The feature around 2.5 GHz corresponds to the noise of the ESA.

similar to that of the master laser. In Fig. 3.4(b), the optical linewidth of the slave laser under stable locking and heterodyne beating tone with the master's laser has been illustrated. As mentioned earlier, when the injected slave laser enters the locked region (frequency locked), the slave laser phase is locked to that of the master in a part of this frequency locked region. Thus, its optical lineshape replicates that of the master and we observe linewidth narrowing, provided the master laser is a narrow linewidth source.




(a) (b)

Figure 3.4: Optical linewidth measurement. (a). Slave laser linewidth free running (dashed line/blue) and stable-locked (solid-line/red) (b). Slave laser linewidth at stable-locked region (solid-line/red) with Master laser linewidth (dashed-line/blue).

## 3.4 Dynamics of DWELL Device

In this section, we show the results on dynamics observed in a DWELL device (4 mm, single-section, $A_1$) under CW injection. The slave laser showed various types of dynamical regimes under optical injection. These dynamics can be classified as unlocked (wave beating), limit cycle category (period-one, period-two and period-four), chaotic oscillation, un-damped relaxation oscillation, stable (phase) locking, and a new region, to the best of our knowledge, that we have named as *Microwave Oscillation*. We believe that this region is an example of *injection-locked mode-locked regime*. We study this dynamical region in more detail as described in this chapter. A description of each dynamical regions is provided below:

**Unlocked (Wave beating)** If the detuning between the master and slave is higher than the locking range, there would be no interaction between the master and slave's modes and the optical spectra of the slave laser remains unchanged (as Fig. 3.2, dashed curve). However, in the RF spectrum, wave beating (or mixing) between the master's mode and slave's injected mode and also between the master's mode and and adjacent slave's mode can be observed. This beating mode can be regarded as the exact value of the detuning in frequency (Hz). A typical RF spectrum of the slave laser in this region is shown in Fig. 3.5.

**Period-one** In this dynamical regime, the slave laser undergoes a limit-cycle oscillation whose period is given by the detuning between the master and slave. Time trace and RF spectra (FFT of the time trace) for this region are shown in Fig. 3.6(a),(b) respectively. The term limit cycle means that the laser in phase space (optical field versus carrier density) has limited states and switching among them generates the limit cycle pulse in the output. The RF spectrum has two components associated with the period of period-one dynamics and higher harmonics.

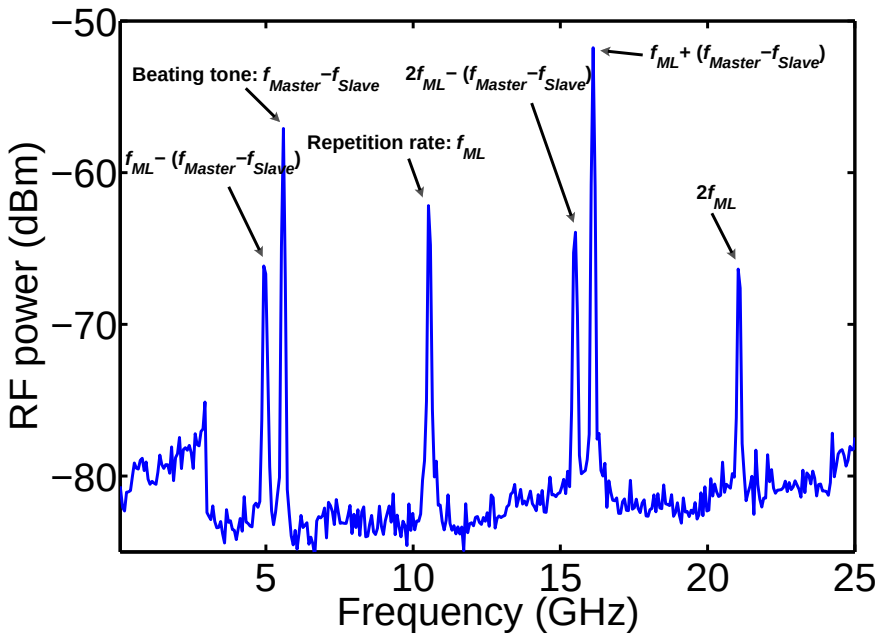
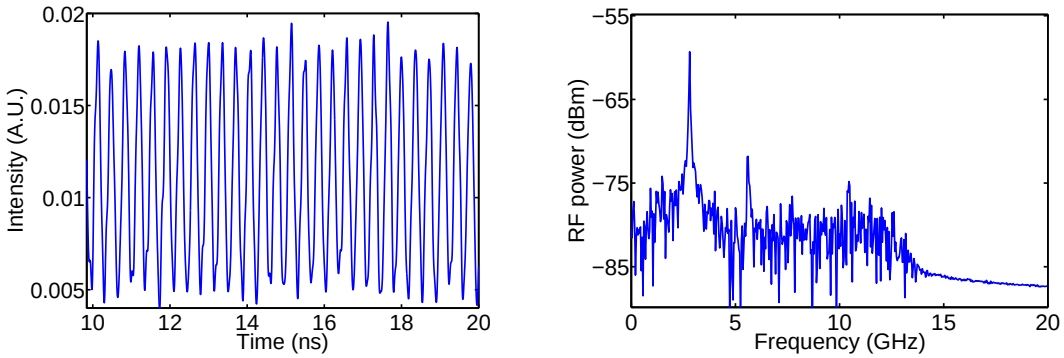



Figure 3.5: Measured RF spectra of the slave laser in the unlocked region. The beating (mixing) tone between master and slave and subsequent generated mixing tones between the master and adjacent modes can be distinguished. The repetition rate and its second harmonic are also denoted by arrows.

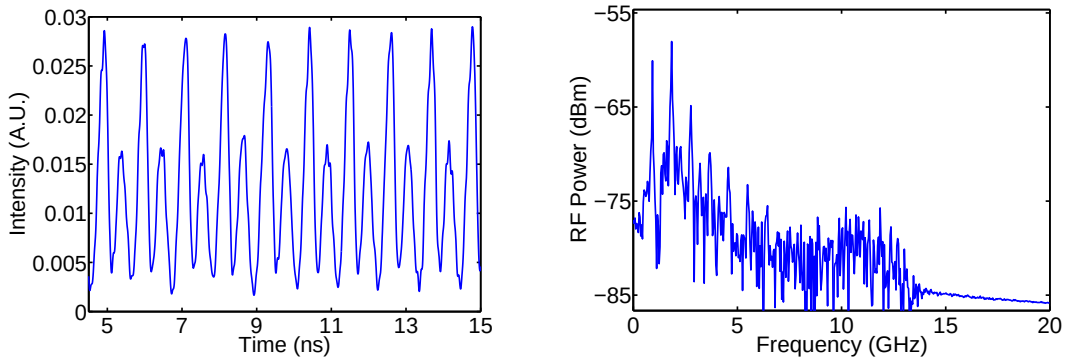



(a) (b)

Figure 3.6: (a). Measured time-trace of the slave laser in the period-one region. (b). Calculated RF spectrum.

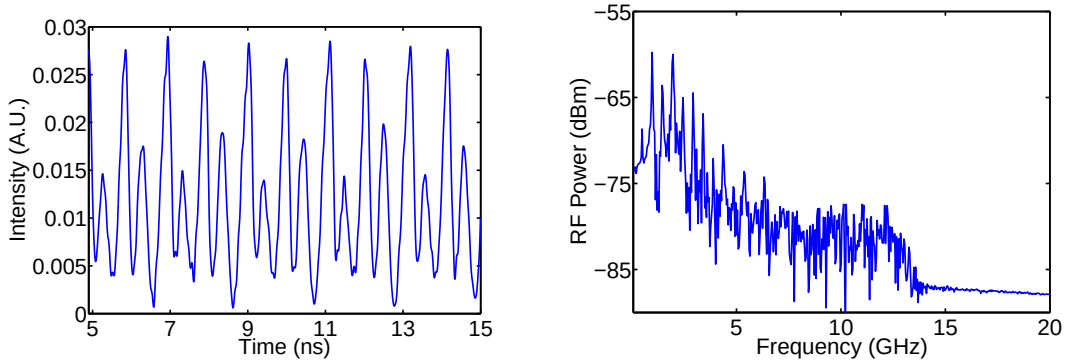
**Period-Two** In this region, the output of the laser undergoes another limit-cycle state whose number of states is four so the laser has two cycles in each periodic oscillation. The frequency of this oscillation is half the original generated frequency or detuning. Time trace and RF spectrum of this region are shown in Fig. 3.7. In the RF spectrum, additional tones between the original detuning tones can be observed which is an indication of doubling the period.

**Period-Four** The slave laser shows the oscillation having a period which is four times greater than that of period-one oscillation which is illustrated in Fig. 3.8(a). This




(a) (b)

Figure 3.7: (a). Measured time-trace of the slave laser in the period-two region. (b). Calculated RF spectrum.



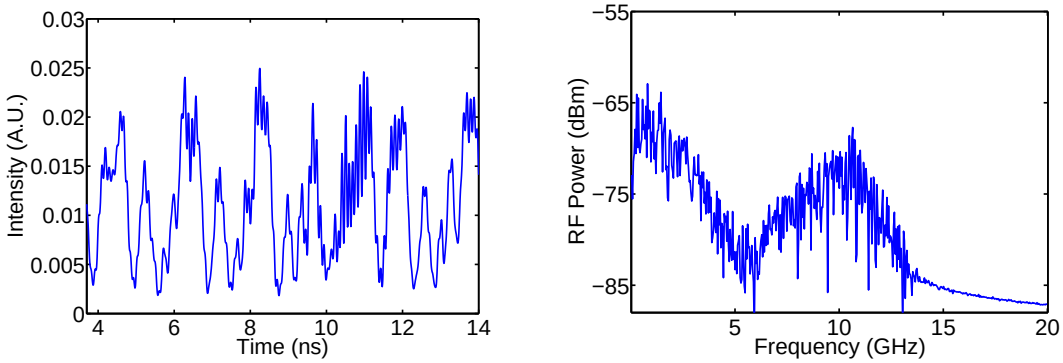

(a) (b)

Figure 3.8: (a). The measured time-trace of the slave laser at period-four region. (b). Calculated RF spectrum.

can be confirmed noting that additional tones have been generated between the tones of period-two region as seen by comparison of Figs. 3.8(b) and 3.7(b).

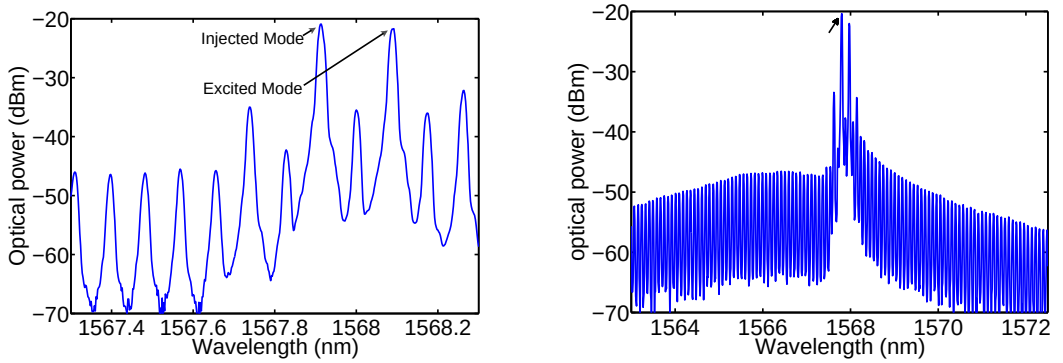
**Chaotic Oscillation (Chaos)** Chaos is a well known dynamical state in nonlinear dynamics of oscillators. Observation of chaos in semiconductor lasers in particular under optical injection is interesting for potential application in secure (chaotic) communications. A good indication of for chaotic oscillation in the output of the slave laser is a continuum RF spectrum. In the time domain, the output looks like a random fluctuation, but there is a difference between a random signal and chaotic one. In the latter, there is some kind of regularity (or being deterministic) in the signal. Time trace and RF spectrum of the laser in chaos is shown in Fig. 3.9. In the chaotic oscillation, the optical spectrum is multi mode indicating that the power is distributed among several modes.

**Stable-(phase) Locking** The characteristics of this region in general was described in § 3.3.




(a) (b)

Figure 3.9: (a) Measured time-trace of the slave laser in the chaotic oscillation. (b) Calculated RF spectrum.




(a) (b)

Figure 3.10: Optical spectrum of the slave laser in the microwave oscillation region. (a)Zoom of the spectrum. The injected mode is denoted in the figure; the excited mode is spaced at twice of mode-locked frequency. (b) Wider span of the spectrum. The injected mode is denoted by an arrow.

**Microwave Oscillation** This dynamical regime exists at low injection levels (0.1% to 1%). The zoom of optical spectrum of the slave laser at this region is shown in Fig. 3.10(a). As can be seen, there are four excited optical modes and the other modes are suppressed. Wider span of the optical spectrum is shown in Fig. 3.10(b). The spectral spacing of the modes is twice the cavity's free spectral range (repetition rate). In addition to the injected mode and *excited* mode having similar intensity, there are two modes located on either side of these modes with the same frequency spacing. The measured optical linewidth of the injected mode at this region indicates that this mode is phase-locked to the master as its optical linewidth is the same as in the phase-locked region; the optical linewidth measurement is shown in Fig. 3.15. As we will see in detailed analysis of this region in § 3.5, the output of the slave laser would be a strong microwave oscillation at twice slave laser's repetition rate.

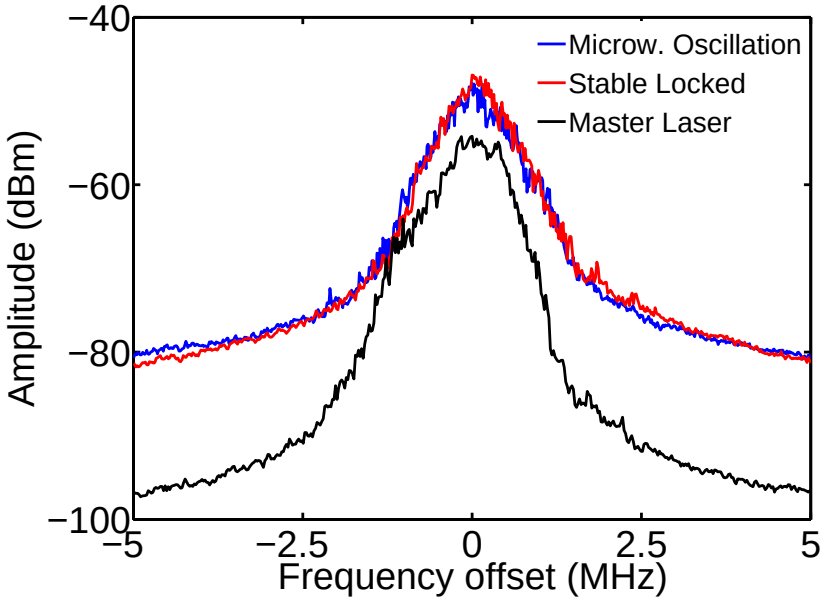



Figure 3.11: Heterodyne measurements of the optical linewidth of the injected mode at the microwave oscillation (solid-line/blue) and stable-locked (solid-line/red) regions. The optical line-shape of the master (solid-line/black) is also shown for comparison.

### 3.4.1 Analysis of Dynamics Versus Injection Parameters

We analyse the evolution of such dynamics when the detuning (frequency difference between the master and injected mode of the slave) and injection power while varied. We always refer to the intensity graph of the measured (or calculated) RF spectrum versus detuning for fixed injection power. The graph was obtained by automatic measurement of the time-trace or RF spectrum when the injection power was constant and detuning was changing by automatic sweeping of the master laser. The bias current of the slave laser was kept constant at 165 mA (14% above threshold).

The intensity graph for injection ratio of 28% is shown in Fig. 3.12. The dynamical regions are denoted by numbers described as follows: 1: Unlocked, 2: Period-One, 3: Period-Two, 4: Period-Four, 5: Period-Two, 6: Period-Four, 7: Period-Two, 8: Period-One, 9: Chaos. Interestingly, no stable-locking region was observed for this injection level. The chaotic regime existed for the injection ratio between 6-40% where theese strong instabilities existed. For injection ratio higher than 40%, a region of stable-locking evolved at the corner of locking region with negative frequency detuning where the wavelength of master was higher than slave's injected mode. There was also a hysteresis associated with the border of stable-locked, unlocked in negative frequency detuning and the evolution from stable-locked to unlocked in that corner is abrupt. At injection level below 1%, the microwave oscillation regime evolved at frequency detuning before the evolution of stable locking. In summary, the various dynamical regimes, particularly limit cycle and chaotic oscillations remind the instabilities observed in

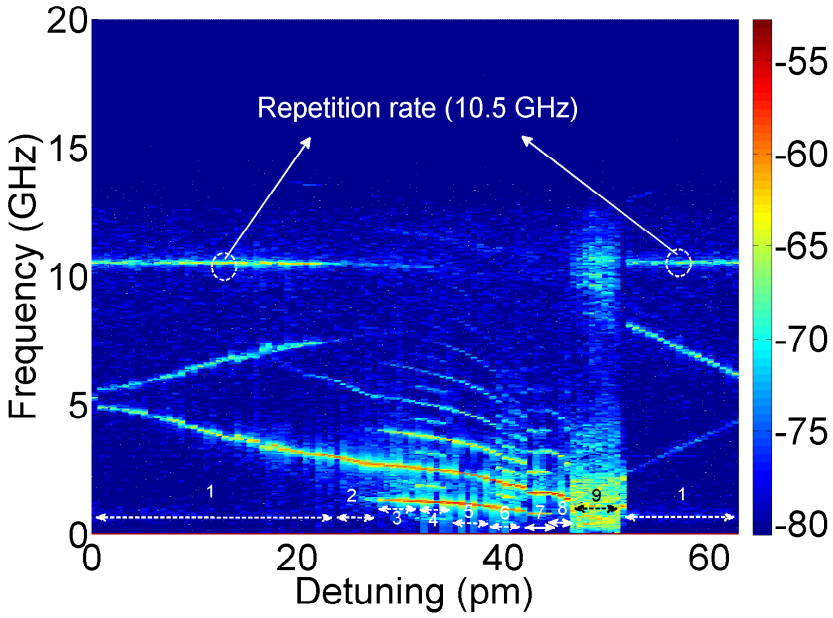


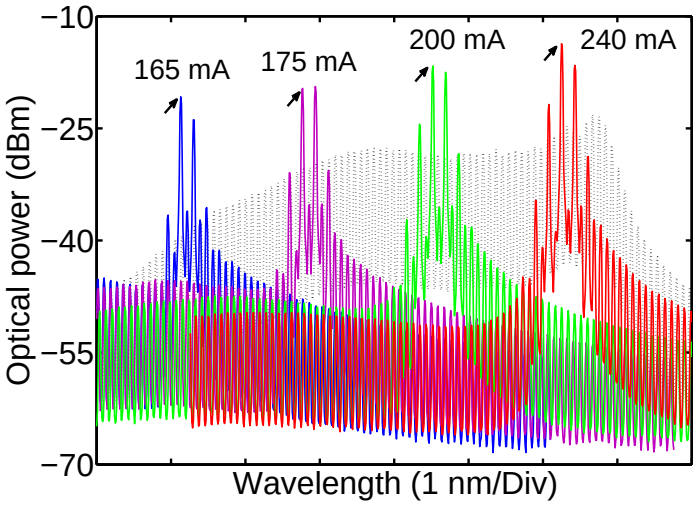

Figure 3.12: The intensity graph for dynamics at injection level of ≈28%. The dynamics are as follows: 1: Unlocked, 2: Period-One, 3: Period-Two, 4: Period-Four, 5: Period-Two, 6: Period-Four, 7: Period-Two, 8: Period-One, 9: Chaos.

quantum-well lasers [152]. This is contrast with quantum dot lasers based on the GaAs material system, where significantly more stable operation was observed under optical injection [153–155].

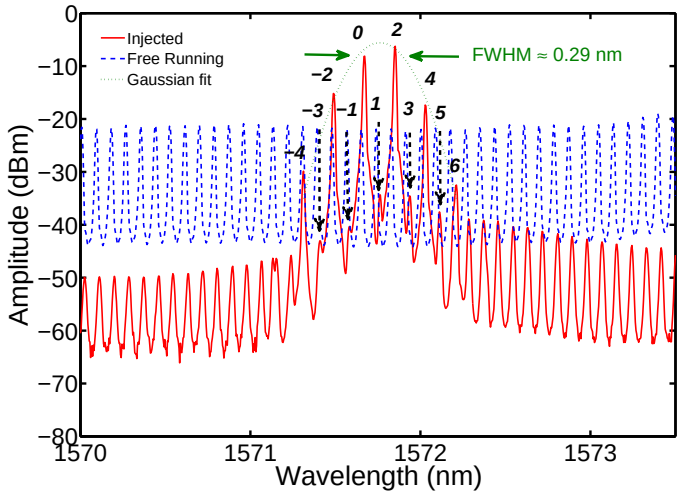
## 3.5 Microwave Generation in DWELL Device

In this section, we analyse the characteristics of DWELL 10.5 GHz device (A1) in microwave oscillation (MWO) region. The experimental arrangement remained the same as Fig. 3.1 except for replacing the powermeter with an autocorelator in the port 3 of the circulator. As briefly described in § 3.4, few modes of the slave laser were selected by optical injection. This region existed consistently at all currents above threshold as shown in Fig. 3.13(a). As can be seen, as the bias current was increased, the envelope of the optical spectrum in the MWO region broadened. The zoom of the optical spectrum at bias current 250 mA is shown in Fig. 3.13(b). The modes are marked based on their relative distance from the injected mode, 0. The modes with odd indices relative to the injected mode (0) were suppressed by more than 25 dB and the modes with even indices were strengthened. The envelope of the spectrum was close to Gaussian with full-width at half-maximum (FWHM) ≈ 0.29 nm as shown. This region was observed for injection ratio 0.5%-3% at this bias current.

Since the optical injection selected modes with spacing at twice the cavity's fundamental frequency (in this case 10.5 GHz), we expected a peak around twice the 10.5 GHz




(a)




(b)

Figure 3.13: Optical spectrum of the slave laser in microwave oscillation region. (a). Optical spectrum versus changing the current. The injected mode is denoted by an arrow. (b). Zoom of the optical spectrum of the slave laser when free running (blue-dashed) and MWO regime (red-solid). The Gaussian fit of the envelope is shown in green-dotted curve. Bias current was $1.6I_{th}$ and injection ratio 3%. The injected mode is 0.

resulted from beating of the dominant modes in the RF spectrum. The corresponding RF spectrum of Fig. 3.13(b) is shown in Fig. 3.14 (red-solid line). In comparison with the free running RF spectrum (the blue-dashed line), several features are of note. First, the original mode-locked frequency and its second harmonic were slightly shifted to the higher values. Second, the component at higher frequency (close to second harmonic) was amplified by more than 15 dB and the one at the frequency close to the mode-locked frequency was attenuated by more than 20 dB. Finally, the relaxation oscillation

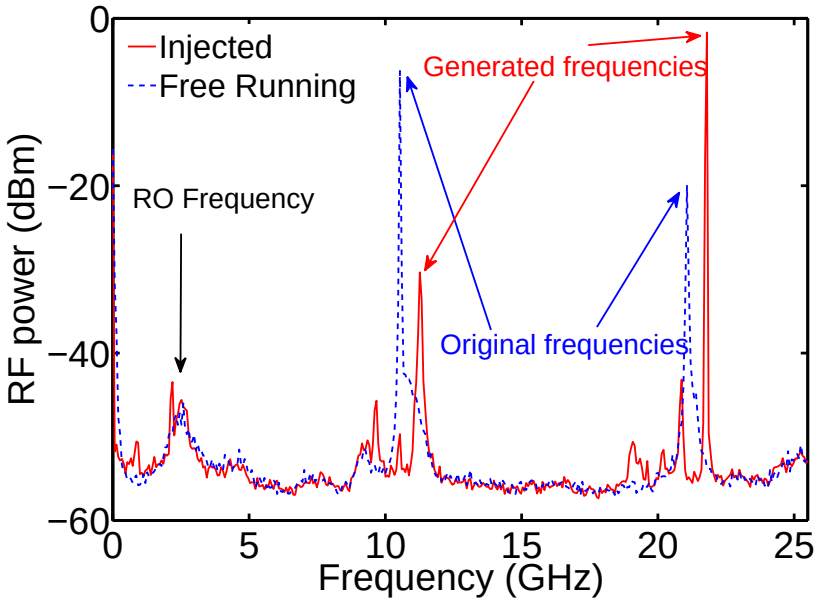



Figure 3.14: RF spectrum of free running (dashed-line/blue) and injection (solid-line/red) corresponding to the optical spectrum of Fig. 3.13(b).

(RO) peak (≈2.6 GHz) was present at both free-running and injected cases, which was weaker than the peak by more than 30 dB. The presence of such a weak relaxation oscillation was also observed in injection-locking of actively mode-locked lasers [85].

Also, no strong frequency component associated with beating between master and slave's modes or any amplitude instabilities was observed. This is an indication of injection-locking as already shown in optical linewidth of the injected mode in Fig. 3.15. We then measured the optical linewidth of the all dominant modes in the optical spectrum of injected laser. The results at bias current of 1.6 Ith at free running and injected, at three wavelengths, are shown in Fig. 3.15. Regardless of the modal linewidth when free running, significant linewidth narrowing occurred for the all of the dominant modes within the range 200 kHz-1 MHz. The linewidths of the modes are close to that of the master and indicates the phase coherence between all the modes and the master laser.

The linewidth narrowing of the optical modes suggests a narrow RF beating tone among the modes. A higher resolution RF spectrum shows narrowing of the generated RF tone in comparison to the free running case as shown in Fig. 3.16(a). The RF spectrum for both cases was shifted to the peak frequency for clear comparison. The RF linewidth of the second harmonic, when free running, was around 1 MHz which reduced to 160 kHz when injected. This value is an order of magnitude lower than the sum of the optical linewidths obtained for the modes which could be an indication of phase-locking among them. The autocorrelation measurement of the laser when free running and with injection in this region is shown in Fig. 3.16(b). The free running trace (solid-line/blue) did not show any clear pulsed trace as explained in previous chapter (§ 2.4.1).

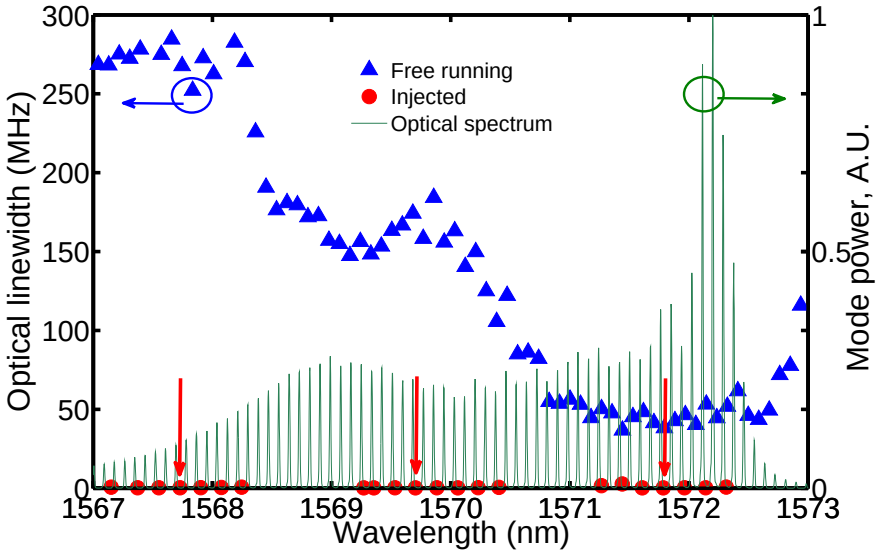
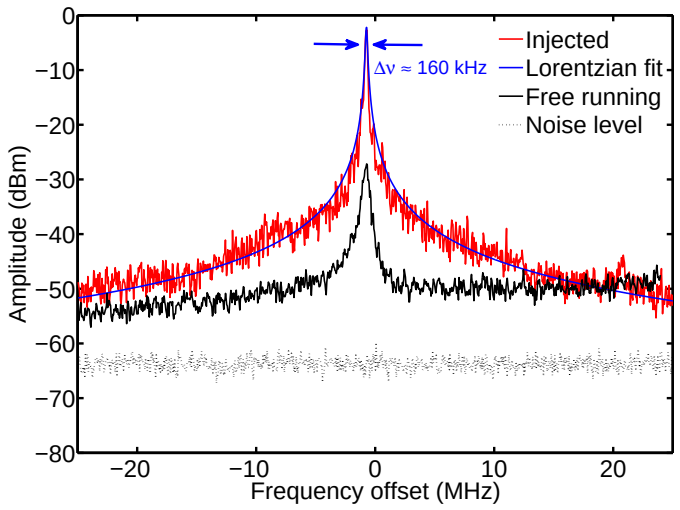



Figure 3.15: Measured optical linewidths of individual modes when free running (blue-diamonds) and injected, MWO (red-circles) for three wavelengths of injection shown by arrows. The free running optical spectrum in linear scale is shown on the right axis.

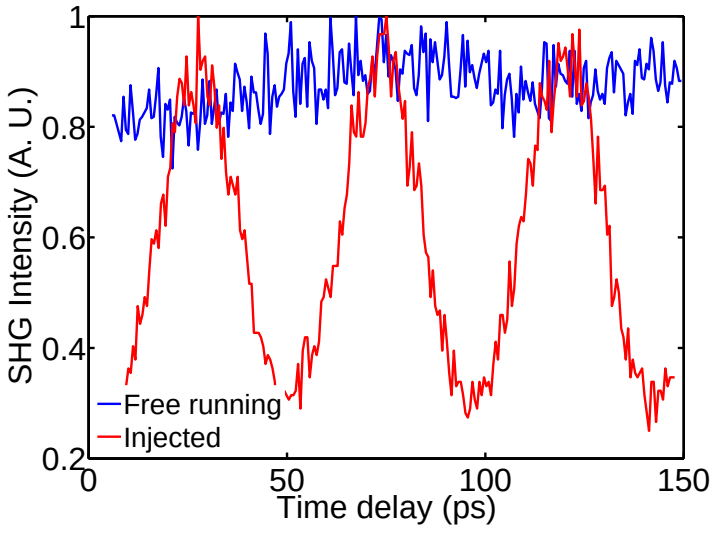
The injected trace, however, showed features with higher extinction ratio which is an indication of selecting few modes with low static phase difference. The measured width of the Gaussian fit (after deconvolution) was about 17 ps indicating broad pulses which is expected as only two modes were dominant in the optical spectrum of Fig. 3.10(b). The estimated time-bandwidth product of such a pulse considering the FWHM spectral width $\approx$ 0.29 nm was around 0.6 which is slightly above the Fourier limit for a Gaussian pulses (0.44).

We also checked the spectral tunability in this region; as seen in Fig. 3.17, this behaviour is tunable across the slave laser's optical spectrum (>6 nm). Finally, we located the MWO region in the 2D global dynamical map (Fig. 3.18). The horizontal axis is the ratio of the injected power at the facet of the slave laser to its free running power. The vertical axis is the frequency difference between the master and slave ($f_{Master} - f_{Slave}$). The region filled in red indicates the MWO region; the width of the region (locking range) depended on the injection level, but the maximum value was around 600 MHz. Adjacent to the MWO region there is another regime with the pure MWO and strong low frequency oscillations at RO frequency (MWO + RO), as shown in Fig. 3.19(a). The low frequency oscillation come from undamped relaxation oscillation. Strong and pure oscillations around the RO frequency and its harmonics (<10 GHz) co-existed with some mixed terms generated by mixing of the RO tones and generated microwave signal (>10 GHz). The optical spectrum at this region remained the same as that of MWO, but there was broadening observed in the individual modes as shown in Fig. 3.19(b). Above the MWO region, there is a wide region designated as Incomplete MWO. The corresponding RF spectrum of the laser is dominated by strong, but broad

(in the order of free running modal linewidth, indicating absence of phase coherence among the modes) components at MWO frequency and its sub-harmonic and presence of oscillations associated with RO of the laser. P1 represents the limit cycle operation at the RO frequency and presence of original mode-locked tone because of less perturbation in the optical spectrum. The laser at P2 (period-doubling), URO (undamped RO), and SL (stable locking) regions operates at single mode. In P2 and URO cases, several harmonics of RO frequency are present in the RF spectrum. Finally, complete coherence from the master is transferred to the slave at SL region which indicates phase locking




(a)




(b)

Figure 3.16: (a). 50 MHz span of the microwave tone (injected, red curve) and second harmonic of mode-locked tone (free running, black curve). Resolution band-width (RBW) was 300 kHz and video band-width (VBW) wass 30 kHz. The blue curve shows the Lorentzian fit of the microwave tone. (b). Autocorrelation trace of the laser under MWO region (solid-curve/red) and free running (solid-curve/blue).

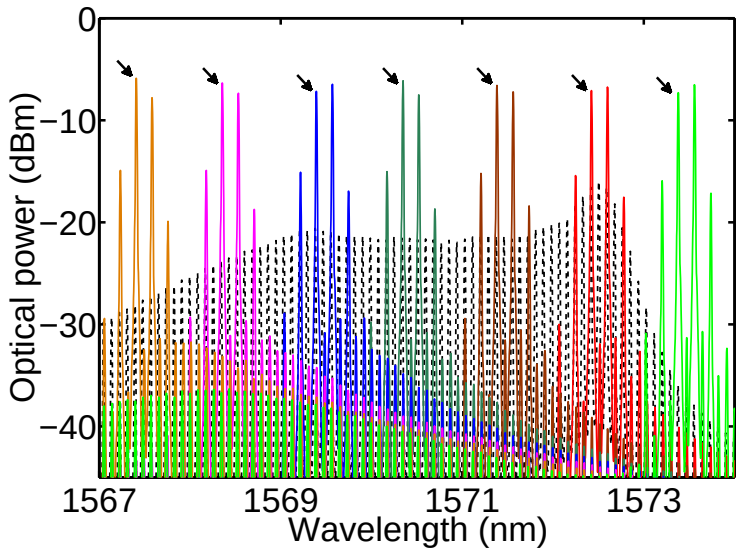



Figure 3.17: Spectral tunability in the MWO regime. The dashed curve is the optical spectrum of the slave laser when free running ($1.6I_{th}$). The arrows show the location of the optical injection.

phenomenon az explained in § 3.4 with single-mode operation.

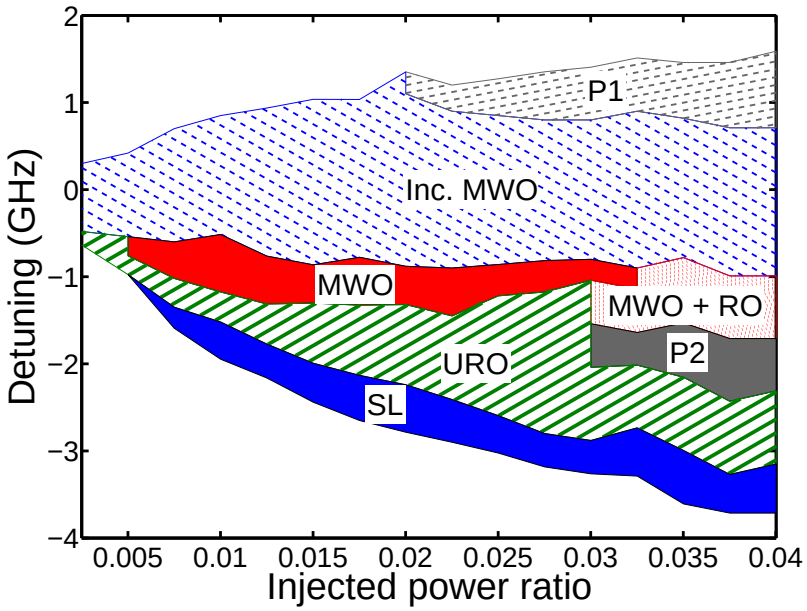
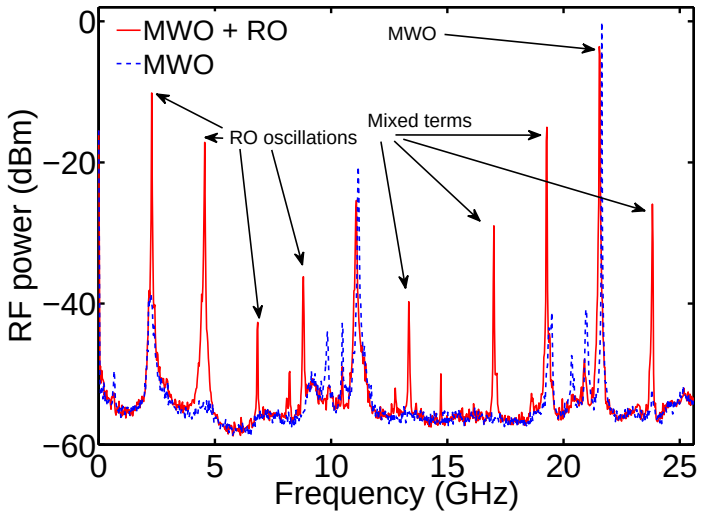
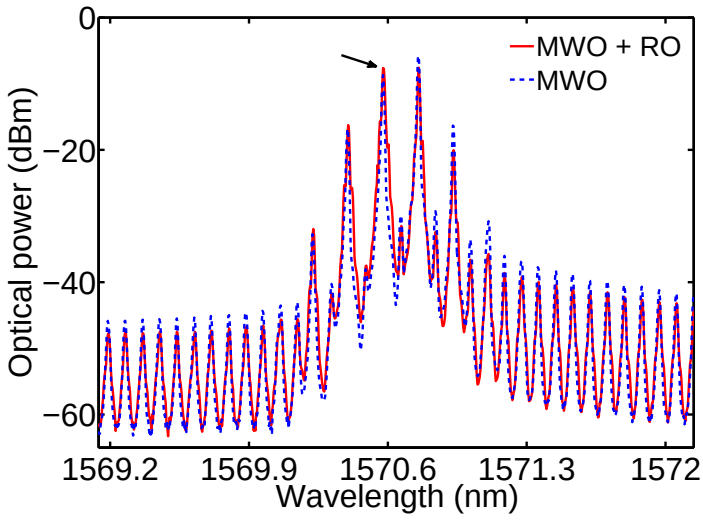



Figure 3.18: 2D operational map of dynamics at $1.6I_{th}$. The symbol definitions are as follows: MWO: Microwave oscillation, MWO+RO: Narrow tone MWO with undamped RO. P2: Period doubling oscillation. URO: Undamped RO only. Inc MWO: Incomplete MWO (refer to the text). P1: Period one oscillation. SL: Stable locking or phase locked with single-mode operation.




(a)

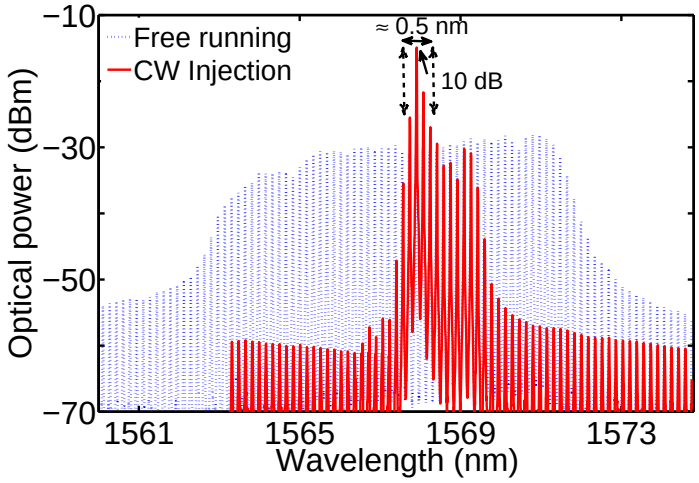



(b)

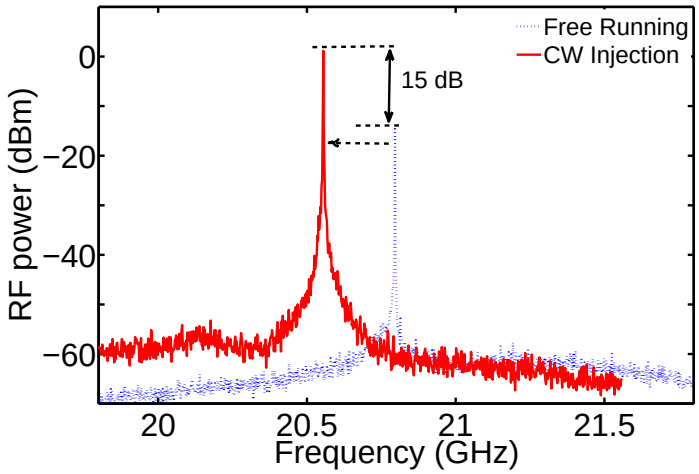
Figure 3.19: (a). RF spectrum of MWO + RO region (solid-line/red curve). The RF spectrum of MWO is also shown for comparison (dashed-line/blue curve). (b). Optical spectrum of MWO + RO region (solid-line/red curve). The optical spectrum of MWO is also shown in dashed-line/blue. The arrow denotes the location of injection; the OSA resolution bandwidth for both cases was at the minimum (0.01 nm).

## 3.6 Microwave Generation in DBARR Device

Following MWO analysis under CW injection in DWELL device, we studied the CW injection properties of DBARR devices with the same experimental arrangement as for DWELL devices. Typical optical and RF spectra of the laser when free running and injected are shown in Fig. 3.20(a) and (b), respectively. In the optical spectrum, the CW light (denoted by an arrow) selected a group of modes: in this group, majority of power was in the modes around the injected one. Such a narrow spectrum (comparing




(a)




(b)

Figure 3.20: (a). Optical spectrum of the DBARR SML (I3-1, $I = 85$ mA, Absorber: 2.0%, floating), injection ratio≈7%) at free running (dashed-line/blue) and locked (solid-line/red). (b). Corresponding RF spectrum; free running (dashed-line/blue) and locked (solid-line/red).

to free running, with only 3 modes within 10 dB of the peak) was tunable by more than 10 nm when the master laser was tuned in the free running optical spectrum. In the RF spectrum, the mode-locked peak shifted to lower frequency than that of the free running laser when locked to the master laser. Unlike DWELL device, we observed the injection-locked mode-locking at the same harmonic of the free running repetition rate. The RF linewidth of the injection locked laser was still narrow (≈200 kHz) slightly higher than that of free-running, ≈ 100 kHz. Also, the increase in the peak of the RF frequency when locked by ≈15 dB is notable. As we discussed in Chapter 2, one

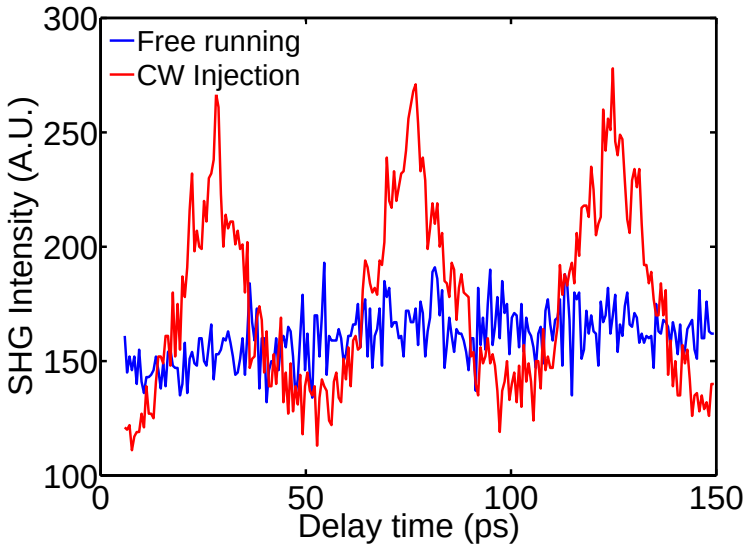



Figure 3.21: Autocorrelation trace of SML DBARR device, CW injection-locked (solid-line, red) and free running (solid-line, blue), injection ratio ≈16.6%.

difference in the mode-locking performance of SML and SAML was the difference in RF power of the two cases. With the same averaged optical power, the SML device had less RF power compared to the SAML device. Here, the CW injection selects few modes and the resulting RF power of beating between these injection-locked modes create more RF power than the free running SML device.

The autocorrelation trace of injection-locked and free running for DBARR SML device is shown in Fig. 3.21 in red and blue solid-lines, respectively. Unlike the free-running trace (no pulsation), the injection-locked trace showed some pulsed features with low extinction ratio due to narrow optical spectrum which limited the pulsed performance in this region. The region was observed at negative frequency detuning between the master and the slave ($f_{Master} < f_{Slave}$) at the boundary of locking range and injection ratio in the order of 1-10%. In the low frequency range of the RF spectrum (0-few GHz) no beating tone, instabilities, or undamped RO were observed. Also, the low frequency noise level (0-200 MHz) was suppressed under CW injection. This regime of operation was reproducible for both single-section and two-section devices when the absorber was floated/forward biased to produce SML operation. Unlike the dynamics of DWELL device discussed in previous section, no limit-cycle and chaotic dynamical regimes observed for these devices. The injection-locked region broadened when the injection power was increased. The optical locking range versus injected power ratio is shown in Fig. 3.22. As can be seen, wide locking range was obtained from this device which is an indication of more stable operation under injection-locking. Also, the locking range increased with increasing the injection power, in contrast with DWELL device. Despite the narrow optical spectrum and pulses with low extinction ratio, this locking region showed wide tuning of RF frequency as we show in the next section.

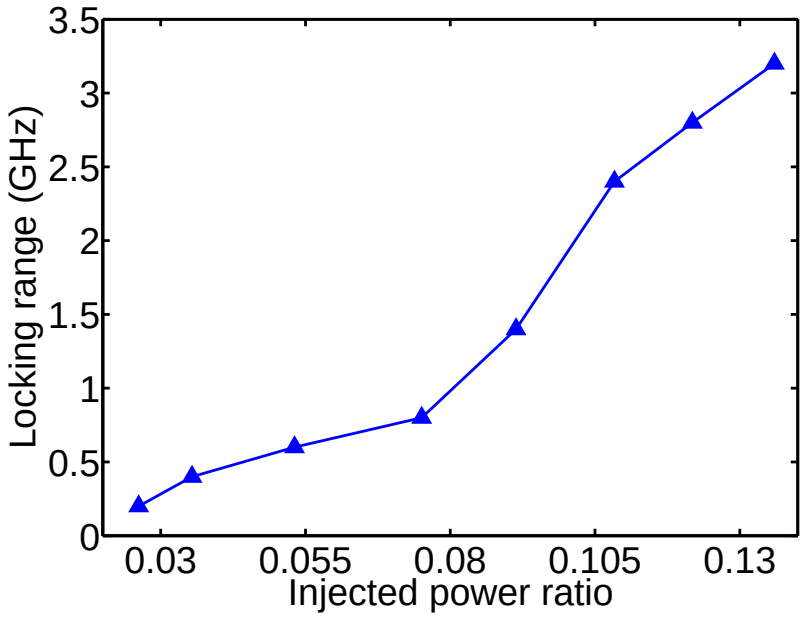



Figure 3.22: Optical locking range of CW injection for SML 21 GHz DBARR device (I3-1, 85 mA) versus injection power ratio.

## 3.7 Tuning and Scaling Properties

We demonstrated microwave generation in both DWELL and DBARR devices with SML operation. In a practical view, the range of RF tunability of the generated microwave signals is important. In Fig .3.23, the RF tuning (the change in RF frequency) of generated microwave signal for both DWELL (10.5 GHz, A1) and DBARR (21 GHz, I3-1) devices versus injection ratio, within the locking range, is shown. The tuning range corresponds to the frequency generated at the first harmonic of the repetition rate for DBARR, and the second harmonic for DWELL SMLL at bias currents 85 mA and 250 mA, respectively, ($\approx 1.6 I_{th}$). From Fig .3.23, we see that up to 730 MHz tunability is possible from DBARR SMLL, which is obtained simply by tuning the master laser within the locking range. Comparing the tuning ranges for both devices, we see that the tuning range for DWELL laser is much smaller than that of DBARR. Also, the injection ratio corresponding to microwave generation region for DWELL laser was smaller that DBARR laser. As we showed, for DWELL device this region was surrounded by regions of dynamic behavior associated with relaxation oscillation (RO) of the laser. This effectively limited the locking-range and associated RF tuning whereas for the DBARR device the locking region was present at the negative boundary of locking range and we observed no dynamical instabilities around that region. The maximum RF frequency tuning for the DWELL was around 60 MHz as shown in Fig. 3.24. As can be seen, the frequency changes monotonically as the master laser was swept. An example of RF spectra superimposed for maximum RF tuning DBARR device (injection ratio 0.136) is shown in Fig. .3.25. As the detuning between master

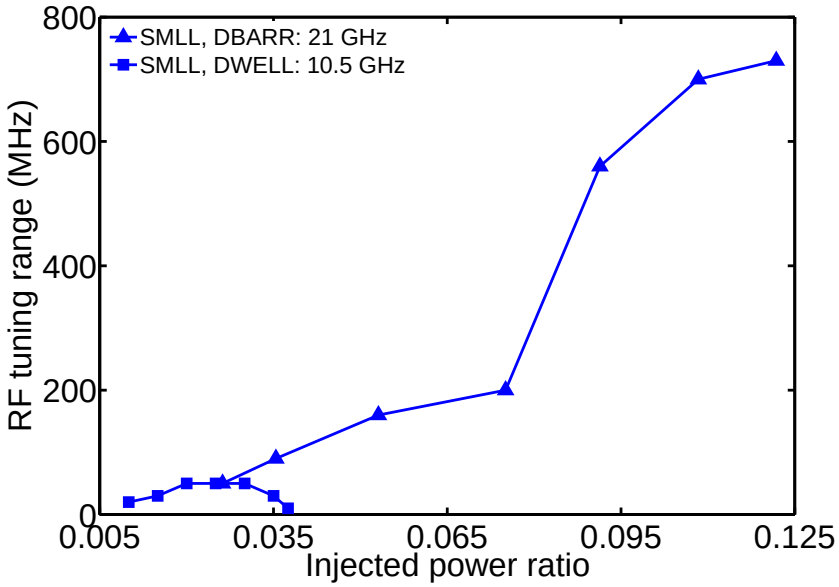



Figure 3.23: RF tuning of generated microwave signal for DBARR SML device at 21 GHz (filled triangles) and DWELL SML at 10.5 GHz ($A_1$, filled squares). The bias current for DBARR and DWELL devices were 85 mA and 250 mA, respectively ($1.6I_{th}$).

and slave is linearly increased, the frequency of generated signal tuned monotonically.

The RF linewidth <1 MHz was measured for the peak frequency for both the cases within the locking range. The optical spectra of slave laser at different frequencies within the locking range for injection ratio 13.6% are shown in Fig. 3.26. The spectra were offset for better viewing. As can be seen, the optical spectrum of the slave laser

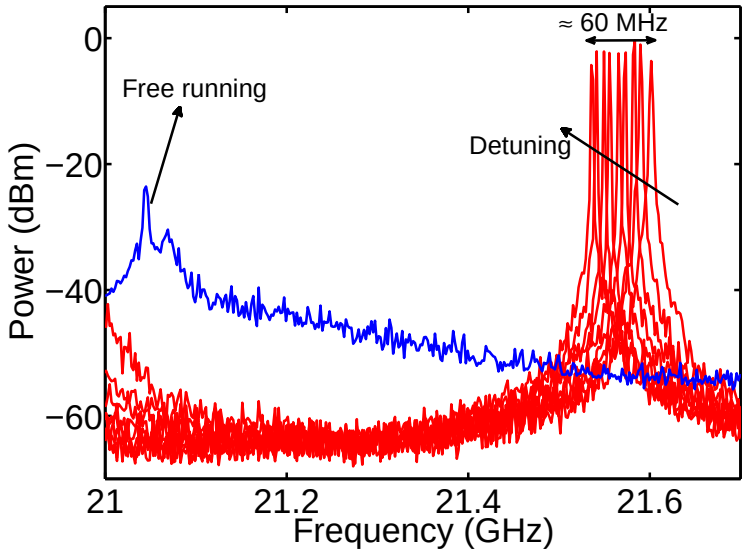



Figure 3.24: RF tuning of generated microwave frequency within the locking range (red) and second harmonic of repetition rate when free running (blue).

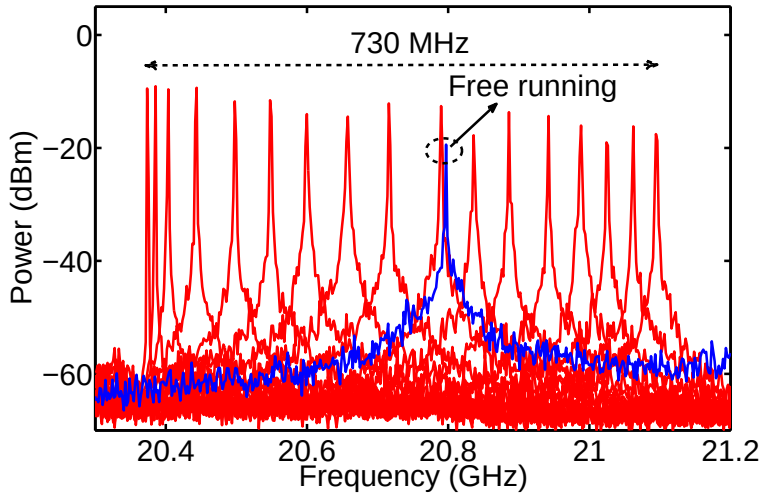



Figure 3.25: RF tuning range as wide as 700 MHz for injection-locked DBARR SMLL with injection ratio ≈13.6%. The frequency of the injection-locked laser decreased while the frequency detuning between the master and slave was increased. The free running RF frequency is shown in blue curve.

remained narrow at all points, but the number of modes was sufficient to generate a strong microwave signal. Despite the fact that such a spectral width is narrow for frequency comb generation, this locking behavior is interesting due to the wide tunability of the RF peak frequency. This tuning range could be extended to 1 GHz

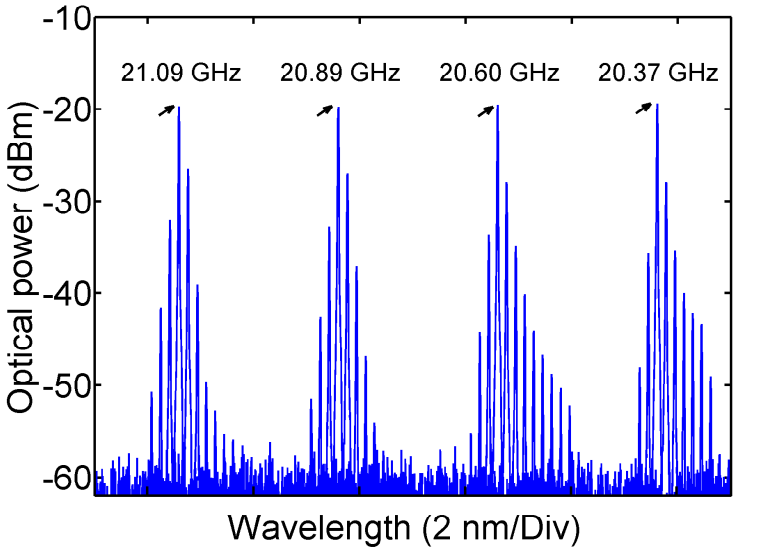



Figure 3.26: The optical spectrum of the injection-locked slave laser (injection ratio 13.6%) at selected points in the locking range. The generated frequency is shown for each spectrum and injection wavelength denoted by arrow. The spcetra were offset for clear view.

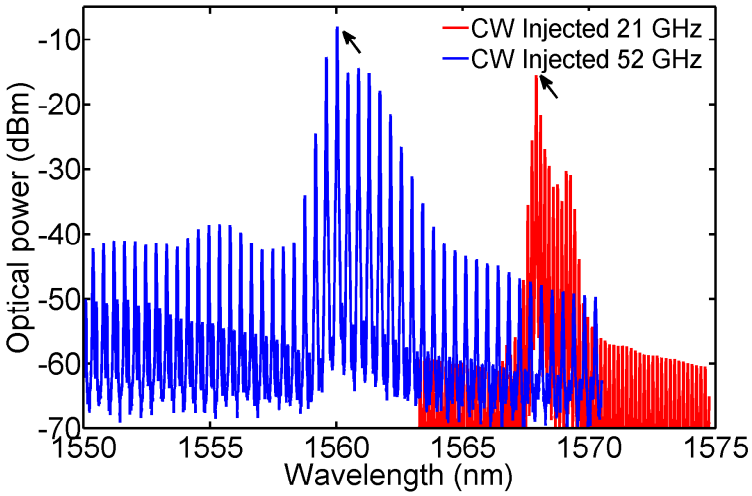



Figure 3.27: Optical spectra of CW injection-locked 52 GHz DBARR SML (solid-line/red, bias current of 120 mA, $2.3I_{th}$) and injection-locked (solid-line/blue) 21 GHz device with the same active region. The arrows denote the wavelength of injection.

for higher injection powers. If this is followed by narrow RF linewidth required for a practical application, this scheme will be attractive for monolithic tunable microwave generation.

Following the analysis of RF tuning properties, a study on the injection-locking properties of shorter devices was carried out. This problem is important for two reasons: First, as a mode-locked laser, are there any cavity effects on stability under injection locking? Second, for microwave generation, is this effect reproducible for devices with different cavity lengths. Ideally, this will be a scheme to generate microwave signals with repetition rates from few GHz to >50 GHz. This scheme is comparable to other semiconductor laser based schemes such as utilizing nonlinear dynamics [156–159]. In the latter, the microwave signal was generated by P1 operation of CW injected semiconductor laser. The frequency of the signal can be extended beyond the free running RO frequency as a result of strong injection [158]. However, the generated signal has a broad RF linewidth with instabilities of the peak in the order of 10-100 MHz and a stabilisation is required to narrow the RF linewidth [156]. The scheme proposed here demonstated microwave signal with sub MHz RF linewidth of without stabilisation. This coherence comes from retaining mode-locking between the group of injection-locked modes from the CW light.

For this purpose the same study was repeated for a 52 GHz device (G4-3, absorber length: 14.8%). The absorber section device was left open (floating) to allow for SML operation. The optical spectrum of injection-locked laser is shown in Fig. 3.27 (solid-line, blue). The CW injection-locked spectrum of 21 GHz device are shown for comparison. As can be seen, the optical spectrum clearly reproduces the same regime for

the shorter device. In the RF spectrum, no beating tone, undamped RO or any other instabilities were observed. Since the repetition rate of the device was higher than the maximum frequency of the electronic spectrum analyser, we could not measure the RF linewidth. However, we used the linewidth measurements of heterodyne beat note of individual modes as an indication of injection locking. The optical linewidth of the modes at free running was $\sim$ 100 MHz. Under injection-locking, the linewidth of the injected mode was similar to the master laser; the linewidth of the other modes slowly increased when the modes were further the linewidth was higher. The maximum value of the linewidth was less than 10 MHz which is a clear indication of phase-locking of the modes to the master laser. The intensity graphs of beat notes for three different modes measured automatically while the master laser was sweeping along one mode of the slave laser are shown in Fig. 3.28(a), (b), and (c). The (a) corresponds to one mode adjacent to the injected mode on the blue side ($M_{-1}$), (b) second mode after

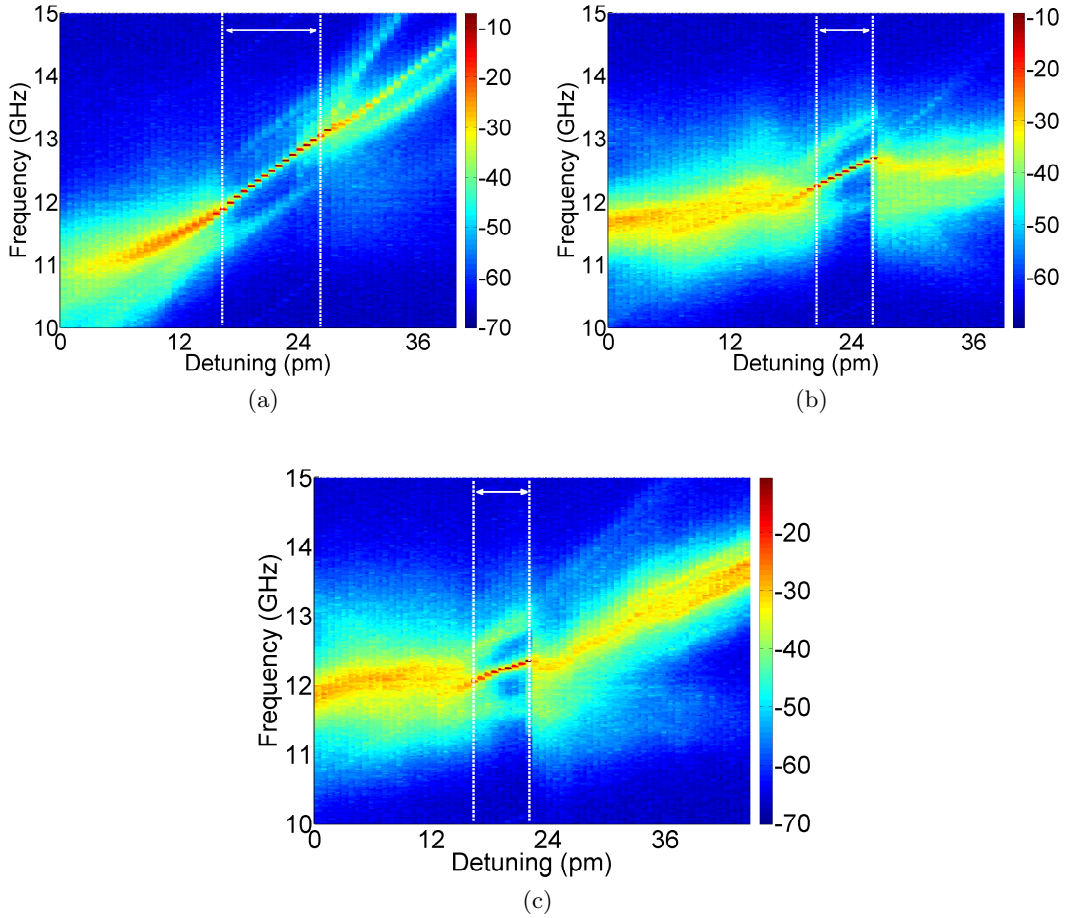



Figure 3.28: Intensity graph of heterodyne beat notes measured automatically while the master laser was sweeping for a few of modes around injection wavelength for 52 GHz DBARR device. (a). The mode adjacent to the injected mode on the blue side ($M_{-1}$). (b). Second mode after injection on the red side ($M_2$). (c). Third mode after injection on red side ($M_3$).

injection on the red side ($M_2$), and (c) the third mode after injection on red side ($M_3$). The locking range where the linewidth of the modes became significantly narrower is denoted by dashed lines.

We demonstrated the reproducibility of this microwave generation injection-locked region for a shorter device. This is a confirmation of the possibility to scale this behavior. However, a few points should be considered in this regard:

1. The optical locking-range was limited for 52 GHz device compared to our observation for a longer (21 GHz) device. This could be due to change of RO parameters (damping factor) for a shorter device despite the fact that they were from the same grown wafer. Experimental work on feedback sensitivity of QDMLLs demosntrated that shorter devices had more feedback sensitivity than longer ones [160]. Similar study on GaAs quantum dot lasers showed that longer devices had more tolerance to the optical feedback [161].

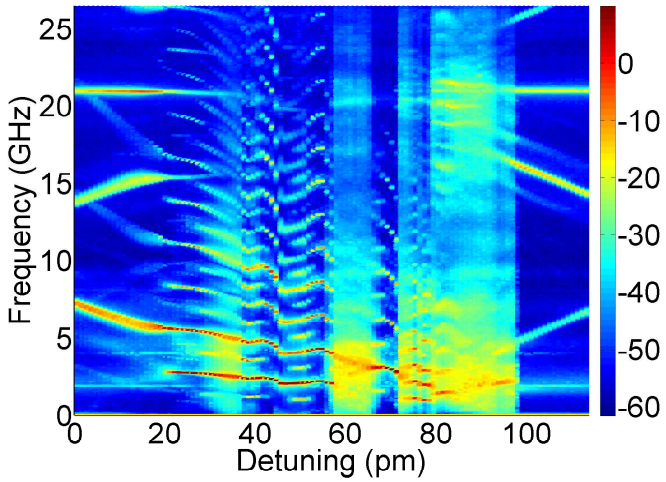
2. We only observed stable injection-locking operation when the device was biased haigher above threshold ($>2I_{th}$). At lower bias currents, the extension of undamped RO dynamics limited the observation of the stable type of locking operation we showed above. Again, this could be due to increase of damping factor and effectively more stable laser at higher currents. It is worth noting that compared to 21 GHz device and similar bias currents, we expect carrier density twice as high in the cavity.

3. Also, the device showed more tendency to single mode operation at the negative corner of locking range. This in contract with 21 GHz devices, where the injection-locked microwave oscillation was present in the majority of negative corner of locking range. For the shorter device, however, the injection-locked microwave oscillation only covered a small part of the negative boundary (about 500 MHz). Then, it followed by region where majority of power was in the injected mode. At higher injection, again the undamped RO did not allow the injection-locked microwave oscillation region to evolve.

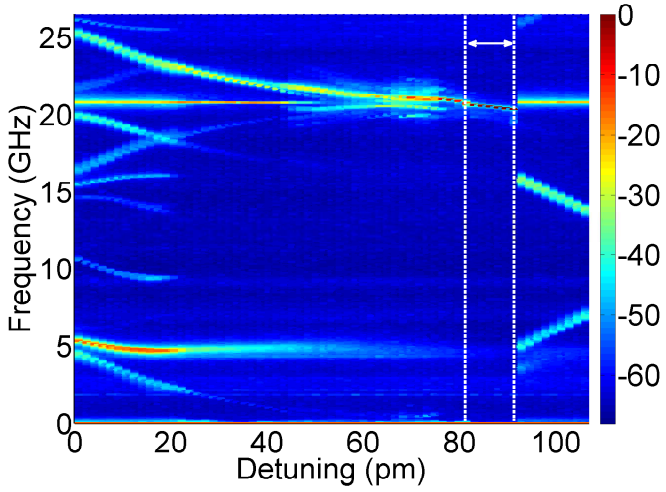
## 3.8 Comparison of DWELL and DBARR Devices

The CW optical injection experiment was repeated with a DWELL device at 21 GHz (B3) to enable side by side comparison with the 21 GHz DBARR devices. Unlike the DBARR device, the DWELL device at 21 GHz did not show stable injection-locked (either single mode or multi-mode) regime as presented above for DBARR devices. We observed strong dynamical instabilities such as chaos and limit cycles of different types, at injection levels available in our experiment. An example of dynamics, represented by intensity graphs of RF spectra obtained by automatic measurement of CW injection

for DWELL and DBARR devices, is shown in Fig. 3.29(a) and (b), respectively. The injection ratio was almost the same for both (≈9%). For the DWELL device, large amplitude instabilities such as limit cycle dynamics with different periods and transition to and from chaos to limit cycle were observed and no region of stable-locking (phase-locking) was present. In contrast, for DBARR device (Fig. 3.29(b)), no particular dynamics or instabilities such as undamped RO were observed. In addition, a wide region (1.6 GHz) of stable locking with multi-mode operation manifesting as microwave oscillation observed, denoted by double arrows. This difference could be attributed to the RO parameters of the lasers, particularly the damping parameter which is responsible for strong instabilities under optical injection [155].




(a)




(b)

Figure 3.29: Comparison of dynamics of DWELL and DBARR devices under CW optical injection. (a). Intensity graph of RF spectra for DWELL SML (B3, $I$ =120 mA, $1.4I_{th}$), injection ratio≈ 9%. (b). Intensity graph of RF spectra for DBARR SML (I3-1, $I$ =85 mA, $2I_{th}$ Absorber: 2.0%, floating) , injection ratio≈ 9%.

As we showed, the DWELL device at 10.5 GHz (4 mm length) showed limited microwave oscillation with the onset of dynamical instabilites under optical injection. The DWELL device at 21 GHz showed strong instabilities without any phase-locking (stable-locking) under optical injection. For DBARR devices, the 21 GHz device showed stable operation under optical injection representing as MWO region with reproduction of the same region for 52 GHz DBARR devices with limited locking range compared to 21 GHz device. If we consider that shorter devices have lower damping of RO than longer ones, we can conclude that DWELL devices have lower damping factor than DBARR devices and therefore are less stable under optical injection.

## 3.9 Summary and Discussions

In this chapter, we analysed the behavior of SML-QDMLLs under CW optical injection. Despite the fact that their free running mode-locking performance did not show significant difference, we observed distinct differences in their behaviour with optical injection. In particular, we found a region of multi-mode injection-locked operation for some devices. This multi-mode injection-locked behavior is believed to be an injection-locked mode-locked region where microwave signals at the first or second harmonic of the free running repetition rate could be generated.

Devices with different cavity lengths and active region types were analysed. The DWELL devices showed classic dynamical regimes observed for bulk or quantum-well lasers with optical injection with a narrow region of MWO at the second harmonic of the free running repetition rate. The latter was observed for the longest device which still showed regions of instabilities associated with un-damping of RO of the laser.

The DBARR devices, however, showed much more stable operation as well as injection-locked MWO with wide tuning of RF frequency and the possibility of scaling for shorter devices. Side by side comparison of DWELL and DBARR devices with the same cavity length revealed significant performance difference for the two types of devices. The DBARR device did not show instabilities and wide region of injection-locking (MWO operation) was observed which is in contrast to DWELL device.

In general, we believe that DBARR devices are more stable under optical injection than their DWELL counterparts. The wide RF tuning and scaling capabilities of MWO region observed under CW optical injection could be potentially used for microwave or THz generation. As we will show later, the optical feedback can be used to reduce the RF linewidth of an injection-locked mode-locked laser. We will also show in the next chapter, the injection-locking properties of two-section QDMLLs operating as SAML devices based on DBARR active region, leading to generation of high quality frequency combs.

# Chapter 4

# Optical Injection of Saturable-Absorber Dominated Mode-Locked Lasers (SAMLs)

## 4.1 Introduction

In this chapter, we analyse the behaviour of SAML devices based on DBARR type active region under optical injection. The results on CW injection as well as dual-mode injection (injection of two coherent CW lines) are presented. We show how the external injection improves the mode-locking performance of QDMLLs in several aspects such as time-bandwidth product, timing jitter, optical linewidth of individual modes as well as waveform noise/instabilities. Furthermore, we address the problem of limited repetition rate tuning in monolithic two-section mode-locked lasers. We show that optimisation is possible to widen the repetition rate tuning under optical injection utilizing the nonlinear characteristics of optical injection in a two-section SAML device. The RF tuning ratio achieved for a two-section 21 GHz device is highest than values reported for any semiconductor monolithic mode-locked laser with hybrid mode-locking technique.

First, we introduce the CW injection properties then the results on dual-mode injection is explained. A comprehensive analysis on RF tuning in free running, CW injection and dual-mode injection will be presented.

## 4.2 CW Injection

The schematic of the experimental arrangement for optical injection of SAML devices is shown in Fig. 4.1. The master laser was a commercial external cavity tunable laser (New

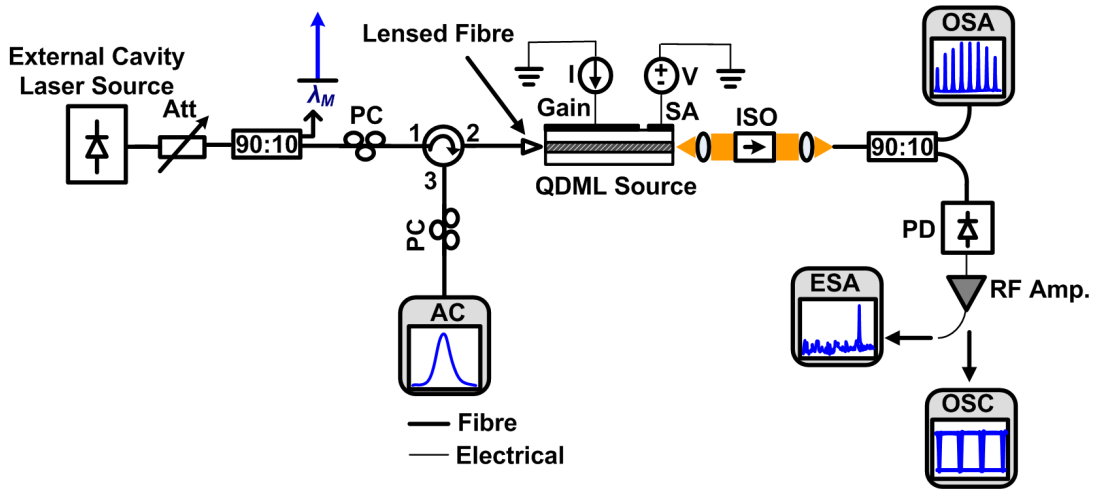
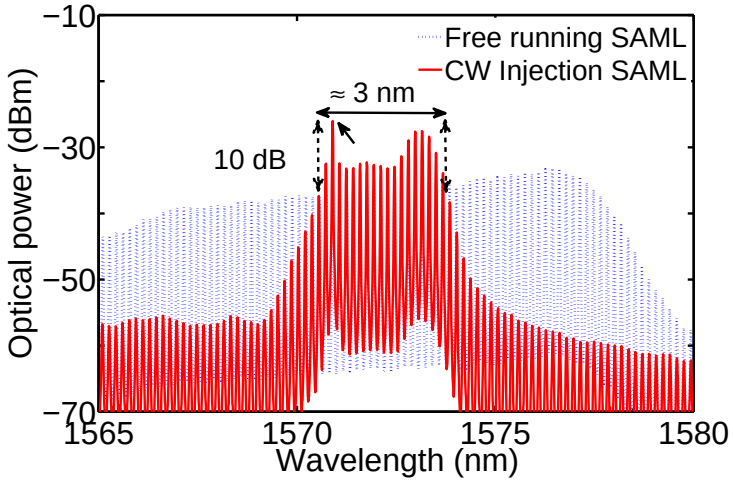



Figure 4.1: Schematic diagram of CW injection experiment for SAML device. List of acronyms: AC: Autocorrelator, Att.: Variable Optical Attenuator, PC: Polarization Controller, QDML: Quantum-Dash Mode-Locked, ISO: Isolator, OSA: Optical Spectrum Analyser, PD: Photodetector, RF Amp.: RF Amplifier, ESA: Electrical Spectrum Analyser, OSC: Digital Oscilloscope, ECL: External Cavity Laser.

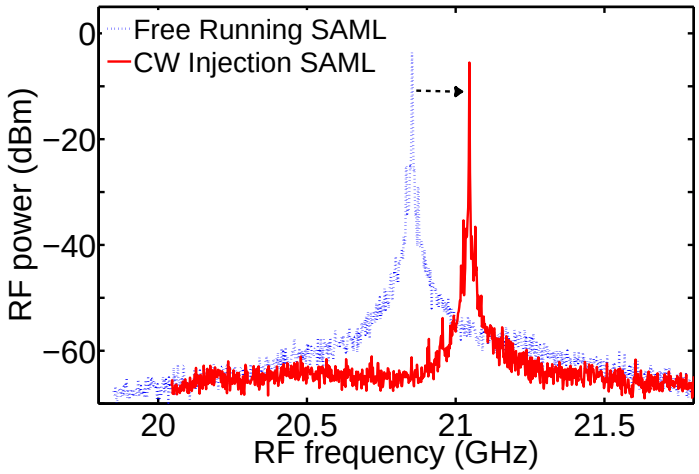
Focus 6328, 1520-1570 nm) with optical linewidth <1 MHz and fine tuning resolution of ≈ 0.5 pm. The details of the arrangement remained the same as Chapter 3.

The optical and RF spectra of the SAML device (I3-3, Absorber: 6.9%, $I$ =110 mA, $V_{Abs}$ =0.0 V) for free-running and CW injection are shown in Fig. 4.2(a) and (b), respectively. In comparison with the optical spectra of the injection locked SML, shown in Chapter 3, several differences could be seen. The locked optical spectrum was much wider for SAML (with 18 modes within 10 dB down from the peak). Also, the majority of the optical spectrum was shifted to the red by ≈ 2.3 nm from the injected mode. Experimental work on injection locking of 1.3 $\mu$m quantum dot mode-locked lasers showed a similar kind of *red shift* [96]. The latter was attributed to a difference in the alpha factor of the gain and absorber sections in a theoretical work carried out on quantum-dot mode-locked lasers [89]. Comparing the RF spectrum of the free running and locked SAML in Fig. 4.2(b), in contrast with SML, we observed an increase in the repetition rate of the laser when locked. The RF linewidth of the mode-locked tone was ≈165 kHz, lower than free running (≈600 kHz) showing increased coherence of the locked modes. Note that RF linewidth reduction under CW optical injection occurred at optimised injection parameters. Similar to injection-locked SML devices, we did not observe any low frequency components associated with the beating of master and slave or RO of the laser which is an indication of stable-locking present between the master and slave.

Injection-locking was only observed at injection ratios ∼ 1-10% at positive frequency detuning where ($f_{Master} > f_{Slave}$), unlike the SML. Here, stable locking is defined as the regime where the laser operation met the following criteria. First, in the RF do-




(a)




(b)

Figure 4.2: (a) Optical spectrum of the SAML laser (I3-3, Absorber: 6.9%, $I$ =110 mA, $V_{Abs}$ =0.0 V), injection ratio ≈2%) free running (dashed-line/blue) and locked (solid-line/red). The injected mode is denoted by an arrow. (b). RF spectrum corresponding to Fig. 4.2(a), free running (dashed-line/blue) and locked (solid-line/red).

main, no beating frequency or oscillations associated with relaxation oscillation (RO) frequency (instabilities under optical injection) existed at low frequency range (0- few GHz). Along with the shift of repetition rate, more than 20 dB suppression of laser's original RF spectral peak was also considered to determine the unlocking-locking transition. For positive values of the absorber voltage, there was an abrupt frequency shift by >150 MHz whereas at negative bias gradual shift by ∼10 MHz was observed. Second, when the free-running laser exhibited autocorrelation traces with coherence spike, injection-locking removed such spikes in the measured autocorrelation trace. This is

a likely indication of suppression of free-running instabilities in pulses generated by the injection-locked mode-locked laser. Third, in the optical spectrum of the injection-locked laser, spectral narrowing around the location of injection with significant portion of the entire power in modes shifts to longer wavelengths as shown in Fig. 4.2. As we will show later, the width of the optical locking-range (the master slave frequency range where locking occurs) could be optimised to be up to 5 GHz extending to negative detuning ranges.

### 4.2.1 Pulse Measurement and Time-Bandwidth Product Control

CW injection-locking also reduced the pulse chirp which was observed previously in Chapter 2. The free running and injection-locked pulses, measured from the autocorrelator, are shown in Fig. 4.3. As can be seen, when the laser was injection-locked, the pulse-width remained unaffected. This was achieved under optimised injection parameters and considerable reduction in the time-bandwidth product is expected considering the optical spectrum of the slave laser (Fig. 4.2(a)).

For calculation of the time-bandwidth product, we obtained the resulting pulse-width from the captured optical spectrum considering zero chirp or flat spectral phase. In other words, constructive superposition of the longitudinal modes was numerically carried out taking their relative amplitudes from the optical spectrum measurement. The procedure is depicted in Fig. 4.4; as can be seen the electric field was calculated from the

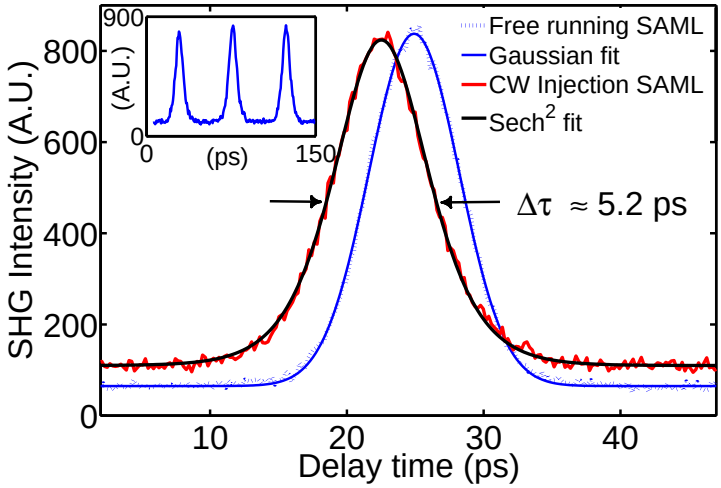



Figure 4.3: Autocorrelation traces of a single pulse for SAML laser (I3-3, Absorber: 6.9%, $I$ =110 mA, $V_{Abs}$ =0.0 V) free running (dotted-line/blue), CW injection-locked (solid-line/red), and their Gaussian (solid-line/blue) and Sech$^2$ fit (solid-line/black) with the same injection power as Fig. 4.2. The inset shows the time trace of three consecutive injection-locked pulses.

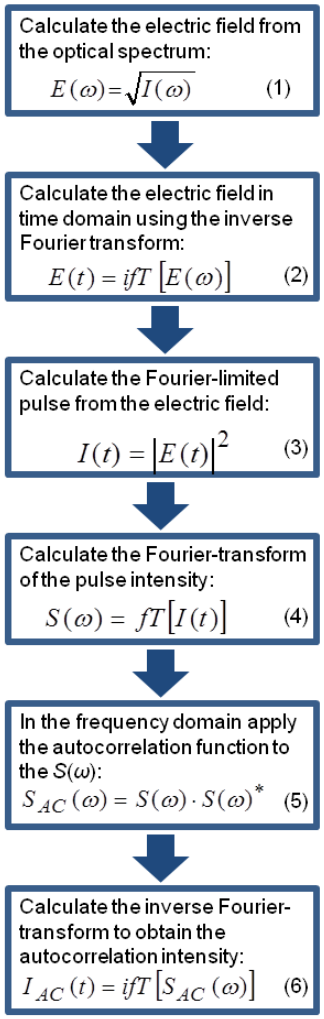



Figure 4.4: Flowchart for calculation of transform limited pulse and autocorrelation trace from the captured optical spectrum for exact time-bandwidth product calculation.

peaks of captured optical spectrum. Then, the resulting Fourier-limited pulse was calculated using the inverse Fourier-transform (Eq. 2) of the electric field with assumption of zero/constant spectral phase. The autocorrelation trace can also be calculated from the pulse shape calculating the Fourier transform of the pulse intensity and substituting into the formula for the Fourier transform of the autocorrelation function (Eq. 5). The time-bandwidth product then was calculated having the pulsewidth of transform limited and de-convolved pulses and assumption of the usual pulse shape(Gaussian or $\text{Sech}^2$). This method gives an accurate indiction of time-bandwidth product as we had a flat part in the spectra of free-running and injection-locked laser which cannot be fit to either Gaussian or $\text{Sech}^2$ distribution. Using this method, the free running laser had time-bandwidth product of 5.40 (Gaussian 5.4 ps pulses, spectral width ≈8.2 nm) reduced to to 1.08 ($\text{Sech}^2$, 5.2 ps pulses, spectral width ≈1.7 nm) when locked, indicating more than 4× reduction in time-bandwidth product. This reduction in the chirp was

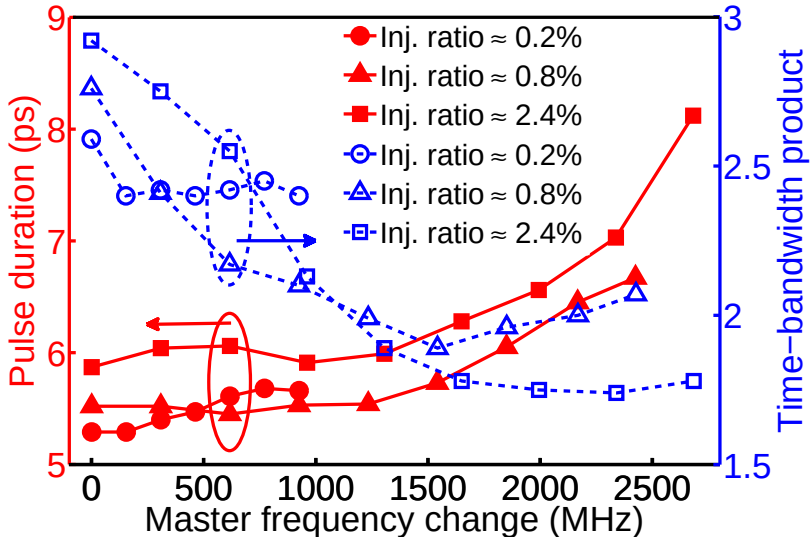


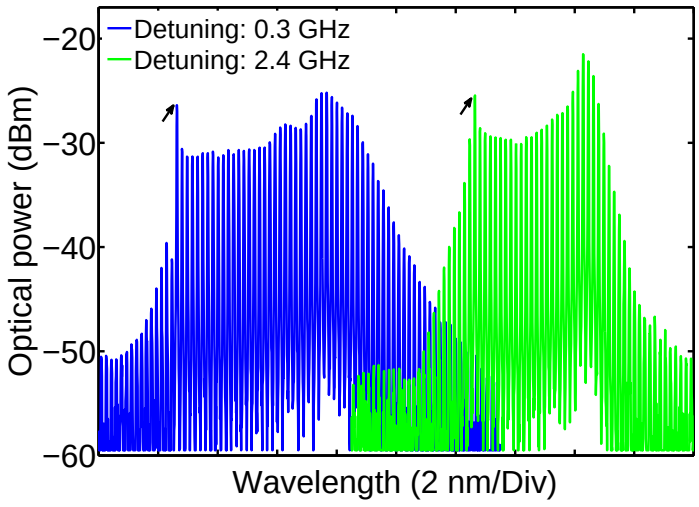

Figure 4.5: Measured pulsewidth (left axis) and calculated time-bandwidth product (right axis) for CW injection-locked SAML (I3-4, Absorber: 9.4%, $I$ =160 mA, $V_{Abs}$ =0.1 V) versus master laser wavelength change within the locking range for different injection powers.

followed by decrease of extinction ratio (ratio of the peak to the minimum in the trace) of the pulses from 11.1 dB to 8.8 dB when locked.

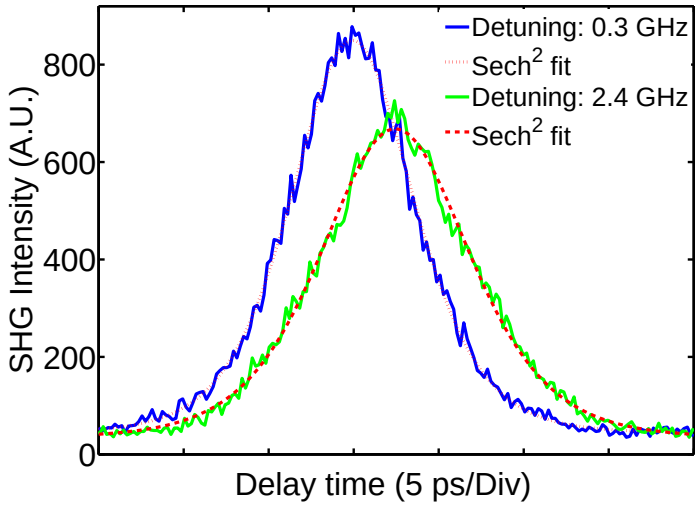
We also analysed the change of the pulse-width and time-bandwidth product of the slave laser within the locking range as the master laser's wavelength was swept as shown in Fig. 4.5 in left and right axes. The x axis is the change in the detuning (in Hz) while the master laser's wavelength was swept. The onset of the locking range was considered as the reference (set to 0 Hz). We observed an increase in the pulsewidth within the locking range when the wavelength of master laser or injection ratio were increased. The increase in the pulsewidth in either cases was followed by a decrease in the time-bandwidth product of the slave laser. This arises from a decrease in the effective spectral width (calculated from the transform limited pulsewidth) when increasing the injection ratio or increasing the master wavelength within the locking range. The optical spectra and the pulsewidths of the slave laser around two boundaries of locking range for injection ratio of 0.8% are shown in Fig. 4.6(a) and (b), respectively. The master laser wavelength was increased within the locking range. The free-running pulsewidth and time-bandwidth product were 7.2 ps and 7.17 for this bias parameters, indicating both the pulsewidth and time-bandwidth product improved with CW injection.

## 4.3 Dual-Mode Injection

We studied the behaviour of the slave laser under dual-mode optical injection when two coherent CW lines were injected to the slave laser. The experimental arrangement




(a)




(b)

Figure 4.6: (a). Optical spectra of slave SAML laser (I3-4, $I$ =160 mA, Absorber: 9.4%, $V_{abs}$ =0.1 V) for two master-slave detunings around the boundaries inside the locking range, injection ratio ≈0.8%. The spectra were offset for better viewing. (b). Corresponding autocorrelation traces with their Sech$^2$ fit; the traces were offset for better viewing.

(shown in Fig. 4.7) remained the same as Fig. 4.1 except for the master source. For generating the two coherent CW modes, the light from the master laser passed through a Mach-Zehnder modulator driven by an RF source and DC biased (at minimum) to generate two coherent CW side-bands and suppress the original master laser mode. Using this method, the spacing of the side-bands became twice the frequency of the RF source as shown in Fig. 4.7. The optical linewidth of the longitudinal modes of the slave laser was measured using heterodyne detection with another narrow linewidth

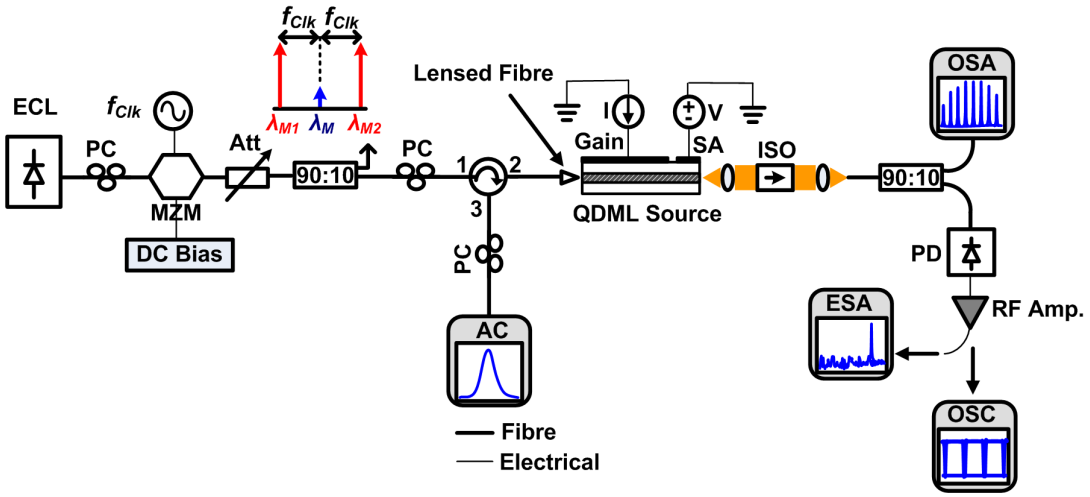



Figure 4.7: Schematic diagram of dual-mode injection experiment for SAML device. List of acronyms: AC: Autocorrelator, Att.: Variable Optical Attenuator, PC: Polarization Controller, QDML: Quantum-Dash Mode-Locked, ISO: Isolator, OSA: Optical Spectrum Analyser, PD: Photodetector, RF Amp.: RF Amplifier, ESA: Electrical Spectrum Analyser, OSC: Digital Oscilloscope, ECL: External Cavity Laser.

tunable laser source.

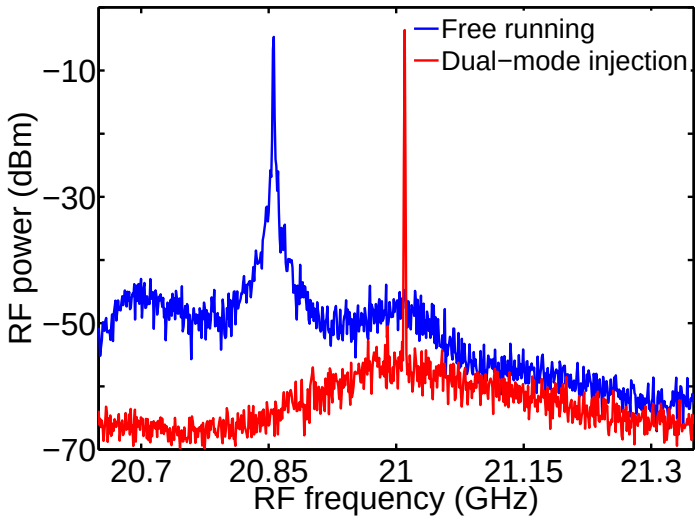
### 4.3.1 Timing Jitter Reduction

One advantage of dual-mode injection over CW injection is the significant reduction in timing jitter of the injection-locked laser. Indeed, in the case of dual-mode injection, the beating of the injected CW lines modulates the carriers, and synchronisation of pulse to pulse timing with that of the dual-modes (equal to RF source) occurs. This has a similar effect as to hybrid-mode-locking where the RF source modulates the absorber-section to synchronise the absorber timing with that of the RF source.

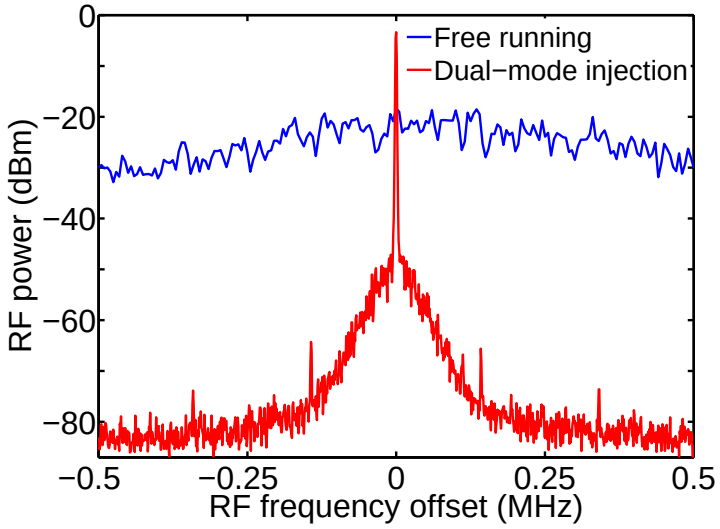
The RF spectra of the laser in free-running and dual-mode injection are shown in Fig. 4.8 (a), and (b). As can be seen when injection-locking occurred, the RF linewidth significantly narrowed forming a delta-like RF lineshape (beyond the resolution limit of the electrical spectrum analyser), similar to hybrid mode-locking, along with a lowered noise level. We expected a significant reduction of timing jitter similar to reports on GaAs quantum-dot mode-locked lasers [96].

The timing-jitter was calculated from single-side band (SSB) phase-noise spectrum of the fundamental RF frequency (21 GHz) using the following formula for RMS timing-jitter [162, 163]:

$$\sigma_{rms} = \frac{1}{2\pi f_{ML}} \sqrt{2 \int_{f_{low}}^{f_{high}} L(f)\, df} \tag{4.1}$$




(a)




(b)

Figure 4.8: (a). RF spectrum of free running SAML laser (I3-4, $I$ =160 mA, Absorber: 9.4%, $V_{abs}$ =0.1 V), solid-line/blue and dual-mode injection, solid-line/red. (b). Zoom of the RF spectra for free-running and dual-mode injection with the peak frequency shifted to zero. Resolution bandwidths for free running and dual-mode injection were 100 kHz and 1 kHz (instrument limit), respectively.

where $f_{ML}$ is the repetition rate, $f_{low}$ and $f_{high}$ are the lower and upper frequency limits for integration. $L(f)$ is the SSB phase noise spectrum, normalised to the carrier power per 1 Hz. The factor of 2 in the integral comes from the assumption of a symmetric phase noise spectrum versus the centre frequency which was the case for our measurements. Care has to be taken for integration ranges for the free running and CW injection cases where we were limited by the RF linewidth of measured data by Lorentzian fit. For the two cases, the integration should cover to the range that

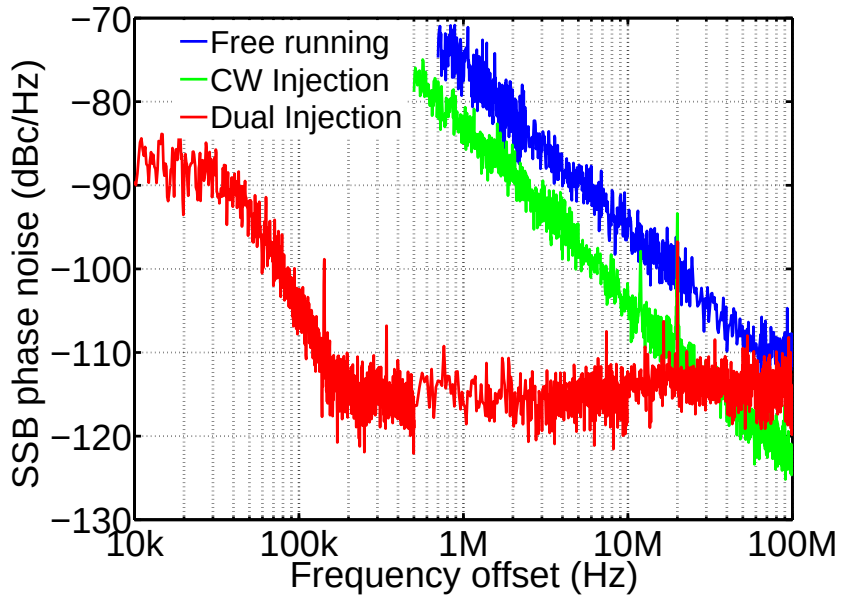



Figure 4.9: The measured SSB noise spectra for free-running (solid-line/blue), CW injection (solid-line/green) and dual-mode injection (solid-line/red) for SAML laser (I3-4, $I$ =160 mA, Absorber: 9.4%, $V_{abs}$ =0.1 V).

phase noise has 20 dBc per decade slope for Eq.4.1 to apply [164, 165]. The onset of this region is around the 3 dB frequency offset. The RF linewidth of free-running laser was ≈ 430 kHz which was reduced to 100 kHz under CW injection. We set the lower integration limit to 1 MHz for free-running and 500 kHz for CW injection. For dual-mode injection, the RF source controlled the repetition rate and the phase noise did not have low frequency fluctuations of free-running or CW injection and the RF linewidth was limited to the instrument resolution. Thus, the lower integration limit was set to 20 kHz similar to hybrid-mode-locking [166]. The upper limit of integration for all cases was set to 100 MHz [45, 166], limited by the instrument noise. The SSB spectra for free-running, CW and dual-mode injection are shown in Fig. 4.9. The calculated timing jitter using Eq. 4.1 for free-running was 1.89 ps reducing to 1.08 ps when locked by CW optical injection. The calculated timing jitter for dual-mode injection (20 kHz-100 MHz) was 229 fs which is close to the value reported for dual-mode injection of GaAs quantum-dot mode-locked lasers [96] and hybrid-mode-locking of quantum well and quantum-dot mode-locked lasers [166, 167]. The SSB noise spectrum for dual-mode injection was similar in trend to what reported in [167] indicating the major contribution of RF clock phase noise in total phase noise of the injection-locked laser (RF source: Rohde&Schwarts, Model SMR60). Further reduction of timing jitter is possible using an RF source with lower noise performance [167].

### 4.3.2 Optical Linewidth

An important advantage of dual-mode injection over electronic synchronisation techniques such as hybrid mode-locking is the modal linewidth narrowing as a result of optical injection-locking. In Fig. 4.10(a), the heterodyne beating tone of the several modes in different locations of the dual-mode injection-locked comb (solid-lines) and free-running 20th mode away from second injected mode (dashed-line/blue) are shown. As can be seen, a significant narrowing of the tone occurs for all the modes, close to that of the master laser, when the laser was injection-locked whereas the free running optical linewidth was measured to be ≈270 MHz. The normalised lineshape of this mode (solid-line/red) along with the lineshape of one of the master lasers's modulated sidebands (dashed-line/black) is shown in Fig. 4.10(b). It is evident that the lineshape of the measured mode follows that of the master laser which is a clear indication of the presence of complete coherence between this mode and the dual-modes. As we will show in Chapter 6, this characteristic is very useful for applications requiring comb generation with optical phase synchronisation of the comb lines to that of the master.

The additional performance improvement observed by dual-mode injection leads to generation of coherent narrow linewidth optical frequency combs (OFCs) from SAML lasers. Later, we show how the tuning of mode spacing in such OFCs can be optimised.

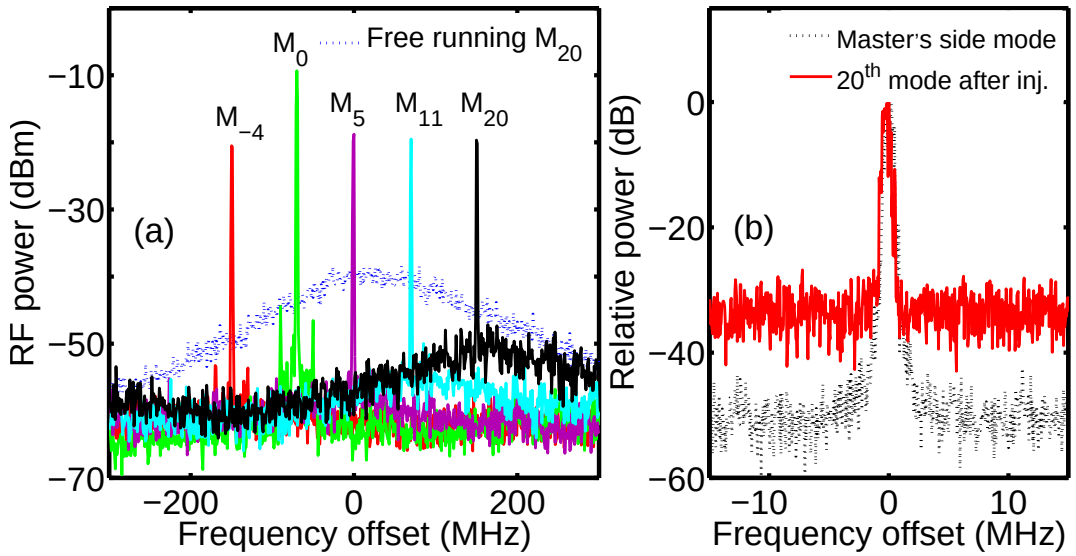



Figure 4.10: (a). Heterodyne beat note of several modes at different locations of the OFC (solid-lines) along with free running (dashed-line/blue) 20th mode away from second injected mode. The modes are denoted based on their relative modal distance from injected modes; mode with negative indice located at the blue side of injection. (b). Zoom (30 MHz span) of the normalised RF beat note for the mode (solid-line/red) and one of the master's modulated side bands (dashed-line/black), injected power ratio ≈3%.

## 4.4 Analysis of Repetition Rate Tuning

In this section, we analyse the dependence of the optical locking range and the amount of repetition rate tuning on the bias parameters. It will be shown that the locking characteristics, particularly the amount of repetition rate tuning could be significantly improved by careful adjustment of the bias parameters. For this purpose, the devices were biased under two different gain current and absorber voltages to show *distinct* SAML operation in terms of RF linewidth and pulse-width without injection. The optical spectra of I3-4 and I3-3 for two different bias parameters are shown in Fig. 4.11(a) and (b), respectively. As can be seen, decreasing the absorber bias to the corner of the SAML operating range (-0.5 V for I3-4 and -1.0 V for I3-3) caused narrowing of the optical spectrum. Spectral narrowing was accompanied by a decrease in the output power and an increase in threshold current. The gain current for the negative absorber case was increased so that the average power of the devices remained the same as that of the positive absorber voltage.

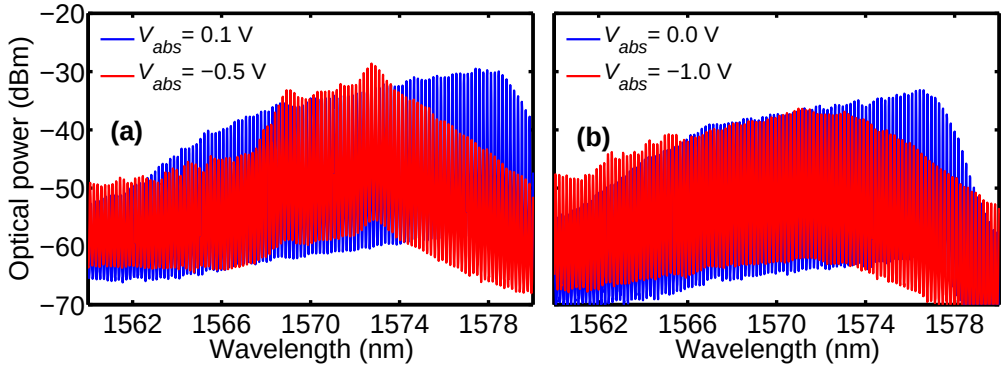



Figure 4.11: Optical spectra of two-section QDMLLs in free running operation. (a) I3-4, Gain current: 160 mA, Absorber voltage: 0.1 V and Gain current: 200 mA, Absorber voltage: -0.5 V. (b) I3-3, Gain current: 110 mA, Absorber voltage: 0.0 V and Gain current: 135 mA, Absorber voltage: -1.0 V.

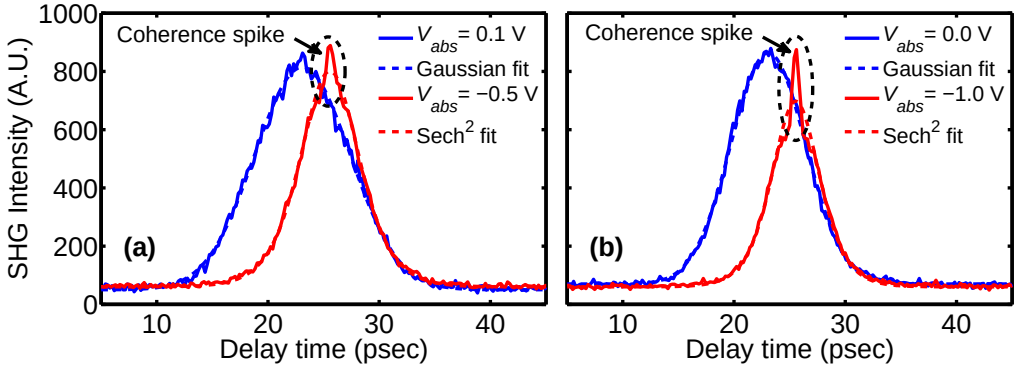



Figure 4.12: Autocorrelation measurement of two-section QDMLLs in free running operation. (a) I3-4 corresponding to Fig. 4.11(a). (b) I3-3 corresponding to Fig. 4.11(b).

The corresponding intensity autocorrelation traces of the pulses are shown in Fig. 4.12(a) and (b). The traces were intentionally offset for better viewing. The pulse-width after deconvolution for I3-4 was 7.2 ps (Gaussian fit) reducing to 4.0 ps ($Sech^2$ fit). For I3-3 the pulsewidths were 5.6 ps (Gaussian fit) reducing to 3.3 ps ($Sech^2$ fit) when the absorber was negatively biased. For both cases a clear coherence spike could be seen in the traces for negative absorber voltages. It is unlikely that these come from partial dispersion compensation in the fibre as only a few meters of single-mode fibre was used in the signal path to the autocorrelator. The existence of such peaks could indicate instabilities or some excess noise in the mode-locking operation. The RF linewidths of the devices in these two regions also showed significant differences. For I3-4 the RF linewidth at positive absorber voltage was $\sim$ 100s of kHz which increased to a few MHz for negative absorber voltage. The same trend was observed for I3-3 where the RF linewidth of a few 10s of kHz at positive absorber voltage increased to a few 100s of kHz when the absorber was negatively biased. These RF linewidth and autocorrelation traces could be an indication of *less stable* mode-locking operation for absorber biased close to the negative boundary of mode-locking operation. From here on, measurement results on I3-4 will be presented which were qualitatively similar to those of I3-3.

Repetition rate tuning is an important parameter to assess the suitability of mode-locked semiconductor lasers for real applications where some frequency deviation exists between the laser repetition rate (given by its optical length) and that of the system. In the following, we analyse the amount of repetition rate tuning in the free running and CW-injection cases.

### 4.4.1 Free Running

Fig. 4.13 shows the amount of frequency change for I3-4 in two cases: (a) when the absorber voltage and temperature of the mount are fixed and only the gain current is changed, (b) where both the bias parameters are fixed and the temperature of the mount is changed. Several differences can be seen in Fig. 4.13(a): first, an increase in the repetition rate was observed when the absorber voltage was decreased from positive to negative values. Second, the trend of frequency tuning versus the gain current for positive absorber bias is descending while it is ascending for negative absorber voltages. Third, the amount of tuning was $\sim$ 30 MHz for positive absorber voltage while it increased to 100 MHz when the absorber was negatively biased. The same kind of trend was observed when the bias parameters were fixed and only the temperature of the mount was changed. The trend for positive absorber voltage was ascending for positive absorber bias in the range of $\approx$3 MHz (not visible in Fig. 4.13(b)). When the temperature was changed with a negative absorber bias, the trend of frequency tuning was descending and large tuning ($\approx$100 MHz) could be seen.

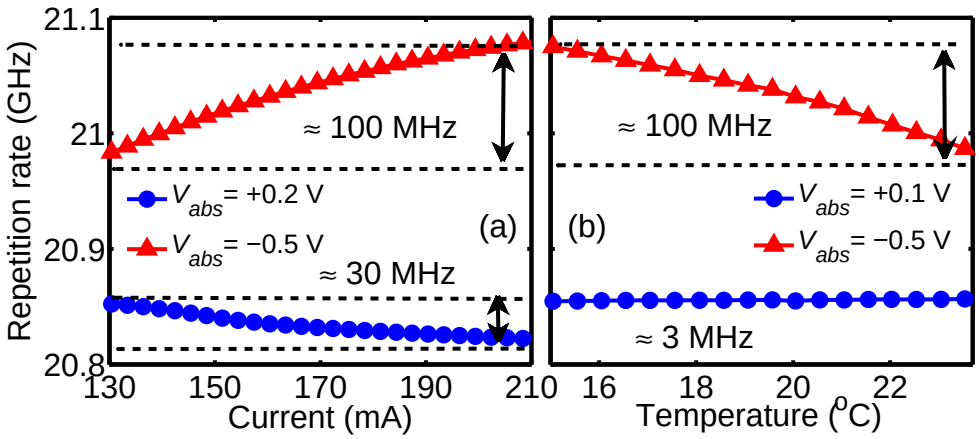



Figure 4.13: Free-running repetition rate of I3-4 for different bias parameters. (a) Absorber voltages: 0.2 V and -0.5 V, mount temperature: 20.0 $^{o}$C, gain current ranging from 130 to 210 mA. (b) Absorber voltages: 0.1 V and -0.5 V, gain current: 160 mA and mount temperature 15-23.5 $^{o}$C.

The mechanism for the difference in the sign and magnitude of frequency tuning for the two cases seems not to be only a function of change in the refractive index. For example, if we consider plasma effect (change of refractive index due to change in the carrier density) the repetition rate should always increase when the gain current is increased. This occurs because the refractive index decreases with increase of carrier density in III-V semiconductor materials and the repetition rate is inversely proportional to the refractive index. However, we observed both ascending and descending trends for different absorber voltages. Another explanation could be presented using the definition of the detuning time (the actual arrival time of the pulse according to the gain/absorption saturation time). This will cause the pulse repetition rate to deviate from the Fabry-Pérot fundamental frequency [168]. It was shown that the detuning time is primarily a function of pulse energy, the pulsewidth and detailed saturation dynamics which are governed by gain/absorber bias parameters [169]. Therefore, it is possible that the laser could be biased in a region so that the detuning time will be an ascending or descending function of the gain current and also with more or less sensitivity.

### 4.4.2 CW Optical Injection

Following study of repetition rate detuning in free running mode-locked operation, we analysed the CW injection-locking behaviour of the laser at the same bias parameters as shown in Fig. 4.11.

In Fig. 4.14, the optical locking-range (filled markers) and the amount of repetition rate tuning (empty markers) within the locking-range for two absorber voltages are shown in the left and right axes, respectively. The injection ratio (x axis) is defined

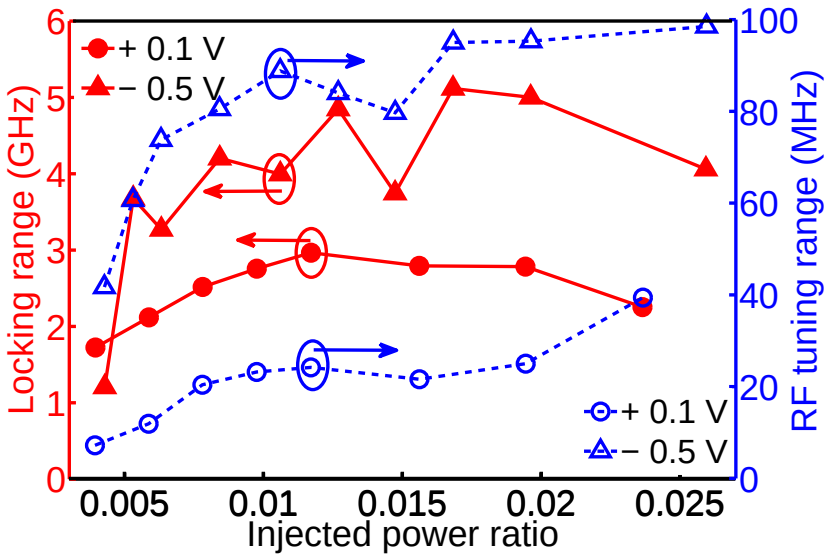



Figure 4.14: Optical locking-range (left axis) at positive absorber voltage (full circles) and negative absorber voltage (full triangles) and repetition rate tuning (right axis) at positive absorber voltage (empty circles), and negative absorber voltage (empty triangles) versus injected power ratio. The bias parameters are the same as in Fig 4.11(a).

as the ratio of injected power to the free running slave's power. As can be seen, the locking-range for the negative absorber voltage was significantly wider than for the positive absorber voltage. For this device, a locking-range up to 5.1 GHz was found which is a large fraction of the longitudinal mode-spacing (≈ 21 GHz). This widening of the locking-range was predicted theoretically in a model for GaAs quantum-dot mode-locked lasers around the boundaries of operational map for passive mode-locking, where *unstable* mode-locking evolves in free running operation [91]. In our case, the wider optical locking-range corresponded to an absorber voltage of -0.5 V while the negative boundary of passive mode-locking operation was -0.6 V. In addition to the wide optical locking-range, the amount of repetition rate tuning within the locking-range was considerably different in the two cases. The maximum amount of repetition rate tuning for the positive absorber voltage (empty circles, right axis) is ∼40 MHz while it increases to ≈ 100 MHz for the negative absorber voltage (empty triangles, right axis). This difference might arise from the initial bias conditions for the gain and absorber sections that provided a significant repetition rate tuning difference in free-running operation. However, the contribution of injection-locking in changing the detuning time and refractive index when the master laser's frequency is swept across the locking-range is unclear and requires separate investigation. Fig. 4.15 shows the change in the repetition rate within the locking-range for positive (filled circles) and negative (filled triangles) absorber voltages when the master laser is swept. The point where stable locking emerges was considered as the reference for the master frequency set (0). The injected power ratio was almost the same (1.1 % for positive and 1.2 % for negative absorber voltage) for the two cases. The free running repetition rate for

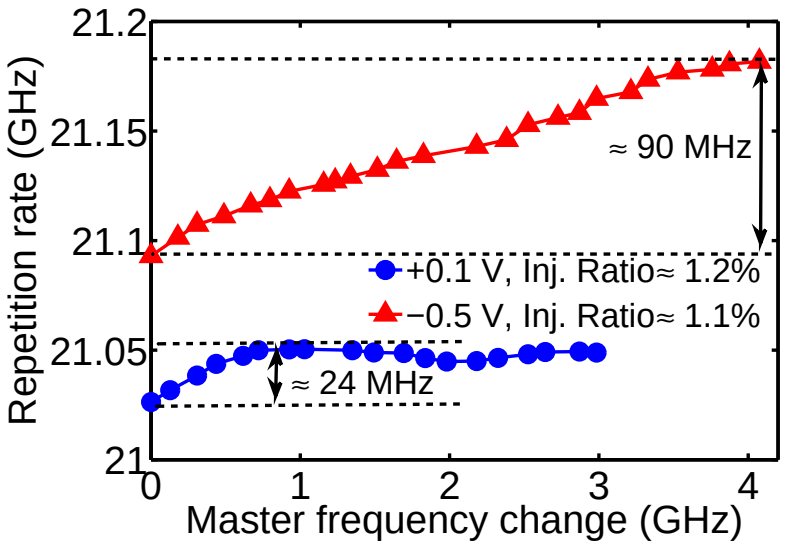



Figure 4.15: Repetition rate within the locking-range as a function of master laser frequency change for positive absorber voltage (circles, injected power ratio ≈1.1%) and negative absorber voltage (triangles, injected power ratio ≈1.2%). Bias parameters were the same as Fig. 4.14.

the positive absorber bias was ≈20.858 GHz which was up-shifted by ≈168 MHz under stable injection-locking. For negative absorber voltage, the free running repetition rate was ≈21.026 GHz (already shifted to higher frequencies than that of positive absorber voltage) was up-shifted by ≈66 MHz at the evolution of stable locking. A noticeable difference could be seen for the trend of repetition rate tuning for both cases: the repetition rate monotonically increased within the locking-range for negative absorber bias. However, for the positive absorber bias, a non-monotonic trend (first ascending followed by a descending trend and some leveling of the maximum frequency) could be observed within the locking-range. This kind of trend was observed for other injection levels depicted in Fig. 4.14. Total repetition rate tuning of ≈ 24 MHz was achieved for positive absorber voltage while it increased to ≈ 90 MHz for negative absorber voltage.

As will be shown later, the combination of wide locking-range and large repetition rate tuning range under CW injection-locking leads to much larger RF locking-range under dual-mode injection.

## 4.5 Versatile Optical Frequency Comb Generation Using Dual-Mode Optical Injection

The locking characteristics of CW injection showed that the lasers operating at negative absorber bias have a wider optical locking-range and larger tuning of repetition rate within the locking-range. Injection of two coherent CW lines (dual-mode injection),

bringing the two lines close enough (in wavelength) to two slave laser modes, caused modulation of the carriers due to saturation of the gain. Careful adjustment of this modulation frequency resulted in RF frequency locking, as well as enhanced optical injection-locking. The modulation frequency is the spacing of the two lines, or a sub-harmonic where dual-mode injection is done at an integer harmonic of the repetition rate. The spacing of the two coherent modes should be consistent with the shift of the repetition rate associated with the injection-locking process (for example, see Fig. 4.15).

### 4.5.1 Wide RF Locking-Range

We compared the RF locking-range in dual-mode injection for the two absorber voltages studied in § 4.4. The RF locking-range is defined here as the spectral region where strong narrowing of the RF linewidth occurred accompanied by a lowering of the noise level by >30 dB (resolution bandwidth: 100 kHz). In the presence of any sidebands, possibly due to self-phase modulation, an additional criterion of side band suppression by more than >30 dB was also applied. Similar to CW optical injection, the 20 dB suppression of free-running RF peak was applied for unlocked-locked transition as well. An example of such wide RF locking-range for negative absorber voltage is shown as intensity graphs in Figs. 4.16(a)-(d). The frequency spacing and wavelengths of the dual-modes were designed initially to match the RF peak in the CW injection-locked case. RF locking in this regime (Fig. 4.16(a)) was limited to a range of 92 MHz. However, by slightly increasing the master laser wavelength (center wavelength of the dual-modes) and keeping the RF spacing fixed, the slave laser transitioned from unlocked to injection-locked. Then, by increasing the frequency of the RF source, new frequencies could be included in the second locking region (Fig. 4.16(b)). Following this method, more locked regions were found, thereby widening the *effective* RF locking-range significantly.

RF locking-ranges at various injected powers available in our experiment showed significant difference for negative and positive absorber voltages. The RF locking-range versus injected power ratio for different SAML devices and for two absorber voltages (positive and negative) is shown in Fig. 4.17. As can be seen, the differences in locking-ranges for these cases are considerable due to the existence of several overlapping locked regions which broaden the upper bound of the total effective RF locking-range. The maximum RF locking-range for negative absorber voltage was $\approx$ 400 MHz corresponding to an injection ratio of $\approx$5%. Extra locked regions were mostly absent or co-existed with much lower RF locking-ranges at positive absorber voltage except for highest available injection power (last two points in Fig. 4.17), with maximum injected power at port 2 of the circulator $\approx$330 $\mu$W. Also, the length of the absorber did not seem to have a significant effect on the locking-range for positive absorber bias. It is worth noting that for negative absorber voltage locking-ranges >100 MHz occurred at even small

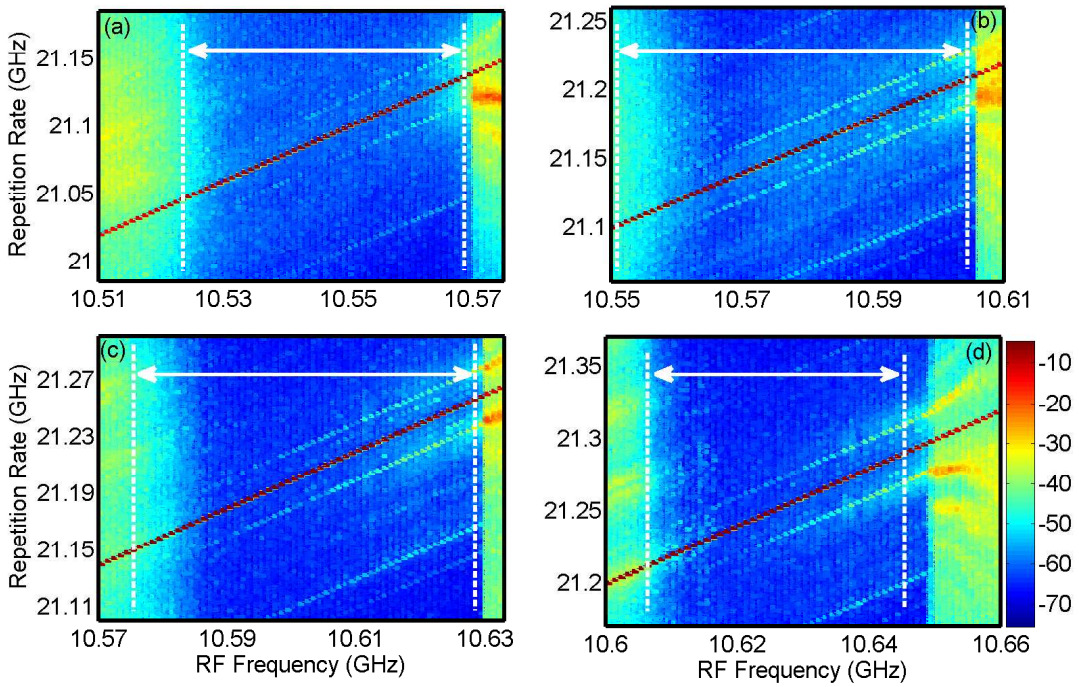



Figure 4.16: Intensity graphs for the RF spectrum under dual-mode injection with negative absorber voltage, injected power ratio ≈2.1%, the locking regions denoted by arrows (resolution bandwidth: 100 kHz). (a) Master laser wavelength: $\lambda_m$. (b) Master laser wavelength: $\lambda_m + 0.015$ nm (1.85 GHz). (c) Master laser wavelength: $\lambda_m + 0.024$ nm (2.90 GHz). (d) Master laser wavelength: $\lambda_m + 0.028$ nm (3.45 GHz).

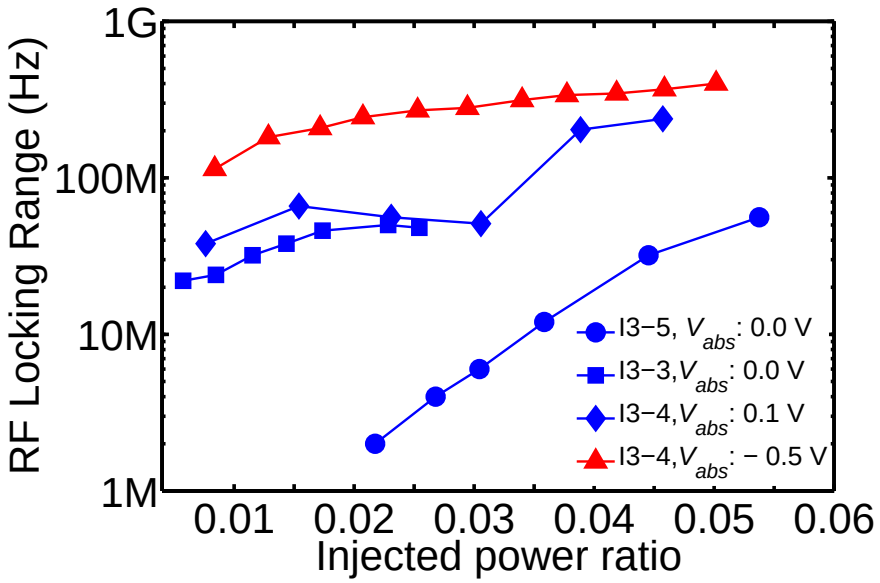
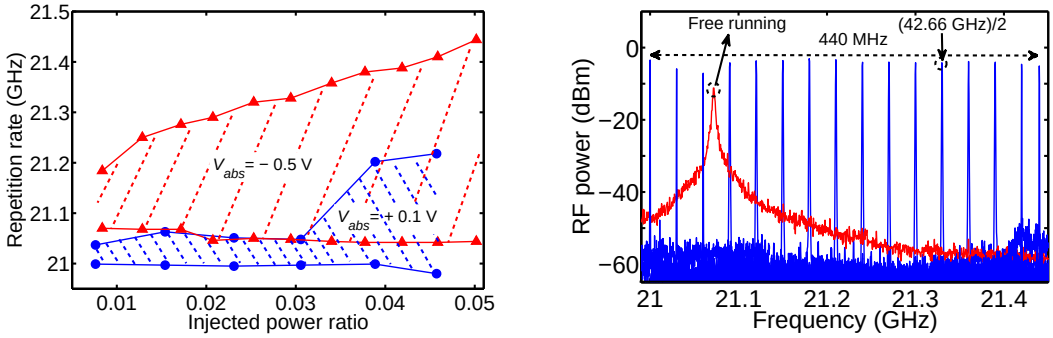



Figure 4.17: RF locking-range for dual-mode injection versus injected power for positive absorber voltage (blue marks) for I3-3 (6.9% absorber, square), I3-4 (9.4%, diamond), and I3-5 (11.9%, circle). The negative absorber voltage (red triangle) was demonstrated for I3-4 with the same bias parameters as Fig. 4.12(a).




(a) (b)

Figure 4.18: (a) Repetition rate coverage of dual-mode injection versus injected power for positive absorber voltage (region surrounded by filled triangles) and negative absorber voltage (region surrounded by filled circles) and same bias parameters as Fig. 4.12 for I3-4. (b). Demonstration of wide (≈ 440 MHz) repetition rate tuning by combining the locking-ranges for negative and positive absorber voltages. The RF spectrum of the free-running mode-locked laser is shown for comparison.

amounts of injected power.

Combining both frequency ranges covered by the injection-locked laser for the two absorber voltages, one can extend the overall locking-range to 440 MHz, as shown in Fig. 4.18(a) and (b). A typical cleaving error of 20 $\mu$m gives a device-to-device variation in designed repetition rate of ∼200 MHz which can be covered easily by such a wide RF locking-range. Also, the locking range seemed to be asymmetric with increase from the upper bound of locking range as shown in Fig. 4.18(a). The wide locking-range for negative absorber voltage also included 21.33 GHz, locking to the sub-harmonic of 42.66 GHz a defined frequency used in optical communication systems as shown in Fig. 4.18(b). This is >300 MHz higher than that of the free-running laser with negative absorber bias (21.026 GHz) and >470 MHz from free-running positive absorber bias (20.858 GHz).

The total RF locking-range of 440 MHz for a 21 GHz device means the tuning percentage of more than 2% is higher than the record achieved using monolithic hybrid mode-locked lasers at 1.55 $\mu$m [39, 40] and comparable to the widest ranges reported in monolithic actively mode-locked lasers [41]. Moreover, these published results were achieved with special RF impedance matching circuits plus multi-section devices to extend the locking-range. Here, we used simple two-section lasers without any mechanism for extra RF or phase tuning (such as passive section). Also, the optical nature of this synchronisation mechanism makes this technique transparent with respect to the RF spectrum of the injected signal, unlike hybrid/active mode-locking where impedance matching is crucial to increase the actual amount of injected RF power versus frequency. As we will show, injection-locking to a dual-mode spacing at higher harmonics of the repetition rate is also possible using this technique. Also, the shift of repetition

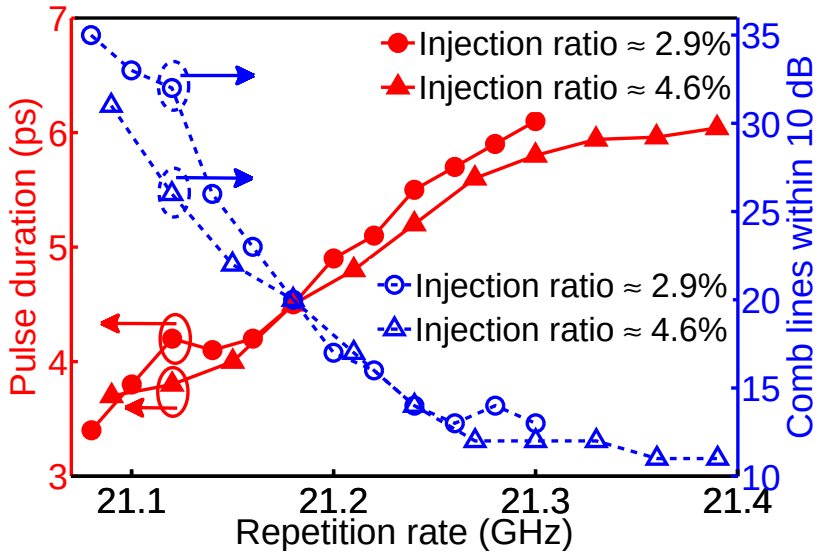



Figure 4.19: Comb pulse-width (filled marks, left axis) and number of comb lines within 10 dB spectral width (empty marks, right axis) versus repetition rate of injection-locked laser ($f_{rep}$) for injection ratios of ≈2.9% and ≈4.6%).

rate observed in dual-mode injection versus free-running values gives an extra degree of freedom in frequency coverage, where a separate frequency range could be covered using hybrid mode-locking.

### 4.5.2 Optical Spectral Properties

In addition to the RF properties of the comb, optical spectral properties such as comb spectral width and pulse characteristics are important parameters that need to be considered in real applications.

The width of pulses generated by the dual-mode injection-locked comb, and 10 dB spectral width versus locked frequency for two injection powers, are shown in Fig. 4.19. The pulse-width (FWHM of $\text{Sech}^2$ fit to the autocorrelation trace after deconvolution) of the comb started from 3.4 and 3.7 ps for injection ratio of 2.9% and 4.6%, respectively. As the frequency spacing of the comb increased within the locking-range, the pulses broadened monotonically up to ≈6 ps. The increase in the pulse-width was followed by decrease of the 10 dB comb spectral width. The number of comb lines within 10 dB of the peak started at 35 and 31 for injection ratios of 2.9% and 4.6%, respectively; then, decreased as the frequency increased with final counts 13 and 11 lines within 10 dB.

The optical spectra of the comb at selected locking frequencies separated by 60 MHz from Fig. 4.19 are shown in Fig. 4.20. The general shape of the comb consisted of two prominent modes at the location of injection, followed by an almost flat range and a group of a few modes having the highest powers among the comb lines on the red side of the comb. As the frequency increased, the spectral distance between this part and

the injected modes decreased, forming a comb with a narrower 10 dB width. This was also followed by presence of lines with unequal power at the location of injection despite the fact that the dual-modes had equal powers before injection. The comb's spectral width could be further expanded using an optical amplifier and highly nonlinear fibre to be tailored to a particular application [170]. The autocorrelation traces with their $\text{Sech}^2$ fit and transform limited autocorrelation traces for the same injection parameters as Fig. 4.20 are shown in Fig. 4.21. The transform limited traces were calculated as explained in §4.2.1. The calculated time-bandwidth product was 1.38 for the widest optical spectrum decreasing to 0.65 for the narrowest spectrum indicating residual chirp in the injection-locked laser. The free-running time-bandwith products were 7.17 for positive and 2.54 for negative absorber bias indicating reduction of time-bandwidth product due to optical injection.

### 4.5.3 On the Scaling Properties

We repeated the optical injection experiment for the shorter SAML device with the same active region (G4-3, 52 GHz). As we showed in §2.5.2, the laser showed narrow pulsewidths (around 1 ps) with lower time-bandwidth product compared to the longer SAMLs at 21 GHz. The laser, however, showed instabilities under similar injection parameters manifesting as undamped RO oscillations inhibiting stable locking operation.

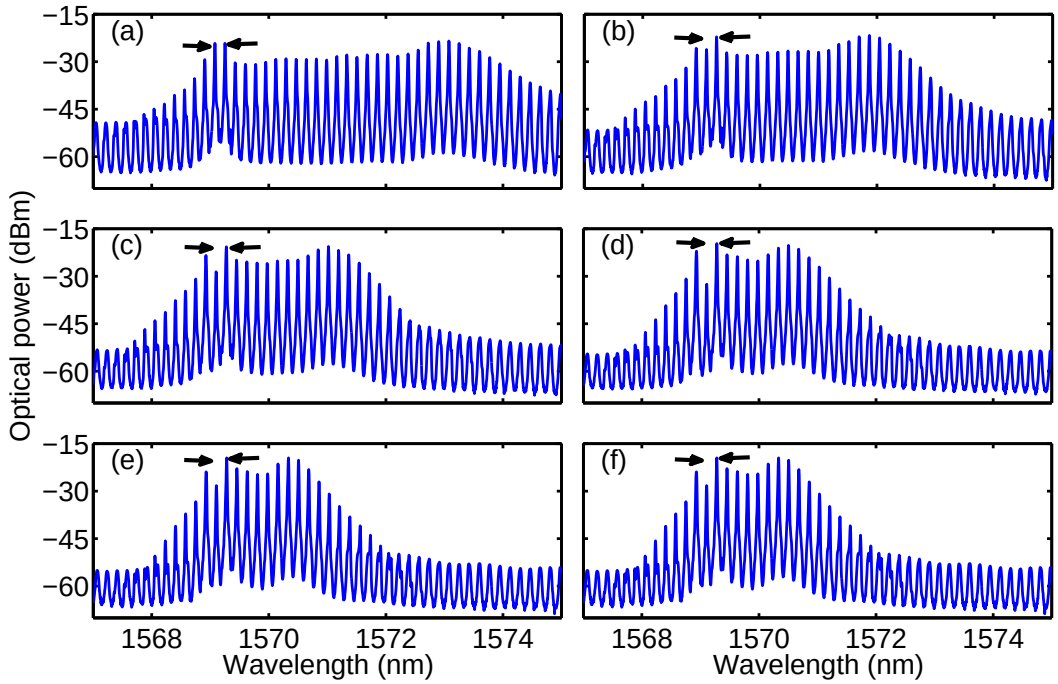



Figure 4.20: Optical spectra of OFC for injection ratio of ≈4.6% at selected frequencies with the step of 60 MHz corresponding to Fig. 4.19. (a) $f_{rep}$ = 21.09 GHz. (b) $f_{rep}$ = 21.15 GHz. (c) $f_{rep}$ = 21.21 GHz. (d) $f_{rep}$ = 21.27 GHz. (e) $f_{rep}$ = 21.33 GHz. (f) $f_{rep}$ = 21.39 GHz. The arrows denote the spectral location of injected dual-modes.

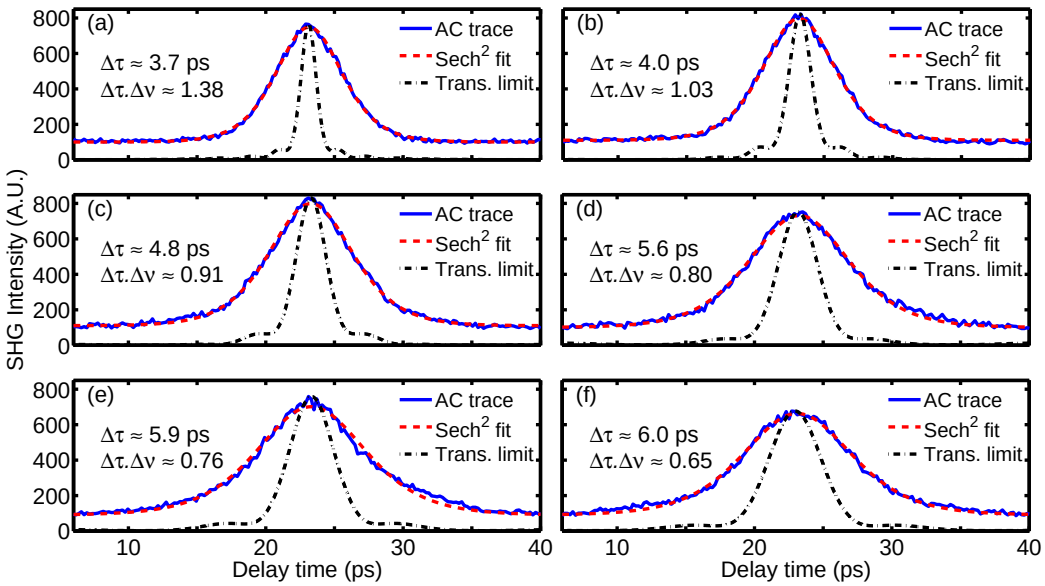



Figure 4.21: Autocorrelation traces (blue/solid-lines) along with $\text{Sech}^2$ fit (red/dashed-line) and transform limited autocorrelation traces (black/dashed-dot line) corresponding to the optical spectra in Fig. 4.20. $\Delta\tau$: Actual pulsewidth after deconvolution, $\Delta\nu$: Spectral width (Hz).

The major difference observed in the free-running operation was the onset of distinct regions of Q-switching starting near threshold and extending to about 10 mA above threshold. This regime of operation was not observed for longer SAML lasers which can be regarded as an indication of less damping of RO for shorter SAMLs [171–173].

## 4.6 Summary and Discussions

In this chapter, we described the behaviour of DBARR SAML lasers at 21 GHz repetition under optical injection. It was shown that CW injection could select a group of modes locked to the master laser and these remained phase locked together. The RF linewidth of the injection-locked laser could be lower than that of the free running laser. The injection-locked laser with optimised injection parameters can also reduce the chirp of the pulses with the pulsewidth remaining unchanged.

Injection-locking of two coherent CW lines, (dual-mode injection) demonstrated additional advantages compared to CW injection in several aspects. The RF linewidth of the laser showed strong narrowing, to a delta-like intsrument-limited lineshape, with reduction of RMS timing jitter by an order of magnitude in the sub-ps range. This value for the timing jitter is close to the best values reported in hybrid mode-locked quantum well lasers emitting at 1.55 $\mu$m. In addition, the modal linewidths of the modes in the injection-locked laser were reduced to that of the master laser.

We also carried out a further study on tuning of the repetition rate within the locking range, to optimise the RF locking-range of the injection-locked laser under dual-mode injection. Following the study of CW injection and free running laser under different absorber voltages, it was shown that the laser showed wider tuning range of the repetition rate under negative absorber voltages where the mode-locked operation is less stable. Dual-mode injection-locking of laser at the optimised bias parameters showed more than 2% the repetition rate tuning. This was a significant range obtained from a simple two-section laser without in-built tuning mechanism such as a passive section. This can cover process related deviation in the designed repetition rate for a specific application. Demonstration of wide optical spectrum along with the with narrow modal linewidths, RF beating with sub-ps timing jitter, wide RF locking-range, picosecond pulsewidth, and low chirp are essential performance requirements for high quality optical frequency combs.

# Chapter 5

# All Optical Stabilisation of Quantum Dash Mode-Locked Lasers

## 5.1 Introduction

Following the studies on CW and dual-mode optical injection of SAML lasers resulting in simultaneous improvement of timing jitter, time-bandwidth product, repetition-rate tuning and optical linewidth, we introduce a novel all optical stabilisation scheme in this chapter including simultaneous optical injection and filtered optical feedback. The optical injection-locked laser, double-locked with optical feedback showed 2× chirp reduction and RF linewidth reduction by 2 orders of magnitude. This stabilisation technique is implemented in an all-optical arrangement without optical/electrical conversion which is ideal for high repetition-rate devices and photonic integration. The chapter is structured as follows: in § 5.2 the experimental arrangement and results are described. Further discussions on the scheme are presented in § 5.3.

As we showed in previous chapters, direct pulses from semiconductor mode-locked lasers have significant chirp and poor timing jitter. Several techniques based on external stabilisation have been demonstrated to improve these two key characteristics, summarised in table 5.1.

In hybrid mode-locking [39, 40, 167], the timing of the pulses is synchronised to an external RF source by electrical modulation of the absorber section of the laser. While sub-ps timing jitter with RF linewidth limited by the RF source can be achieved with this technique, the time-bandwidth product (TBP) of the pulses does not improve significantly. Also, the electrical bandwidth is limited for a laser with high repetition-rate (40 GHz or more) and special care has to be taken in the design of appropriate

Table 5.1: Comparison of different techniques for stabilisation of mode-locked lasers based on external control.

| **Technique** | **RF-Source** | **RF-Linewdith Improvement** | **TBP Improvement** | **O/E conversion** | **Electrical BW Limitation** |
|---|---|---|---|---|---|
| Hybrid mode-locking [39, 40, 167] | Required | Yes | No | Not required | ~ Limited |
| Dual-mode optical injection [92, 94] | Required | Yes | Yes | Not required | Not limited |
| Optoelectronic feedback [174, 175] | Not required | Yes | No | Required | Limited |
| Optical feedback [90, 176–180] | Not required | Yes | No | Not required | Not limited |
| CW optical injection [81, 83, 89] | Not required | No[1] | Yes | Not required | Not limited |

impedance matching circuits [39, 41]. As we showed in Chapter 4, dual-mode optical injection, has demonstrated both timing jitter and TBP improvement simultaneously [92, 94]. Also, this technique is not limited by available electrical bandwidth as the injection/synchronisation mechanism is all-optical. However, both of these techniques require an external RF source as a reference clock for improvement of timing jitter. Optoelectronic feedback [174, 175] can also be utilised to stabilise timing jitter by conversion of the optical oscillation (using a fast photodetector) to an electrical oscillation for use in a long feedback loop. This technique does not require an RF source, but requires optical to electrical conversion and the repetition-rate of the laser determines the electrical bandwidth required. A simpler version of this technique without optical/electrical conversion has been demonstrated to improve timing jitter of the laser in a form of optical feedback [90, 176–180]. It should be noted that none of the above feedback-based techniques contribute to the improvement of the TBP. These techniques improve the mutual coherence of the laser modes by re-injecting a part of the pulsation from an auxiliary cavity with higher quality factor. CW optical injection has demonstrated the improvement of TBP [83], and waveform stabilisation[89]. While the timing jitter improvement as a result of CW optical injection has been reported [81] due to super-mode noise reduction, only slight improvement in RF linewidth was observed. This contrasts with feedback based techniques which achieve RF linewidth improvement by more than one order of magnitude. This is to be expected as CW optical injection does not produce direct carrier modulation and the interaction of external

light is mostly with the optical field in the cavity.

For stabilisation of a mode-locked laser a scheme which improves both the timing jitter and TBP without an RF source, optical/electrical conversion, and RF bandwidth limitation is desirable. We introduce a novel scheme for simultaneous improvement of timing jitter and TBP of a quantum-dash mode-locked semiconductor laser (QDMLL). For the first time, incorporation of CW optical injection and filtered optical feedback has resulted in simultaneous improvement of timing jitter and TBP. In this scheme, a narrow band-pass filter in a ring-based all-optical feedback loop was used to double-lock the injection-locked optical spectrum by self injecting a part of the spectrum. Deliberate optimisation of feedback strength and filtered spectrum leads to further narrowing the RF linewidth relative to injection-locked case, maintaining the reduction of TBP achieved by injection-locking. This scheme is all-optical and no optical/electrical conversion or an RF source is required.

Note that a semiconductor laser system with optical injection and/or optical feedback is a complex nonlinear dynamical system showing various regimes of unstable operation. Addition of optical feedback to a semiconductor laser with optical injection adds an extra level of external perturbation to the system which can force the system to become more susceptible to nonlinear dynamical instabilities [181]. Nevertheless, a quantum dot semiconductor laser with highly damped relaxation oscillation (RO) under optical injection does not appear to display RO induced instabilities, which is qualitatively similar to behavior of RO free class A laser under optical injection [155, 182]. Experimental results for such a system showed very stable operation under optical injection [182]. Here, we demonstrate simultaneous injection-locking and feedback based self-injection for a quantum-dash mode-locked laser. We believe this laser is closer to a quantum dot laser in terms of dynamical properties than its quantum well or bulk

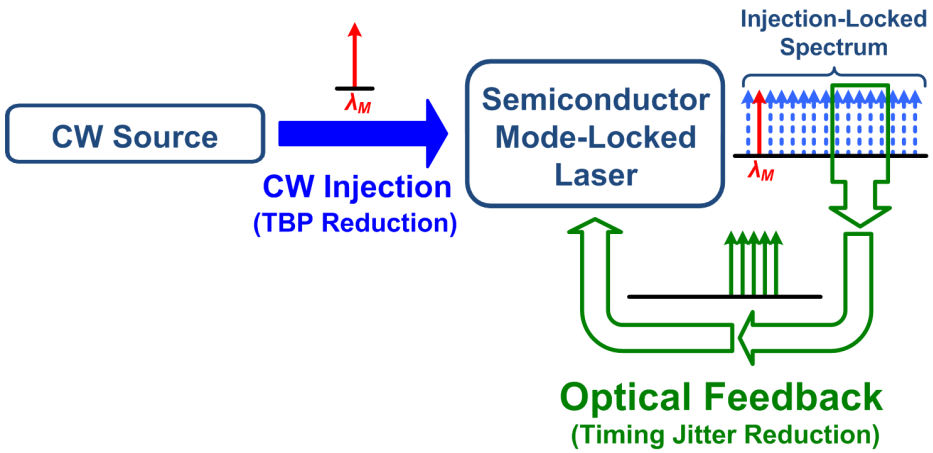



Figure 5.1: The basic diagram of the proposed scheme for stabilisation of semiconductor mode-locked lasers.

[1]Slight improvement in RF linewidth might be possible with optimised injection parameters.

counterparts. This scheme is, however, applicable for any mode-locked laser system which is stable under optical injection.

A schematic diagram for the proposed technique is shown in Fig. 5.1, a mode-locked laser was stabilised by optical injection from an external CW source in a master-slave configuration. Then, part of the optical spectrum of the injection-locked laser is fed back to the slave laser in a ring-based feedback loop to self-injection-lock the laser, effectively double-locking.

## 5.2 Experimental Arrangement and Results

The diagram of the experimental arrangement for the proposed scheme is shown in Fig. 5.2. For the optical injection part, a commercial single-mode tunable laser (New Focus 6328) with sub MHz optical linewidth was used in a master-slave (uni-directional) optical injection configuration. Light from the master laser passed through a polarisation controller and was fed into the gain side of the two-section slave laser using a lensed fiber and a circulator. Light from the absorber side was coupled to a single-mode fibre (SMF) through free-space lenses for feedback part. The ring-based feedback loop comprised a fibre-based isolator, a semiconductor optical amplifier (SOA), a 0.8 nm full-width at half maximum (FWHM) tunable band pass filter (C-band), a variable optical delay, a polarisation controller, a spool of SMF , and a variable optical attenuator

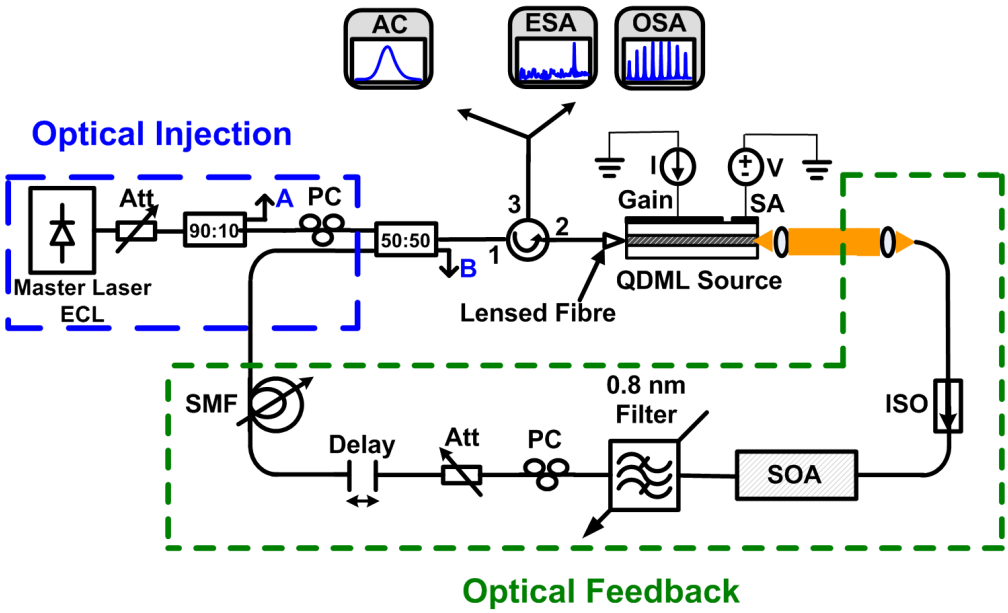



Figure 5.2: Schematic of the experimental arrangement for simultaneous optical injection and feedback. A: Optical injection monitor point. B: Optical feedback monitor point. Acronyms: AC: Autocorrelator, Att.: Attenuator, ECL: External cavity laser, ESA: Electrical spectrum analyser, ISO: Isolator, OSA: Optical spectrum analyser, PC: Polarisation controller.

to control the feedback strength. The feedback loop with different spools of SMF in length was examined to investigate the effect of delay time. The feedback signal was combined with the master laser output using a 3 dB coupler and injected through port 1 of the circulator. Port 3 of the circulator was used for analysis of optical, RF spectra and intensity autocorrelation. Taps of power at points A and B shown in Fig. 5.2 were utilised to calculate the optical injection and optical feedback strength.

The slave laser was the two-section QDMLL with DBARR active region, cavity length of $\approx$ 2030 $\mu$m, and 11.9% (240 $\mu$m) of which formed the absorber section (I3-5), giving pulsed repetition frequency of 20.7 GHz ($I_{Gain}$ = 320 mA, $V_{Abs.}$ = -0.06 V) and typical average power of $\sim$ 0.8 mW in fibre, per facet. The mode-locking mechanism was dominated by saturable-absorption as a conventional passive mode-locker when the absorber was biased well below the transparency point ($\approx$0.9 V). The gain and absorber layers were electrically isolated by $\approx$ 9 k$\Omega$. SAML operation was observed at gain currents above 250 mA and for absorber voltage of $\approx$ 0 V to +0.3 V.

Fig. 5.3(a)-(h) shows the optical spectra (left side) and corresponding autocorrelation traces (right side) for the slave laser for four cases: free-running, CW optical injection only, optical feedback only, and combination of optical injection and optical feedback with a 20 m spool of SMF in the feedback loop. The pulsewidth ($\Delta\tau$) and TBP ($\Delta\tau\Delta\nu$) are shown for each case. The TBP was calculated by determining the Fourier-limited pulse-width from the captured optical spectrum considering the zero static phase among the modes. The free-running laser ($I_{Gain}$ = 320 mA, $V_{Abs.}$ = -0.06 V) showed the pulse-width of 8.4 ps (Gaussian fit after deconvolution) with TBP of 9.48 (Fig. 5.3(b)). CW optical injection reduced the TBP to 4.77 with slight increase in the pulse-width to 9.6 ps (Fig. 5.3(d)). Spectral narrowing as a result of optical injection (Fig. 5.3(c)) with the majority of modes on the red side of injected wavelength (denoted by arrow) was observed. The laser with optical feedback only showed minor change of the optical spectrum (Fig. 5.3(e)), resulting in the TBP close to the free running with minor change in pulse-width. The laser under optical injection and feedback, had the same narrowing of the optical spectrum (Fig. 5.3(g)) as only with optical injection and similar amount of TBP reduction. The part of the spectrum which was used to re-inject as the feedback is also denoted by an arrow in Fig. 5.3(g).

The RF spectra for the laser with the four cases (free-running, CW optical injection, optical feedback, CW optical injection + optical feedback) are shown in Fig. 5.4. The laser with optical feedback showed slight decrease of repetition-rate with strong narrowing of the RF linewidth (Lorentzian fit, $\approx$ 10 kHz) compared with free-running case ($\approx$ 1.09 MHz). The CW optical injection caused an increase in the repetition-rate compared to the free-running case which again slightly pulled to lower frequencies when the optical feedback was applied to the injection-locked laser. The RF linewidth of injection-locked laser increased to $\approx$ 1.62 MHz compared to free-running; it was

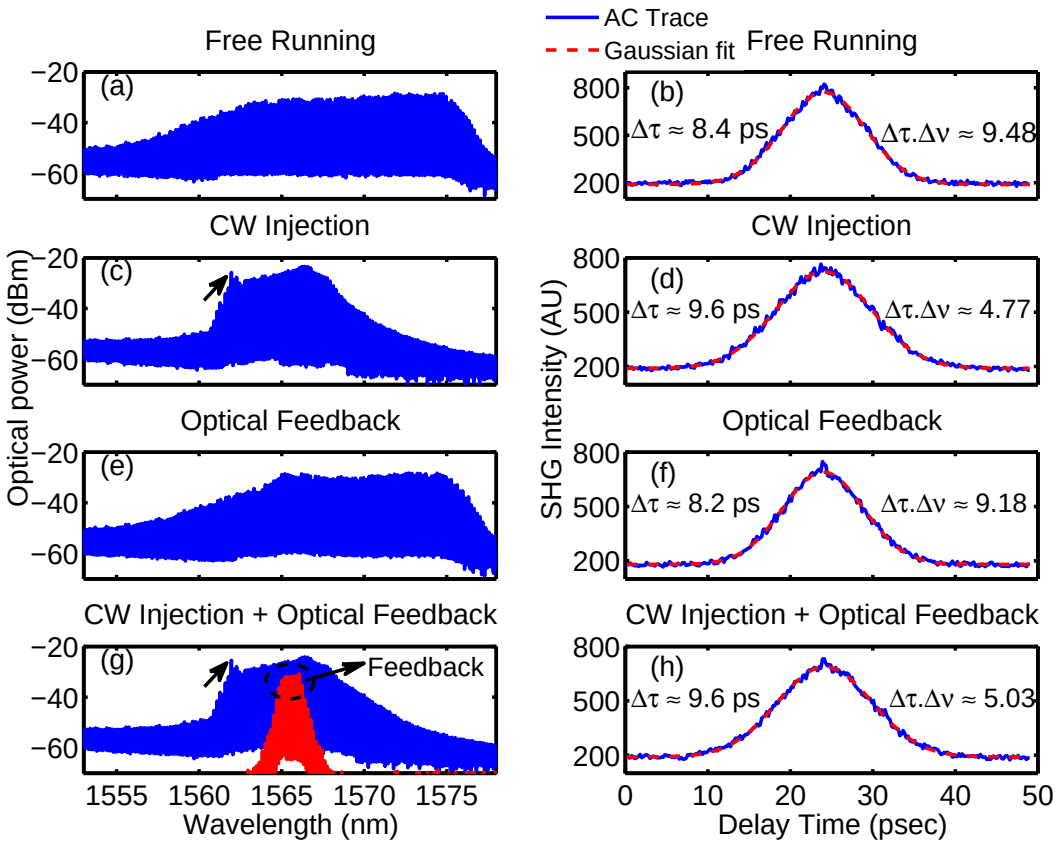



Figure 5.3: (a) Optical spectra of QDMLL when free-running ($I_{Gain}$ = 320 mA, $V_{Abs.}$ = -0.06 V). (b) Autocorrelation trace (solid-line, blue) with Gaussian fit (dashed-line, red) of QDMLL when free-running. (c) Optical spectrum of QDMLL under CW optical injection (injection strength ≈ -13.7 dB). (d) Autocorrelation trace (solid-line, blue) with Gaussian fit (dashed-line, red) of QDMLL under CW optical injection. (e) Optical spectrum of QDMLL under optical feedback (feedback strength ≈ -22.8 dB). (f) Autocorrelation trace (solid-line, blue) with Gaussian fit (dashed-line, red) of QDMLL with optical feedback (g) Optical spectrum of QDMLL under optical injection and optical feedback (-22.8 dB). The filtered spectrum used to re-inject to the laser was denoted by arrow. (h) Autocorrelation trace (solid-line, blue) with Gaussian fit (dashed-line, red) of QDMLL with optical injection and optical feedback.

reduced to ≈ 35 kHz when optical feedback was also applied, along with optical injection. The existence of external cavity side-modes (spacing ≈ 5.4 MHz in this case) was clear for the laser with optical feedback, both with and without optical injection. The RF linewidth reduced to its minimum when the round-trip time of the feedback loop became an integer multiplier of the laser's round-trip time which was slightly modified by optical injection. This was achieved by fine tuning the length of the external cavity by tuning the delay line. Changing the delay from this optimum value led to increase in RF linewidth, with continuous tuning of the repetition-rate until dominated by the next available external cavity side-mode. The trend for change of RF linewidth and repetition-rate was periodic with delay, similar to the behavior of laser under feedback only [74]. Care has to be taken in controlling the feedback strength not to de-stabilise

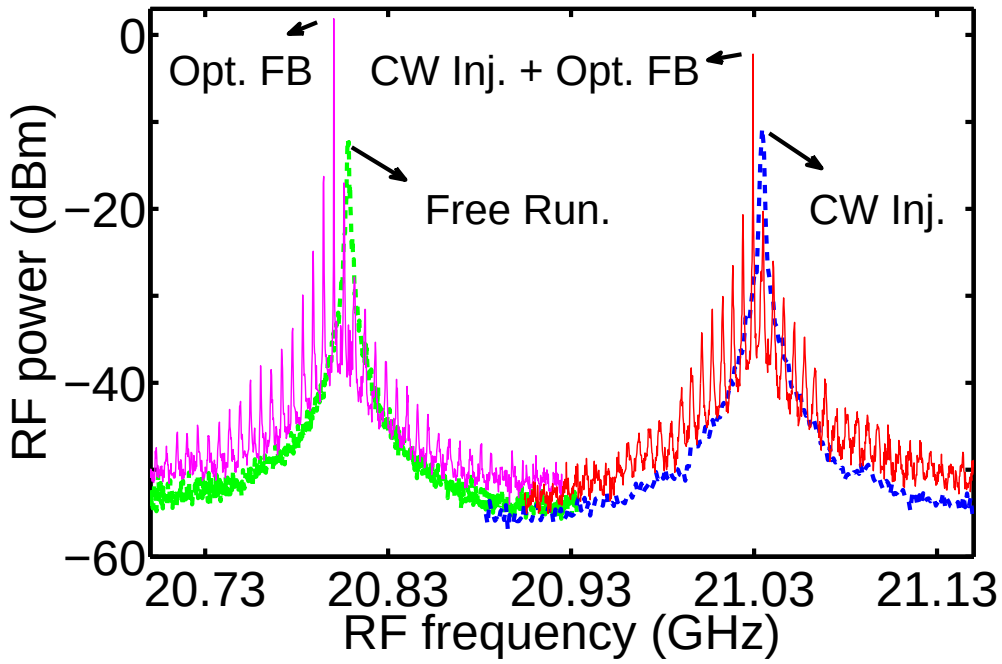



Figure 5.4: RF spectra of the mode-locked laser when free-running (dashed curve) and optical feedback only (solid curve), CW optical injection only (dashed curve) and both with CW optical injection and optical feedback (solid curve). Each case was denoted by an arrow.

the laser to the region where the external cavity modes dominate with significant broadening in the envelope of the modal peaks. The feedback strength was held below -20 dB to avoid the coherence collapse region [183]. Also, to stabilise the mode-locked laser through feedback circuit, a part of the injection-locked spectrum was selected which was far from the injection wavelength, an effect to be discussed in § 5.2.1.

We also observed dependence of the optimum RF linewidth under feedback on the wavelength detuning of master and slave lasers within the locking-range. This slightly compromised the optimum value of TBP as usually the TBP is minimum at the negative boundary of the locking-range where spectral narrowing is maximized due to optical injection. To achieve the minimum RF linewidth with optical feedback, the master laser wavelength was slightly detuned from the negative boundary which is an advantage in terms of long-term stability of master-slave locking caused by thermal drift. When the master laser wavelength was tuned within the optical locking-range, the corresponding tuning of the repetition-rate only occurred in discrete values of the external cavity side-mode spacing $\approx$ 5.5 MHz.

The reduction in RF linewidth of the laser under optical feedback mainly depends on the quality factor ($Q$) of the external cavity which is determined by the round-trip time (optical length) of the external cavity. It is expected that the RF linewidth of the injection-locked laser under optical feedback follows the same trend as laser with

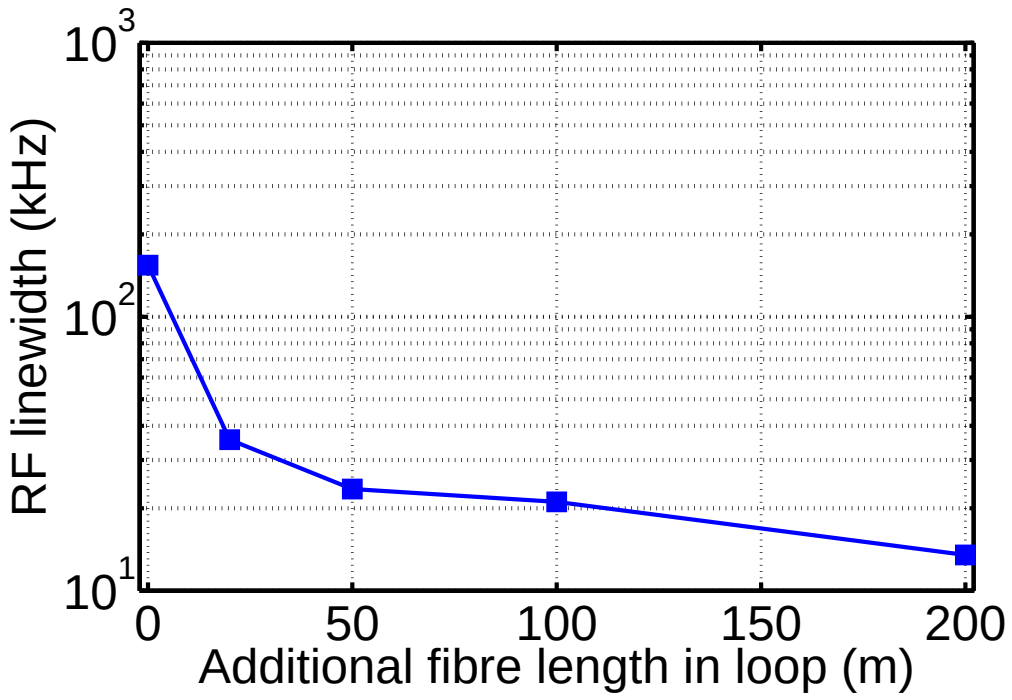



Figure 5.5: Minimum RF linewidth of the injection-locked QDMLL with additional optical feedback loop using SMF with different lengths.

feedback only when the external cavity length is varied. The effect of the external cavity length on the minimum RF linewidth of the injection-locked laser is shown in Fig. 5.5. For each cavity length, the minimum RF linewidth was obtained by optimizing the feedback strength, polarization, optical delay, and master-slave detuning within the locking-range. As can be seen, the RF linewidth of the injection-locked laser with feedback loop of minimum length (14.6 m) without additional fibre in the loop was 162 kHz, decreasing to 36 kHz by adding 20 m of SMF and to 13 kHz with addition of SMF with length 200 m. The injection-locked laser was more prone to feedback instabilities with a longer external cavity, so the maximum feedback strength for stable operation decreased with longer feedback loop.

In order to analyze the phase noise properties of the laser in more detail, the single side-band (SSB) noise spectra for the laser when free-running (with Lorentzian fit) and under CW optical injection, and with feedback of two different lengths (no additional SMF and 200 m SMF) are shown in Fig. 5.6. The external cavity modes can be seen in the SSB spectra of the injection-locked laser with feedback; these are spaced 12.5 MHz for the minimum feedback length, and 850 kHz for the longest feedback loop. For the calculation of RMS timing jitter from SSB phase noise spectra in each case, the lower integration bound was selected around the 3 dB frequency at which 20 dB/Hz slope was observed per decade of frequency offset. The higher frequency bound was set to 100 MHz which was limited by the noise level of the instrument. With these assumptions, the timing jitter of the free-running (1-100 MHz) was 4.32 ps, which increased to

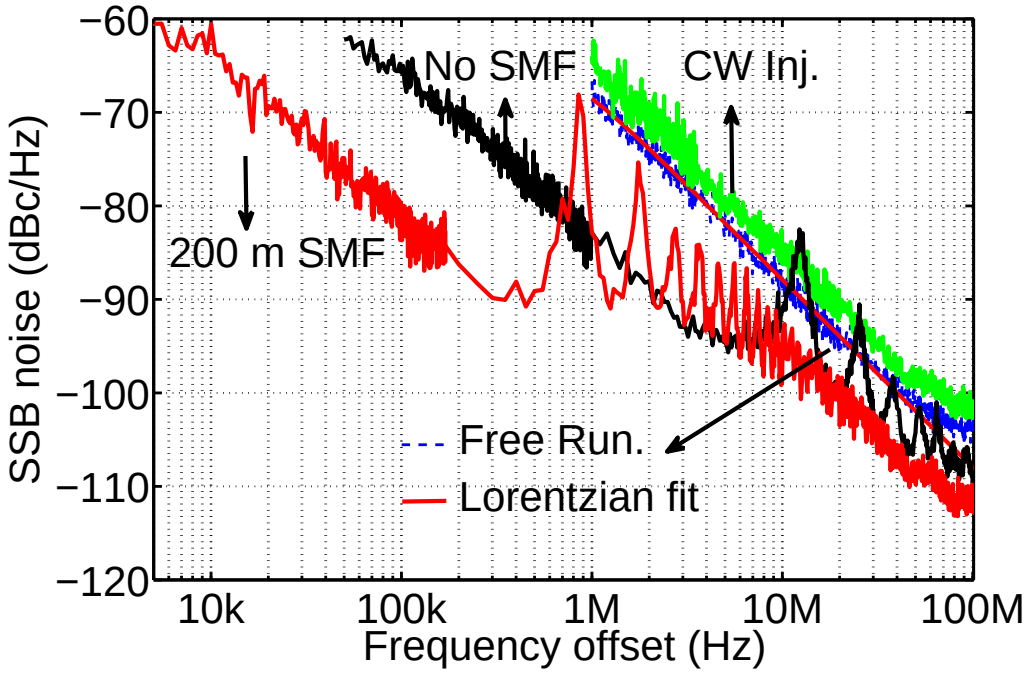



Figure 5.6: SSB phase noise spectra for the laser when free-running (with its Lorentzian fit) and CW optical injection only and optical injection + feedback for minimum and maximum length of the external cavity.

6.26 ps under CW optical injection (same integration range). For the feedback with minimum external cavity length, the calculated timing jitter (150 kHz-100 MHz) was 2.23 ps. The CW injection-locked laser with the feedback loop of maximum length (SMF 200 m) showed timing jitter (10 kHz-100 MHz) of 2.09 ps. It should be noted that the reduction in timing jitter for the last two cases was lower than expected from RF linewidth reduction. As can be seen, the SSB of the laser with feedback followed the Lorentzian distribution having the same slope per decade compared to the free-running and CW injection cases. For the SSB with Lorentzian distribution, the major contribution to the timing jitter ($> 90\%$) lies within the first decade from the lower frequency bound which means 150 kHz-1.5 MHz for the first feedback case and 10 kHz-100 kHz for the latter. If we modify the integration to exclude the external cavity modes (150 kHz- 6.25 MHz for minimum length feedback and 10 kHz-425 kHz for the maximum length feedback) the timing jitter for the minimum and maximum feedback lengths are 1.74 ps and 790 fs, respectively. This indicates that the contribution of the external cavity side-modes to the timing jitter is significant, particularly for the longer cavities as they are closer to the main peak and are less suppressed. The external cavity modes can be suppressed by using an additional loop shorter than the main loop, in a dual-loop scheme. Precise alignment of the length of the two loops will lead to resonance at certain modes which are a harmonic of those of the main (longer) loop, as well as interference effect from the different delays in the two paths [175]. These two phenomena effectively reduce the timing jitter due to suppressing the side-

modes. While the utilisation of dual-loop feedback has been implemented in coupled optoelectronic oscillators (COEO) [174, 175], an optical feedback equivalent of this scheme was recently implemented for a 1.55 $\mu$m quantum-well mode-locked laser [180].

### 5.2.1 Mechanism in Filtered Feedback

The feedback scheme used in this experiment was a selective one, which a part of the injection-locked spectrum was fed back to the slave laser. This filtering scheme was essential to prevent the system de-stabilising from the double-locked state. Moving the center frequency of the filter towards the injection wavelength forced the system to instabilities, mainly resulting in slow and strong fluctuations of the repetition-rate. We investigated the possible reason of such instabilities by measuring the optical (modal) linewidths of the modes, measured by heterodyne technique, in the injection-locked spectrum. The modal linewidth (Lorentzian fit) versus the mode index (with respect to the injected mode) with their corresponding coherence lengths are shown in Fig. 5.7. The coherence length was calculated from $\frac{c}{\pi\Delta\nu_M}$, where $c$ is the vacuum velocity of light and $\Delta\nu_M$ is the optical linewidth of each mode (in Hz). As can be seen, the modal linewidth increased rapidly after the injected mode, leading to decrease in the coherence length. This is in contrast to dual-mode optical injection where all modes have similar linewidths to the master laser (Chapter 4). The coherence length decreased to a few meters beyond the 10th mode after injection, which is significantly smaller than the minimum feedback length (14.6 m in our experiment). This was close to the minimum

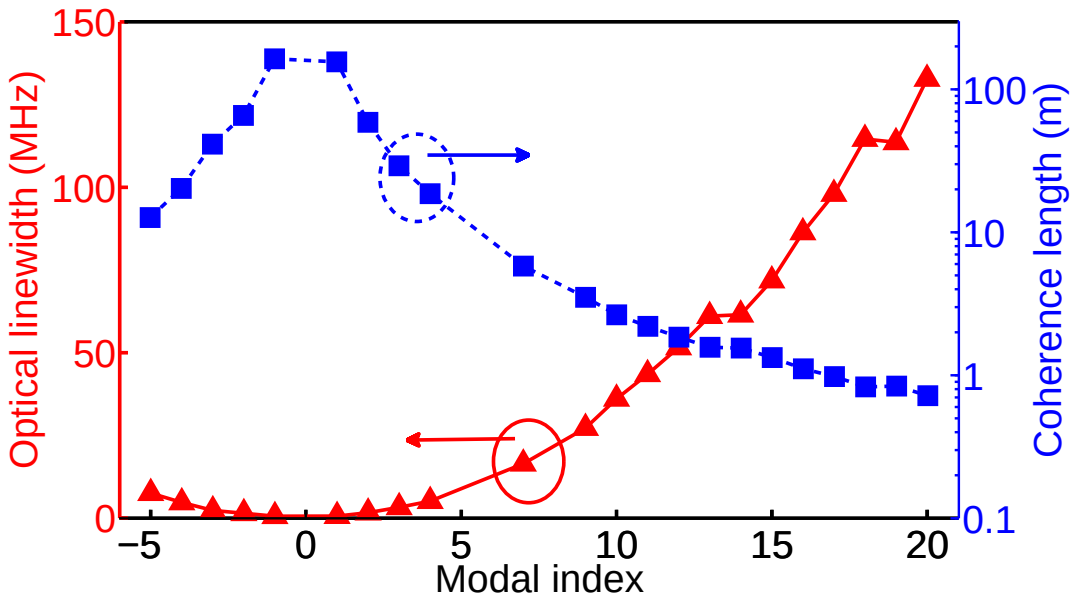



Figure 5.7: The modal (optical) linewidth of the injection-locked laser (left axis) and their associated coherence length (right axis) versus modal index (relative distance from the injected mode).

center wavelength of the BPF to keep the self-injected feedback stable. This is likely due to the fact that selection of modes away from the injection led to modes with coherence lengths much shorter than the external cavity length. Each such mode lacks the phase information with respect to its equivalent in the injection-locked spectrum while the mutual coherence among all the selected modes is maintained due to propagation in the same path. As a result, the feedback is effectively incoherent where the interaction of optical fields in the cavity is minimized. However, the selected modes are interacting with the carriers leading to carrier modulation due to the coherent beating of the modes.

## 5.3 Summary and Discussions

In this chapter, we have demonstrated the potential of the combination of optical injection and optical feedback; this should be regarded as a proof of concept rather than achieving the record values. For example, more reduction in TBP to the values below 1.00 with narrower pulses is possible by optical injection-locking of a two-section device with shorter absorber length and negative bias (refer to the results in Chapter 4 for I3-3 and I3-4). The device used in this experiment had a long absorber so that no lasing was observed under negative absorber voltage due to excessive absorption. In addition, a master laser with sub MHz optical linewidth was utilised in this experiment which necessitated the use of filtered optical feedback with a SOA because of the relatively low output power after filtering. It should be possible to remove the filter and SOA in the loop to use the whole injection-locked spectrum as feedback by using a CW line with moderate optical linewidth (∼MHz range). Ideally, this CW line could be selected from the optical spectrum of a Fabry-Pérot laser, which eases the selection of master source compared to an external cavity or DFB laser and also facilitating the photonic integration. In addition to the dual feedback loop suggested to remove the contribution of external cavity side-modes in timing jitter, we expect further reduction of RF linewidth using a longer feedback loop with higher quality factor and/or optimized RF injection, as optoelectronic feedback, to the cavity. This requires investigation of other limiting effects in such a long feedback loop like dispersion, which will be investigated in a separate study. In an ideal picture, utilisation of external cavities with very high quality factors should result in SSB phase noise spectra comparable to those from an RF source and timing jitters as low as values reported in hybrid mode-locking or dual-mode optical injection.

Another potential application of this scheme is to stabilise the microwave generation previously reported in CW optical injection-locking of SML QDMLLs in Chapter 3. This requires optimization of our scheme to work for a relatively narrow optical spectrum. While the scaling of the microwave generation for lasers with frequencies up to 52 GHz was demonstrated under CW injection, the optical feedback stabiliser loop has the advantage of no limitation for electrical bandwidth for such high-speed lasers. The

optimized scheme with a bank of lasers each spanning a range from ∼1-50 GHz with repetition-rate extended with optical injection and stabilised with optical feedback can be a simple, cost effective system of microwave oscillators.

# Chapter 6

# Application of Injection-Locked Mode-Locked Lasers for Phase Sensitive Amplifiers

## 6.1 Introduction

Following the results on injection-locking and coherent optical frequency comb generation from quantum-dash mode-locked lasers (QDMLL), we show an important application of injection-locking in this chapter. We demonstrate the utilisation of QDMLL injection-locking in a phase-sensitive amplifier (PSA). Implementation of a phase-synchronisation scheme is a critical part of a "black-box" (practical) PSA. The idea of synchronisation of many comb lines with injection-locking of two coherent lines to a QDMLL was extended here to generate a comb of coherent lines used as suitable pumps for a PSA. This new phase-synchronisation scheme is particularly important when the PSA is supposed to have more than one input signal at different channels (multi-wavelength PSA). With the currently available practical scheme one injection-locking stage per channel is required. We show that it is possible to merge all injection-locking (phase-synchronisation) stages into one laser.

The contents are presented as follows: first, we present a brief background on PSAs, particularly a practical, black-box PSA scheme. Then, the experimental arrangement to use a QDMLL for phase-synchronisation of a two-channel PSA is introduced. With focus on noise properties of carrier extraction stage, we analyse the injection-locking performance under different situations. Finally, the PSA basic performance including phase-sensitive gain and bit-error rate measurements are demonstrated for the optimum injection-locking case.

## 6.2 Basics of Phase Sensitive Amplifiers

Differential phase shift keying (DPSK) modulation formats have proven several advantages over amplitude encoding schemes such as 3 dB more sensitivity at the receiver and robustness against impairments caused by components in an optical communication system [184]. However, transmission over long distance in optical fibre imposes inevitable impairments, particularly accumulated phase noise in the signal [184]. This necessitates utilisation of signal regenerators to remove the phase noise and clean the signal before the receiver. PSAs have recently attracted a lot of interest due to their unique phase squeezing capabilities, which make them an ideal technology platform for regenerating phase encoded modulation formats, e.g. DPSK [185, 186].

The main difference between a phase-insensitive amplifier and a PSA, known as *phase squeezing*, is illustrated in the form of phase diagrams in Fig. 6.1(a) and (b), respectively. For a phase-insensitive amplifier (like an EDFA or SOA) the amount of gain available for the input signal is independent of its phase, so the phase of the output will be the same as that of the input. On the other hand, for a PSA the amount of gain available for the signal depends on the phase of input signal. For example, the in-phase component of the signal will experience higher gain ($g$) than that of quadrature component ($\frac{1}{g}$). Therefore, the phase of the output signal will be a "squeezed" version of the input in favor of the in-phase component. This characteristic which has been well known for more than a decade [187] makes the PSAs ideal for signal regeneration.

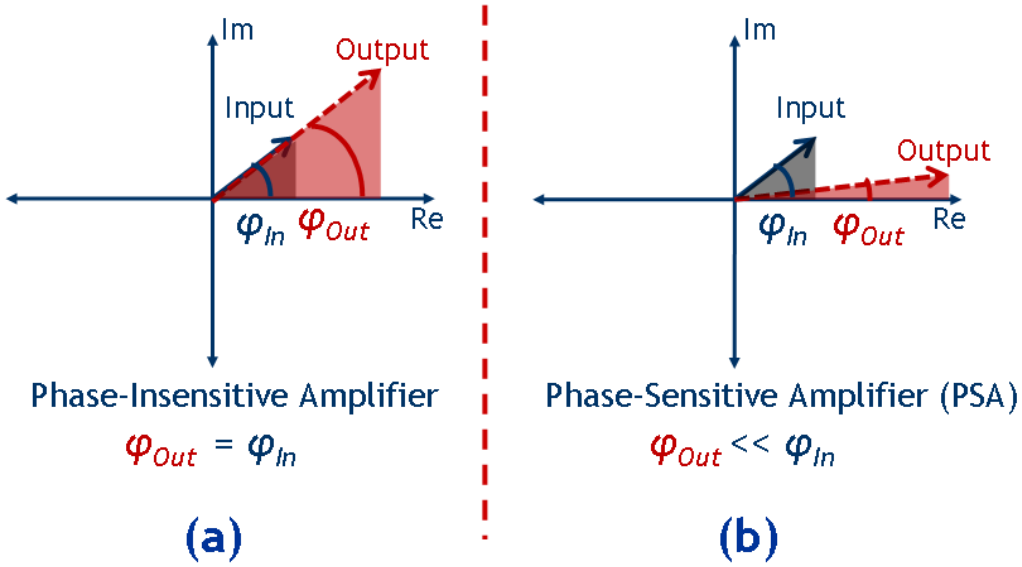



Figure 6.1: Comparison of a phase-sensitive amplifier (PSA) and phase-insensitive amplifier (PIA) in terms of phase diagram. (a) Phase-insensitive amplifier. (b) A PSA.

## 6.3 PSA Schemes

The PSA has been realised experimentally in several different schemes. All these schemes are common in utilising pump(s) and idler(s) to amplify the signal upon the phase difference between the signal and that of the idler and pump. For example, in a PSA based on degenerate four-wave mixing (FWM), the idler is generated at the same frequency of the signal and the amplification or attenuation is dependent of constructive or destructive interference between them. In this case, the signal experiences maximum gain if its phase is the average of those of the pumps [188]. One important difference between these schemes is whether the signal and idler have the same frequencies (degenerate PSA) or different frequencies (non-degenerate PSA). The basic block diagram of these schemes are shown in Fig. 6.2(a), (b), and (c). In Fig. 6.2(a), a noisy signal was combined with a pump for PSA operation, propagating in opposite directions in a nonlinear loop mirror. Phase-sensitive amplification occurred based on the phase difference between the signal and the pump at the input [185, 189] leading to significantly reducing the phase noise of the input signal. As shown in Fig. 6.2(b), the PSA can also be implemented in a non-degenerate scheme where an idler at frequency symmetric with respect to the signal was utilised to perform phase-sensitive amplification [190]. Finally, a PSA can be realised in a degenerate dual-pump scheme [186] where two pumps were utilised for phase-sensitive amplification of a signal whose frequency is the average of the pump frequencies (Fig. 6.2(c)). In the latter, the idler is generated in the same frequency as the signal and phase-sensitive performance can be achieved depending on the difference between the phase of the idler and those of the signal and pumps. In any PSA, the main requirement is to have the phase of the signal(s) and corresponding pump(s) synchronised together.

In a real optical communication system, only the signal carying the modulated data is sent through the optical link. Therefore, a practical PSA that can be used as an inline

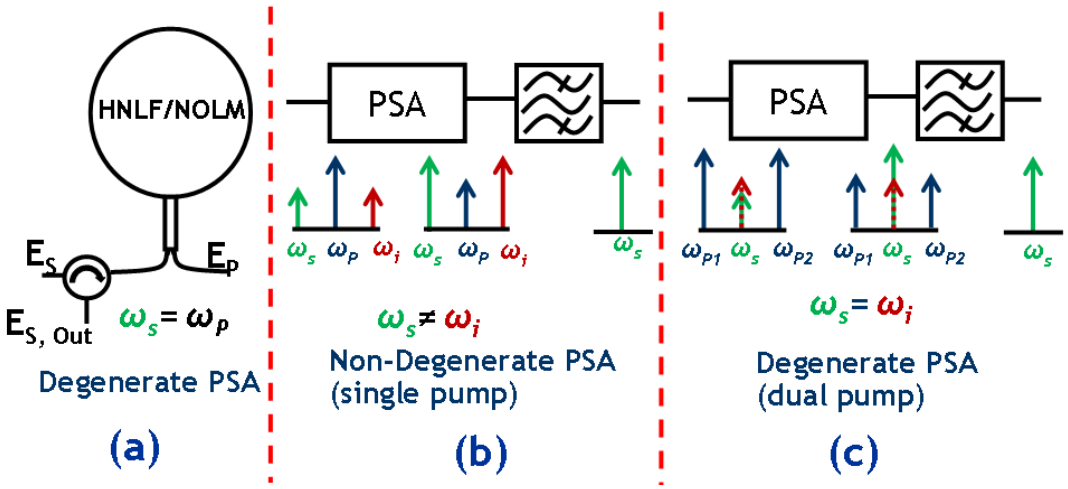



Figure 6.2: Block diagram of a different PSA schemes experimentally realised [191].

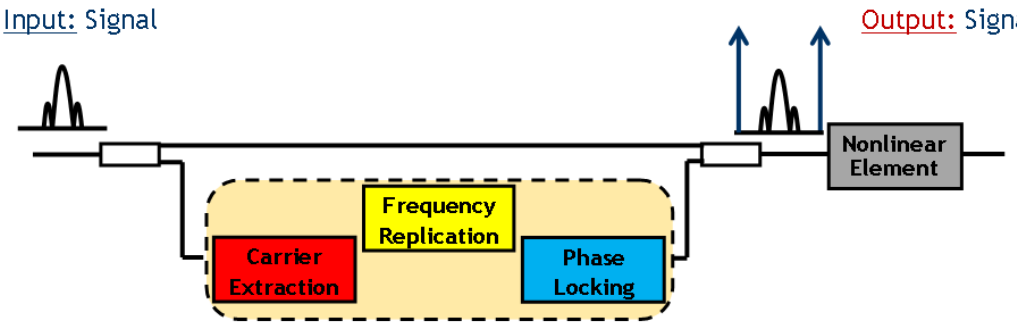



Figure 6.3: Schematic diagram of PSA with different schemes. (a) Degenerate PSA with pump at the same frequency of the signal in a nonlinear loop mirror. (b) Non degenerate PSA with single pump. (c) Degenerate PSA with two pumps (dual-pump) [191].

module should enable generation of the necessary components with only one input from the link: the signal. A schematic diagram of a black-box PSA is depicted in Fig. 6.3. As can be seen at the input of the PSA, the signal (a modulated channel) is divided into two paths. In one path, the original signal is transmitted without any further processing. In the other path, three main processes are carried out to generate phase synchronised pump(s) to form the PSA. First, the modulation should be stripped off from the signal (carrier extraction). Then, the pumps should be generated at required frequencies symmetric to the signal(s) (frequency replication). In addition, new pumps generated at desired frequencies should be phase synchronised with the original signal(s) (phase synchronisation) [191]. Then, the generated components, at the other arm, are combined with the original signal as an interferometer in a nonlinear medium to form the PSA.

### 6.3.1 Practical Implementation of Carrier-Extraction and Frequency Replication

As described earlier, in a practical PSA the pump(s) phase-locked to the signal should be generated from the signal only. This can be achieved using the inherent properties of FWM in a highly nonlinear medium [192]. Assume a DPSK channel and a local pump interact in a highly nonlinear medium as shown in Fig. 6.4; the signal is depicted in green with frequency $\omega_S$ and the pump in blue with frequency $\omega_P$. Due to the FWM process between the pump and the signal, two idler components are generated at frequencies symmetric to the signal and the pump at frequencies $\omega_{i1}$ and $\omega_{i2}$. The frequencies and phases of the idlers are related to those of the signal and pump as follows:

$$\omega_{i1} = 2\omega_S - \omega_P; \tag{6.1}$$

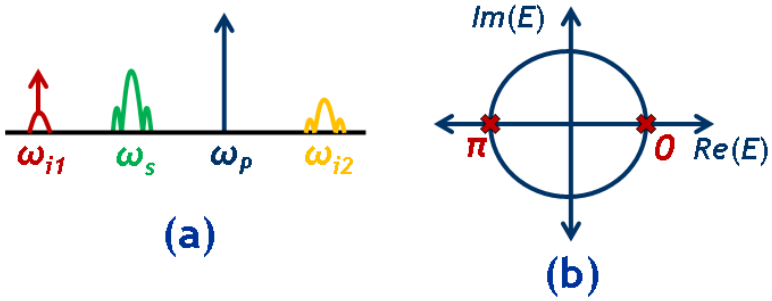



Figure 6.4: (a) Carrier extraction using FWM in a nonlinear medium. The signal is depicted in green with frequency $\omega_S$ and the pump in blue with frequency $\omega_P$ (b) Phase diagram of a binary phase encoded signal (DPSK).

$$\varphi_{i1} = 2\varphi_S - \varphi_P; \tag{6.2}$$

$$\omega_{i2} = 2\omega_P - \omega_S; \tag{6.3}$$

$$\varphi_{i2} = 2\varphi_P - \varphi_S; \tag{6.4}$$

From Eqs. 6.1 and 6.3 it can be seen that the two idlers are distributed symmetric with respect to the pump and the signal. Also, Eqs. 6.2 and 6.4 show that the generated idlers are self phase-locked to the pump and the signal. In addition, the idler2 contains phase modulation as the signal, but the idler1 has different phase properties than idler2. Since the DPSK modulation can have phases of either "0" or "$\pi$" (Fig. 6.4(b)), the term $2\varphi_S$ will be either "0" or "$2\pi$". This means that the modulation is stripped off from the idler1, as shown in Fig. 6.4(a). As a result, a pump with symmetric frequency with respect to the signal and self-phase locked to the signal and pump is generated. Care has to be taken about spectral noise accumulated in this pump: since the FWM is an ultra fast process any noise present in the signal, pump or amplifiers will be transferred to the signal. This generated pump will need spectral filtering/cleaning and amplification prior to usage as a PSA pump. These can ideally be accomplished by injection-locking of this pump to a CW laser to suppress the additional noise in the extracted carrier and increase its power. Since the slave laser is phase-locked to the master laser (here the extracted carrier), the phase-synchonisation of the injection-locked laser with the signal and local pump is maintained. The synchronisation scheme proposed in [193] combined carrier extraction and frequency generation functionalities along with optical injection-locking of a local oscillator laser to create the synchronised pumps of the PSA. This lead to the first practical implementation that would allow the PSAs to stand as independent, black-box elements in transmission links [188].

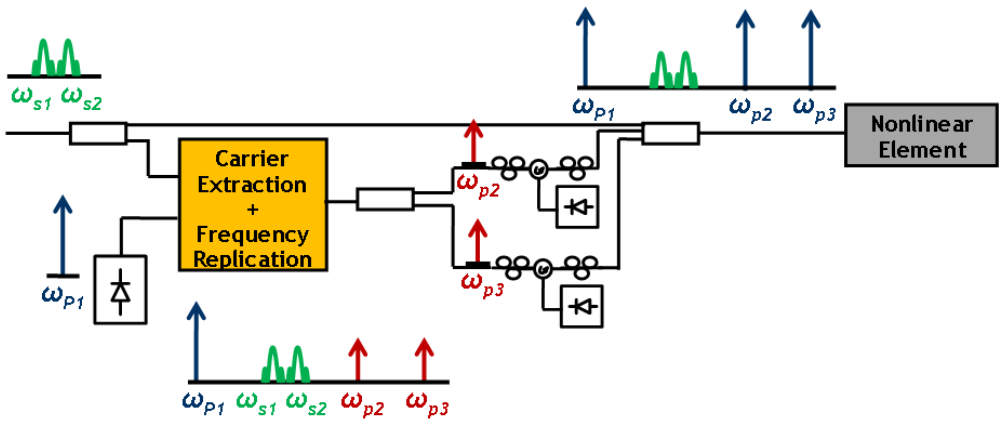



Figure 6.5: Schematic diagram of a multi pump black-box PSA based on conventional injection-locking scheme.

## 6.4 PSA Based on Injection-Locked Quantum Dash Mode-Locked Lasers

We showed the scheme of a single-channel practical PSA; recently, this scheme was extended to demonstrate the first two-channel DPSK PSA using optical injection-locking of two independent single-mode lasers [194]. Increasing the number of channels in such a black-box PSA requires at its synchronisation stage an equal number of additional local pumps. Each one of these pumps should be phase-locked to the corresponding extracted carrier. For instance, for a 10 channel PSA regenerator, 10 local pumps and 10 independent injection-locking setups are required. This makes the overall setup complicated and bulky, effectively undermining the *multi-wavelength processing* capability of such regenerators. Therefore, a solution that would enable multiple pump generation by synchronising a single laser frequency comb would be advantageous. Schematic descriptions of a two-channel black-box PSA with conventional injection-locking scheme and our proposed scheme are shown in Fig. 6.5 and Fig. 6.6 respectively. As depicted, with injection-locking to the QDMLL both synchronisation can be carried out in one injection-locking process with a single slave laser. In this section, we demonstrate a powerful application of the dual-mode injection-locking technique described in § 4.5, which allowed us to create multiple synchronised pumps for phase sensitive amplification using a single QDMLL which was injection-locked by two extracted carriers from the FWM process introduced in § 6.3.1.

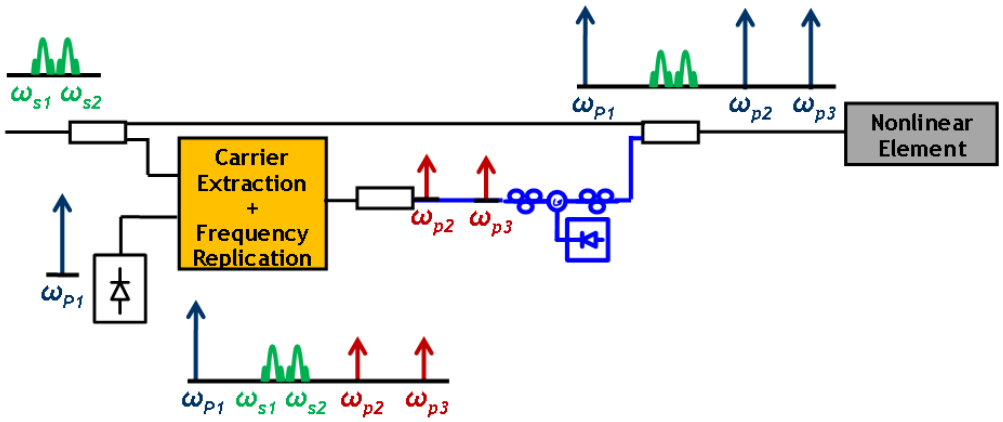



Figure 6.6: Schematic diagram of a multi pump black-box PSA based on injection-locking of quantum-dash mode-locked laser.

### 6.4.1 Experimental Arrangement

The experimental set-up for implementation of the PSA based on QDMLL is illustrated in Fig. 6.7. At the transmitter, a comb generator consisting of two cascaded Mach-Zehnder modulators was used to create synchronised optical carriers spaced at 41.496 GHz. Two of them were selected at $\lambda_{s1}$ = 1558.431 nm and $\lambda_{s2}$ = 1558.759 nm and modulated in DPSK format at 10.374 Gbit/s with a pseudorandom binary sequence (PRBS) of $2^7$-1. To enable phase modulation, a Mach-Zehnder modulator was modulated to have minimum transitions in order to give $\pi$ phase shifts at the output [195]. Subsequently, the channels were de-correlated by 20 km of conventional single-mode fiber (SMF) and amplified by an EDFA to 11 dBm. At the carrier extraction stage of the PSA, two input signals were mixed with a local DFB laser emitting at $\lambda_{P1}$ = 1554.898 nm, then amplified to 30 dBm in a highly nonlinear fiber (HNLF). The HNLF had a length of 0.198 km, dispersion parameter -0.2 ps/(nm.km) (at 1550 nm), nonlinear coefficient 7.4 $W^{-1}.km^{-1}$ and attenuation of 14 dB/km [196]. At the HNLF output two carriers were generated from the FWM interaction of the corresponding signals and the local pump. The output of the HNLF was divided in two arms. In one arm, we used a band pass filter (3 dB bandwidth 4 nm) and two interleavers (50 GHz and 21.31 GHz) to select the carriers and clean them from the residual frequencies of the FWM process. Then, the filtered spectrum was injected through a circulator to the QDMLL. The circulator was connected to the QDMLL through a lensed fibre introducing a typical loss of 3 dB. The output of the laser from port-3 of the circulator (average power $\approx$ -1.2 dBm) was then amplified to 13 dBm in an EDFA and combined with the pump and signal spectrum of the other arm to a Wavelength Selective Switch (WSS). The WSS also removed unwanted frequencies from the carrier extraction process and selected the two signal channels and the three pumps. The output of WSS was amplified by a 30 dBm high power EDFA before launched to a second HNLF (with

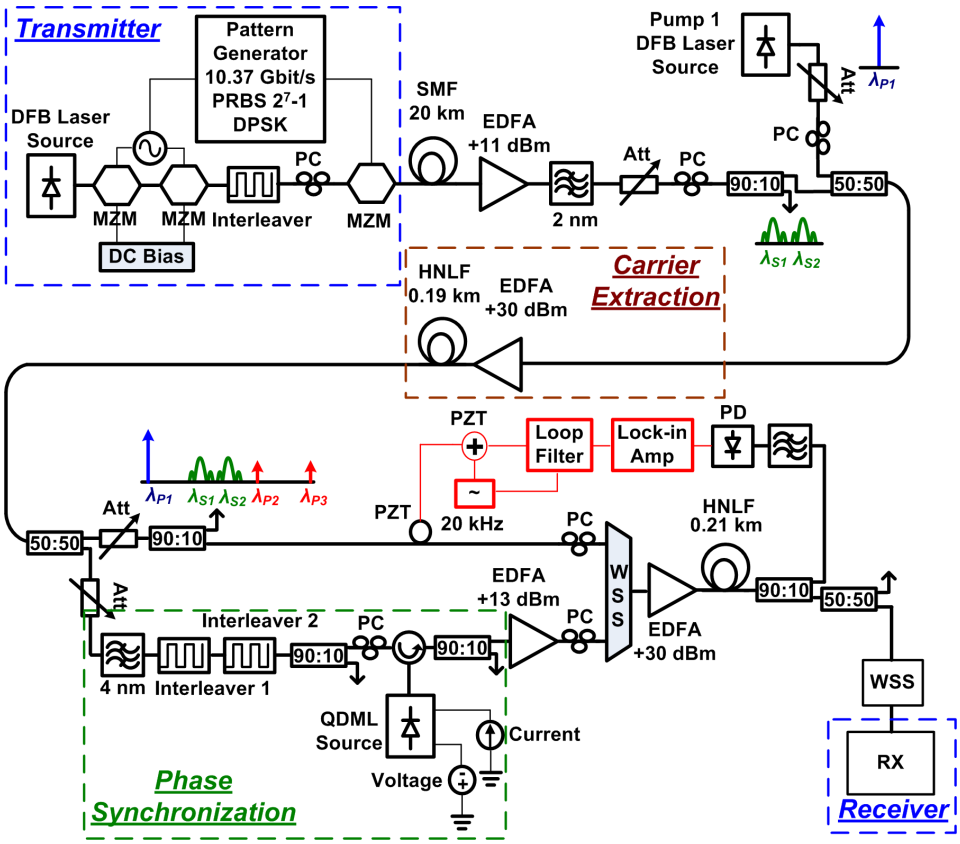



Figure 6.7: Experimental arrangement for two-channel DPSK PSA based on QDML phase synchronisation. List of acronyms used: MZM: Mach-Zehnder Modulator, PC: Polarisation Controller, SMF: Single-Mode Fibre, Att. Variable Optical Attenuator, HNLF: Highly Nonlinear Fibre, PZT: Piezo-Electric Transducer, PD: Photodetector, QDML: Quantum-Dash Mode-Locked Laser, WSS: Wavelength Selective Switch, RX: Receiver.

the same parameters as the first HNLF and with a length of 0.19 km) to form the PSA. We used a conventional feedback based phase-locked loop circuit to control a piezoelectric-based fibre stretcher (PZT) and hence compensate any slow thermal or acoustic induced phase drift between the interacting waves in both paths.

The QDMLL used in this experiment was a two-section device with total cavity length of 2030 $\mu$m, with 40 $\mu$m saturable-absorber section (2%) (I3-1) operating as SML lasers when the absorber was left floating, giving mode-locked frequency around 20.75 GHz and the same mounting configuration as described in § 2.2.2.

### 6.4.2 Analysis of Four-Wave Mixing Terms

In this section we describe study of the FWM terms generated in the carrier extraction process. We compare different channel spacing and the effects of phase modulation on the FWM. The optical spectrum of the HNLF output is shown in Fig. 6.8; the two modulated channels and the local pump along with their corresponding FWM terms are

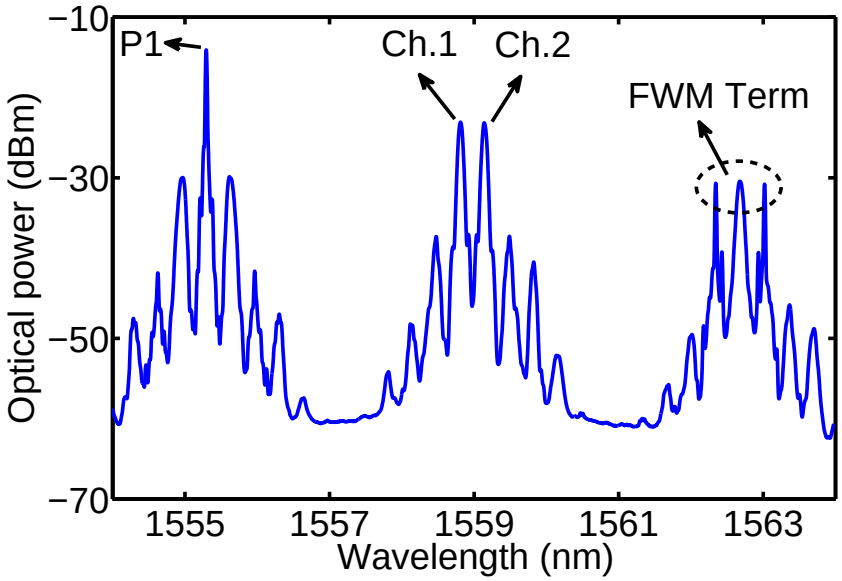



Figure 6.8: Optical spectrum of the HNLF output for carrier extraction process. The arrows denote the two DPSK channels (Ch.1, Ch.2), the local pump (P1), and the pumps generated through FWM process.

denoted by arrows. The two generated carriers were self-locked to the corresponding signals and the local pump and located at symmetric wavelengths with respect to them, due to the inherent properties of the FWM process.

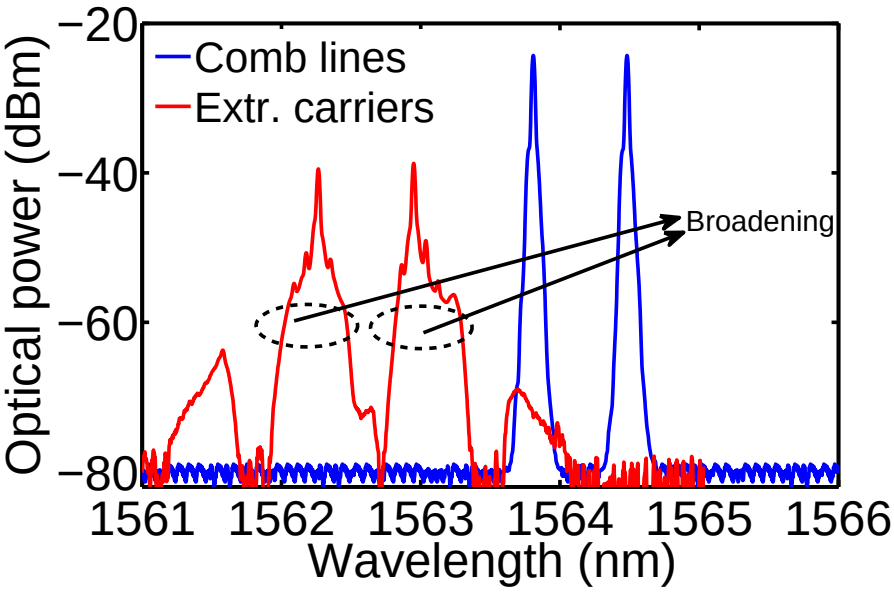



Figure 6.9: Comparison of the optical spectra for the extracted carriers (after filtering) through FWM of local pump and two de-correlated DPSK channels (red curve) and original CW lines(blue curve). Broadening clearly seen in the spectrum of extracted carriers are denoted by arrows.

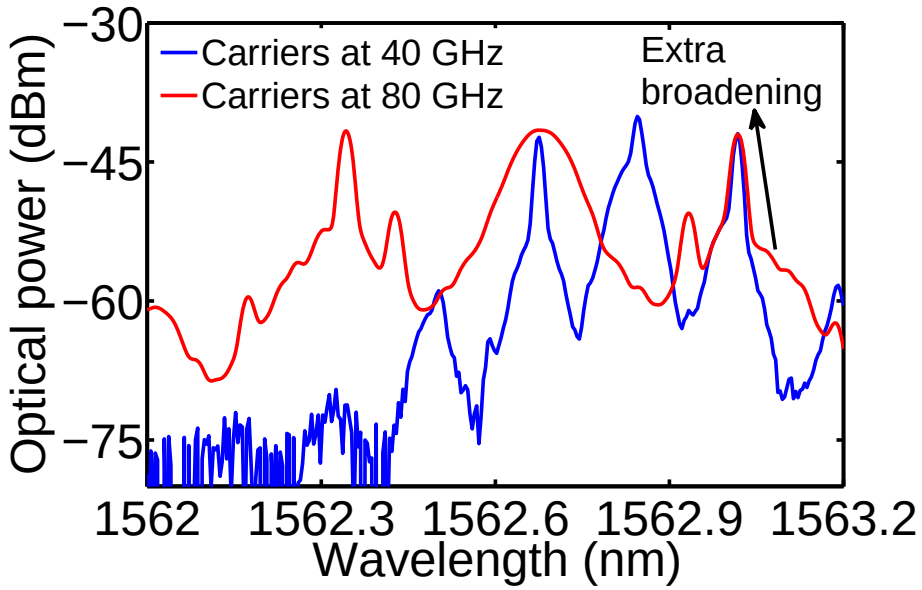



Figure 6.10: Comparison of the optical spectra for the extracted carriers through FWM of local pump and two de-correlated DPSK channels at 20 GHz spacing (blue curve) and 40 GHz spacing (red curve). Note that the spacing of carriers generated through FWM is twice of that of channels. Extra broadening of FWM carriers with larger channel spacing is denoted by an arrow.

A comparison of carriers generated from the FWM process and original CW lines is shown in Fig. 6.9. The blue curve is the two CW modes selected from the comb generator and the red curve the generated carriers through FWM process after filtering. Significant broadening of the carriers can be seen for generated carriers compared to the CW comb lines (blue curve). This is a result of transferring the noise from the modulated signals to the generated carriers through FWM process.

We also studied the effect of spacing of the modulated channels in the generated FWM term and whether the channels were correlated or de-correlated. A comparison of the FWM term for modulated channels around 20 GHz and 40 GHz spacing is shown in Fig. 6.10 in blue and red curves, respectively. A zoom in the FWM term shows generated carriers with lower signal to noise ratio when the spacing of the signals increased. As will be shown in the next section, this spectral broadening affects the injection-locking performance of the laser.

We also compared the FWM terms when the channels were de-correlated to the case where both channels were amplified and launched to the first HNLF without any phase de-correlation. The signal-pump power ratio were the same for both cases and the only difference was the omission of the 20 km SMF used for de-correlation. As shown in Fig. 6.11, the FWM term with de-correlated channels showed higher noise level and side-bands around the carriers. The component in the middle of the carriers resulted from the mixing of both channels with the pump. For the phase of the component we

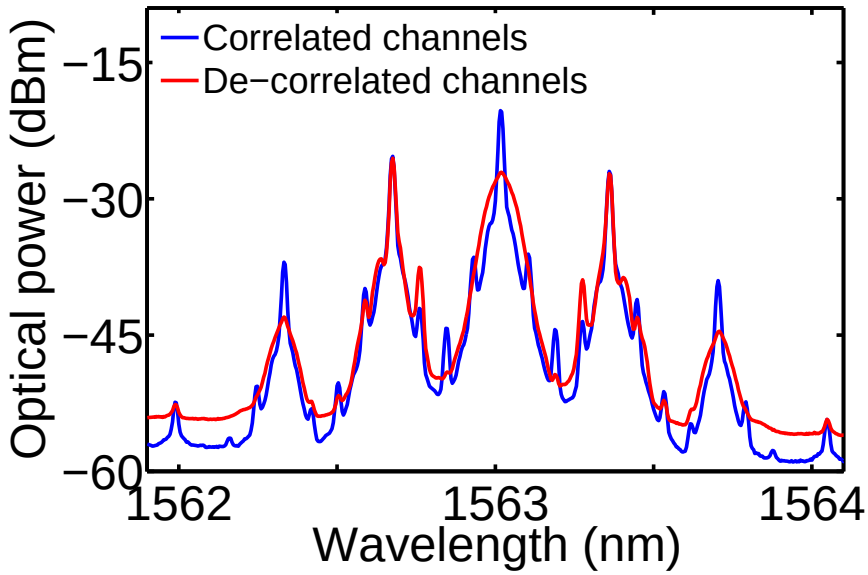



Figure 6.11: Optical spectra for the extracted carriers with channels at 40 GHz spacing with correlated (blue curve) and de-correlated cases (red curve).

have the following:

$$\varphi_o = (\varphi_{S1} + \varphi_{S2}) - \varphi_P \tag{6.5}$$

For the case of correlated channels, both signals contained the same pattern having either "0" or "$\pi$" for the value of phase. Therefore, the phase of FWM term will be either $(0 - \varphi_P)$ or $(2\pi - \varphi_P)$ indicating that the modulation is stripped off from this component. This explains why we saw a CW line in the middle of the correlated channels. On the other hand, when the channels were de-correlated the term in Eq. 6.5 becomes a summation of two independent modulations. As a result, the term in the middle became a time-varying signal rather than a CW line as can be seen in Fig. 6.11 in the red curve. The side-bands present around the carriers come from the residual modulation present in the carriers and were higher for the case of de-correlated channels.

### 6.4.3 Injection-Locking Performance

In this section, we analyse the slave laser performance under optical injection of the FWM terms introduced in the previous section. Our interest is to obtain optimum injection-locking performance in terms of timing jitter, as was demonstrated in Chapter 4. We use the RF linewidth of the injection-locked laser as an indication of timing jitter reduction. A delta-like (instrument-limited) RF lineshape was regarded as an indication of complete injection-locking. We show that this condition is not met for all cases, and care has to be taken to the OSNR of the FWM term.

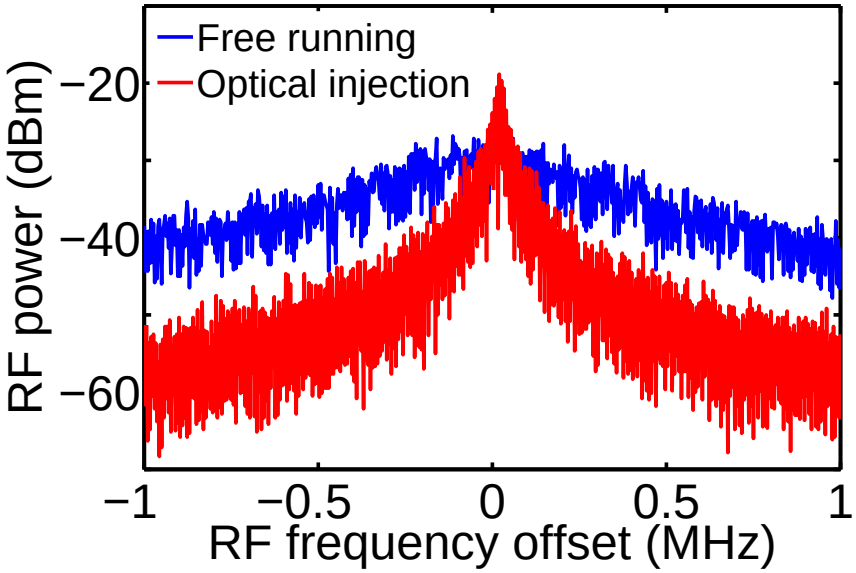



Figure 6.12: RF spectrum of the slave laser when free-running (blue curve) and under optical injection to the FWM generated carriers (red curve), offset to the peak frequency. The modulated channels where de-correlated channels at 40 GHz spacing with two independent RF sources for comb generation and phase modulation. The resolution bandwidth for free-running and injection-locked was 10 kHz, and 3 kHz, respectively.

Under injection-locking, we observed similar phenomena as discussed in Chapter 4, such as increase in the repetition rate and narrowing of the optical spectrum with the majority of the power on the red side. The key parameter here to asses the quality of locking was the RF linewith of injection-locked laser. The FWM carriers were generated from de-correlated channels with spacing around 40 GHz, giving the FWM carriers spaced by ∼80 GHz. Two independent RF sources were used to generate comb lines and phase modulation. The zoom around the RF spectrum of the slave laser when free-running and under optical injection with FWM carriers is shown in Fig. 6.12 (offset to the peak frequency). The RF linewidth (Lorentzian fit) of free-running was ≈ 500 kHz reducing to ≈ 50 kHz when injection-locked. This was in contrast to what was demonstrated for RF linewidth under dual-mode injection in Chapter 4. Indeed, we expected strong narrowing of RF linewidth to the value of the beating of the injected FWM carriers which were expected to have same level of coherence as the two comb lines before modulation.

To further investigate this discrepancy, we checked the mutual coherence of one mode before and after each injected mode to see how the coherence is transferred from the injected modes to the neighboring ones. The optical spectrum of the injection-locked laser with the spectral position of each case is shown in Fig. 6.13. The RF linewidth measured corresponding to each case is shown in Fig. 6.14(a-c) which is in the same order (∼ 30 kHz) for all the cases. This confirms that the mutual coherence is similar for all the modes and this is an indication on incomplete coherence transfer from the extracted carriers to the injection-locked comb.

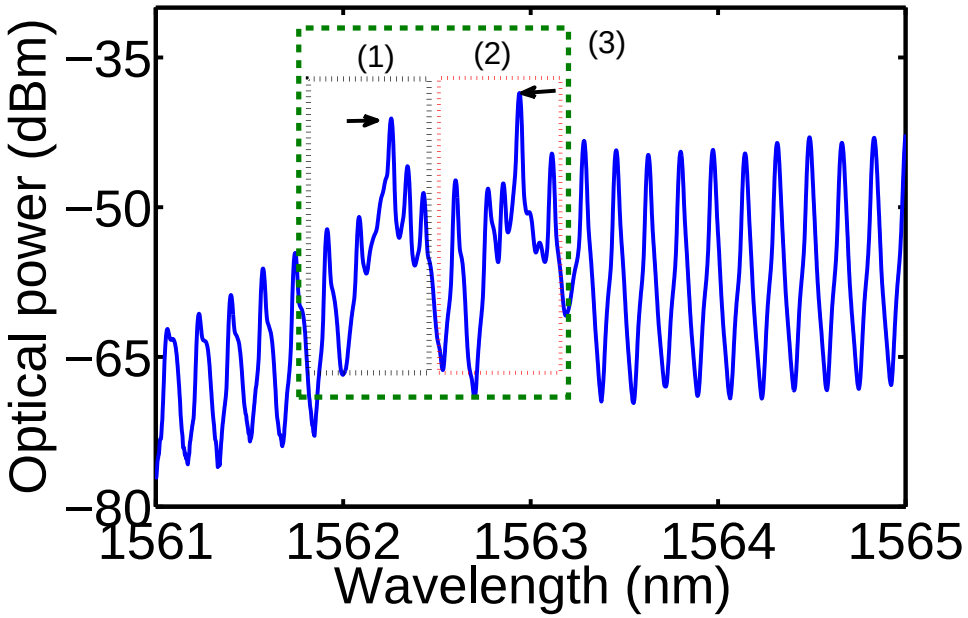
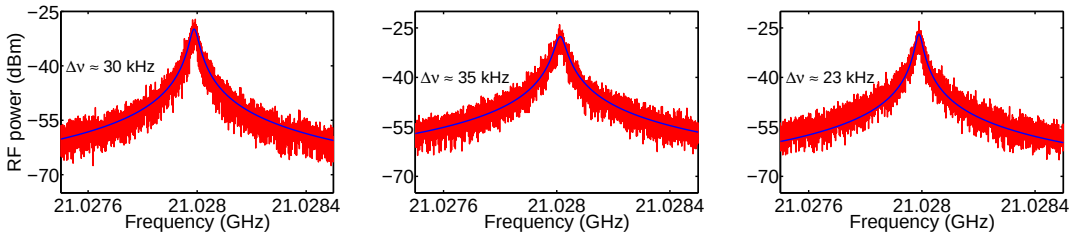



Figure 6.13: Optical spectrum of the slave laser under optical injection to the FWM generated carriers (blue curve), and spectral position of programmable filter (WSS) for each case. Case 1: Dotted black rectangle, Case 2: Dotted red rectangle, Case 3: Green dashed rectangle. The injected modes are denoted by arrows.




(a) (b) (c)

Figure 6.14: RF linewidth of mode beating around each injected mode (red curve) along with its Lorentzian fit (blue curve) corresponding to spectral filtering cases in Fig. 6.13. (a). Case 1. (b). Case 2. (c) Case 3. Resolution bandwidth for all the cases was 3 kHz, $\Delta\nu$: RF linewidth.

We then considered several configurations for channel spacing of 40 GHz to explore the effect of injection-locking performance. First, injection-locking to the FWM carriers generated from correlated channels. Second, using synchronised (or the same) RF sources for comb generation and phase modulation. The results are summarised in table 6.1. As can be seen, the locking showed sensitivity to the channel correlation/de-correlation as we saw differences in the optical spectra of FWM extracted carriers (Fig. 6.11). Also, we observed significant improvement in the performance when the RF sources (clocks) for comb generation and phase modulation were synchronised or one RF source was used for both. The RF spectra for complete injection-locking and

Table 6.1: Injection-locking performance versus different configurations for clock (RF) source and channel correlation/de-correlation. Channel spacing was 40 GHz for all the cases.

| **Case** | **Injection-Locking** | **Comments** |
|---|---|---|
| Independent Clocks<br>Correlated channels | Complete | |
| A: Independent Clocks<br><br>De-correlated channels | Incomplete | Lorentzian linewidth ~10-100 kHz |
| B: Same (synchronised) clocks<br>De-correlated channels | Complete | Smaller locking-range |
| C: Same (synchronised) clocks<br>Correlated channels | Complete | Wider locking-range |

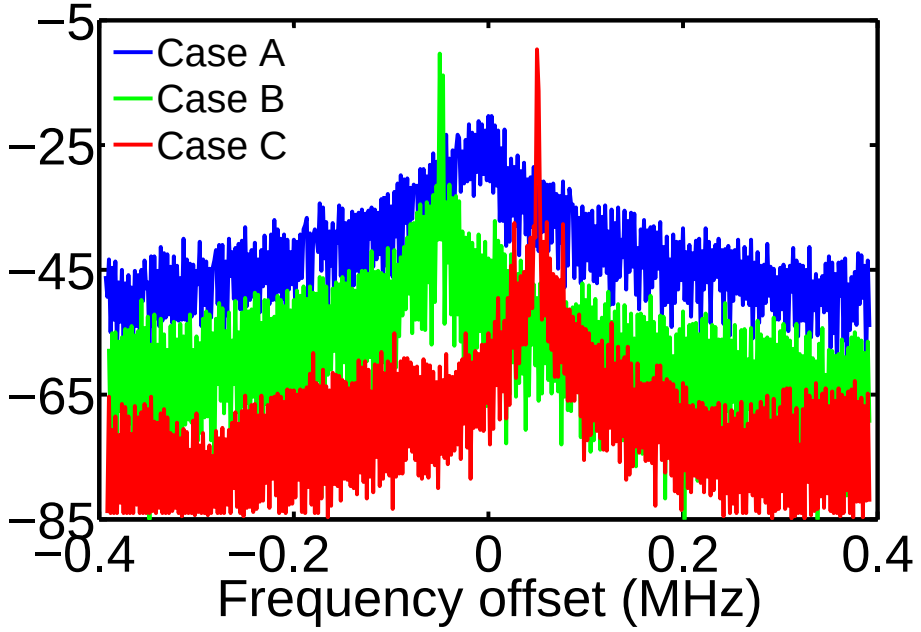



Figure 6.15: RF spectra of the slave laser (SAML) under optical injection for three scenarios. Case A (blue curve): Independent clocks (RF sources) with de-correlated channels. Case B (green curve): Same (synchronised) clocks with de-correlated channels. Case C (red curve): Same (synchronised) clocks with correlated channels. The RF frequency of injection-locked laser was the same for all the cases and the traces were offset for better viewing. The resolution bandwidth was 3 kHz for case A and 1 kHz for case B and case C.

incomplete cases are shown in Fig. 6.15 (offset to the peak) for injection-locking to the same RF frequency. As can be seen, the RF linewidth of injection-locked laser was improved significantly under case B and case C where the same clock was used. The RF lineshape consisted of a very narrow peak (Hz level) with a Lorentzian tail suppressed by 20 dB in case B and 30 dB in case C with respect to the peak. The RF spectra of injected signal and injection-locked laser for the case B are also shown

in Fig. 6.16 in the 0-50 GHz range (maximum frequency of instrument) in blue and red curves, respectively. From the blue curve we observed a broad-band noise spanning from 0 to more than 10 GHz, mainly come from the residual phase modulation in the FWM carriers. This broad band noise was suppressed considerably in the spectrum of injection-locked laser (red curve). Also, the tones associated with the modulation around 10.5 and 15 GHz and between 20-40 GHz were suppressed by more than 40 dB under optical injection. The spacing of extracted carriers was twice of that the channels due to FWM process; this means injection at the 4th harmonic of the repetition rate of the injection-locked laser (84.112 GHz). The beating tone at this frequency contributed to the carrier modulation and injection-locking and was beyond the maximum frequency of instrument (50 GHz). Nevertheless, the OFC with the same line spacing as dual-mode injection at first harmonic was generated as the locking mechanism was governed by the resonance of carrier modulation rate to repetition-rate of the laser (harmonic injection-locking) and not related to any possible FWM process in the QDMLL's cavity [97]. The modulation pattern length for this case was $2^{31} - 1$ creating side-bands with the spacing of few Hz, not resolved with the resolution bandwidth of the instrument in this measurement. Suppression of these sidebands through optical injection is also crucial to ensure PSA output produces minimum error at the receiver.

We repeated this measurement for the SML laser in the same situation as Fig. 6.16 (case B). The RF spectrum of the laser when free running (without injection) and under injection-locking is depicted in Fig. 6.17, where significant RF linewidth narrowing was

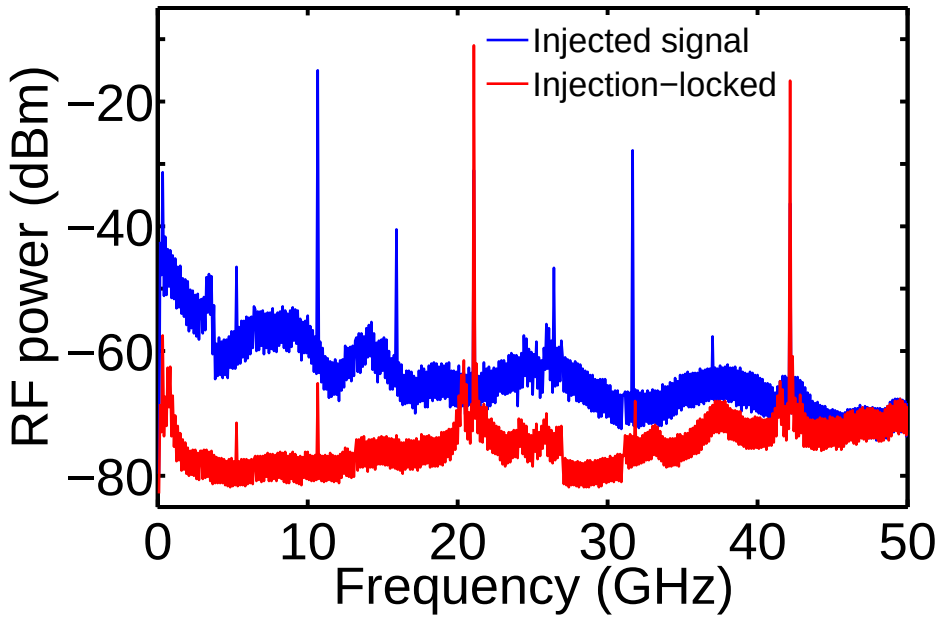



Figure 6.16: RF spectra of the the injected signal (blue curve, FWM carriers) and injection-locked laser (red curve). The modulated channels were de-correlated and same clock was utilised for comb generation and modulation (case B).

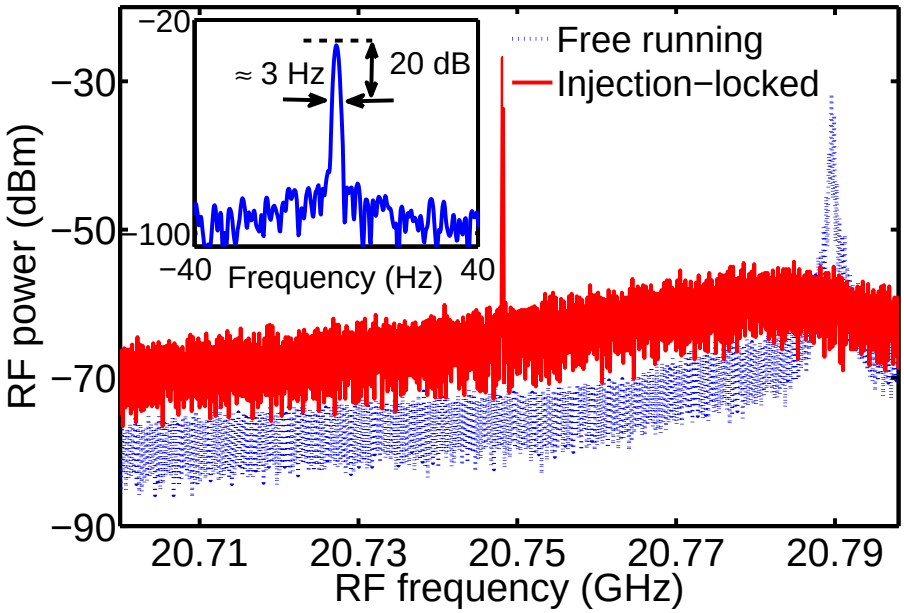



Figure 6.17: RF spectrum of free running (dashed-line/blue) and injection-locked SML (solid-line/red), the inset shows a zoom of the RF tone with 80 Hz span and RBW of 1 Hz. the 20 dB linewidth is ≈ 3 Hz. The FWM carriers were generated through case B scenario.

observed. The Lorentzian fit to the RF linewidth of the free running laser was 270 kHz (not shown) whereas the RF linewidth of the injection-locked laser reduces to the values beyond the resolution bandwidth (RBW) of the instrument. The inset in Fig. 6.17 shows the 80 Hz zoom of the peak with resolution bandwidth of 1 Hz; the 20 dB linewidth of the tone is estimated to be 3 Hz, indicating strong reduction of timing jitter of the laser. This confirms the presence of phase-locking between the injected modes and extracted carriers.

Optical spectra of from SMLs under injection-locking had fewer comb lines with the majority of the power in the injected modes. Combs from SAMLs are much wider (as seen in Chapter 4), with power distributed among many comb lines (see Fig. 6.18). SML combs are beneficial for this scheme, as more power per line was required to observe phase sensitive performance at the output of the PSA.

The major spectral differences of FWM generated carriers and CW lines generated from sideband amplitude modulation was discussed in § 6.4.2. In dual-mode injection, discussed in Chapter 4,the modes were generated from a CW source with high optical signal to noise ratio (OSNR) which indicates dual-modes with high OSNR. In the case of dual-modes generated through FWM in a HNLF, however, any noise present in signals, pump and EDFA will be transferred to the generated carriers. Therefore, special care has to be taken to make sure that the dual-modes are injected with OSNR higher than a threshold ( which requires a separate study) to have complete injection-

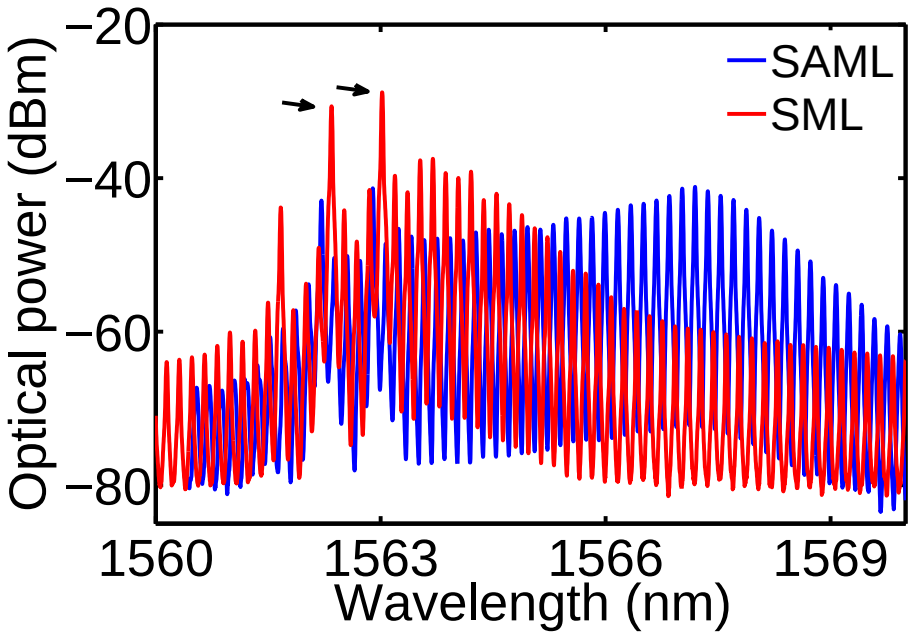



Figure 6.18: Comparison of optical spectra for SML and SAML lasers under optical injection to the extracted carriers. The FWM carriers were generated through case B scenario: same (synchronised) clocks with de-correlated channels. The arrows denote the location of injection.

locking. Correct evaluation of this threshold requires a separate study to investigate the robustness of dual-mode injection scheme against OSNR similar to what has been done in [193] for injection locking to CW slave lasers. In addition to the noise, residual phase modulation is present in the generated carriers. In order to suppress the residual phase modulation, the injection ratio should be kept as low as possible [197] (about -30 dB in this experiment).

In selection of pump and signal power and spectral locations few points should be considered simultaneously:

- The FWM generated carriers located symmetric with respect to the channels. The closer the pump and signals, the higher the power of the FWM generated carriers and the shorter their wavelengths will be. On the other hand, the wavelengths of FWM carriers should be higher than the minimum wavelength that laser can be injection-locked.
- The power of FWM carriers can also be controlled through the power ratio of the pump and signals; care has be to be taken to not decrease this ratio below a certain threshold at which nonlinear distortion of signals occur in the HNLF.
- The frequency spacing of pump-signals should not be an integer multiplier of signal spacing. Otherwise, unwanted components will be generated through the FWM process in the HNLF. In this work, this ratio should be kept withinga ratio

of $m \pm \frac{1}{2}$, where $m$ is an integer.

### 6.4.4 Phase-Sensitive Performance

After successful injection-locking of slave laser, the necessary components were selected from the two arms using the WSS (programmable filter). They included three pumps (two from injection-locked comb and one local pump) and two channels, as shown in Fig. 6.19(a). Before investigating the PSA performance, the relative phases of pumps and signals should be stabilised against any environmental drifts using the feedback circuit shown in Fig. 6.7. The feedback circuit can only stabilise any fluctuations in the frequency range of a few Hz due to low speed of PZT response. Therefore, any source of faster phase fluctuations should be removed before this stage. For example, the optical path length difference between the two arms should be small (less than 1%) compared to the shortest coherence length (largest optical linewidths, the FWM carriers) in the system. In our experiment we used commercial DFB lasers for pump and signals having optical linewidth ≈1 MHz. The optical linewidth of generated FWM carriers will be around twice the signal plus the pump, around 3 MHz for our case. Therefore, the optical path length difference should be limited to the cm range. A tap of the spectrum of one channel at PSA output was utilised for feedback circuit to stabilise the slow phase fluctuations. The WSS was programmed to control the phase of the PSA input components individually, giving freedom in maximising the PSA gain in favor of either of the channels and equalising the channels' power level. This occurred at the expense of limited spectral resolution of the WSS, as can be seen in presence of sidebands around two pumps in the optical spectrum of Fig. 6.19(a).

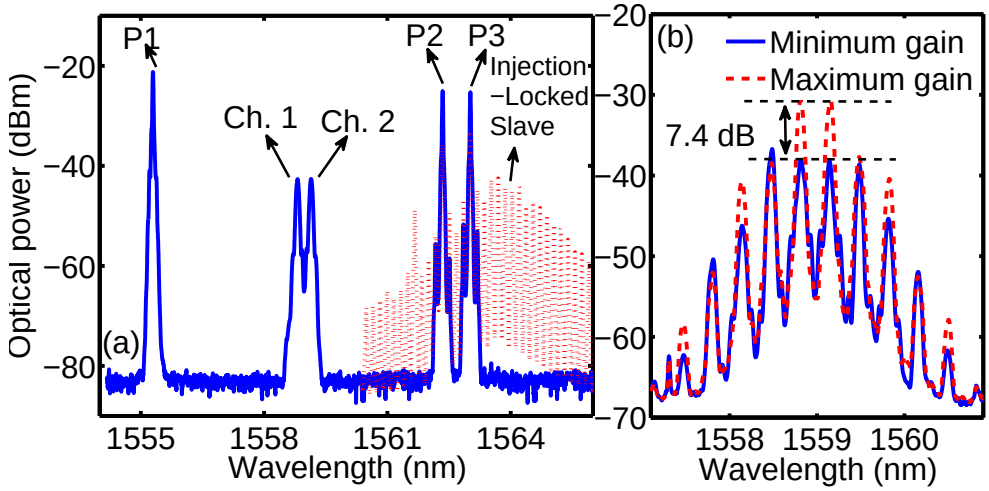



Figure 6.19: (a) Optical spectrum of PSA input, after removing un-wanted components using WSS, the spectrum of OFC from QDMLL is depicted in dashed curve. (b) The zoom of the optical spectrum at the PSA output around channels for maximum (dashed line-red) and minimum (solid-line/blue) gain.

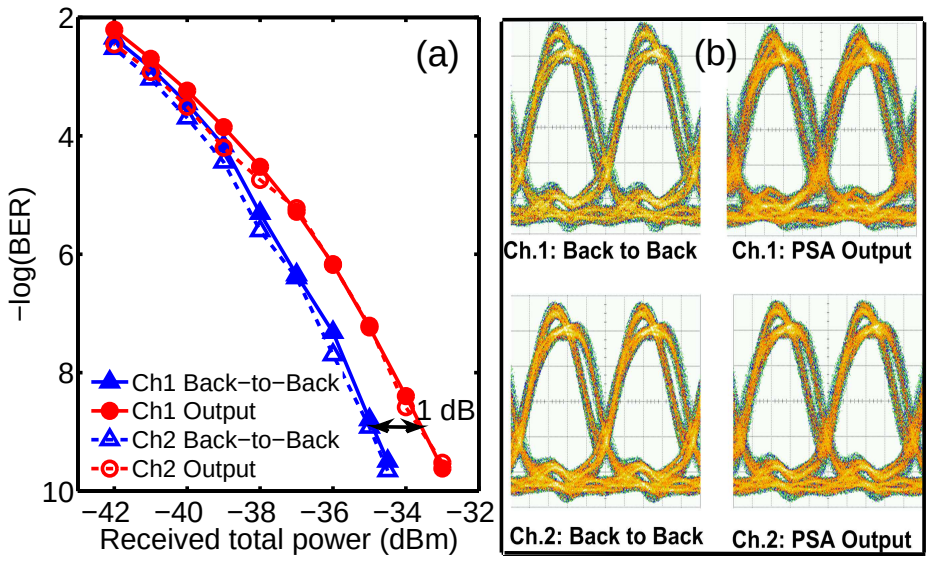



Figure 6.20: (a). BER measurements of both channels versus total received power. (b). Error free eye diagrams for both channels at the input and output of the PSA.

The side-bands were the neighboring comb lines around 20 GHz from optical spectrum of injection-locked QDMLL.

The stabilised output of the PSA against thermal fiber expansion was observed at maximum and minimum gain for both channels, as shown in Fig. 6.19(b). A 7.4 dB on-off gain was measured for both channels which may be increased by using higher pump powers. We also studied the performance of the PSA in terms of BER measurements for both channels. Fig. 6.20(a) depicts the BER for both channels in back-to-back and PSA output (maximum gain) against received power. By comparing the BER curves for both channels at the output, about 1 dB sensitivity penalty for BER of $10^{-9}$ was observed, with negligible penalty at the forward error correction (FEC) threshold around $10^{-3}$. The error-free eye diagrams (shown in Fig. 6.20(b) for both channels at the output are open proving the excellent performance of our scheme.

It should be emphasised that the BER was measured with PRBS length of $2^7$-1, selection of longer patterns caused rapid increase in BER, leading to greater performance penalty. This was because of limitation of our injection-locking scheme in suppression of residual phase modulation, manifesting as the sidebands associated with the pattern length and modulation frequency. Increasing the pattern length causes these side-bands generated closer in frequency and limiting the suppression effect of injection-locking process. A study of injection-locking of CW lasers show that injection ratio should be kept below -40 dB to minimise the penalty associated with residual phase modulation [197]. For our case, however, this injection level was too low to achieve complete stable locking, so we had to set the minimum injection ratio to $\approx$ -30 dB. This requires a detailed investigation to study the suppression effects of dual-mode

injection in QDMLLs with change of injection parameters such as injection power and master-slave frequency detuning. In this case, we also have one more parameter which is RF spacing of dual-modes.

## 6.5 Summary and Discussions

In this chapter, we demonstrated an application for injection-locking of QDMLLs, namely PSA systems with multi-channel inputs. The dual-mode injection-locking scheme analysed in Chapter 4 was extended in a PSA system to phase-lock the QDMLL comb lines to a pair of extracted carriers. Two lines of the phase-synchronised, coherent optical frequency comb after injection-locking was utilised to serve as pumps for PSA operation. A two-channel PSA with two 10.374 Gb/s DPSK input channels was demonstrated based on simultaneous phase synchronisation of local pumps to incoming signals through this novel injection-locking technique using a 21 GHz InP QDMLL. A 7.4 dB phase sensitive gain and only 1 dB sensitivity penalty observed in the BER measurements of two channels at the output of the amplification stage. This scheme has the potential for extension to multiple channels towards more compact and efficient black-box PSAs.

While we demonstrated the basic PSA performance, several issues need to be addresses to make this phase-synchronisation scheme more feasible in a multi-channel practical PSA. First, in analysis of FWM terms the OSNR of the extracted carriers showed dependence on parameters such as presence of correlation/decorrelation in the modulated channels and channel spacing. This, in return affected the quality of injection-locking to the extracted carriers. We also observed sensitivity to the existence of phase synchronisation between RF sources (clocks) used for phase modulation and channels' comb generation. As a result, an incomplete injection-locked case showed kHz range RF linewidth whereas delta-like RF lineshape with RF linewidth close to that of the RF clock was observed when the QDMLL was completely injection-locked. A comprehensive study to examine the robustness of this scheme against OSNR with different parameters such as channel spacing, modulation rate, transmitter noise, nonlinear medium (a nonlinear SOA and EDFA side by side comparision) will be required to understand of the important parameters.

Second, a separate study for suppression of residual phase modulation through injection-locking of QDMLL needs to be carried out to fully understand the optimum injection-locking parameters to have minimum penalty in BER performance. To show regeneration, a nonlinear medium with higher power efficiency will be ideal as the power requirement increases quite rapidly by increasing the number of channels in a PSA based on current power consuming HNLFs.

Third, we showed successful locking to the standard frequency of 42.66 GHz widely

used in WDM systems in Chapter 4 for QDMLL with optimised RF locking-range. Using such a laser in this experiment makes the usage of more robust and less noisy transmitters along with using narrow linewidth fibre laser as a comb source with likelihood of lower contribution to OSNR of FWM based extracted carriers. This will lead to more stable and higher quality of injection-locking process.

Apart from black-box PSA scheme, a PSA with pilot tones as pump sources is another way of implementing such regenerators [198]. In this scheme, the pumps are sent along with the signals and are self-phase locked initially as they are generated from a coherent comb source. The wide coherent optical frequency comb from a QDMLL injection-locked to a pair of coherent CW lines will be an ideal comb source to realise single and multi-channel degenerate or non-degenerate PSAs for regeneration of DPSK modulation format.

# Chapter 7

# Conclusions

## 7.1 Introduction

Following the technical chapters presented, we conclude this thesis by summarising the technical contributions on optical injection, combined optical injection and optical feedback and PSAs. Then, we outline the problems corresponding to each technical contribution, to be investigated for continuation of this work .

## 7.2 Technical Contributions

The focus of this thesis was on characterisations and advanced measurements of behaviour of QDMLLs under external optical injection. The mode-locked lasers were categorized in two types of SML and SAML operation, upon mode-locking mechanism dominated by self-mode-locking or saturable-absorber dominated mode-locking, respectively. In each type of the laser, in depth experimental analysis was carried out in order to understand the stabilities/instabilities and also optimisation possibilities with optical injection.

For SML lasers, when the laser was stably injection-locked to the CW master laser, strong spectral narrowing occurred with narrow RF beating tone. This RF beating appeared at second harmonic of the free-running repetition-rate (harmonic mode-locking) for 10 GHz DWELL lasers. The DBARR SML devices showed similar spectral narrowing without harmonic operation, giving the same repetition-rate under optical injection. While the DWELL lasers showed instabilities associated with RO dynamics of the laser, DBARR devices showed more stable operation under optical injection without RO induced oscillations. With this advantage wider locking range was achieved followed by the extension of the repetition rate by more than 700 MHz (both higher and lower frequencies) and scalability of stable-injection-locking for shorter devices.

The stable injection-locked operation of SAML lasers demonstrated spectral narrowing with majority of power in the wavelengths longer than that of the injection. In contrast with SML lasers, the spectrum was wide enough to reproduce similar or narrower pulses than free-running, leading to significant reduction of the chirp. The optical injection of two coherent CW lines (dual-mode injection) added further optimisations in strong timing jitter reduction to the range of 0.2 ps (similar to hybrid mode-locking) and reduction of the individual mode phase-noise, similar to master laser linewidth. Therefore, the SAML laser under dual-mode optical injection operates as a narrow-linewidth optical frequency comb, where the lines are well coherent to each other as well as the external source. We also investigated the dependence of RF-locking range of the laser on the bias parameters. It was found that under negative absorber voltages, when the free-running mode-locking is less stable and noisier, the optical locking range is extended, followed by wide RF locking-range >400 MHz for a 21 GHz laser. This frequency tuning corresponded to $> 2\%$ ratio which is a record for a monolithic two-section mode-locked laser, without additional section for extra frequency tuning. The synchronisation mechanism is optical rather than electrical, so no limitation due to electrical frequency response of the laser existed, unlike electrical synchronisation techniques which requires specific injection circuit design to minimise reflections at high RF frequencies. The extension in the repetition-rate of injection-locked laser was achieved due to the nonlinear properties of injection-locking phenomenon.

We also showed that a stable mode-locked laser under optical injection can be stabilised in a two level scheme with simultaneous optical feedback. In our all-optical scheme, a part of the spectrum of injection-locked laser was fed-back (filtered feedback) to the laser through a long feedback loop to double-locked the injection-locked laser. With this new stabilisation scheme, we achieved simultaneous reduction of time-bandwidth product and wavelength control with optical injection, and reduction of RF-linewidth and timing jitter as a result of feedback self-injection. This synchronisation scheme was implemented in all-optical format, without RF source, and is not limited to the frequency response of the laser as no optical/electrical conversion is required and is ideal for photonic integration.

Finally, we investigated an application of the optical injection-locking of mode-locked laser in optical communication systems. Recent developments in all-optical signal regenerators have resulted in the first realisation of a practical phase and amplitude regenerator based on phase-sensitive amplifier. This system can be utilised as an inline component in the optical communication systems with multi-wavelength regeneration capabilities. In this scheme, phase-synchronisation of local pumps to the incoming signal(s) is a critical part to preserve the phase information which is carried out using optical injection-locking. To process more than one wavelength for the regeneration, one injection-locking stage per wavelength is required. We showed that with dual-mode injection-locking of a QDMLL, a two-wavelength PSA can be implemented with

single-stage injection-locking where both local pumps were synchronised from the same comb source, injection-locked QDMLL. With this technical achievement, the multi-wavelength capabilities of such PSAs can be preserved in an efficient and practical way using one comb source, paving the way towards compact multi-wavelength PSAs.

## 7.3 Future Works

Probably an important problem which is still open is development of a theoretical model for explanation of the self-mode-locking present in QDMLLs.

With regard to observations of QDMLLs with SML type under optical injection, a theoretical model to explain the locking characteristics and also the major differences between DWELL and DBARR structures, particularly more stable operation of DBARR lasers is desirable. With observations concerning scalability of stable operation under optical injection, it is necessary to explicitly investigate the limiting factor coming from RO parameters and contributions of cavity length and bias parameters in making a mode-locked laser more or less stable under optical injection. This is of particular importance in practical applications as synchronisation to lasers with different repetition-rates, from few to more than 100 GHz is required in different scenarios in optical communication systems.

In the operation of QDMLLs with SAML type under optical injection, the main contribution of this work was on achievement wide tuning of repetition rate combined with broad optical spectrum and narrow pulsewidth and linewidths of comb lines. A theoretical study on optimisation of laser structure (absorber length, gain/absorprtion parameters) is beneficial towards having injection-locked combs with broader spectral width, wider RF-locking range, and higher up-shifting of the repetition-rate than free-running. We showed in Chapter 4 that it is possible to have a separate frequency range covered by optical injection than that of free-running, giving an extra room for tuning the repetition-rate for practical applications. Indeed, optical injection gave a separate range for repetition-rate tuning in addition to the hybrid-mode-locking frequency range which is around the free-running repetition-rate. The successful theoretical study will be helpful in determining how to optimise this up-shift to have wider range of repetition-rates for synchronisation in a mode-locked laser.

For the all-optical stabilisation scheme with combination of optical injection and optical feedback, a separate study is required to investigate the limitation for RF-linewidth reduction in particular any drawback that optical feedback might have in comparison with optoelectronic feedback (optical/electrical conversion) in longer loops. Also, a dual-loop scheme was suggested to suppress the side-modes coming from external cavity limiting the timing jitter improvement caused by RF-linewidth reduction.

Also, this scheme is attractive to stabilise the microwave generation observed in optical injection of SML lasers. In particular, the feedback loop should be optimised to work for a narrow spectrum without need to the use a filter in the feedback loop. Successful, implementation of such system will be an attractive solution towards implementation of tunable microwave/millimetre wave photonic oscillators with all optical stabilisation schemes without need to an RF source.

Finally, for the PSA based on QDMLLs the following problems should be addressed:

- On the laser side, a detailed study of dual-mode injection-locking scheme robustness against optical signal to noise ratio (OSNR).
- On the PSA side, We showed that the existence of decorrelation between the channels and using different clocks for the pattern generator and comb source affects the quality of locking. Detailed study on contributions of any of these factors as well as channel spacing or number of channels on final OSNR of generated pumps from FWM process is necessary for proper understanding the limitations.
- A key part in injection-locking of the local pumps to the incoming extracted carriers is to reduce the injection-power to a level that the modulation response of the slave laser will not be enhanced. This is necessary to filter the residual modulation in the extracted carriers through injection-locking process. An open problem is to study the modulation response of individual lines in the comb of injection-locked mode-locked laser to study the filtering mechanism in such lasers in comparison with CW single-mode lasers [197].
- We showed the successful PSA performance with this novel synchronisation using a QDMLL. The main issue with this PSA scheme was the power level in the comb lines and also the long-term stability of the synchronisation setup. Addressing these problems by either increasing the output power of QDMLLs (such a tapered structure) or using PSAs with lower power consumption (SOA based [199] or photonic-crystal fibres as power efficient nonlinear media) will be desirable.

In this thesis, we showed the application of synchronised mode-locked lasers in PSAs. The nature of coherent narrow-linewidth combs generated by dual-mode injection will be attractive in other applications of optical communication systems requiring coherent combs with narrow linewidths such as coherent WDM [200, 201]. The advantages of QDMLLs in these applications are the broad spectrum, wide RF locking-range (covering the error occurred during cleaving and processing of lasers), scalability for different repetition rates (10, 20, 30, 40 GHz ranges), and optical synchronisation, compared to electrical synchronisation techniques, recently introduced for discrete-mode semiconductor lasers [170].

# References


[1] M. I. Nathan, "Invention of the semiconductor laser," in *CLEO: Science and Innovations*. Optical Society of America, 2012, p. JM2I.1. [Online]. Available: http://www.opticsinfobase.org/abstract.cfm?URI=CLEO: S and I-2012-JM2I.1

[2] R. Dupuis, "An introduction to the development of the semiconductor laser," *IEEE Journal of Quantum Electronics*, vol. 23, no. 6, pp. 651 – 657, Jun. 1987.

[3] H. Kroemer, "A proposed class of hetero-junction injection lasers," *Proceedings of the IEEE*, vol. 51, no. 12, pp. 1782–1783, 1963.

[4] J. J. Coleman, "The development of the semiconductor laser diode after the first demonstration in 1962," *Semiconductor Science and Technology*, vol. 27, no. 9, p. 090207, 2012. [Online]. Available: http://stacks.iop.org/0268-1242/27/i=9/a=090207

[5] *Semiconductor Science and Technology , Special issue on the 50th anniversary of the diode laser*, vol. 27, no. 9, Sep. 2012. [Online]. Available: http://iopscience.iop.org/0268-1242/27/9

[6] Z. Alferov, "Double heterostructure lasers: early days and future perspectives," *IEEE Journal of Selected Topics in Quantum Electronics*, vol. 6, no. 6, pp. 832 –840, 2000.

[7] J. Singh, *Quantum mechanics: fundamentals and applications to technology*, ser. Wiley-Interscience publication, 1997, pp. 78–79. [Online]. Available: http://books.google.ie/books?id=_AJRAAAAMAAJ

[8] E. A. A. Edik U. Rafailov, Maria Ana Cataluna, *Ultrafast Lasers Based on Quantum Dot Structures: Physics and Devices*. Wiley-VCH Verlag & Co. KGaA, 2011.

[9] E. Kapon, *Semiconductor Lasers: Fundamentals*, ser. Optics and Photonics Series. Acad. Press, 1999, no. v. 1. [Online]. Available: http://books.google.ie/books?id=XkNGAAAAYAAJ

[10] Y. Arakawa and A. Yariv, "Quantum well lasers–gain, spectra, dynamics," *IEEE Journal of Quantum Electronics*, vol. 22, no. 9, pp. 1887 – 1899, Sep. 1986.

[11] P. Ho, L. Glasser, E. Ippen, and H. Haus, "Picosecond pulse generation with a cw gaalas laser diode," *Applied Physics Letters*, vol. 33, no. 3, pp. 241–242, 1978.

[12] E. Avrutin, J. Marsh, and E. Portnoi, "Monolithic and multi-gigahertz mode-locked semiconductor lasers: constructions, experiments, models and applications," *Optoelectronics, IEE Proceedings* -, vol. 147, no. 4, pp. 251 –278, Aug. 2000.

[13] K. Williams, M. Thompson, and I. White, "Long-wavelength monolithic mode-locked diode lasers," *New Journal of Physics*, vol. 6, no. 1, p. 179, 2004.

[14] P. Vasil'ev, *Ultrafast Diode Lasers: Fundamentals and Applications*. Boston, MA: Artech House.

[15] K. Sato, I. Kotaka, Y. Kondo, and M. Yamamoro, "Actively mode-locked strained-InGaAsP multiquantum-well lasers integrated with electroabsorption modulators and distributed Bragg reflectors," *IEEE Journal of Selected Topics in Quantum Electronics*, vol. 2, no. 3, pp. 557 –565, Sep. 1996.

[16] S. Sanders, L. Eng, J. Paslaski, and A. Yariv, "108 GHz passive mode locking of a multiple quantum well semiconductor laser with an intracavity absorber," *Applied Physics Letters*, vol. 56, no. 4, pp. 310–311, 1990.

[17] P. Vasil'ev and A. Sergeev, "Generation of bandwidth-limited 2 ps pulses with 100 GHz repetition rate from multisegmented injection laser," *Electronics Letters*, vol. 25, no. 16, pp. 1049 –1050, Aug. 1989.

[18] F. Camacho, E. Avrutin, P. Cusumano, A. Saher Helmy, A. Bryce, and J. Marsh, "Improvements in mode-locked semiconductor diode lasers using monolithically integrated passive waveguides made by quantum-well intermixing," *IEEE Photonics Technology Letters*, vol. 9, no. 9, pp. 1208 –1210, Sep. 1997.

[19] P. A. Morton, J. E. Bowers, L. A. Koszi, M. Soler, J. Lopata, and D. P. Wilt, "Monolithic hybrid mode-locked 1.3 $\mu$m semiconductor lasers," *Applied Physics Letters*, vol. 56, no. 2, pp. 111–113, 1990.

[20] K. Sato, K. Wakita, I. Kotaka, Y. Kondo, M. Yamamoto, and A. Takada, "Monolithic strained-InGaAsp multiple-quantum-well lasers with integrated electroabsorption modulators for active mode locking," *Applied Physics Letters*, vol. 65, no. 1, pp. 1–3, 1994.

[21] K. Sato, I. Kotaka, Y. Kondo, and M. Yamamoto, "Active mode locking at 50 GHz repetition frequency by half-frequency modulation of monolithic semiconductor lasers integrated with electroabsorption modulators," *Applied Physics Letters*, vol. 69, no. 18, pp. 2626–2628, 1996.

[22] G. Agrawal and N. Olsson, "Self-phase modulation and spectral broadening of

optical pulses in semiconductor laser amplifiers," *IEEE Journal of Quantum Electronics*, vol. 25, no. 11, pp. 2297 –2306, Nov. 1989.

[23] D. Derickson, R. Helkey, A. Mar, J. Karin, J. Wasserbauer, and J. Bowers, "Short pulse generation using multisegment mode-locked semiconductor lasers," *IEEE Journal of Quantum Electronics*, vol. 28, no. 10, pp. 2186 –2202, Oct. 1992.

[24] H. Liu, S. Arahira, T. Kunii, and Y. Ogawa, "Generation of wavelength-tunable transform-limited pulses from a monolithic passively mode-locked distributed Bragg reflector semiconductor laser," *IEEE Photonics Technology Letters*, vol. 7, no. 10, pp. 1139 –1141, Oct. 1995.

[25] E. Zielinski, E. Lach, J. Bouayad-Amine, H. Haisch, E. Kuhn, M. Schilling, and J. Weber, "Monolithic multisegment mode-locked DBR laser for wavelength tunable picosecond pulse generation," *IEEE Journal of Selected Topics in Quantum Electronics*, vol. 3, no. 2, pp. 230 –232, Apr. 1997.

[26] M. C. Wu, Y. K. Chen, T. Tanbun-Ek, R. A. Logan, M. A. Chin, and G. Raybon, "Transform-limited 1.4 ps optical pulses from a monolithic colliding-pulse mode-locked quantum well laser," *Applied Physics Letters*, vol. 57, no. 8, pp. 759–761, 1990.

[27] Y. K. Chen, M. C. Wu, T. Tanbun-Ek, R. A. Logan, and M. A. Chin, "Subpicosecond monolithic colliding-pulse mode-locked multiple quantum well lasers," *Applied Physics Letters*, vol. 58, no. 12, pp. 1253–1255, 1991.

[28] Y.-K. Chen and M. Wu, "Monolithic colliding-pulse mode-locked quantum-well lasers," *IEEE Journal of Quantum Electronics*, vol. 28, no. 10, pp. 2176 –2185, Oct. 1992.

[29] J. F. Martins-Filho and C. N. Ironside, "Multiple colliding pulse mode-locked operation of a semiconductor laser," *Applied Physics Letters*, vol. 65, no. 15, pp. 1894–1896, 1994.

[30] J. Martins-Filho, E. Avrutin, C. Ironside, and J. Roberts, "Monolithic multiple colliding pulse mode-locked quantum-well lasers, experiment and theory," *IEEE Journal of Selected Topics in Quantum Electronics*, vol. 1, no. 2, pp. 539 –551, Jun. 1995.

[31] T. Shimizu, X. Wang, and H. Yokoyama, "Asymmetric colliding-pulse mode-locking in InGaAsP semiconductor lasers," *Optical Review*, vol. 2, no. 6, pp. 401–403, 1995.

[32] T. Shimizu, I. Ogura, and H. Yokoyama, "860 GHz rate asymmetric colliding pulse modelocked diode lasers," *Electronics Letters*, vol. 33, no. 22, pp. 1868 –1869, Oct. 1997.

[33] Z. Wang, J. Nielsen, S. Brorsan, B. Christensen, T. Franck, N. Jensen, A. Larsen, J. Norregaard, and E. Bodtker, "15.8 Gbit/s system transmission experiment using a 5.2 mm long monolithic colliding-pulse-modelocked quantum well laser diode," *Electronics Letters*, vol. 31, no. 4, pp. 272 –274, Feb. 1995.

[34] T. Franck, S. Brorson, A. Moller-Larsen, J. Nielsen, and J. Mork, "Synchronization phase diagrams of monolithic colliding pulse-modelocked lasers," *IEEE Photonics Technology Letters*, vol. 8, no. 1, pp. 40 –42, Jan. 1996.

[35] S. Bischoff, J. Mork, T. Franck, S. D. Brorson, M. Hofmann, K. Fröjdh, L. Prip, and M. P. Sørensen, "Monolithic colliding pulse mode-locked semiconductor lasers," *Quantum and Semiclassical Optics: Journal of the European Optical Society Part B*, vol. 9, no. 5, p. 655, 1997.

[36] M. Hofmann, S. Bischoff, T. Franck, L. Prip, S. D. Brorson, J. Mork, and K. Frojdh, "Chirp of monolithic colliding pulse mode-locked diode lasers," *Applied Physics Letters*, vol. 70, no. 19, pp. 2514–2516, 1997.

[37] H.-F. Liu, S. Arahira, T. Kunii, and Y. Ogawa, "Tuning characteristics of monolithic passively mode-locked distributed Bragg reflector semiconductor lasers," *IEEE Journal of Quantum Electronics*, vol. 32, no. 11, pp. 1965 –1975, Nov. 1996.

[38] R. Kaiser, B. Huttl, H. Heidrich, S. Fidorra, W. Rehbein, H. Stolpe, R. Stenzel, W. Ebert, and G. Sahin, "Tunable monolithic mode-locked lasers on InP with low timing jitter," *IEEE Photonics Technology Letters*, vol. 15, no. 5, pp. 634 –636, may 2003.

[39] R. Kaiser and B. Huttl, "Monolithic 40-GHz mode-locked MQW DBR lasers for high-speed optical communication systems," *IEEE Journal of Selected Topics in Quantum Electronics*, vol. 13, no. 1, pp. 125–135, Jan./Feb. 2007.

[40] S. Arahira, N. Mineo, K. Tachibana, and Y. Ogawa, "40 GHz hybrid modelocked laser diode module operated at ultra-low RF power with impedance-matching circuit," *Electronics Letters*, vol. 39, no. 3, pp. 287 – 289, Feb. 2003.

[41] S. Arahira and Y. Ogawa, "40 GHz actively mode-locked distributed Bragg reflector laser diode module with an impedance-matching circuit for efficient RF signal injection," *Japanese Journal of Applied Physics*, vol. 43, no. 4B, pp. 1960–1964, 2004.

[42] E. Rafailov, M. Cataluna, and W. Sibbett, "Mode-locked quantum-dot lasers," *Nature photonics*, vol. 1, no. 7, pp. 395–401, 2007.

[43] M. Thompson, A. Rae, M. Xia, R. Penty, and I. White, "InGaAs quantum-dot mode-locked laser diodes," *IEEE Journal of Selected Topics in Quantum Electronics*, vol. 15, no. 3, pp. 661 –672, 2009.

[44] E. U. Rafailov, M. A. Cataluna, W. Sibbett, N. D. Il'inskaya, Y. M. Zadiranov, A. E. Zhukov, V. M. Ustinov, D. A. Livshits, A. R. Kovsh, and N. N. Ledentsov, "High-power picosecond and femtosecond pulse generation from a two-section mode-locked quantum-dot laser," *Applied Physics Letters*, vol. 87, no. 8, p. 081107, 2005.

[45] M. Todaro, J. Tourrenc, S. Hegarty, C. Kelleher, B. Corbett, G. Huyet, and J. McInerney, "Simultaneous achievement of narrow pulse width and low pulse-to-pulse timing jitter in 1.3 $\mu$m passively mode-locked quantum-dot lasers," *Optics Letters*, vol. 31, Mar. 2006.

[46] M. Cataluna, E. Rafailov, A. McRobbie, W. Sibbett, D. Livshits, and A. Kovsh, "Stable mode-locked operation up to 80 °C from an InGaAs quantum-dot laser," *IEEE Photonics Technology Letters*, vol. 18, no. 14, pp. 1500 – 1502, Jul. 2006.

[47] M. A. Cataluna, E. A. Viktorov, P. Mandel, W. Sibbett, D. A. Livshits, J. Weimert, A. R. Kovsh, and E. U. Rafailov, "Temperature dependence of pulse duration in a mode-locked quantum-dot laser," *Applied Physics Letters*, vol. 90, no. 10, p. 101102, 2007.

[48] J. K. Mee, M. T. Crowley, N. Patel, D. Murrell, R. Raghunathan, A. Aboketaf, A. Elshaari, S. F. Preble, P. Ampadu, and L. F. Lester, "A passively mode-locked quantum-dot laser operating over a broad temperature range," *Applied Physics Letters*, vol. 101, no. 7, p. 071112, 2012.

[49] M. A. Cataluna, W. Sibbett, D. A. Livshits, J. Weimert, A. R. Kovsh, and E. U. Rafailov, "Stable mode locking via ground- or excited-state transitions in a two-section quantum-dot laser," *Applied Physics Letters*, vol. 89, no. 8, p. 081124, 2006.

[50] M. A. Cataluna, D. I. Nikitichev, S. Mikroulis, H. Simos, C. Simos, C. Mesaritakis, D. Syvridis, I. Krestnikov, D. Livshits, and E. U. Rafailov, "Dual-wavelength mode-locked quantum-dot laser, via ground and excited state transitions: experimental and theoretical investigation," *Optics Express*, vol. 18, no. 12, pp. 12 832–12 838, Jun. 2010.

[51] J. Kim, M.-T. Choi, and P. J. Delfyett, "Pulse generation and compression via ground and excited states from a grating coupled passively mode-locked quantum dot two-section diode laser," *Applied Physics Letters*, vol. 89, no. 26, p. 261106, 2006.

[52] M. G. Thompson, A. Rae, R. L. Sellin, C. Marinelli, R. V. Penty, I. H. White, A. R. Kovsh, S. S. Mikhrin, D. A. Livshits, and I. L. Krestnikov, "Subpicosecond high-power mode locking using flared waveguide monolithic quantum-dot lasers," *Applied Physics Letters*, vol. 88, no. 13, p. 133119, 2006.

[53] M. Kuntz, G. Fiol, M. Lammlin, D. Bimberg, M. G. Thompson, K. T. Tan, C. Marinelli, R. V. Penty, I. H. White, V. M. Ustinov, A. E. Zhukov, Y. M. Shernyakov, and A. R. Kovsh, "35 GHz mode-locking of 1.3 $\mu$m quantum dot lasers," *Applied Physics Letters*, vol. 85, no. 5, pp. 843–845, 2004.

[54] H. Schmeckebier, G. Fiol, C. Meuer, D. Arsenijević, and D. Bimberg, "Complete pulse characterization of quantum dot mode-locked lasers suitable for optical communication up to 160 Gbit/s," *Optics Express*, vol. 18, no. 4, pp. 3415–3425, Feb 2010.

[55] G. Fiol, D. Arsenijevic, D. Bimberg, A. G. Vladimirov, M. Wolfrum, E. A. Viktorov, and P. Mandel, "Hybrid mode-locking in a 40 GHz monolithic quantum dot laser," *Applied Physics Letters*, vol. 96, no. 1, p. 011104, 2010.

[56] M. Thompson, C. Marinelli, X. Zhao, R. Sellin, R. Penty, I. White, I. Kaiander, D. Bimberg, D.-J. Kang, and M. Blamire, "Colliding-pulse modelocked quantum dot lasers," *Electronics Letters*, vol. 41, no. 5, pp. 248 –250, Mar. 2005.

[57] Y. C. Xin, Y. Li, V. Kovanis, A. L. Gray, L. Zhang, and L. F. Lester, "Reconfigurable quantum dot monolithic multisectionpassive mode-locked lasers," *Optics Express*, vol. 15, no. 12, pp. 7623–7633, Jun. 2007.

[58] A. Rae, M. Thompson, R. Penty, I. White, A. Kovsh, S. Mikhrin, D. Livshits, and I. Krestnikov, "Harmonic mode-locking of a quantum-dot laser diode," in *Lasers and Electro-Optics Society, 2006. LEOS 2006. 19th Annual Meeting of the IEEE*, Oct. 2006, pp. 874 –875.

[59] J. Renaudier, R. Brenot, B. Dagens, F. Lelarge, B. Rousseau, F. Poingt, O. Legouezigou, F. Pommereau, A. Accard, P. Gallion, and G.-H. Duan, "45 GHz self-pulsation with narrow linewidth in quantum dot Fabry-Perot semiconductor lasers at 1.5 $\mu$m," *Electronics Letters*, vol. 41, no. 18, pp. 1007 – 1008, Sep. 2005.

[60] C. Gosset, K. Merghem, A. Martinez, G. Moreau, G. Patriarche, G. Aubin, A. Ramdane, J. Landreau, and F. Lelarge, "Subpicosecond pulse generation at 134 GHz using a quantum-dash-based Fabry-Perot laser emitting at 1.56 $\mu$m," *Applied Physics Letters*, vol. 88, no. 24, p. 241105, 2006.

[61] C. Gosset, K. Merghem, A. Martinez, G. Moreau, G. Patriarche, G. Aubin, J. Landreau, F. Lelarge, and A. Ramdane, "Subpicosecond pulse generation at 134 GHz and low radiofrequency spectral linewidth in quantum dash-based Fabry-Perot lasers emitting at 1.5 $\mu$m," *Electronics Letters*, vol. 42, no. 2, pp. 91 – 92, Jan. 2006.

[62] Z. G. Lu, J. R. Liu, S. Raymond, P. J. Poole, P. J. Barrios, and D. Poitras, "312-

fs pulse generation from a passive c-band InAs/InP quantum dot mode-locked laser," *Optics Express*, vol. 16, no. 14, pp. 10 835–10 840, Jul 2008.

[63] F. Lelarge, B. Dagens, J. Renaudier, R. Brenot, A. Accard, F. van Dijk, D. Make, O. Le Gouezigou, J. Provost, F. Poingt *et al.*, "Recent advances on InAs/InP quantum dash based semiconductor lasers and optical amplifiers operating at 1.55 $\mu$m," *IEEE Journal of Selected Topics in Quantum Electronics*, vol. 13, no. 1, pp. 111–124, 2007.

[64] H. Bachert, P. Eliseev, M. Manko, V. Strahov, S. Raab, and C. Thay, "Multimode operation and mode-locking effect in injection lasers," *IEEE Journal of Quantum Electronics*, vol. 11, no. 7, pp. 507 – 510, Jul. 1975.

[65] L. Tiemeijer, P. Kuindersma, P. Thijs, and G. Rikken, "Passive FM locking in InGaAsP semiconductor lasers," *IEEE Journal of Quantum Electronics*, vol. 25, no. 6, pp. 1385 –1392, Jun. 1989.

[66] S. Chinn and E. Swanson, "Passive FM locking and pulse generation from 980-nm strained-quantum-well Fabry-Perot lasers," *IEEE Photonics Technology Letters*, vol. 5, no. 9, pp. 969 –971, Sep. 1993.

[67] K. Sato, "Optical pulse generation using Fabry-Perot lasers under continuous-wave operation," *IEEE Journal of Selected Topics in Quantum Electronics*, vol. 9, no. 5, pp. 1288 – 1293, 2003.

[68] J. Renaudier, G.-H. Duan, J.-G. Provost, H. Debregeas-Sillard, and P. Gallion, "Phase correlation between longitudinal modes in semiconductor self-pulsating DBR lasers," *IEEE Photonics Technology Letters*, vol. 17, no. 4, pp. 741 –743, Apr. 2005.

[69] Y. Nomura, S. Ochi, N. Tomita, K. Akiyama, T. Isu, T. Takiguchi, and H. Higuchi, "Mode locking in Fabry-Perot semiconductor lasers," *Physical Review A*, vol. 65, p. 043807, Mar. 2002.

[70] G.-H. Duan, A. Shen, A. Akrout, F. V. Dijk, F. Lelarge, F. Pommereau, O. LeGouezigou, J.-G. Provost, H. Gariah, F. Blache, F. Mallecot, K. Merghem, A. Martinez, and A. Ramdane, "High performance InP-based quantum dash semiconductor mode-locked lasers for optical communications." *Bell Labs Technical Journal*, vol. 14, no. 3, pp. 63–84, 2009.

[71] M. J. R. Heck, E. A. J. M. Bente, B. Smalbrugge, Y.-S. Oei, M. K. Smit, S. Anantathanasarn, and R. Nötzel, "Observation of Q-switching and mode-locking in two-section InAs/InP (100) quantum dot lasers around 1.55 $\mu$m," *Optics Express*, vol. 15, no. 25, pp. 16 292–16 301, Dec. 2007.

[72] M. J. Heck, E. J. Salumbides, A. Renault, E. A. Bente, Y.-S. Oei, M. K. Smit, R. van Veldhoven, R. Nötzel, K. S. Eikema, and W. Ubachs, "Analysis of hybrid

mode-locking of two-section quantum dot lasers operating at 1.5 $\mu$m," *Optics Express*, vol. 17, no. 20, pp. 18 063–18 075, Sep. 2009.

[73] M. Heck, A. Renault, E. Bente, Y.-S. Oei, M. Smit, K. Eikema, W. Ubachs, S. Anantathanasarn, and R. Notzel, "Passively mode-locked 4.6 and 10.5 GHz quantum dot laser diodes around 1.55 $\mu$m with large operating regime," *IEEE Journal of Selected Topics in Quantum Electronics*, vol. 15, no. 3, pp. 634 –643, 2009.

[74] R. Rosales, K. Merghem, A. Martinez, A. Akrout, J.-P. Tourrenc, A. Accard, F. Lelarge, and A. Ramdane, "InAs/InP quantum-dot passively mode-locked lasers for 1.55- $\mu$m applications," *IEEE Journal of Selected Topics in Quantum Electronics*, vol. 17, no. 5, pp. 1292 –1301, 2011.

[75] R. Adler, "A study of locking phenomena in oscillators," *Proceedings of the IRE*, vol. 34, no. 6, pp. 351 – 357, Jun. 1946.

[76] H. L. Stover and W. H. Steier, "Locking of laser oscillators by light injection," *Applied Physics Letters*, vol. 8, no. 4, pp. 91–93, 1966.

[77] S. Kobayashi, J. Yamada, S. Machida, and T. Kimura, "Single-mode operation of 500 Mbit/s modulated algaas semiconductor laser by injection locking," *Electronics Letters*, vol. 16, no. 19, pp. 746 –748, 11 1980.

[78] L. Joneckis, P.-T. Ho, and G. Burdge, "CW injection seeding of a modelocked semiconductor laser," *IEEE Journal of Quantum Electronics*, vol. 27, no. 7, pp. 1854 –1858, Jul. 1991.

[79] M. Margalit, M. Orenstein, and H. Haus, "Injection locking of a passively mode-locked laser," *IEEE Journal of Quantum Electronics*, vol. 32, no. 1, pp. 155 –160, Jan. 1996.

[80] Y. Katagiri and A. Takada, "Supermode selection of a subterahertz-harmonic colliding-pulse mode-locked semiconductor laser using continuous-wave light injection," *IEEE Photonics Technology Letters*, vol. 9, no. 12, pp. 1564 –1566, Dec. 1997.

[81] F. Quinlan, S. Gee, S. Ozharar, and P. Delfyett, "Greater than 20-dB supermode noise suppression and timing jitter reduction via CW injection of a harmonically mode-locked laser," *IEEE Photonics Technology Letters*, vol. 19, no. 16, pp. 1221 –1223, aug.15, 2007.

[82] C. Williams, F. Quinlan, and P. Delfyett, "Injection-locked mode-locked laser with long-term stabilization and high power-per-combline," *IEEE Photonics Technology Letters*, vol. 21, no. 2, pp. 94 –96, Jan. 2009.

[83] S. Arahira, H. Yaegashi, K. Nakamura, and Y. Ogawa, "Chirp control and broad-

band wavelength-tuning of 40-GHz monolithic actively mode-locked laser diode module with an external cw light injection," *IEEE Journal of Selected Topics in Quantum Electronics*, vol. 11, no. 5, pp. 1103 – 1111, 2005.

[84] A. Takada and W. Imajuku, "Linewidth narrowing and optical phase control of mode-locked semiconductor ring laser employing optical injection locking," *IEEE Photonics Technology Letters*, vol. 9, no. 10, pp. 1328 –1330, Oct. 1997.

[85] M. Teshima, K. Sato, and M. Koga, "Experimental investigation of injection locking of fundamental and subharmonic frequency-modulated active mode-locked laser diodes," *IEEE Journal of Quantum Electronics*, vol. 34, no. 9, pp. 1588 –1596, Sep. 1998.

[86] M. Teshima, M. Koga, and K. Sato, "Accurate frequency control of a mode-locked laser diode by reference-light injection," *Optics Letters*, vol. 22, no. 2, pp. 126–128, Jan. 1997.

[87] K. Mori and K. Sato, "Supercontinuum lightwave generation employing a mode-locked laser diode with injection locking for a highly coherent optical multicarrier source," *IEEE Photonics Technology Letters*, vol. 17, no. 2, pp. 480 –482, Feb. 2005.

[88] T. Jung, J.-L. Shen, D. Tong, S. Murthy, M. Wu, T. Tanbun-Ek, W. Wang, R. Lodenkamper, R. Davis, L. Lembo, and J. Brock, "CW injection locking of a mode-locked semiconductor laser as a local oscillator comb for channelizing broadband RF signals," *IEEE Transactions on Microwave Theory and Techniques*, vol. 47, no. 7, pp. 1225 –1233, Jul. 1999.

[89] N. Rebrova, T. Habruseva, G. Huyet, and S. P. Hegarty, "Stabilization of a passively mode-locked laser by continuous wave optical injection," *Applied Physics Letters*, vol. 97, no. 10, pp. 101 105 –101 105–3, sep 2010.

[90] G. Fiol, M. Kleinert, D. Arsenijević, and D. Bimberg, "1.3 $\mu$m range 40 GHz quantum-dot mode-locked laser under external continuous wave light injection or optical feedback," *Semiconductor Science and Technology*, vol. 26, no. 1, p. 014006, 2011.

[91] N. Rebrova, G. Huyet, D. Rachinskii, and A. G. Vladimirov, "Optically injected mode-locked laser," *Physical Review E*, vol. 83, p. 066202, Jun. 2011.

[92] Z. Ahmed, H. Liu, D. Novak, Y. Ogawa, M. Pelusi, and D. Kim, "Locking characteristics of a passively mode-locked monolithic DBR laser stabilized by optical injection," *IEEE Photonics Technology Letters*, vol. 8, no. 1, pp. 37 –39, Jan. 1996.

[93] Z. Ahmed, H. Liu, D. Novak, M. Pelusi, Y. Ogawa, and D. Kim, "Low phase noise millimetre-wave signal generation using a passively modelocked monolithic DBR

laser injection locked by an optical DSBSC signal," *Electronics Letters*, vol. 31, no. 15, pp. 1254 –1255, Jul. 1995.

[94] W. Lee, M. Mielke, S. Etemad, and P. Delfyett, "Subgigahertz channel filtering by optical heterodyne detection using a single axial mode from an injection-locked passively mode-locked semiconductor laser," *IEEE Photonics Technology Letters*, vol. 16, no. 8, pp. 1945 –1947, Aug. 2004.

[95] W. Lee and P. Delfyett, "Dual-mode injection locking of two independent mode-locked semiconductor lasers," *Electronics Letters*, vol. 40, no. 19, pp. 1182–1183, Sep. 2004.

[96] T. Habruseva, S. O'Donoghue, N. Rebrova, D. Reid, L. Barry, D. Rachinskii, G. Huyet, and S. Hegarty, "Quantum-dot mode-locked lasers with dual-mode optical injection," *IEEE Photonics Technology Letters*, vol. 22, no. 6, pp. 359 –361, Mar. 2010.

[97] T. Habruseva, G. Huyet, and S. Hegarty, "Dynamics of quantum-dot mode-locked lasers with optical injection," *IEEE Journal of Selected Topics in Quantum Electronics*, vol. 17, no. 5, pp. 1272 –1279, 2011.

[98] M. Margalit, M. Orenstein, G. Eisenstein, and V. Mikhaelshvili, "Injection locking of an actively mode-locked semiconductor laser," *Optics Letters*, vol. 19, no. 24, pp. 2125–2127, Dec. 1994.

[99] M. Margalit, M. Orenstein, and G. Eisenstein, "High-repetition-rate mode-locked er-doped fiber lasers by harmonic injection locking," *Optics Letters*, vol. 20, no. 17, pp. 1791–1793, Sep. 1995.

[100] ——, "Synchronized two-color operation of a passively mode-locked erbium-doped fiber laser by dual injection locking," *Optics Letters*, vol. 21, no. 19, pp. 1585–1587, Oct. 1996.

[101] H. Kurita, T. Shimizu, and H. Yokoyama, "Experimental investigations of harmonic synchronization conditions and mechanisms of mode-locked laser diodes induced by optical-pulse injection," *IEEE Journal of Selected Topics in Quantum Electronics*, vol. 2, no. 3, pp. 508 –513, sep 1996.

[102] A. Nirmalathas, H.-F. Liu, Z. Ahmed, D. Novak, and Y. Ogawa, "Subharmonic synchronous mode-locking of a monolithic semiconductor laser operating at millimeter-wave frequencies," *IEEE Journal of Selected Topics in Quantum Electronics*, vol. 3, no. 2, pp. 261 –269, Apr. 1997.

[103] I. Kim, C. Kim, P. LiKamWa, and G. Li, "Dynamics of all-optical clock recovery using two-section index- and gain-coupled DFB lasers," *IEEE/OSA Journal of Lightwave Technology*, vol. 23, no. 4, pp. 1704 – 1712, Apr. 2005.

[104] S. Arahira and Y. Ogawa, "Cavity-resonant behaviors of all-optical synchronization and clock recovery in passively mode-locked laser diodes," *IEEE Journal of Quantum Electronics*, vol. 44, no. 5, pp. 410 –423, May 2008.

[105] ——, "Retiming and reshaping function of all-optical clock extraction at 160 Gb/s in monolithic mode-locked laser diode," *IEEE Journal of Quantum Electronics*, vol. 41, no. 7, pp. 937 – 944, Jul. 2005.

[106] S. Arahira, H. Takahashi, K. Nakamura, H. Yaegashi, and Y. Ogawa, "Polarization-, wavelength-, and filter-free all-optical clock recovery in a passively mode-locked laser diode with orthogonally pumped polarization-diversity configuration," *IEEE Journal of Quantum Electronics*, vol. 45, no. 5, pp. 476 –487, May 2009.

[107] S. Arahira, H. Takahashi, and H. Yaegashi, "Optical noise tolerance in a polarization-, wavelength-, and filter-free all-optical clock recovery system based on a monolithic mode-locked laser," *IEEE Journal of Quantum Electronics*, vol. 45, no. 10, pp. 1240 –1247, Oct. 2009.

[108] V. Roncin, A. O'Hare, S. Lobo, E. Jacquette, L. Bramerie, P. Rochard, Q.-T. Le, M. Gay, J.-C. Simon, A. Shen, J. Renaudier, F. Lelarge, and G.-H. Duan, "Multi-data-rate system performance of a 40-GHz all-optical clock recovery based on a quantum-dot Fabry-Pérot laser," *IEEE Photonics Technology Letters*, vol. 19, no. 19, pp. 1409 –1411, Oct. 2007.

[109] B. Lavigne, J. Renaudier, F. Lelarge, O. Legouezigou, H. Gariah, and G.-H. Duan, "Polarization-insensitive low timing jitter and highly optical noise tolerant all-optical 40-GHz clock recovery using a bulk and a quantum-dots-based self-pulsating laser cascade," *IEEE/OSA Journal of Lightwave Technology*, vol. 25, no. 1, pp. 170 –176, Jan. 2007.

[110] L. Goldberg, H. F. Taylor, J. F. Weller, and D. R. Scifres, "Injection locking of coupled-stripe diode laser arrays," *Applied Physics Letters*, vol. 46, no. 3, pp. 236 –238, Feb. 1985.

[111] J. P. Hohimer, A. Owyoung, and G. R. Hadley, "Single-channel injection locking of a diode-laser array with a cw dye laser," *Applied Physics Letters*, vol. 47, no. 12, pp. 1244 –1246, Dec. 1985.

[112] L. Goldberg and J. Weller, "Injection-locked operation of a 20-element coupled-stripe laser array," *Electronics Letters*, vol. 22, no. 16, pp. 858 –859, 31 1986.

[113] S. MacCormack, J. Feinberg, and M. H. Garrett, "Injection locking a laser-diode array with a phase-conjugate beam," *Optics Letters*, vol. 19, no. 2, pp. 120–122, Jan. 1994.

[114] L. Goldberg and J. F. Weller, "Injection locking and single-mode fiber coupling

of a 40-element laser diode array," *Applied Physics Letters*, vol. 50, no. 24, pp. 1713 –1715, Jun. 1987.

[115] H. Tsuchida, "Tunable, narrow-linewidth output from an injection-locked high-power AlGaAs laser diode array," *Optics Letters*, vol. 19, no. 21, pp. 1741–1743, Nov. 1994.

[116] J. P. Hohimer, G. R. Hadley, and A. Owyoung, "Interelement coupling in gain-guided diode laser arrays," *Applied Physics Letters*, vol. 48, no. 22, pp. 1504 –1506, Jun. 1986.

[117] G. Abbas, S. Yang, V. Chan, and J. Fujimoto, "Injection behavior and modeling of 100 mW broad area diode lasers," *IEEE Journal of Quantum Electronics*, vol. 24, no. 4, pp. 609 –617, Apr. 1988.

[118] L. Bartelt-Berger, U. Brauch, A. Giesen, H. Huegel, and H. Opower, "Power-scalable system of phase-locked single-mode diode lasers," *Applied Optics*, vol. 38, no. 27, pp. 5752–5760, Sep 1999.

[119] Y. Liu, H.-K. Liu, and Y. Braiman, "Simultaneous injection locking of couples of high-power broad-area lasers driven by a common current source," *Applied Optics*, vol. 41, no. 24, pp. 5036–5039, Aug. 2002.

[120] Y. Liu, H. K. Liu, and Y. Braiman, "Injection locking of individual broad-area lasers in an integrated high-power diode array," *Applied Physics Letters*, vol. 81, no. 6, pp. 978 –980, Aug. 2002.

[121] Y. Liu and Y. Braiman, "Synchronization of high-power broad-area semiconductor lasers," *IEEE Journal of Selected Topics in Quantum Electronics*, vol. 10, no. 5, pp. 1013 – 1024, sept.-oct. 2004.

[122] M. Silber, L. Fabiny, and K. Wiesenfeld, "Stability results for in-phase and splay-phase states of solid-state laser arrays," *Journal of the Optical Society of America B*, vol. 10, no. 6, pp. 1121–1129, Jun. 1993.

[123] W. Wang, K. Nakagawa, S. Sayama, and M. Ohtsu, "Coherent addition of injection-locked high-power algaas diode lasers," *Optics Letters*, vol. 17, no. 22, pp. 1593–1595, Nov 1992.

[124] L. C. Berger, U. Brauch, A. Giesen, H. Huegel, H. Opower, M. Schubert, and K. Wittig, "Coherent fiber coupling of laser diodes," vol. 39, pp. 39–46, 1996.

[125] C. Chang, L. Chrostowski, and C. Chang-Hasnain, "Injection locking of VCSELs," *IEEE Journal of Selected Topics in Quantum Electronics*, vol. 9, no. 5, pp. 1386–1393, 2003.

[126] L. Chrostowski, X. Zhao, and C. Chang-Hasnain, "Microwave performance of

optically injection-locked VCSELs," *IEEE Transactions on Microwave Theory and Techniques*, vol. 54, no. 2, pp. 788–796, 2006.

[127] L. Chrostowski, B. Faraji, W. Hofmann, M. Amann, S. Wieczorek, and W. Chow, "40 GHz bandwidth and 64 GHz resonance frequency in injection-locked 1.55 $\mu$m VCSELs," *IEEE Journal of Selected Topics in Quantum Electronics*, vol. 13, no. 5, pp. 1200–1208, 2007.

[128] X. Zhao, D. Parekh, E. Lau, H. Sung, M. Wu, W. Hofmann, M. Amann, and C. Chang-Hasnain, "Novel cascaded injection-locked 1.55-$\mu$m VCSELs with 66 GHz modulation bandwidth," *Optics Express*, vol. 15, no. 22, pp. 14 810–14 816, 2007.

[129] J. Georges, M.-H. Kiang, K. Heppell, M. Sayed, and K. Lan, "Optical transmission of narrow-band millimeter-wave signals by resonant modulation of monolithic semiconductor lasers," *IEEE Photonics Technology Letters*, vol. 6, no. 4, pp. 568 –570, Apr. 1994.

[130] A. Kellner, B. Lam, G. Yan, and P. Yu, "Externally modulated mode-locked laser diodes for microwave transmission links," *Electronics Letters*, vol. 25, no. 19, pp. 1291 –1293, Sep. 1989.

[131] Z. Ahmed, D. Novak, R. Waterhouse, and H. Liu, "Optically-fed millimetre-wave (37 GHz) transmission system incorporating a hybrid mode-locked semiconductor laser," *Electronics Letters*, vol. 32, no. 19, pp. 1790 –1792, Sep. 1996.

[132] D. Tong and M. Wu, "Continuously tunable optoelectronic millimetre-wave transmitter using monolithic mode-locked semiconductor laser," *Electronics Letters*, vol. 32, no. 21, pp. 2006–2007, 1996.

[133] M. Pelusi, H. Liu, D. Novak, and Y. Ogawa, "THz optical beat frequency generation from a single mode locked semiconductor laser," *Applied physics letters*, vol. 71, no. 4, pp. 449–451, 1997.

[134] L. A. Jiang, E. P. Ippen, and H. Yokoyama, "Semiconductor mode-locked lasers as pulse sources for high bit rate data transmission," *Journal of Optical and Fiber Communications Reports*, vol. 2, pp. 1–31, 2005. [Online]. Available: http://dx.doi.org/10.1007/s10297-004-0022-0

[135] P. Hansen, G. Raybon, U. Koren, B. Miller, M. Young, M. Newkirk, M.-D. Chien, B. Tell, and C. Burrus, "Monolithic semiconductor soliton transmitter," *IEEE/OSA Journal of Lightwave Technology*, vol. 13, no. 2, pp. 297 –301, Feb. 1995.

[136] P. Hansen, C. Giles, G. Raybon, U. Koren, S. Evangelides, B. Miller, M. Young, M. Newkirk, J.-M. Delavaux, S. Korotky, J. Veselka, and C. Burrus, "8.2 Gbit/s,

4200-km soliton data transmission using a semiconductor soliton source," *IEEE Photonics Technology Letters*, vol. 5, no. 10, pp. 1236 –1238, Oct. 1993.

[137] A. Sano, T. Kataoka, H. Tsuda, A. Hirano, K. Murata, H. Kawakami, Y. Tada, K. Hagimoto, K. Sato, K. Wakita, K. Kato, and Y. Miyamoto, "Field experiments on 40 Gbit/s repeaterless transmission over 198 km dispersion-managed submarine cable using a monolithic mode-locked laser diode," *Electronics Letters*, vol. 32, no. 13, pp. 1218 –1220, Jun. 1996.

[138] A. Gnauck, R. Tkach, A. Chraplyvy, and T. Li, "High-capacity optical transmission systems," *IEEE/OSA Journal of Lightwave Technology*, vol. 26, no. 9, pp. 1032–1045, May 2008.

[139] U. Feiste, R. Ludwig, C. Schubert, J. Berger, C. Schmidt, H. Weber, B. Schmauss, A. Munk, B. Buchold, D. Briggmann, F. Kueppers, and F. Rumpf, "160 Gbit/s transmission over 116 km field-installed fibre using 160 Gbit/s OTDM and 40 Gbit/s ETDM," *Electronics Letters*, vol. 37, no. 7, pp. 443 –445, Mar. 2001.

[140] L. Davis, M. Young, and S. Forouhar, "Mode-locked laser arrays for WDM applications," in *Vertical-Cavity Lasers, Technologies for a Global Information Infrastructure, WDM Components Technology, Advanced Semiconductor Lasers and Applications, Gallium Nitride Materials, Processing, and Devi.* IEEE, 1997, pp. 68–69.

[141] H. Shi, G. Alphonse, J. Connolly, and P. Delfyett, "20× 5 Gbit/s optical WDM transmitter using single-stripe multiwavelength modelocked semiconductor laser," *Electronics Letters*, vol. 34, no. 2, pp. 179–181, 1998.

[142] H. Murai, H. Yamada, K. Fujii, Y. Ozeki, I. Ogura, T. Ono, and H. Yokoyama, "3 × 80 Gbit/s WDM-transmission over 600 km using mode-locked laser diodes with an 80 Gbit/s OTDM module," in *Optical Communication, 2001. ECOC '01. 27th European Conference on*, vol. 2, 2001, pp. 180 – 181 vol.2.

[143] M. Attygalle, C. Lim, and A. Nirmalathas, "Dispersion-tolerant multiple WDM channel millimeter-wave signal generation using a single monolithic mode-locked semiconductor laser," *IEEE/OSA Journal of Lightwave Technology*, vol. 23, no. 1, p. 295, Jan 2005.

[144] J. Hayau, O. Vaudel, P. Besnard, F. Lelarge, B. Rousseau, L. Le Gouezigou, F. Pommereau, F. Poingt, O. Le Gouezigou, A. Shen *et al.*, "Optical injection of quantum dot and quantum dash semiconductor lasers," in *Lasers and Electro-Optics 2009 and the European Quantum Electronics Conference. CLEO Europe-EQEC 2009. European Conference on.* IEEE, 2009.

[145] E. A. Viktorov, private communication, 2011.

[146] S. Bouchoule, S. Azouigui, G. Patriarche, S. Guilet, L. Le Gratiet, A. Martinez,

F. Lelarge, and A. Ramdane, "Processing of InP-based shallow ridge laser waveguides using a HBr ICP plasma," in *Indium Phosphide Related Materials, 2007. IPRM '07. IEEE 19th International Conference on*, may 2007, pp. 218 –221.

[147] D. Derickson, Ed., *Fiber Optic Test and Measurement.* Upper Saddle River: NJ: Prentice-Hall, 1998.

[148] APE Pulsecheck. [Online]. Available: http://www.ape-berlin.de/sites/default/files/pulseCheck_1.pdf

[149] S. G. Murdoch, R. T. Watts, Y. Q. Xu, R. Maldonado-Basilio, J. Parra-Cetina, S. Latkowski, P. Landais, and L. P. Barry, "Spectral amplitude and phase measurement of a 40 GHz free-running quantum-dash modelocked laser diode," *Optics Express*, vol. 19, no. 14, pp. 13 628–13 635, Jul 2011.

[150] M. Radziunas, A. Vladimirov, E. Viktorov, G. Fiol, H. Schmeckebier, and D. Bimberg, "Pulse broadening in quantum-dot mode-locked semiconductor lasers: Simulation, analysis, and experiments," *IEEE Journal of Quantum Electronics*, vol. 47, no. 7, pp. 935 –943, 2011.

[151] G. Fiol, C. Meuer, H. Schmeckebier, D. Arsenijevic, S. Liebich, M. Laemmlin, M. Kuntz, and D. Bimberg, "Quantum-dot semiconductor mode-locked lasers and amplifiers at 40 GHz," *IEEE Journal of Quantum Electronics*, vol. 45, no. 11, pp. 1429 –1435, Nov. 2009.

[152] T. B. Simpson, J. M. Liu, K. F. Huang, and K. Tai, "Nonlinear dynamics induced by external optical injection in semiconductor lasers," *Quantum and Semiclassical Optics: Journal of the European Optical Society Part B*, vol. 9, no. 5, p. 765, 1997.

[153] S. P. Hegarty, D. Goulding, B. Kelleher, G. Huyet, M.-T. Todaro, A. Salhi, A. Passaseo, and M. D. Vittorio, "Phase-locked mutually coupled 1.3 $\mu$m quantum-dot lasers," *Optics Letters*, vol. 32, no. 22, pp. 3245–3247, Nov. 2007.

[154] D. Goulding, S. P. Hegarty, O. Rasskazov, S. Melnik, M. Hartnett, G. Greene, J. G. McInerney, D. Rachinskii, and G. Huyet, "Excitability in a quantum dot semiconductor laser with optical injection," *Physical Review Letters*, vol. 98, p. 153903, Apr. 2007.

[155] T. Erneux, E. A. Viktorov, B. Kelleher, D. Goulding, S. P. Hegarty, and G. Huyet, "Optically injected quantum-dot lasers," *Optics Letters*, vol. 35, no. 7, pp. 937–939, Apr. 2010.

[156] S.-C. Chan and J.-M. Liu, "Tunable narrow-linewidth photonic microwave generation using semiconductor laser dynamics," *IEEE Journal of Selected Topics in Quantum Electronics*, vol. 10, no. 5, pp. 1025 – 1032, Sep.-Oct. 2004.

[157] S.-C. Chan, S.-K. Hwang, and J.-M. Liu, "Period-one oscillation for photonic

microwave transmission using an optically injected semiconductor laser," *Optics Express*, vol. 15, no. 22, pp. 14 921–14 935, Oct. 2007.

[158] S.-C. Chan, "Analysis of an optically injected semiconductor laser for microwave generation," *IEEE Journal of Quantum Electronics*, vol. 46, no. 3, pp. 421 –428, Mar. 2010.

[159] X.-Q. Qi and J.-M. Liu, "Photonic microwave applications of the dynamics of semiconductor lasers," *IEEE Journal of Selected Topics in Quantum Electronics*, vol. 17, no. 5, pp. 1198 –1211, Sep.-Oct. 2011.

[160] S. Azouigui, B. Dagens, F. Lelarge, J.-G. Provost, D. Make, O. Le Gouezigou, A. Accard, A. Martinez, K. Merghem, F. Grillot, O. Dehaese, R. Piron, S. Loualiche, Q. Zou, and A. Ramdane, "Optical feedback tolerance of quantum-dot- and quantum-dash-based semiconductor lasers operating at 1.55 $\mu$m," *IEEE Journal of Selected Topics in Quantum Electronics*, vol. 15, no. 3, pp. 764 –773, May-Jun. 2009.

[161] O. Carroll, S. Hegarty, G. Huyet, and B. Corbett, "Length dependence of feedback sensitivity of InAs/GaAs quantum dot lasers," *Electronics Letters*, vol. 41, no. 16, pp. 39 – 40, Aug. 2005.

[162] D. Linde, "Characterization of the noise in continuously operating mode-locked lasers," *Applied Physics B: Lasers and Optics*, vol. 39, pp. 201–217, 1986.

[163] D. J. Derickson, P. A. Morton, J. E. Bowers, and R. L. Thornton, "Comparison of timing jitter in external and monolithic cavity mode locked semiconductor lasers," *Applied Physics Letters*, vol. 59, no. 26, pp. 3372 –3374, dec 1991.

[164] J. P. Tourrenc, A. Akrout, K. Merghem, A. Martinez, F. Lelarge, A. Shen, G. H. Duan, and A. Ramdane, "Experimental investigation of the timing jitter in self-pulsating quantum-dash lasers operating at 1.55 µm," *Optics Express*, vol. 16, no. 22, pp. 17 706–17 713, Oct. 2008.

[165] R. Poore. (2001) Overview of phase noise and jitter. [Online]. Available: http://cp.literature.agilent.com/litweb/pdf/5990-3108EN.pdf

[166] G. Carpintero, M. Thompson, R. Penty, and I. White, "Low noise performance of passively mode-locked 10-GHz quantum-dot laser diode," *IEEE Photonics Technology Letters*, vol. 21, no. 6, pp. 389 –391, Mar. 2009.

[167] K. Yvind, D. Larsson, L. Christiansen, C. Angelo, L. Oxenløwe, J. Mørk, D. Birkedal, J. Hvam, and J. Hanberg, "Low-jitter and high-power 40-GHz all-active mode-locked lasers," *IEEE Photonics Technology Letters*, vol. 16, no. 4, pp. 975 –977, Apr. 2004.

[168] H. Haus, "Theory of mode locking with a slow saturable absorber," *IEEE Journal of Quantum Electronics*, vol. 11, no. 9, pp. 736 – 746, Sep. 1975.

[169] S. Arahira and Y. Ogawa, "Repetition-frequency tuning of monolithic passively mode-locked semiconductor lasers with integrated extended cavities," *IEEE Journal of Quantum Electronics*, vol. 33, no. 2, pp. 255 –264, Feb. 1997.

[170] P. Anandarajah, R. Maher, Y. Xu, S. Latkowski, J. O'Carroll, S. Murdoch, R. Phelan, J. O'Gorman, and L. Barry, "Generation of coherent multicarrier signals by gain switching of discrete mode lasers," *IEEE Photonics Journal*, vol. 3, no. 1, pp. 112 –122, Feb. 2011.

[171] E. A. Viktorov, P. Mandel, M. Kuntz, G. Fiol, D. Bimberg, A. G. Vladimirov, and M. Wolfrum, "Stability of the mode-locked regime in quantum dot lasers," *Applied Physics Letters*, vol. 91, no. 23, pp. 231 116 –231 116–3, dec 2007.

[172] A. G. Vladimirov, U. Bandelow, G. Fiol, D. Arsenijević, M. Kleinert, D. Bimberg, A. Pimenov, and D. Rachinskii, "Dynamical regimes in a monolithic passively mode-locked quantum dot laser," *Journal of the Optical Society of America B*, vol. 27, no. 10, pp. 2102–2109, Oct 2010.

[173] T. Kolokolnikov, M. Nizette, T. Erneux, N. Joly, and S. Bielawski, "The Q-switching instability in passively mode-locked lasers," *Physica D: Nonlinear Phenomena*, vol. 219, no. 1, pp. 13 – 21, 2006. [Online]. Available: http://www.sciencedirect.com/science/article/pii/S0167278906001801

[174] X. S. Yao, L. Davis, and L. Maleki, "Coupled optoelectronic oscillators for generating both RF signal and optical pulses," *IEEE/OSA Journal of Lightwave Technology*, vol. 18, no. 1, p. 73, Jan 2000. [Online]. Available: http://jlt.osa.org/abstract.cfm?URI=jlt-18-1-73

[175] F. van Dijk, A. Enard, X. Buet, F. Lelarge, and G.-H. Duan, "Phase noise reduction of a quantum dash mode-locked laser in a millimeter-wave coupled opto-electronic oscillator," *IEEE/OSA Journal of Lightwave Technology*, vol. 26, no. 15, pp. 2789 –2794, Aug. 2008.

[176] O. Solgaard and K. Lau, "Optical feedback stabilization of the intensity oscillations in ultrahigh-frequency passively modelocked monolithic quantum-well lasers," *IEEE Photonics Technology Letters*, vol. 5, no. 11, pp. 1264 –1267, Nov. 1993.

[177] K. Merghem, R. Rosales, S. Azouigui, A. Akrout, A. Martinez, F. Lelarge, G.-H. Duan, G. Aubin, and A. Ramdane, "Low noise performance of passively mode locked quantum-dash-based lasers under external optical feedback," *Applied Physics Letters*, vol. 95, no. 13, p. 131111, 2009.

[178] C.-Y. Lin, F. Grillot, N. A. Naderi, Y. Li, and L. F. Lester, "rf linewidth reduction in a quantum dot passively mode-locked laser subject to external optical feedback," *Applied Physics Letters*, vol. 96, no. 5, p. 051118, 2010.

[179] S. Breuer, W. Elsaer, J. McInerney, K. Yvind, J. Pozo, E. Bente, M. Yousefi, A. Villafranca, N. Vogiatzis, and J. Rorison, "Investigations of repetition rate stability of a mode-locked quantum dot semiconductor laser in an auxiliary optical fiber cavity," *IEEE Journal of Quantum Electronics*, vol. 46, no. 2, pp. 150 –157, Feb. 2010.

[180] M. Haji, L. Hou, A. E. Kelly, J. Akbar, J. H. Marsh, J. M. Arnold, and C. N. Ironside, "High frequency optoelectronic oscillators based on the optical feedback of semiconductor mode-locked laser diodes," *Optics Express*, vol. 20, no. 3, pp. 3268–3274, Jan 2012.

[181] M. Nizette and T. Erneux, "Stability of injection-locked CW-emitting external-cavity semiconductor lasers," *IEEE Journal of Selected Topics in Quantum Electronics*, vol. 10, no. 5, pp. 961 – 967, sept.-oct. 2004.

[182] S. P. H. G. H. E. A. V. B. Kelleher, D. Goulding and T. Erneux, *Quantum Dot Devices*, ser. Lecture notes in nanoscale science and technology. New York: Springer, 2012, vol. 13, pp. 1–22.

[183] D. Lenstra, B. Verbeek, and A. Den Boef, "Coherence collapse in single-mode semiconductor lasers due to optical feedback," *IEEE Journal of Quantum Electronics*, vol. 21, no. 6, pp. 674 –679, Jun. 1985.

[184] A. Gnauck and P. Winzer, "Optical phase-shift-keyed transmission," *IEEE/OSA Journal of Lightwave Technology*, vol. 23, no. 1, pp. 115 – 130, Jan. 2005.

[185] K. Croussore, I. Kim, Y. Han, C. Kim, G. Li, and S. Radic, "Demonstration of phase-regeneration of dpsk signals based on phase-sensitive amplification," *Optics Express*, vol. 13, no. 11, pp. 3945–3950, May 2005.

[186] K. Croussore and G. Li, "Phase and amplitude regeneration of differential phase-shift keyed signals using phase-sensitive amplification," *IEEE Journal of Selected Topics in Quantum Electronics*, vol. 14, no. 3, pp. 648 –658, 2008.

[187] M. Marhic, C. Hsia, and J.-M. Jeong, "Optical amplification in a nonlinear fibre interferometer," *Electronics Letters*, vol. 27, no. 3, pp. 210 –211, Jan. 1991.

[188] R. Slavik, F. Parmigiani, J. Kakande, C. Lundstrom, M. Sjodin, P. A. Andrekson, R. Weerasuriya, S. Sygletos, A. D. Ellis, L. Gruner-Nielsen, D. Jakobsen, S. Herstrom, R. Phelan, J. O'Gorman, A. Bogris, D. Syvridis, S. Dasgupta, P. Petropoulos, and D. J. Richardson, "All-optical phase and amplitude regenerator for next-generation telecommunications systems," *Nature Photonics*, vol. 4, pp. 690 – 695, 2010.

[189] K. Croussore, I. Kim, C. Kim, Y. Han, and G. Li, "Phase-and-amplitude regeneration of differential phase-shift keyed signals using a phase-sensitive amplifier," *Optics Express*, vol. 14, no. 6, pp. 2085–2094, Mar 2006.

[190] R. Tang, J. Lasri, P. S. Devgan, V. Grigoryan, P. Kumar, and M. Vasilyev, "Gain characteristics of a frequency nondegenerate phase-sensitive fiber-optic parametric amplifier with phase self-stabilized input," *Optics Express*, vol. 13, no. 26, pp. 10 483–10 493, Dec 2005.

[191] S. Sygletos, R. Weerasuriya, S. Ibrahim, F. Gunning, R. Phelan, J. O'Gorman, J. O'Carrol, B. Kelly, A. Bogris, D. Syvridis, C. Lundström, P. Andrekson, F. Parmigiani, D. Richardson, and A. Ellis, "Phase locking and carrier extraction schemes for phase sensitive amplification," in *Transparent Optical Networks (ICTON), 2010 12th International Conference on*, 27 2010-july 1 2010, pp. 1 –4.

[192] G.-W. Lu and T. Miyazaki, "Optical phase add-drop for format conversion between DQPSK and DPSK and its application in optical label switching systems," *IEEE Photonics Technology Letters*, vol. 21, no. 5, pp. 322 –324, Mar. 2009.

[193] R. Weerasuriya, S. Sygletos, S. Ibrahim, R. Phelan, J. O'Carroll, B. Kelly, J. O'Gorman, and A. Ellis, "Generation of frequency symmetric signals from a BPSK input for phase sensitive amplification," in *Optical Fiber Communication (OFC), 2010 Conference on (OFC/NFOEC)*, Mar. 2010,, p. Paper OWT6.

[194] S. Sygletos, P. Frascella, S. K. Ibrahim, L. Grüner-Nielsen, R. Phelan, J. O'Gorman, and A. D. Ellis, "A practical phase sensitive amplification scheme for two channel phase regeneration," *Optics Express*, vol. 19, no. 26, pp. B938–B945, Dec. 2011.

[195] J.-M. Liu, *Photonic Devices*. Cambridge University Press, 2005.

[196] L. Gruner-Nielsen, S. Dasgupta, M. Mermelstein, D. Jakobsen, S. Herstrom, M. Pedersen, E. Lim, S. Alam, F. Parmigiani, D. Richardson, and B. Palsdottir, "A silica based highly nonlinear fibre with improved threshold for stimulated brillouin scattering," in *Optical Communication (ECOC), 2010 36th European Conference and Exhibition on*, Sep. 2010.

[197] S. Sygletos, S. K. Ibrahim, R. Weerasuriya, R. Phelan, L. G. Nielsen, A. Bogris, D. Syvridis, J. O'Gorman, and A. D. Ellis, "Phase synchronization scheme for a practical phase sensitive amplifier of ASK-NRZ signals," *Optics Express*, vol. 19, no. 13, pp. 12 384–12 391, Jun. 2011.

[198] P. Frascella, S. Sygletos, F. Gunning, R. Weerasuriya, L. Grüner-Nielsen, R. Phelan, J. O'Gorman, and A. Ellis, "DPSK signal regeneration with a dual-pump nondegenerate phase-sensitive amplifier," *IEEE Photonics Technology Letters*, vol. 23, no. 8, pp. 516 –518, Apr. 2011.

[199] S. Sygletos, M. Power, F. Garcia Gunning, R. Webb, R. Manning, and A. Ellis, "Simultaneous dual channel phase regeneration in SOAs," in *European Conference and Exhibition on Optical Communication*. Optical Society of America, 2012.

[200] R. Maher, P. Anandarajah, S. Ibrahim, L. Barry, A. Ellis, P. Perry, R. Phelan, B. Kelly, and J. O'Gorman, "Low cost comb source in a coherent wavelength division multiplexed system," in *Optical Communication (ECOC), 2010 36th European Conference and Exhibition on*, Sep. 2010, pp. 1 –3.

[201] A. Ellis and F. Gunning, "Spectral density enhancement using coherent WDM," *IEEE Photonics Technology Letters*, vol. 17, no. 2, pp. 504–506, Feb. 2005.